



**UNIVERSITY** *of the*  
**WESTERN CAPE**

**A comparative analysis of long-term variations of temperature  
and rainfall in rural and urban areas, and their effects on the  
estimation of design storms in Kenya**



LYDIAH WANGECHI GACHAHI  
UNIVERSITY *of the*  
WESTERN CAPE

A thesis submitted in partial fulfilment of the requirements for the degree of  
Doctor of Philosophy in the Department of Earth Sciences, Faculty of Natural  
Science, University of the Western Cape.

**August 2016**

Supervisor:

Professor Dominic Mazvimavi

## KEY WORDS

Nairobi

Mombasa

Equatorial East Africa

Temperature

Global warming

Rainfall

Continuous wavelet transform

Quantile regression

Urban heat island

Land surface temperature

Extreme value

Climate covariates

Storm designs

Return period



## ABSTRACT

My Thesis aimed at expanding the current knowledge on how variations of temperature characteristics including the possible existence of urban heat islands (UHI) over urban areas of Kenya could be influencing rainfall characteristics, and to examine if the stationary extreme value distribution is still suitable for modeling urban storm designs in view of the global climate change. My hypothesis was that the flooding occurring frequently in major urban areas of Kenya are due to increased rainfall caused by global climate change, and the urban heat island (UHI) effect. To put this perception into perspective, temperature and rainfall characteristics and their inter-relationships, of four of the major urban areas in Kenya namely, Nairobi, Mombasa, Kisumu, and Nakuru, were investigated. I obtained data from meteorological stations in and around each urban area, which had at least thirty (30) years of continuous monthly (or daily) temperatures and rainfall values, from the Kenya Meteorological Department. I checked the datasets for quality and missing values and adjusted where necessary before commencing with analysis. I sourced other supporting global dataset from various websites' data banks. I used various methods of data analysis which included; i) exploratory data analysis techniques such as the continuous wavelet transform (CWT), geographical information system (GIS) maps, and visual time series plots. In particular and unique in my Thesis was the use of the CWT method as a diagnostic tool to examine non-stationarities and variability of temperature and rainfall time series. The use of land surface temperature data to investigate UHIs was also adopted to supplement the air temperature; ii) statistical methods including parametric (linear and quantile regression) and non-parametric (Mann-Kendal) trend tests, Pearson's correlation analysis and the extreme value analysis. Statistical hypotheses were stated and tested at the 5% level of significance. Particularly unique in the statistical analysis is the use of the quantile regression which has not been used to investigate trends of the highly variable rainfall of the equatorial East

African (EEA) region, and the generalized extreme value analysis (GEV) analysis which has virtually no published literature for the EEA rainfall extreme value analysis. Most of the analysis was carried out in the *R* environment. I established that; i) there is warming due to urbanization as well as global warming within and in the neighbourhood of each of the four urban areas especially for the night-time temperature; ii) there was generally no significant change over time of rainfall at the monthly, seasonal and annual time scales; however, there were few exceptions where stations close to urban areas, had trends of monthly and seasonal rainfall. In particular, I observed that June-July-August (JJA) seasonal rainfall was decreasing over the coastal region and increasing over Nairobi. On further analysis of inter-relationships between rainfall and temperature I established fairly strong statistical relationships between rainfall and temperature. For instance, I found that JJA seasonal rainfall in Nairobi at the Dagoretti corner station was strongly associated with JJA temperature of the stations to the northeast of Mombasa town ( $R^2 \sim 0.7$ ,  $p$ -value 0.001). Such relationships were attributed to the changes in local and regional thermal circulations resulting from enhanced temperatures; iii) Urban heat islands (UHIs) exist in Nairobi and Mombasa which were observable more clearly from the land surface temperature (LST). The UHIs are strongest during the dry season (DJF). For instance, Nairobi urban area has a strong day-time and weak night-time UHI, particularly within the CBD and heavily built up areas, while Mombasa has a weaker UHI than Nairobi during both daytime and nighttime. However, the UHIs in both cities are more distinguishable in the night-time than in the day-time LST. I found no evidence in general, that urbanization and/or UHI have directly influenced seasonal rainfall within Mombasa but there was evidence of changes downwind of Nairobi and; iv) lastly, I carried out the extreme value analysis of rainfall under stationary and non-stationary conditions using the generalized extreme value (GEV) method and established that stationary GEV models of the Gumbel type were applicable to produce design storms for each town. The



implications of these outcomes to urban stormwater management in Kenya are that; a) changes in temperatures due to global warming and UHI effect in urban areas are influencing (positive or negative) changes in rainfall characteristics, which will affect urban hydrology; b) the day-time UHI effect especially over Nairobi, has the potential to strengthen the convective activities in urban areas and their downwind neighborhoods, and in the presence of moisture could intensify the rainfall storms with consequences of urban flooding. Thus there is need to extend this study to investigate the effects of UHI and global warming on storm intensities; iii) although stationary GEV models are adequate in producing design storms, there is need to understand the non-stationarity of rainfall, and the influence of climate modes of variability on the occurrence of extreme rainfall events in the EEA region, since such events will cause flooding even when urban stormwater management systems are adequately put in place.



**DECLARATION**

I declare that this thesis “*A comparative analysis of long-term variations of temperature and rainfall in rural and urban areas, and their effects on the estimation of design storms in Kenya*” is my own work and has not been presented before for any degree or examination in any other university and that all the information sources I have used or quoted have been indicated and acknowledged by means of complete references.

Lydia W. Gachahi



Signature.....date.....

UNIVERSITY of the  
WESTERN CAPE

## **DEDICATION**

To the entire Githaiga's Family headed by my dear mother Gladys Nyokabi

To my beloved children, Nguyo, Kirigo and Nyokabi, niece Wanjiku and nephew Githaiga



## ACKNOWLEDGEMENT

My sincere gratitude first of all goes to my supervisor, Dominic Mazvimavi, Professor of Environmental and Water Science, Department of Earth Sciences, University of the Western Cape, and Director, Institute for Water Studies, for his continuous guidance, constructive criticisms, encouragement and tireless review of the various scripts that culminated into successive and timely completion of this Thesis. I am deeply indebted to the Government of the Netherlands through its NUFFIC, NICHE project at the Technical University of Kenya (TUK) for offering me a scholarship. Special thanks go to the TUK members of staff managing the NUFFIC NICHE project headed by Prof. Paul Shiundu for giving me the opportunity for my Ph.D. degree to be an outcome of one of the objectives of the project. Thanks to the Vice Chancellor of TUK Prof. Francis Aduoland his deputy Prof Paul Shiundu for granting me paid study leave and also arranging for financial support to supplement the Nuffic funding. I am sincerely indebted to Bobby Russel of Euroconsult Mott Macdonald Company (the Netherlands) for his timely imbursement of all the monies needed for this study on behalf of Nuffic. Special thanks are due to the Department of Meteorology in Kenya for providing me with the necessary data sets, and all other individual persons who gave me their personal data to supplement. Thanksto Mandy Naidoo (Postgraduate administrator), for her tireless effort to remind us of important deadlines, Dr. Kanyerere for his support in settling us down on arrival in SA, and in particular giving me insights on how to write a Ph.D. proposal. I am sincerely and greatly indebted to my friend and colleague Mr. Kiplagat Ayabei of UWC, Department of Chemistry, who together with others supported me in all ways when I was taken ill during the course of my study. I am equally indebted to my children Alex Nguyo, Karen Kirigo and Joy Nyokabi, together with my entire family for the support they provided to me during this trying period. And thanks to all those who provided voluntary assistance of any kind, God bless you all.

## TABLE OF CONTENTS

KEY WORDS.....	ii
ABSTRACT.....	iii
DECLARATION .....	vi
DEDICATION.....	vii
ACKNOWLEDGEMENT .....	viii
TABLE OF CONTENTS.....	ix
LIST OF FIGURES .....	xii
LIST OF TABLES.....	xiv
LIST OF ABBREVIATIONS.....	xvi
<b>CHAPTER 1: INTRODUCTION.....</b>	<b>1</b>
1.1 Temperature variability and change.....	2
1.2 Rainfall variability and change .....	3
1.3 The urban heat island (UHI), and temperature-rainfall relationships .....	4
1.4 Change detection and the extreme value analysis.....	6
1.5 Research questions and objectives .....	8
1.6 Significance of the study .....	10
1.7 The study area .....	12
1.7.1 Nairobi city .....	14
1.7.2 Mombasa city.....	15
1.7.3 Kisumu town.....	15
1.7.4 Nakuru town.....	16
1.7.5 Justification of the choice of study area.....	17
1.8 Thesis outline .....	18
<b>CHAPTER 2: TEMPORAL VARIATIONS OF TEMPERATURE .....</b>	<b>21</b>
2.1 Introduction .....	21
2.2 Data types and sources .....	23
2.2.1 Infilling of missing data .....	25
2.3 Description of urban and rural stations .....	26
2.4 Data analysis .....	28
2.4.1 Continuous wavelet transform (CWT) as an exploratory tool.....	31
2.4.2 Trend analysis .....	38
2.5 Results and discussion.....	42
2.5.1 Spatial and temporal variations of temperature .....	42
2.5.2 Continuous wavelet transform (CWT) analysis of temperature .....	45

2.5.3	Trend analysis .....	59
2.5.4	Influence of global temperature anomalies.....	66
2.5.5	Discussion.....	69
2.6	Summary .....	71
<b>CHAPTER 3: TEMPORAL VARIATIONS OF RAINFALL.....</b>		<b>73</b>
3.1	Introduction .....	73
3.1.1	Climatology of rainfall over the EEA region.....	75
3.2	Data types and sources .....	77
3.2.1	Description of rainfall stations.....	78
3.2.2	ENSO and IOD data.....	80
3.3	Data quality control and methods of analysis .....	81
3.3.1	Quantile regression .....	82
3.4	Results and discussion.....	84
3.4.1	Estimating missing values and homogeneity test .....	84
3.4.2	Spatial and temporal variability of rainfall .....	85
3.4.3	Exploring rainfall variability using CWT .....	93
3.4.4	Effects of ENSO and IOD on rainfall variability.....	101
3.4.5	Trend analysis of rainfall .....	106
3.4.6	Discussion.....	112
3.5	Summary .....	115
<b>CHAPTER 4: URBAN HEAT ISLAND.....</b>		<b>118</b>
4.1	Introduction .....	118
4.1.1	Generation of UHI .....	120
4.1.2	Determination of UHI intensity .....	123
4.2	Methodology .....	127
4.2.1	Description of urban and rural temperature measuring stations .....	128
4.2.2	Data and methodology .....	134
4.3	Results and discussion.....	140
4.3.1	The difference of means of $T_{max}$ and $T_{min}$ in urban and rural stations .....	140
4.3.2	UHI over Nairobi .....	142
4.3.3	UHI over Mombasa.....	156
4.3.4	Discussion .....	167
4.4	Summary .....	171
<b>CHAPTER 5: EFFECTS OF TEMPERATURE ON URBAN RAINFALL.....</b>		<b>173</b>
5.1	Introduction .....	173
5.1.1	Effects of urban temperature on urban precipitation patterns.....	174
5.1.2	The mechanisms of temperature enhancement on urban rainfall .....	176

5.1.3	Influence of thermally induced motions on rainfall.....	178
5.2	Materials and methods .....	183
5.3	Results and discussion.....	188
5.3.1	Urban and UHI effects on rainfall .....	188
5.3.2	Spatial influence of temperature on urban rainfall .....	194
5.3.3	Discussion.....	201
5.4	Summary .....	204
<b>CHAPTER 6: EXTREME VALUE DISTRIBUTION MODELS OF URBAN RAINFALL.....</b>		<b>207</b>
6.1	Introduction .....	207
6.2	Data sources .....	212
6.3	Data analysis .....	213
6.3.1	Generalized extreme value (GEV) distribution .....	214
6.3.2	Estimation of parameters of GEV distribution .....	217
6.3.3	Model diagnostics .....	218
6.3.4	Choice of model.....	220
6.3.5	Return period and return level .....	220
6.4	Results and discussion.....	222
6.4.1	Correlations between annual daily maximum rainfall and climate covariates .....	222
6.4.2	GEV analysis results.....	223
6.4.3	Predicting return levels and return periods with the GEV models .....	232
6.4.4	Discussion.....	234
6.5	Summary .....	236
<b>CHAPTER SEVEN: CONCLUSION .....</b>		<b>238</b>
7.1	Significance of the outcomes .....	242
7.2	Implications of the findings to urban hydrology.....	243
7.3	Recommendations .....	244
7.3.1	Recommendations to climate scientists and research institutions .....	244
7.3.2	Recommendations to urban environmentalist and hydrologists .....	247
7.3.3	Recommendations to urban planners .....	247
References.....		248
Appendices.....		278

## LIST OF FIGURES

<b>Figure 1.1:</b> A photograph of a flooded road in the city of Nairobi during the long rains of March to May 2016.....	12
<b>Figure 1.2:</b> The relief map of Kenya.....	14
<b>Figure 1.3:</b> Location of counties and the major towns .....	17
<b>Figure 2.1:</b> Locations of meteorological stations and the acronyms used for the analysis of temperature .....	28
<b>Figure 2.2:</b> An illustrative diagram (WPS map) of an output of a time series variable analysed using the CWT method .....	37
<b>Figure 2.3:</b> Annual temperature cycle of the mean monthly $T_{max}$ and $T_{min}$ .....	43
<b>Figure 2.4:</b> Spatial and temporal variations of the mean seasonal temperature for urban and rural stations.....	44
<b>Figure 2.5:</b> The wavelet power spectrum plots of $T_{max}$ over Nairobi .....	46
<b>Figure 2.6:</b> The wavelet power spectrum plots of $T_{min}$ over Nairobi .....	48
<b>Figure 2.7:</b> The wavelet power spectrum plots of $T_{max}$ over Mombasa.....	50
<b>Figure 2.8:</b> The wavelet power spectrum plots of $T_{min}$ over Mombasa.....	51
<b>Figure 2.9:</b> The wavelet power spectrum plots of the $T_{max}$ over the Lake region .....	53
<b>Figure 2.10:</b> The wavelet power spectrum plots of the $T_{min}$ over the Lake region.....	54
<b>Figure 2.11:</b> The wavelet power spectrum plots of the $T_{max}$ in Nakuru .....	55
<b>Figure 2.12:</b> The wavelet power spectrum plots of the $T_{min}$ in Nakuru.....	56
<b>Figure 2.13:</b> Linear regression trend test results of $T_{max}$ .....	60
<b>Figure 2.14:</b> Mann-Kendall trend test results of $T_{max}$ .....	61
<b>Figure 2.15:</b> Linear regression trend test results of $T_{min}$ .....	62
<b>Figure 2.16:</b> Mann-Kendall trend test results of $T_{min}$ .....	63
<b>Figure 2.17:</b> Relationship between global temperature anomalies (GT) and the urban and rural temperature .....	67
<b>Figure 3.1:</b> The eight homogeneous rainfall zones of East Africa .....	79
<b>Figure 3.2:</b> Mass curves of rainfall of some stations showing rainfall homogeneity .....	85
<b>Figure 3.3:</b> Spatial variation of the mean annual and seasonal rainfall .....	86
<b>Figure 3.4:</b> An example from NU station showing the mean pentad distribution of rainfall within a year.....	87
<b>Figure 3.5:</b> Spatial variability of the mean monthly rainfall depicting the bimodal rainfall characteristics and seasonal peak months of some stations from each climatic zone .....	88
<b>Figure 3.6:</b> Temporal variability of annual total rainfall for urban and rural stations.....	89
<b>Figure 3.7:</b> Temporal variability of MAM seasonal rainfall for urban and rural stations .....	90
<b>Figure 3.8:</b> Temporal variability of OND seasonal rainfall for urban and rural stations .....	92
<b>Figure 3.9:</b> The wavelet power spectra of rainfall time series of Nairobi .....	94
<b>Figure 3.10:</b> The wavelet power spectra of rainfall time series of Mombasa.....	96
<b>Figure 3.11:</b> The wavelet power spectrum of rainfall time series of Nakuru .....	98
<b>Figure 3.12:</b> The wavelet power spectra of rainfall time series of Kisumu.....	99
<b>Figure 3.13:</b> The wavelet power spectra of the annual time series of NINO3.4 and IOD indices	



<b>Figure 3.14:</b> The wavelet power spectra of annual rainfall of stations of Nairobi, Mombasa and Kisumu .....	103
<b>Figure 3.15:</b> Linear correlations between annual rainfall with NINO 3.4 and IOD indices respectively .....	105
<b>Figure 3.16:</b> Quantile regression analysis of rainfall .....	109
<b>Figure 3.17:</b> Temporal variation of indices of rainfall extreme at Nakuru station .....	112
<b>Figure 4.1:</b> Schematic diagram of daytime convective UBL with wind flowing from left to right.....	119
<b>Figure 4.2:</b> A typical rural and urban surface energy balance .....	120
<b>Figure 4.3:</b> Factors that influence the generation of Urban Heat Island.....	122
<b>Figure 4.4:</b> The ‘local climate zone’ (LCZ) classification scheme.....	125
<b>Figure 4.5:</b> Map of Kenya showing the locations of Nairobi and Mombasa.....	128
<b>Figure 4.6:</b> Location of three of the four weather stations used to study UHI in Nairobi .....	131
<b>Figure 4.7:</b> Locations of urban and rural stations at the coast .....	133
<b>Figure 4.8:</b> Google Earth map showing the N-S and W-E transects used to compute temperature profiles for Nairobi and Mombasa.....	139
<b>Figure 4.9:</b> Comparison between the rates of change of seasonal $T_{min}$ between urban and rural stations in Nairobi area.....	143
<b>Figure 4.10:</b> Temporal variations of annual $\Delta T_{max}(u-r)$ and $\Delta T_{min}(u-r)$ for urban-rural pair of station in Nairobi.....	144
<b>Figure 4.11:</b> Seasonal and annual mean values of $\Delta T_{max}(u-r)$ and $\Delta T_{min}(u-r)$ over Nairobi .....	145
<b>Figure 4.12:</b> Linear relationships between $\Delta T_{max}(u-r)$ and the rural $T_{max}$ over Nairobi.....	148
<b>Figure 4.13:</b> N-S land surface temperature profiles of Nairobi .....	151
<b>Figure 4.14:</b> W-E land surface temperature profiles of Nairobi .....	152
<b>Figure 4.15:</b> Mean monthly distribution of land surface temperature for 2015 .....	153
<b>Figure 4.16:</b> Comparison of the rates of change of $T_{min}$ between the urban station and the rural stations for Mombasa .....	157
<b>Figure 4.17:</b> Temporal Variation of annual mean temperature differences ( $\Delta T_{max}(u-r)$ and $\Delta T_{min}(u-r)$ ) over Mombasa .....	158
<b>Figure 4.18:</b> Long-term mean monthly and seasonal values of $\Delta T_{max}(u-r)$ and $\Delta T_{min}(u-r)$ .....	158
<b>Figure 4.19:</b> Linear relationships between urban-rural temperature differences and the urban $T_{min}$ over Mombasa .....	160
<b>Figure 4.20:</b> N-S land surface temperature profiles for Mombasa. ....	162
<b>Figure 4.21:</b> W-E land surface temperature profiles for Mombasa. ....	164
<b>Figure 4.22:</b> Mean monthly distribution of night-time LST of 2005 and 2015 January and July.....	166
<b>Figure 5.1:</b> A schematic diagram showing elements of precipitation in an urban and a rural area.....	178
<b>Figure 5.2:</b> Temporal and spatial extent of different scales of atmospheric motions.....	182
<b>Figure 5.3:</b> Mean westerly and easterly winds and pressure systems across the globe.....	182
<b>Figure 5.4:</b> Temporal variability of rainfall differences for Nairobi .....	189
<b>Figure 5.5:</b> Temporal variability rainfall differences for Mombasa .....	190

<b>Figure 5.6:</b> Trends of log (U/R) for Nairobi .....	191
<b>Figure 5.7:</b> Rainfall-temperature relationships. ....	201
<b>Figure 6.1:</b> Temporal variability of the annual daily maximum rainfall series .....	223
<b>Figure 6.2:</b> Diagnostic plots comparing the stationary and non-stationary GEV distributions for Nairobi.....	225
<b>Figure 6.3:</b> Diagnostic plots comparing the stationary and non-stationary GEV distributions for Mombasa .....	228
<b>Figure 6.4:</b> Diagnostic plots comparing the stationary and non-stationary GEV distributions for Kisumu .....	230
<b>Figure 6.5:</b> Diagnostic plots for stationary GEV distributions for Nakuru .....	232
<b>Figure 6.6:</b> Estimating return levels of each the four stations; .....	233

## LIST OF TABLES

<b>Table 1.1:</b> Kenya’s major towns and their population .....	16
<b>Table 2.1:</b> Stations used for analyses of air temperature: .....	27
<b>Table 2.2:</b> Indices of daily temperature extremes selected .....	30
<b>Table 2.3:</b> Definition of terms and formulas used in computing regression and correlation coefficients .....	39
<b>Table 2.4:</b> Variation of annual mean temperature with altitude.....	42
<b>Table 2.5:</b> Trend results of the extreme temperature indices .....	66
<b>Table 2.6:</b> Proportion of variance of temperature explained by variation of global temperature .....	68
<b>Table 3.1:</b> Indices of daily rainfall extremes used in this study.....	77
<b>Table 3.2:</b> Stations used for analysis of rainfall.....	80
<b>Table 3.3:</b> Quantile regression trend results of MAM seasonal rainfall .....	107
<b>Table 3.4:</b> Quantile regression trend results of JJA seasonal rainfall .....	107
<b>Table 3.5:</b> Quantile regression trend results of OND seasonal rainfall .....	108
<b>Table 3.6:</b> Trend analysis of monthly and seasonal rainfall .....	110
<b>Table 4.1:</b> Urban and rural stations used to investigate UHI.....	133
<b>Table 4.2:</b> Urban-rural pair of stations used to compute temperature differences.....	135
<b>Table 4.3:</b> The long-term mean of seasonal and annual $T_{max}$ and $T_{min}$ .....	141
<b>Table 4.4:</b> Analysis of difference of means of $T_{max}$ and $T_{min}$ between urban and rural stations over Nairobi and Mombasa.....	141
<b>Table 4.5:</b> Assessment of temporal trends of $\Delta T(u-r)$ for Nairobi.....	146
<b>Table 4.6:</b> Temporal trends of temperature differences between Mombasa urban and rural stations .....	159
<b>Table 5.1:</b> Pairs of urban-rural stations used in investigating urban and UHI effects on rainfall.....	185
<b>Table 5.2:</b> Correlations coefficients of MAM rainfall and mean MAM temperature.....	196
<b>Table 5.3:</b> Correlations coefficients of JJA rainfall and mean JJA temperature.....	198
<b>Table 5.4:</b> Correlations coefficients of OND rainfall and mean OND temperature .....	199

<b>Table 6.1:</b> Location of stations in each urban area with daily rainfall data used in GEV analysis.....	213
<b>Table 6.2:</b> Correlations of the Annual daily maximum series with climate covariates .....	222
<b>Table 6.3:</b> Comparison of model parameters of a stationary and non-stationary GEV distribution model fitted for Nairobi.....	224
<b>Table 6.4:</b> Comparison of model parameters of a stationary and non-stationary GEV distribution model for Mombasa.....	227
<b>Table 6.5:</b> Comparison of model parameters of a stationary and non-stationary GEV distribution model fit for Kisumu .....	229
<b>Table 6.6:</b> Parameters of a stationary GEV distribution model for Nakuru .....	231
<b>Table 6.7:</b> Return levels for some selected return periods for each of the four urban areas; the errors were estimated by the Normal method for the 95% level of confidence .....	234



## LIST OF ABBREVIATIONS

<b>DJF</b>	December-January-February
<b>CBD</b>	Central Business District
<b>CWT</b>	Continuous Wavelet Transform
<b>COI</b>	Cone of Influence
<b>EALLJ</b>	East Africa Low Level Jet
<b>EEA</b>	Equatorial Eastern Africa
<b>ENSO</b>	El Niño / Southern Oscillation
<b>EVA</b>	Extreme Value Analysis
<b>GHA</b>	Greater Horn of Africa
<b>GEV</b>	Generalized Extreme Value
<b>GPD</b>	Generalized Pareto Distribution
<b>IOD</b>	Indian Ocean Dipole
<b>IPCC</b>	U Intergovernmental Panel on Climate Change
<b>ISC</b>	WESTERN CAPE Inter-station correlations
<b>ITCZ</b>	Inter-Tropical Convergence Zone
<b>JJA</b>	June-July-August
<b>KARI</b>	Kenya Research Institute
<b>KMD</b>	Kenya Meteorological Department
<b>KNBS</b>	Kenya National Bureau of Statistics
<b>LST</b>	Land Surface Temperature
<b>MAM</b>	March-April-May
<b>MODIS</b>	Moderate Imaging Spectroradiometer
<b>NCAR</b>	National Centre for Atmospheric Research
<b>NCC</b>	Nairobi City Council

<b>NCDC</b>	National Climate Data Centre
<b>NCEP</b>	National Centre for environmental prediction
<b>NE</b>	North Easterlies
<b>NOAA</b>	National Oceanic and Atmospheric Administration
<b>OND</b>	October-November-December
<b>PBL</b>	Planetary Boundary Layer
<b>QR</b>	Quantile Regression
<b>SE</b>	South Easterlies
<b>SOI</b>	Southern Oscillation Index
<b>SON</b>	September-October-November
<b>SST</b>	Sea Surface Temperature
<b>TOA</b>	Top of the atmosphere
<b>UBL</b>	Urban Boundary layer
<b>UHI</b>	Urban Heat Island
<b>UHII</b>	Urban Heat Island Intensity
<b>UCI</b>	Urban Cool Island
<b>WPS</b>	Wavelet Power Spectrum
<b>WMO</b>	World Meteorological Organizations

## 1 CHAPTER 1: INTRODUCTION

Activities of a rapidly increasing and industrializing human population have added significant quantities of greenhouse gases in the atmosphere. The increased greenhouse gases have affected the radiative balance of the earth's atmosphere resulting in climate change. According to the Intergovernmental Panel on Climate Change (IPCC)(Stocker, 2013),there is evidence of an increase in atmospheric and sea surface temperatures which is likely to intensify the hydrological cycle, leading to increased intensity and frequency of rainfall. Urban areas are faced with special climatic conditions owing to the enhanced temperatures caused by the Urban Heat Island (UHI) effect that may contribute to increasing rainfall intensities (Wang, et al., 2008; Rosenzweig, et al., 2011). Regional studies have indicated changes in temperature and rainfall patterns in several parts of the world (New, et al., 2006; Skansi, et al., 2013; Omondi, et al., 2014). However, these regional studies have coarse spatial resolution and the results may not be applicable at local (urban) scale, such as determining possible changes in both frequencies and magnitude of rainfall that is likely to impact on urban stormwater management systems.

Studies that have investigated possible changes of spatial and temporal characteristics of temperature and rainfall at the local scale over the equatorial east African (EEA) region are very few. Omondi, et al. (2014) analysed daily temperature and rainfall extreme indices over the Greater Horn of Africa (GHA) and the results indicated a significant decreasing trend in total rainfall during wet days (for rainfall greater than 1mm/day), increasing warm extremes and decreasing cold extremes in temperature. While Kenya is a part of the GHA, only three stations were included in the study and one method of change detection was used which may not give conclusive evidence for change as suggested by Sonali and Kumar, (2013).Moreover, indices of extreme temperature and rainfall were the only variables used in

this study. Furthermore, the study by Omondi et al. (2014) did not investigate the possible existence of the urban heat island effect within the fast growing cities of the EEA region and its possible impacts on rainfall characteristic. In my Thesis, I sought to provide an improved understanding of how possible changes in temperature and rainfall characteristics within and around urban areas of the equatorial region may influence extreme rainfall events considered important for urban stormwater management. A brief discussion of the research gaps that exist in this regard is presented below.

### **1.1 Temperature variability and change**

Climate change studies have reported global warming in some parts of the world. Skansi, et al. (2013) reported warming across South America since the mid-twentieth century. Jhahharia and Singh, (2010) analysed maximum, minimum and mean temperatures over northeast India and found no trends in winter and pre-monsoon seasons and increasing trends in both minimum and maximum temperatures in the monsoon and post monsoon seasons. Sonali and Kumar (2013) found increasing trends of minimum temperatures over the whole of India. Kruger and Sekele, (2013) using climate indices of daily temperature extremes, found increasing trends of warm extremes and decreasing trends of cold extremes over South Africa, while Omondi, et al. (2014) analysed daily temperature extremes over the Greater Horn of Africa (GHA) and New, et al. (2006) over the southern and western African region; the results from both studies indicate increasing trends of surface temperatures extremes. These studies indicate a general increase in regional surface temperatures which was also reported in global climate studies by the IPCC (Stoker, 2013).

However, regional studies of temperature variability and changes at small spatial scales and in the EEA region have not been investigated especially for the rapidly growing urban areas

of this region. Different methods of change detection in urban and rural temperature have not been employed to explore the possible influence of urbanization on temperature. I, therefore, endeavoured to examine temperature variations at small spatial scales in and around urban areas of Kenya using different methods of data exploration and trend analysis in order to provide new knowledge on the variability and possible changes in temperature at various time scales. Any changing patterns of temperature characteristics at different time scales in and around the major urban areas of Kenya, was then used to investigate their influence on rainfall characteristics, that may in turn influence stormwater generation.

## 1.2 Rainfall variability and change

Rainfall is the main input in the terrestrial hydrologic system and its variability has a direct impact on urban stormwater systems. Noticeable influence of human activities on rainfall patterns has been reported in some parts of the world especially in urban areas. For example, Marengo et al. (2013) found an increase in total and heavy rainfall and decrease in light rains over São Paulo metropolitan area (Brazil) and suggested that effects of urbanization are significant. Some studies on rainfall distribution over the eastern African region have shown that there is a decreasing trend in annual rainfall amounts (Omondi, et al., 2014). However (Opija et al. (2007) indicated that the Nairobi (Kenya) urban area showed increasing trends of high-intensity rainfall and attributed it to the effects of urbanization. Rainfall over the equatorial region is seasonal and highly variable. Kenya has two main rainy seasons; the March to May (MAM) season locally referred to as the '*long rain season*', and the '*short rain season*' from October to December (OND). The onset and cessation of each season coincide with the arrival and withdrawal respectively of the Inter-Tropical Convergence zone (ITCZ) which is mainly responsible for the high inter-annual and intra-seasonal variability (Okoola, 1998). The spatial and temporal variability of seasonal rainfall



in EEA region has mainly been linked to changes in the sea surface temperatures (SSTs) of the Indian and Atlantic oceans (Mukabana and Pielke, 1996), the El-Nino Southern Oscillation (ENSO) and the Indian Ocean Dipole (IOD) anomalies (Indeje et al., 2000; Clark et al., 2002; Black, et al., 2003; Nicholson, 2014; Nicholson, 2015). Decadal variability of the East African rainfall has been established and linked to different modes of SST anomalies over the Indian and Atlantic oceans (Omondi, et al., 2012; Omondi, et al., 2013).

A comparative study of rainfall variability and possible changes at various temporal scales over urban areas and their rural surroundings and especially in relation to urban storm designs has not yet been carried out in the EEA region. The urban areas of this region have been expanding rapidly over the last few decades (Mundia and Aniya, 2006). Furthermore, rigorous methods of change detection at small spatial scales have not been employed in the Kenyan rainfall although reported cases of increased damage by urban floods have been on the rise. More details on rainfall temporal and spatial variability including change detection methods are discussed in Chapter 3.

### **1.3 The urban heat island (UHI), and temperature-rainfall relationships**

Most of the regional studies over the EEA region have not shown if there are differences in trends and variabilities of temperatures and rainfall between urban and rural areas. Studies of UHI effects over EEA urban areas are few. For example Opija and Mukabana, (2004) examined the effects of urbanization on the water budget over Nairobi, and indicated that the presence of the city has influence on the water budget. Opija et al. (2007) further indicated that the urban effects are modifying the heat budget over the city of Nairobi. Apart from the likely increase in surface temperatures resulting from global warming in a given region, the development of large cities creates UHIs which may further influence local climate and

especially rainfall characteristics. UHI is an urban area which is significantly warmer than its surrounding rural areas. The 'island' designation is due to the circular isothermal patterns of the near-surface air temperature surrounded by a 'sea' of the cooler area (Oke, 1995). The UHI has been studied widely especially for the megacities of the world (Peng, et al., 2011; Vardoulaski, et al., 2013; Ahmed, et al., 2014). The intensity of the UHI is mainly measured as the difference between the surface temperature of the urban area and a neighbouring rural area (Oke, 1995; Rosenberg, et al., 2010). The UHI intensity (UHII) in a city has been found to be apparent when winds are weak and skies are clear. For instance, Murphy, et al. (2011) computed urban heat island intensities for San Juan metropolitan area (Puerto Rico) using data collected by mobile and fixed stations for various seasons and different spatial locations; Vardoulaski, et al. (2013) studied UHI in Agrinio city in Greece that has high summer temperature using a network of air sensors located at different locations in the city. Both studies indicated that night-time UHI was on average stronger than day-time UHI. Studies have also shown that UHI is a phenomenon that is common regardless of the climatic region and is manifested more strongly in winter than summer (Peng, et al., 2011) for temperate regions, and more strongly during dry seasons than wet seasons in tropical regions.

The urban UHI effect is likely to affect urban stormwater generation through enhancing convective activities. Studies have shown that the presence of the UHI enhances urban rainfall. According to Bornstein and Lin, (2000), under calm regional wind flow, a relatively low pressure may be created over the city by the anomalously high temperature of the UHI and cooler air rushes into the urban area causing warm air to rise. This vertical motion can create convective thunderstorms that may produce rainfall in the city and mostly at night when the UHI is strongest. On the other hand, when the regional flow is unstable, winds tend to diverge around the city because of increased surface roughness thus creating maximum

precipitation on the lateral and downwind edges of the city with minimum precipitation located over the urban area (Shepherd, 2005). Other factors that may induce changes in the natural precipitation in an urban environment include modification of microphysical and dynamical processes of passing clouds through the addition of condensation nuclei from industrial pollutants, increase in low level mechanical turbulence from urban obstructions and modification of low level atmospheric moisture content by additions of industrially generated plumes from cooling towers (Huff and Changnon, 1973; Stewart and Oke, 2012). Studies that examine possible relationships between enhanced urban surface temperatures (resulting from UHI effect and/or global warming) and urban rainfall characteristics in the African region are few (Efe and Eyefia, 2014). Opija, et al. (2007) used dynamical simulations and suggested a possible influence of enhanced urban temperatures on convective activities over Nairobi (Kenya) although the study did not establish the existence of UHI. Studies that improve the understanding of the UHI, and the interaction between the enhanced urban temperatures and urban rainfall characteristics in the rapidly growing cities of the equatorial African region are lacking. My Thesis, therefore, forms a basis upon which such understanding is improved and new knowledge provided.

#### **1.4 Change detection and the extreme value analysis**

Changes in temperature and rainfall characteristics due to climate and other factors are not consistent even at regional or country levels (New et al., 2006; Mazvimavi, 2010; Murphy and Elis, 2014; Omondi, et al., 2014). Furthermore, information of any changes at small spatial scales is important for water resources management particularly for urban catchments where even small changes in rainfall intensity or duration of storms may result in floods due to the high proportion of imperviousness (Jacobson, 2011). Different approaches to change detection are therefore needed particularly, in the equatorial region where rainfall is highly

variable and with multi-temporal cycles (Omondi et al., 2012; Gitau, et al., 2014). In this study in order to improve the understanding of the temporal and spatial variability of temperature and rainfall respectively, various methods of variability and change detection were employed which include parametric and non-parametric statistical methods, and the wavelet transform spectral analysis method. A wavelet transform is an approach being applied in change detection to overcome some of the challenges of conventional parametric and non-parametric methods that are particularly sensitive to temporal cycles. The wavelet analysis method extracts the relevant information from a time series by transforming it from one variable (time) function to a two variables (time and scale) function. Several studies have used wavelet spectral based analysis on climatic and hydrologic data (Nakken, 1999; Prokoph and Patterson, 2004; Adamowski, et al., 2013; Adamowski, et al., 2013) and have found this method to be valuable in investigating variability and changes in time series that have inter-annual, inter-decadal and other temporal cycles which would impede the detection of trends. In my Thesis, the wavelet analysis was particularly used as a diagnostic tool to assess variability before change detection analysis was done. The use of wavelet spectral analysis, together with other conventional methods of trend detection in meteorological data provides stronger evidence of change and helps understand the nature of the underlying factors causing such changes.

Significant changes in rainfall characteristics in urban areas may influence magnitude and severity of flooding (Biggs and Atkinson, 2011). In most urban areas, the design of the drainage systems has been based on historical rainfall intensities. Changes in rainfall characteristics such as increasing daily intensity may result in the drainage systems being ineffective in controlling flooding (Milly, et al., 2008; Efstratiadis, et al., 2013). Mailhot and Duchesne, (2009) suggested that assumptions made during the statistical analysis of design

storms for urban stormwater systems should be regularly revised to integrate the changes in rainfall that may be brought about by climate change and other anthropogenic changes, such as urbanization. The starting point in the estimation of design storms is the extreme value analysis (EVA) of the rainfall time series (Liu et al., 2013). The extreme value theorem forms the basis for EVA (Coles, 2001) which uses the assumptions that a series of the extreme values (e.g., annual daily maximum values) is suitably long, the elements of the series are independent and identically distributed and that the series is stationary. However, there is evidence that the hydro-meteorological elements such as rainfall can be non-stationary either due to natural climatic variability and/ or climate change (Milly et al., 2008; Cannon, 2010). The EVA has therefore been extended to include non-stationarity (Beguería et al., 2011; Gilleland et al., 2006; Gilleland et al., 2013). Studies that have examined the suitable extreme value models that are applicable to storm water modelling systems in Kenya are lacking. To reduce this knowledge gap, my Thesis examined the suitability of the stationary against several non-stationary models that can be used to produce design storms in Kenyan towns.

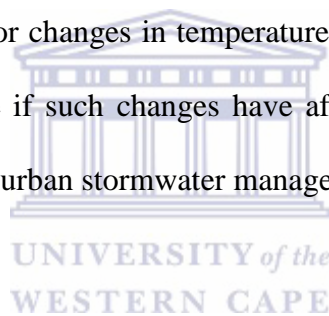
## **1.5 Research questions and objectives**

This study was motivated by the need to improve the understanding of the variations of temperature and rainfall at spatial scales relevant to urban storm water management, and would form a basis for further urban hydro-climatological studies. This knowledge is lacking in most of the climate studies carried out in Kenya. Hence, the study endeavored to answer the following questions:

1. Are there significant changes over time in temperature and rainfall characteristics in the urban and neighbouring rural areas of Kenya?

2. Do urban heat islands (UHI) exist in urban areas of Kenya, and if they do what are the characteristics of their intensities?
3. Do changing urban and rural (maximum and minimum) temperatures influence rainfall characteristics within and around the urban areas?
4. If temperatures have changed and also affected rainfall, is the assumption of a stationary extreme value distribution of maximum rainfall series valid in the estimation of design storms for urban stormwater management systems in Kenyan towns?

The main aim of this study was, therefore, to improve the knowledge of the current understanding of variability and/or changes in temperature and rainfall characteristics in and around urban areas and examine if such changes have affected the stationarity of extreme value distribution that may affect urban stormwater management in Kenyan towns.



To address the research questions and achieve the main aim of this study, specific objectives were addressed in Chapters 2 to 6 of the thesis and a summary of the findings given in chapter 7; the objectives are:

1. To establish if there have been changes over time in temperature and rainfall characteristics within and in the neighborhood of the major urban areas of Kenya. (Chapters 2&3),
2. To determine whether urban heat islands exist in the rapidly expanding towns within an equatorial climatic region (Chapter 4),
3. To examine if changes in surface air temperature influence rainfall in the urban areas (Chapter 5)

4. To establish if the assumption of stationary extreme value distribution model is suitable for describing rainfall events used for estimating storm designs in view of the possible effects of urban heat island and global climate change.

## **1.6 Significance of the study**

Even as more evidence is gathered about climate change (Stocker, 2013), there is still limited information in the EEA about possible changes over time of the maximum and minimum temperature and rainfall characteristics at small spatial scales needed in storm water management and especially within urban areas. Various studies of trends of extreme values over the African region indicate increasing trends in temperature but mixed trends in the rainfall characteristics (New, et al., 2006; Omondi et al., 2014). These studies were carried out over large areas (covering a number of countries) and used a limited number of stations in each country. For storm water management, a rigorous analysis of data from a denser network of meteorological stations is needed (Sonali and Kumar, 2013). Changes in temperatures and rainfall patterns in many parts of the world have been reported to result in increased frequency and intensity of weather-related hazards such as floods particularly in the urban areas (Skansi, et al., 2013). Enhancement of temperature through the urban heat island (UHI) and global warming have also been suggested to have possible enhancement of convective activities (Shepherd, 2005; Shepherd 2006). Although the UHI is a well-studied phenomenon in many parts of the world (Peng, et al., 2011; Vardoulaski, et al., 2013; Ahmed, et al., 2014), its existence and/or influence on hydro-climatic processes of urban areas of equatorial African region have not yet been fully investigated.

As the atmosphere in urban areas becomes warmer due to climate change and possible UHI effect, and alters the hydrological cycle, changes in the amount, timing, form and intensity of

rainfall are likely to be witnessed (Opija, et al., 2007; Marengo, et al., 2013). These changes are likely to affect the systems designed to protect the quantity of storm water and hence affect public health and safety. Frequent news that makes headline locally and internationally about the serious damage of property and even loss of lives especially during seasonal rains in Kenya provides evidence of how vulnerable a country could be to water-related extreme events. For instance, there have been scores of injuries and even deaths reported in Nairobi and Mombasa urban areas and damages to houses and roads in the recent past following heavy rainfall (e.g., April 2012, November, 2015 and April-May, 2016) (Fig 1.1). Such water related incidences are usually loosely attributed to climate change. There is however, not enough scientific evidence to support the claims of climate change or even changes in rainfall variability. These reports are pointers to the vulnerability of the urban environment to changes in rainfall characteristics and or poor urban stormwater infrastructure. Therefore, proper scientific documentation of rainfall variability and possible changes in urban areas is a starting point to improving urban flooding. Again, the design storms used in the engineering of storm water drainage systems have been based on the assumption that rainfall characteristics are stationary in time. The validity of this assumption is now questionable in view of climate change and urban heat island effect (Milly, et al., 2008). The revision of many aspects of stormwater management procedures such as the design storm models can only be carried out if local environmental and climatic conditions are understood. Kenya in particular lacks studies on extreme value distribution that may be used in the development of urban stormwater design manuals for its towns. Hence, there is the need to explore and establish if the stationary statistical distributions of the extreme values that may be used to prepare design storms for the development of stormwater management systems in the urban areas of Kenya are still valid. By incorporating the changes needed in the development of the



design storms in urban infrastructure, other non-climatic factors influencing urban flooding may be effectively established.



Figure 1.1: A photograph of a flooded road in the city of Nairobi during the long rains of March to May 2016 (source: <https://www.kenyans.co.ke/news>).

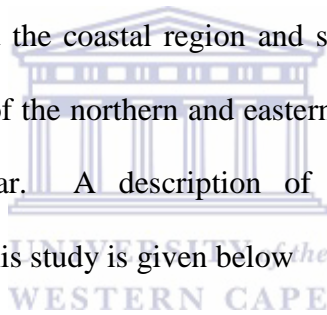
## 1.7 The study area

Kenya lies on the equator between about 5°N, 5°S, and 34°E, 42°E (Fig 1.2). From the coast of the Indian Ocean, the low plains rise to the central highlands. The highlands are bisected by the Great Rift Valley. Kenya has a population of about 40 million people (KNBS 2010) and covers an area of 581,309 square kilometres. Climatologically, Kenya lies within the tropical equatorial climate which is greatly modified by altitude and influenced by the monsoon wind systems. The climate of Kenya may be broadly classified into four categories based on the winds and the averaged weather characteristics including:

- the north-easterly monsoon season from December to February (DJF) characterized by windy, sunny and warm conditions with generally clear skies, especially in December and January. The prevailing winds during this season are northeast monsoon winds

- the long rain season from March to May (MAM). The prevailing winds are North-easterlies (NE) becoming South-easterlies (SE) later in the season. The season is characterized by heavy stormy rains with increasing cloudiness towards the end of May
- Southeast monsoon from June to September (JJAS) characterized by prevailing SE winds and generally cloudy with overcast days. Low temperatures are experienced with occasional drizzles during this period and;
- the short rain season between October to December (OND), characterized by light SE winds changing NE towards the end of the season.

However, the varied topography makes the climates within these seasons to vary with wetter conditions over the highland and the coastal region and semi-arid and arid conditions over parts of the rift valley and most of the northern and eastern Kenya. The mean annual rainfall in Kenya is about 630mm/year. A description of the locations and demographic characteristics of towns used in this study is given below



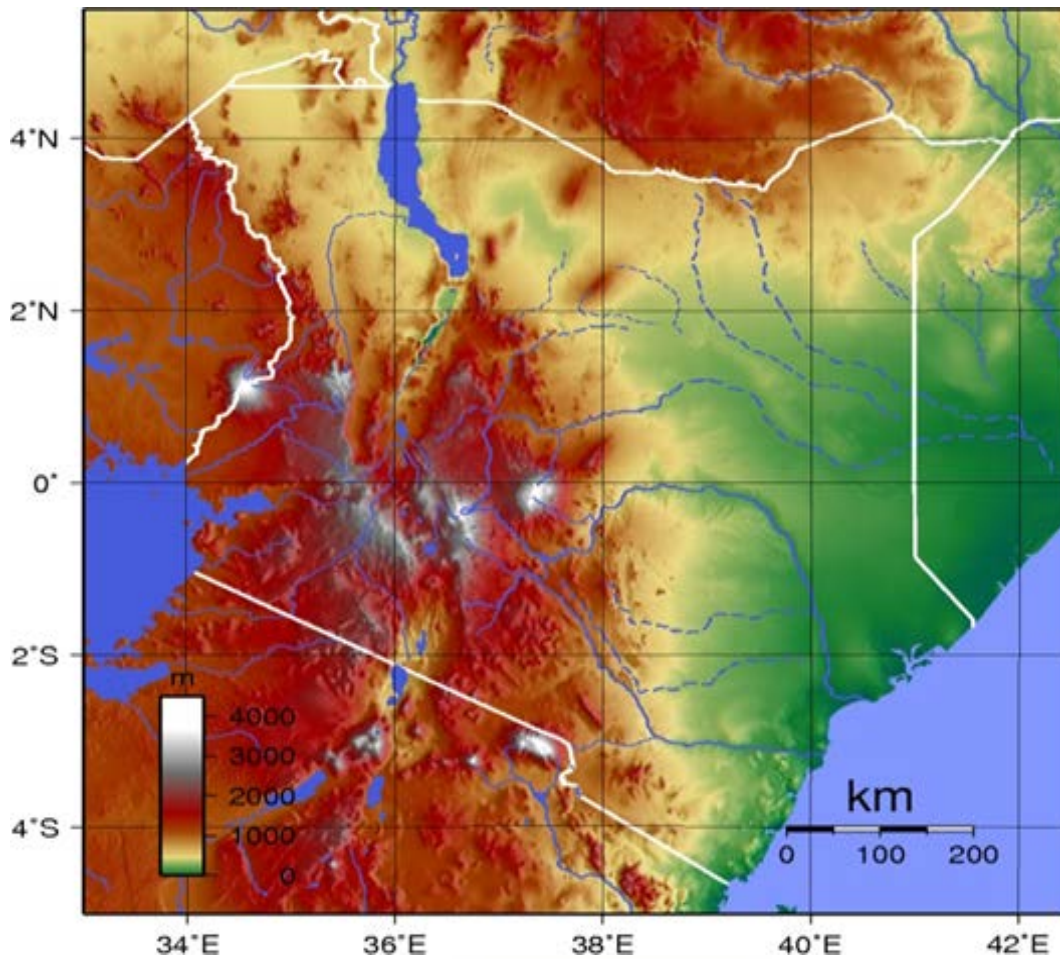


Figure 1.2: The relief map of Kenya (Source: [www.map.library.com/](http://www.map.library.com/))

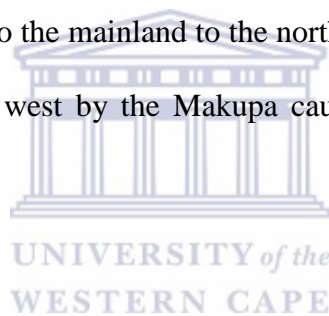
### 1.7.1 Nairobi city

The Nairobi urban area extends between 36° 4' and 37° 10' east and approximately between 1° 9' and 1° 28' south, covering an area of 689km<sup>2</sup> (Fig 1.3). The average altitude is approximately 1700m above sea level. The population of Nairobi has increased almost tenfold in the last five decades mainly due to rural-urban migration and natural population growth. In the early 1960's Nairobi had a population of about 350,000 and by 2009 more than 3.1 million people live within the city (Table 1.1). The main central business district (CBD) contains the commercial buildings, government and state premises, and the industrial area. The population densities vary widely within the city. High-income locations have average

densities as low as 500 people/km<sup>2</sup> while low-income locations such as those in the slums have densities as high as 63 000 people/km<sup>2</sup> (UN Habitat Report, 2008).

### **1.7.2 Mombasa city**

Mombasa is located about 3° 8', 4° 10' south of the equator and 39° 6', 39° 8' east of the Greenwich (Fig 1.3). It has a total landmass of 230 km<sup>2</sup> and 65 km<sup>2</sup> of in-show waters. The city has two parts referred to in this study as the Mombasa Island and the mainland towns. The city has a population of about 1.0 million people (Table 1.1) and is located mainly on Mombasa Island and sprawls to the surrounding mainland to the west, north and south of the island. The Island is separated from the mainland by two creeks; Tudor creek and Kilindini harbour. The Island is connected to the mainland to the north by the Nyali Bridge, to the south by the Likoni Ferry, and to the west by the Makupa causeway, alongside which runs the Kenya-Uganda railway.



### **1.7.3 Kisumu town**

Kisumu town, lies about 0°00' and 0°13'S and 34°35' and 35° East. It lies between Lake Victoria to the west and the Nyando escarpment to the north at a mean altitude of 1160 mamsl. It covers an area of 417 square kilometres (Fig 1.3). The town has a population of over 0.4 million people as of the 2009 Kenya National census (KNBS, 2010). The climate is sub-humid tropical with a high mean temperature of about 28°C and mean annual rainfall varying between 1100mm/ year in the south to 1500mm/year in the north (Indeje, et al., 2000).

#### 1.7.4 Nakuru town

Nakuru town lies in the central Rift Valley between the latitude 0°15' and 0°31'South and longitude 36°35' and 36°12 'East with an average altitude of 1860 mamsl (Fig 1.3). It covers an area of 290 km<sup>2</sup> which includes the area covered by Lake Nakuru. The urban growth pattern of this town is such that it is characterized by intense urban pressure along the main highways and then sprawls into sub-urban areas. The current population is about 310,000 people (KNBS, 2010).

**Table 1.1:Kenya’s major towns and their population (Kenya National Bureau of Statistics (KNBS) 2010)**

City/ Town	Location	Size in km <sup>2</sup>	Population
Nairobi	1°S,36°E	689	3,138,369
Mombasa	3°S,39°E	230	1,200,000
Kisumu	0°S,34°E	417	409,928
Nakuru	0°S,36°E	290	307,990

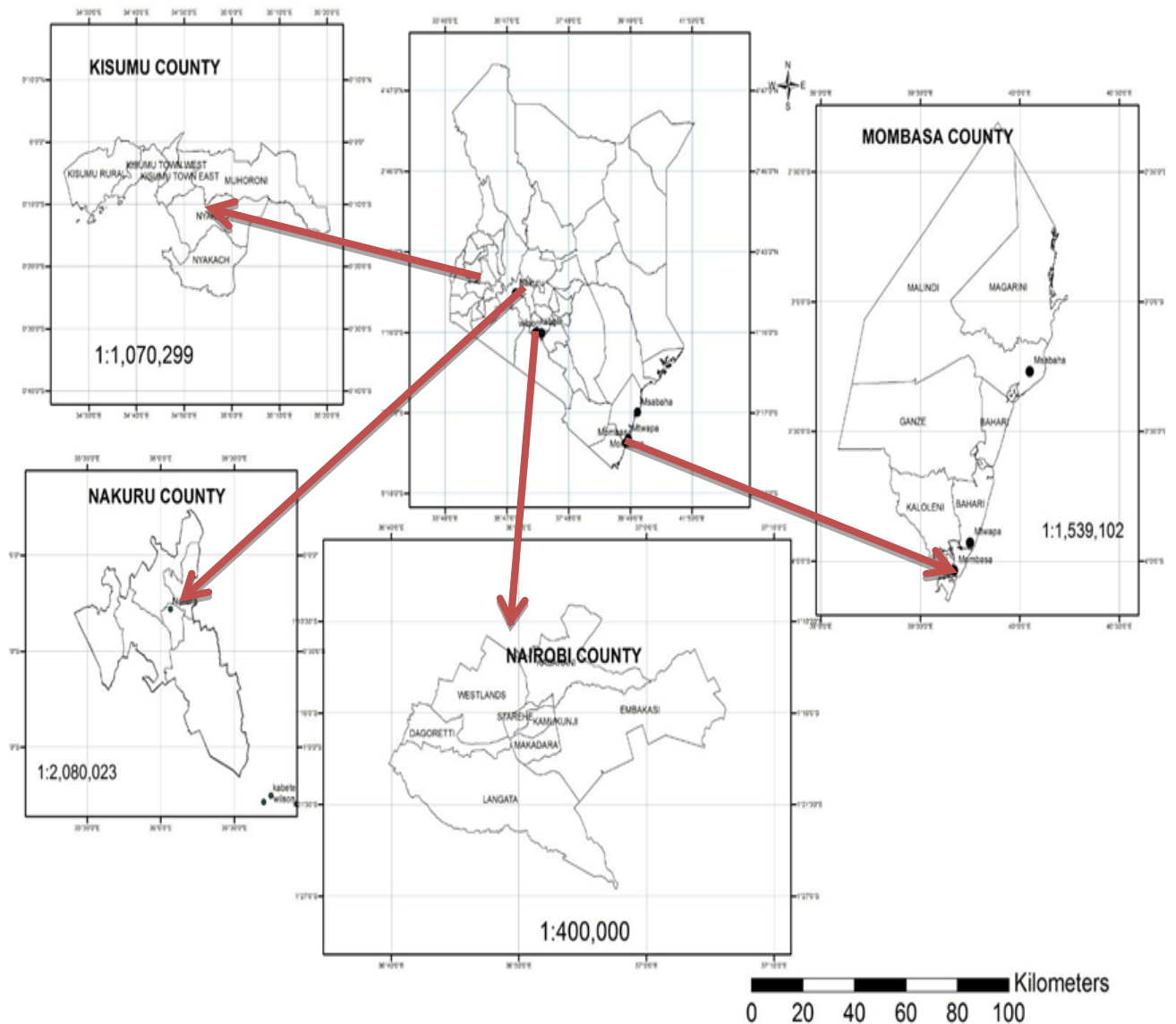


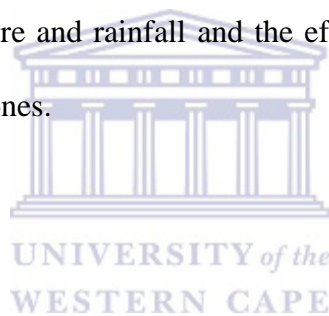
**Figure 1.3: Location of counties and the major towns**

### 1.7.5 Justification of the choice of study area

Kenya is among the countries in the equatorial African region where there is limited literature on the variability of temperature, rainfall and UHI effect especially in relation to water resources management. Kenya has experienced rapid urbanization during the last five decades and the existence of UHIs and their possible effect on rainfall characteristics have not been fully investigated. Rainfall in Kenya exhibits high variability over time and space (Opija, et al., 2007) which is a challenge for effective stormwater management and hence any



changes brought about by urbanization and/or climate change would further affect the management of storm water. Kenya has a fairly dense network of meteorological stations with relatively long time data series (more than 30 years) that have less than 10% of missing values compared to other countries in this region (Omondi, et al., 2012; Omondi et al., 2014), which makes it comparatively ideal for my study. Other records such demographic and urban development data that may be needed to investigate factors influencing the formation of urban heat islands are also available. The major cities and towns in Kenya are distributed in different climatic zones (e.g., Nairobi in the central highlands east of the Rift Valley, Nakuru within the Rift Valley, Kisumu in the Lake Victoria region west of the Rift Valley and Mombasa a coastal town bordering the Indian Ocean) which enabled an assessment of the temporal variability of temperature and rainfall and the effects of the UHI (where possible) on rainfall in different climatic zones.



## 1.8 Thesis outline

This thesis is formulated in such a way that it follows the 'Chapter Format'. In this format a general discussion of the research problem, statement of the objectives and description of the study area are given in Chapter one (1). Subsequent Chapters answer the specific research questions. Each Chapter has a background and literature review relevant to it, description of data and methods of data analysis and, results, their discussion, and summary. However, where methods of data analysis are common to Chapters, they are not repeated in subsequent Chapters. The motivation of using this format is that each chapter is covering an independent objective which is linked to the overall aim, and is envisioned to be a publication after the Thesis is completed. The Thesis is organized into seven (7) chapters as follows:

- **Chapter 1** has provided the background information of temporal variability and changes of temperature and rainfall from global, regional and local scales, the urban heat islands and

their influence on local microclimates. The main and specific objectives were stated. Various methods used for analysis of variability and change detection, and extreme value distribution were highlighted. The study area was described together with its suitability for this study. The significance of the study particularly with respect to management of storm water in urban areas of the equatorial East African region was highlighted.

- In **Chapter 2**, temperature characteristics of urban and neighbouring rural areas of four towns in Kenya were investigated. This chapter starts by presenting the relevant literature review of temporal and spatial characteristics of temperature at global, regional and local scales. Description of data used and the various methods of change detection and trend tests are described. Particularly, the spectral-based method using continuous wavelet transform is discussed in detail as a diagnostic method that has become valuable in detecting multi-temporal cycles that act to influence variability in meteorological variables. The results are presented and discussed, and findings from this Chapter summarized.
- In **Chapter 3** rainfall variability and change were investigated. A literature review regarding rainfall variability and change in EEA is given. Various variables obtained from the daily and monthly rainfall time series are described and some of the methods used for analysis that were not already discussed in Chapter 2 are highlighted and discussed. The results are presented and discussed and a summary drawn for this Chapter.
- **Chapter 4** presents the investigations of the possible existence of urban heat islands (UHI) in Nairobi and Mombasa, which are the two major towns of Kenya by population size and spatial extent and had an adequate number of stations with air temperature of data. Literature of UHI formations and factors that influence their development from cities of different regions of the world is reviewed. Data required for UHI analysis and various methods used to determine the existence and the intensity of UHI are discussed together with methods for testing for statistical significance of the rural-urban temperature



differences. Trend analysis methods are referred to from Chapter 2. The results from this Chapter are presented, discussed and summarized.

- **Chapter 5** links the results of Chapters 2-4 and addresses the effects of enhanced temperature within and close to urban areas due to global warming and/or UHI effects on urban rainfall characteristics. The literature on the effect of urbanization on precipitation patterns in some cities in the world was reviewed. Various methods used to determine relationships between precipitation and temperature were discussed. Results for this Chapter are presented, discussed and summarized.
- In **Chapter 6**, the extreme value analyses under stationarity and non-stationarity conditions of annual daily maximum rainfall series are done. An introduction and literature review of the extreme value analysis is discussed. The theory of the generalized extreme value (GEV) distribution under stationarity and non-stationarity condition, together with the theories of estimating the model parameters, choice of models, and the statistical tests required are discussed. The rainfall and other climate covariates data series required for GEV analysis were described. The results are presented, discussed and summarized.
- **Chapter 7** summarizes the results from all the analyses done from chapter 2 to 6 and highlights the major findings and conclusions. The implications of these findings, limitations and challenges are highlighted and finally, recommendations and suggestions for future work are highlighted.

## 2 CHAPTER 2: TEMPORAL VARIATIONS OF TEMPERATURE

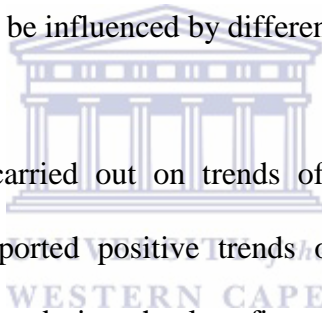
### 2.1 Introduction

The aim of this Chapter is to investigate variability and possible changes over time of maximum and minimum air temperature of urban and nearby rural areas. The results from this Chapter will form a basis for the investigations of the influence of temperature and the urban heat island (UHI) (Chapter 4) on urban rainfall. This Chapter starts by a review of the literature on the spatial and temporal variations and changes of temperature from the global, regional and local perspectives.

The radiation budget of the earth is a fundamental element of the climate system. The earth is considered to be in radiative imbalance with more energy from the sun entering than exiting at the top of the atmosphere since about 1970 (Stocker, 2013). This has resulted in positive radiative forcing (RF); a phenomenon used to describe the net change in the energy balance of the earth's system in response to some external influence. Positive RF leads to a warming while a negative RF would lead to a cooling of the climate system. The spatial and temporal energy imbalance due to radiation and latent heat flux between low and high latitudes produce the general circulation of the atmosphere and oceans. The general circulation transports heat from warm to cold regions and acts to reduce the spatial imbalance in the available energy. Anthropogenic influence on the climate system occurs mainly through perturbations of the components of the earth's radiation budget such as through increase of concentrations of greenhouse gases and aerosols into the atmosphere, thus increasing the atmospheric greenhouse effect. Land surface changes, such as deforestation and urbanization may have impacts on local and regional climate change through processes that are not always directly radiative in nature but have the potential to influence temperature changes. According to the IPCC (Stocker, 2013), human activities have caused more than

half of the observed global increase in average surface temperature from 1951-2010.

Air temperature has been used globally as an indicator of the state of climate mainly due to its ability to represent the energy exchanges over the earth's surface with reasonable accuracy (Jhajharia and Singh 2011; Zhang, et al., 2011). According to Braganza et al. (2004), changes in the mean temperature indicate climate variability and Jhajharia and Singh (2011) indicated that the diurnal range of temperature may be used as an index for climate change since recent surface warming has been attributed more to increase in global minimum temperatures rather than the maximum. Further, Christy, et al. (2009) indicated that the maximum and minimum temperatures should be treated as separate datasets in climate studies since they seem to be influenced by different factors.



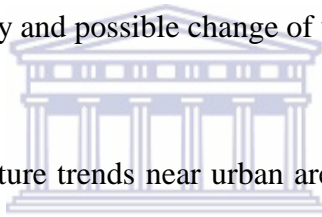
There are a number of studies carried out on trends of temperature over the African continent and most of them reported positive trends of the minimum more than the maximum temperatures especially during the last five decades (King'uyu, et al., 2000; Kruger and Shongwe, 2004; Christy, et al., 2009; Collins, 2011; Nicholson, et al., 2013). Other regional studies of temperature extremes have also reported increasing trends in the minimum temperature indices. For example, Jury and Funk (2013) over Ethiopia, Funk, et al. (2012) over Senegal, Nsubuga, (2011) over Uganda, and Anguilar et al. (2009) over equatorial western and central Africa have reported increasing trends in the minimum temperature. Over the EA region, King'uyu, et al. (2000) further reported that the coastal and the Lake Victoria region showed night-time cooling during the (1939-1992) period. This cooling was attributed to thermally induced mesoscale circulations which act to modify patterns of the large-scale circulations and thus modulate temperature.

In general air temperature in the East African region is controlled by complex maritime (from the adjacent Indian and Atlantic Oceans and inland water bodies) and terrestrial interactions that produce a variety of climates (Indeje, et al., 2000; Christy, et al., 2009). The variability of temperature in space and time poses a challenge in understanding the response of local changes caused by rapid urbanization and environmental degradation to the global warming. Kenya has diverse climatological zones owing to its heterogeneous relief (Fig 1.2). Localized circulations of thermal and orographic origins greatly influence the climatic patterns and hence, there exist spatial differences of temperature variability even over short distances (Christy, et al 2009). Githui (2008) indicated that the western side of the Rift Valley in Kenya had increasing temperatures with higher rates of increase over the lowlands than the highlands. Omumbo et al. (2011) reported evidence of warming trends of the maximum ( $T_{max}$ ), minimum ( $T_{min}$ ) and mean temperature over western Kenya highland region using meteorological data for Kericho station for the 1979-2009 period. However, the variations of temperature on small spatial scales that may exist between the urban and neighbouring rural areas within the same climatic zones are still under-investigated. Moreover, wavelet aided studies of temperature variability and trend analysis are lacking although such information is important for change detection of temperature over time in a region where climate variability is high and fast urbanization has taken place over the last five decades.

## **2.2 Data types and sources**

The variability and/or changes of the  $T_{max}$  and  $T_{min}$  for areas within urban and neighbouring rural areas were investigated. The various time scales used to analyse trends include daily temperature extremes indices, the monthly, seasonal and annual means of  $T_{max}$  and  $T_{min}$ . The rationale of using these time scales is that the analyses of temperature forms the basis of which the influence of changes of urban temperature on rainfall was investigated (Chapter

5) and each of the time scales is important since rainfall in Kenya is seasonal. Mean daily and monthly  $T_{\max}$  and  $T_{\min}$  time series for urban, sub-urban and rural stations around the four main towns of Kenya (Nairobi, Mombasa, Kisumu and Nakuru) were collected from Kenya Meteorological Department (KMD). I used the location of stations' closeness to central business district CBD of each town and the availability of continuous data for at least thirty years as criteria an urban station (Kruger and Shongwe, 2004). Neighbouring rural stations were those that are in the same climatic zone with the urban station and are in relatively less built up area or in complete rural environments (Steward and Oke, 2012); the choice of rural stations also depended on the availability of continuous daily and/or monthly data for at least thirty years. Ten stations (Table 2.1) that met the above criteria were selected for the comparative analyses of variability and possible change of urban and rural temperature.



Studies have shown that temperature trends near urban areas are being influenced by global warming as well as urbanization effects (Kruger and Shongwe, 2004), however, no studies in EEA have tried to separate the effects of urbanization and global warming in temperature studies. I sought to statistically examine the influence of global warming on the variability and change of the urban and rural temperatures using the global monthly mean temperature anomaly indices (designated here as GT). GT data were obtained from the National Oceanic and Atmospheric Administration (NOAA) database (<http://www.ncdc.noaa.gov/monitoring>); the data was obtained as monthly mean values of the standardized anomalies of land and ocean surface temperatures from the National Climate Data Centre (NCDC). The global temperature anomalies describe climate variability over large areas and have the advantage over absolute temperature since they offer a frame of reference that allows assessments between locations (Smith et al., 2008). The gradual rise in the average global temperature has

been used as an indicator of global warming which represents one aspect of climate change and has been used in climate studies as a proxy for global warming (Stocker, 2013).

While a sufficiently long-term (at least 30 years) data series from a dense network of stations is ideal for trend analysis of climate data, the acquisition of continuous daily (and or monthly) temperature data from Kenya Meteorological Department (KMD) is a constraint due to lack of completeness of data for many weather stations (i.e., most stations have data with long periods of missing values). Network of stations that are spatially close and have sufficient longtime series are also sparse (King'uyu et al., 1999; Christy et al., 2009; Omumbo, et al., 2011). However, for the purposes of this study, the ten stations that had temperature data for the last three decades (1980-2013) were sufficient to examine temperature changes when rapid urbanization has been taking place over the study areas (Makokha and Shisanya, 2010; Muthoka and Ndegwa, 2015), and also give an indication of the state of regional warming of different climatic zones of Kenya both within urban areas and in the rural neighbourhoods.

### **2.2.1 Infilling of missing data**

Climatological records often contain errors, missing values, and other inconsistencies that should be checked before analysis. I estimated the missing monthly values using regression methods. The station with the highest correlation coefficient ( $> 0.5$ ) with the station with missing value (s) was used to develop a linear regression equation between the observations at the station with a missing value(s) and the observations of the station it is highly correlated with (King'uyu et al., 2000). The missing value was then estimated. For the daily data, only years with complete daily data were analysed since estimating daily values would cause accuracy challenges.

### 2.3 Description of urban and rural stations

Table 2.1 gives the description and Figure 2.2 shows locations of urban and rural stations for each of the four urban areas. The areas represented are as follows:

a) Nairobi urban area, which is in the central highlands of Kenya east of the Rift valley, and the largest city by population and spatial extent was represented by; i) Wilson airport (NU) as the urban station which is within a moderately high density built up area (Makokha and Shisanya 2010); it is 4 km south of the Nairobi CBD and 2 km southwest of main industrial area; ii) Dagoretti Corner (NR<sub>D</sub>) a station which is 8 km to the west of the CBD and 10 km from the main industrial area; it is in a less populated area compared to NU as it is located on the outer fringes of the city and bordered by a natural (Ngong) forest to the north and west and thus was considered rural with respect to NU; iii) Kabete (NR<sub>K</sub>) station is 20 km northwest of the CBD and is used as a rural station relative to NU and; iv) Thika (NR<sub>T</sub>) station is in a rural area within the central highlands, 50 km north-east of Nairobi CBD, and outside Nairobi urban area. The four stations are used in this Chapter to investigate the variability and trends of temperature within and close to Nairobi city.

b) Mombasa is the second largest town in Kenya, and was represented in this study by; i) Mombasa airport station (MU) representing the urban station located 10 km to the northwest of Mombasa Island; it was the only station within Mombasa town that had temperature data. This station was used to study the effect of urbanization on wind speed and direction in Ongoma et al. (2013); ii) Mtwapa (MR<sub>Mt</sub>) station which is 16 km northeast of from MU and situated in a rural area north of Mtwapa town and; iii) Msabaha (MR<sub>Ms</sub>) station which is about 90 km northeast of MU and a station in a coastal rural area.

- c) Over the highlands west of the Rift Valley and Lake Victoria region there is Kisumu urban area, represented by; i) Kisumu (**KU**) urban station and; ii) Kisii (**KR**) station representing a rural station about a 150 km southeast of Kisumu town (note: there were no other stations close to Kisumu town that had complete data for at least thirty years).
- d) Nakuru urban area was only presented by Nakuru station (**NKU**) due to lack of other stations within the Rift valley and close to Nakuru with complete data which is sufficiently long for long-term analysis.

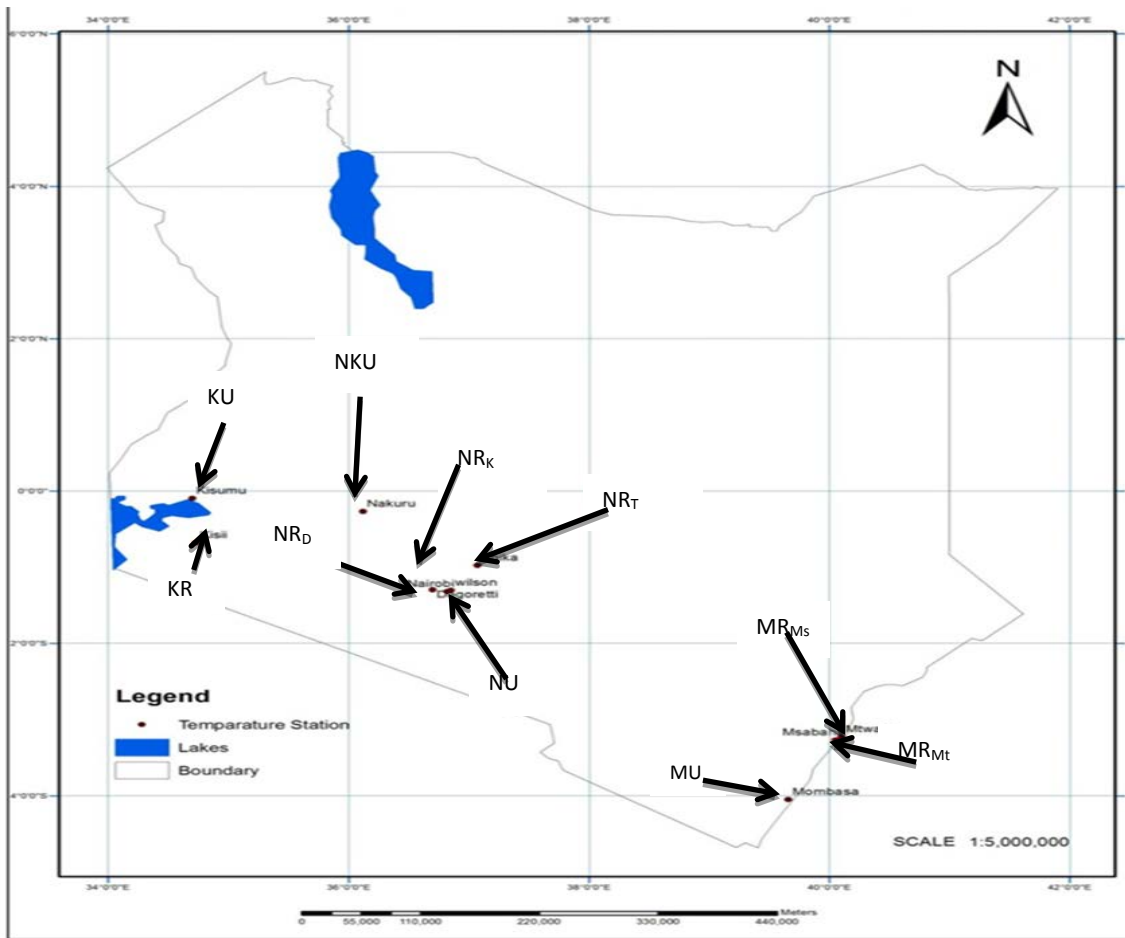
The acronyms and designations of these stations remain the same throughout my Thesis.

**Table 2.1: Stations used for analyses of air temperature:**

Meteorological Station Number	Station name	Station acronym	Lat. (°S)	Long. (°E)	Altitude (m)	Temperature data period	Type of data
9136130	Wilson	NU-Urban	1.32	36.82	1679	1984-2013	Daily
9136164	Dagoretti	NR <sub>D</sub>	1.30	36.70	1798	1980-2013	Monthly
9136208	Kabete	NR <sub>K</sub>	1.27	36.75	1820	1980-2013	Monthly
9137048	Thika	NR <sub>T</sub>	0.98	37.07	1549	1980-2013	Monthly
9334021	Mombasa	MU-urban	4.03	39.60	55	1980-2013	Daily
9339036	Mtwapa	MR <sub>Mt</sub>	3.93	39.73	20	1980-2013	Monthly
9340007	Msabaha	MR <sub>M<sub>s</sub></sub>	3.27	40.05	91	1974-2013	Monthly
9034025	Kisumu	KU-urban	0.10	34.75	1146	1980-2013	Daily
9034088	Kisii	KR	0.67	34.78	1493	1976-2013	Monthly
9036261	Nakuru	NKU-urban	0.267	36.10	1901	1980-2013	daily

Note: that continuous daily data were only available in a few stations, while the rest of the data was available as monthly means.





UNIVERSITY of the  
WESTERN CAPE

**Figure 2.1: Locations of meteorological stations and their acronyms as used for the analysis of temperature**

## 2.4 Data analysis

The quality controlled temperature data were used to develop variables that were used to investigate possible existences of trends and other temporal cycles. The variables included:

- the monthly mean  $T_{\max}$  and  $T_{\min}$  for each month of the year. The monthly means are normally computed by time averaging the daily  $T_{\max}(T_{\min})$  of a given month, i.e

$$\text{Monthly mean } T_{\max} = \frac{1}{t} \sum_1^t \text{daily } T_{\max} \quad (2.1)$$

where  $t$  is the number of days in a given month; the same is done for the  $T_{\min}$

- b) the seasonal mean  $T_{\max}$  and  $T_{\min}$  for the seasons: i) December, January, and February (DJF); ii) March, April, and May (MAM); iii) June, July and August (JJA) and ; iv) September, October and November (SON); which represent the dry, wet (long rains), cool and wet (short rains ) seasons respectively in the EEA region, are computed by averaging the  $T_{\max}$  ( $T_{\min}$ ) of the three months that make the season; i.e.,

$$\text{Seasonal mean } T_{\max} = \frac{1}{3} \sum_{1}^3 \text{monthly } T_{\max}, \quad (2.2)$$

where monthly  $T_{\max}$  is as computed in Equation (2.1); the same is computed for  $T_{\min}$

- c) the annual mean  $T_{\max}$  and  $T_{\min}$  for each station and each year. Here the  $T_{\max}$  ( $T_{\min}$ ) for all the months are averaged into one variable; thus,

$$\text{Annual mean } T_{\max} = \frac{1}{12} \sum_{1}^{12} \text{monthly } T_{\max} \quad (2.3)$$

- d) Daily temperature indices as specified in Table 2.2. Four stations that adequately represented each urban area, and had adequate length of daily data, were used to compute the temperature indices of extremes. The behaviour of temperature extremes in urban is important in relation to urban rainfall (Shepherd, 2006) and hence their analyses were included. A total of nine indices were obtained from the daily  $T_{\max}$  and  $T_{\min}$  using the ClimDex software; a Microsoft Excel-based program for the calculation of indices of climate extremes for monitoring, and detecting climate change. ClimDex software is run in R language as

RclimDex(<http://cccma.seos.uvic.ca/ETCCDMI/RclimDex/rclimdex.r>) (Zhang and Yang 2004). It has been used in the Commission of Climatology/Climate Variability and Predictability (CCI/CLIVAR) workshops to prepare temperature indices for climate studies.

**Table 2.2:Indices of daily temperature extremes selected**

<b>Index ID</b>	<b>Indicator Name</b>	<b>Indicator definition</b>	<b>units</b>
<b>TXx</b>	Max $T_{\max}$	Monthly max value of daily max temperature	°C
<b>TNx</b>	Max $T_{\min}$	Monthly max value of daily min temperature	°C
<b>TXn</b>	min $T_{\max}$	Monthly min value of daily max temperature	°C
<b>TNn</b>	Min $T_{\min}$	Monthly min value of daily min temperature	°C
<b>TN10p</b>	Cool nights ( $T_{\min}10p$ )	% of time when daily min temperature < 10 <sup>th</sup> percentile	%
<b>TX10p</b>	Cool days ( $T_{\max}10p$ )	% of time when daily max temperature < 10 <sup>th</sup> percentile	%
<b>TN90p</b>	Warm nights ( $T_{\min}90p$ )	% of time when daily min temperature > 90 <sup>th</sup> percentile	%
<b>TX90p</b>	Warm days ( $T_{\max}90p$ )	% of time when daily max temperature > 90 <sup>th</sup> percentile	%
<b>DTR</b>	Diurnal temperature range	Monthly mean difference between daily max and min temperature	°C

Several methods of data analysis were applied to the above variables. The methods included: i) Exploratory data analysis (time series plots, temporal averages and the continuous wavelet transform (CWT)); ii) trend analysis using linear regression and Mann-Kendall (MK) tests and; iii) correlations for testing relationships between temperature and global warming at seasonal and annual time scales. The detailed description of each method of analysis is outlined in the next sub-sections.

### **2.4.1 Continuous wavelet transform (CWT) as an exploratory tool**

CWT was mainly used in this Chapter as a diagnostic tool to explore the variability of monthly temperature time series before trend analysis was carried out. The purpose of CWT as an exploratory data analysis (EDA) tool in time series analysis is to reveal the properties of the underlying processes within the observations so as to get a preliminary indication of the characteristics of the variability of the time series (Labat, 2005).

The wavelet analysis has become an important diagnostic tool for analysing non-stationarity in climatological time series. CWT is based on the convolution of one variable function (in this case temperature)  $T(t)$  into a function of two variables (time and scale). Basically, the wavelet analysis allows for the determination of the frequency (scale) of the time series signal and to assess the temporal variations of the frequency content. The CWT analysis, in particular, improves the determination of the temporal variations by allowing isolation of the dominant multi-scale processes in a time series signal that is characterized by multiple variable processes (Torrence and Compo, 1998) (e.g., high-frequency and low-frequency modes of variability forced by local and global factors respectively). Land use changes due to urbanization and the effects of climate change may be influencing temperature characteristics that may not be differentiated by the use of the conventional trend analysis methods alone. Since CWT analysis allows a time series signal to be localized in both scale (period) and time, the evolution of processes in the signal can be tracked at different scales (Labat 2005; Sen and Ogrin 2015) which can be attributed to local or large-scale forcing ( Prokoph and Patterson 2004).

The fundamental objective of a wavelet transform is to obtain a complete time/scale representation of localized and transient systems occurring at different periods in a time

series. It is considered as a time slided windowed Fourier transform with the advantage of having resolution properties of time and scale (period) domain and has been applied in hydro-meteorological long-term data analysis to search for change signals (Bejranonda and Koch, 2010). In the wavelet analysis unlike classical Fourier transform, the basis function in Fourier transform is replaced by a two parameter basis  $\{\psi_{s, s}(t), (s, s) \in \mathcal{R}^* \times \mathcal{R}\}$ , where  $\psi_{s, s}(t)$  is wavelet function which allows time-scale discrimination of the processes (Labat 2005) (see CWT theory below). The functions of the CWT are derived from the translation and dilation of a ‘mother’ wavelet  $\psi(t)$ . The mother wavelet must be a function centred at zero and in the limits as  $t \rightarrow \infty$ ,  $\psi(t) \rightarrow 0$  and also  $\psi(t)$  must have a mean of zero (known as the admissibility condition) for the invertibility of wavelet transform. The CWT serves as a continuously sweeping ‘microscope’ in examining the spectral components of a dataset (Kumar and Georgiou, 1997; Wang and Lu, 2009). The CWT as an diagnostic tool therefore improves the determination of temporal and spatial variations and permits the detection of multiple scales in a given time that are not apparent using the conventional data exploration methods such as time series plots (Labat, 2005; Sang, et al., 2013; Sen and Ogrin, 2015). I used the CWT method of time series analysis to explore comparatively the temporal and spatial variations of urban and rural  $T_{\max}$  (and  $T_{\min}$ ) time series respectively, and further to help me interpret the nature of the variability and changes that may have occurred in temperature over time.

### ***CWT analysis theory***

The CWT of a temperature  $T(t)$  time series signal is defined as the convolution of the time series with an analysing wavelet function and may be expressed as:

$$\check{T}_{\psi}(s, s) = \int_{-\infty}^{+\infty} T(t) \psi_{s, s}(t) dt \quad (2.4)$$

where  $\tilde{T}_\psi(s, \tau)$  is the transform of the time series  $T(t)$ ;  $T(t)$  is a temperature random variable with values at  $t=1, \dots, n$  taken at equal time intervals  $\partial t$  (e.g. daily, monthly or annually), the functions  $\psi_{s, \tau}(t)$  are the wavelets with scaling parameter  $s$  and translating parameter  $\tau$  and is given by:

$$\psi_{s, \tau}(t) = \frac{1}{\sqrt{s}} \psi\left(\frac{t - \tau}{s}\right), s > 0, \tau \in \mathcal{R} \quad (2.5)$$

where  $\mathcal{R}$  is set all real numbers. The set of analysing wavelets  $\psi_{s, \tau}(t)$  are produced from a single wavelet called the mother wavelet,  $\psi(t)$ , by scaling and shifting it. The shifting parameter  $\tau$  is responsible for time location while  $s$  is the scaling parameter used for stretching ( $s > 1$ ) and compressing ( $s < 1$ ) the mother wavelet. The choice of a sine-like wavelet as the mother wavelet such as the Morlet wavelet, after Morlet (1982), allows the value  $s$  to be approximated as wavelength and the reciprocal value  $\frac{1}{s}$  to be interpreted as frequency. The Morlet wavelet is expressed as:

$$\psi = \pi^{-\frac{1}{4}} \left[ \exp(-i2\pi f_0 t) \left( \exp\left(-\frac{1}{2}(t)^2\right) \right) \right] \quad (2.6)$$

and for the set of shifted wavelets it follows that:

$$\psi_{(s, \tau)} = \pi^{-\frac{1}{4}} \left[ \exp\left(-i2\pi f_0 \left(\frac{t - \tau}{s}\right)\right) \left( \exp\left(-\frac{1}{2}\left(\frac{t - \tau}{s}\right)^2\right) \right) \right] \quad (2.7)$$

where parameter  $f_0$  defines the basic frequency of the mother wavelet and controls the number of oscillations below the Gaussian envelope, and other symbols are as defined in Equation 2.4 and 2.5 (Prokoph and Barthelmes 1996). The Morlet wavelet has both complex

and real parts and therefore offers the advantage that it combines wavelet power both positive and negative peaks into a single broad peak.

***Choice of scales and the cone of influence (COI)***

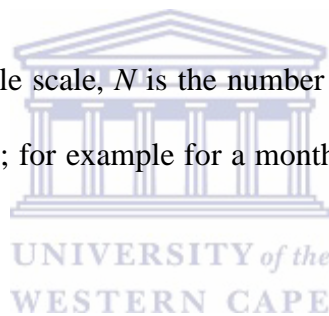
The scaling factor for the Morlet wavelet used in the transformation of the temperature time series was chosen following Torrence and Compo,(1998) as a discrete set of scales that are powers of 2 according to the equation:

$$s_j = s_0 2^{j\Delta_j} \tag{2.8}$$

$j=0,1,\dots,J$  and

$$J = \Delta_j^{-1} \log_2 \left( \frac{N\Delta t}{s_0} \right) \tag{2.9}$$

where  $s_0$  is the smallest resolvable scale,  $N$  is the number of data points,  $\Delta t$  is the time step and  $j$  determines the largest scale; for example for a monthly time series  $\Delta t=1$  month and  $s_0$  is 2 (*i.e.*,  $2 \Delta t$ ).



Dealing with finite length time series introduces errors at the beginning and end in CWT analysis since the classical Fourier transform assumes the data to be cyclic. In wavelet transform of the temperature series, I used the method of padding with zeros before the transformation and then removing them afterwards so as to reduce the edge effects in the CWT wavelet power spectrum plots (Torrence and Compo1998). For example for a time series of thirty (30) years of monthly data,  $N\Delta t= 408$  which is not a power of two. Therefore 104 zeros would be padded at the end of the series to make it 512 ( $2^9$ ). However the padding with zero produces discontinuities at the end points and for larger scales decreases the amplitude near the edges as more zeros enters the analysis. The cone of influence (COI) of a power spectrum defines the region where the effects of padding becomes important and is

defined as the e-folding time of the auto-correlation of the wavelet power at each scale. The e-folding time is chosen so that the wavelet power for a discontinuity at the edges drops by a factor  $e^{-2}$ , and ensures that the edge effect are negligible beyond this point. For the Morlet wavelet function the, e-folding time at each scale is computed as:

$$\tau_e = \sqrt{2}s \quad (2.10)$$

where  $\tau_e$  is the e-folding time and  $s$  is the scale (Torrence and Compo, 1998).

### ***The wavelet power spectrum (WPS)***

The WPS represents the signal energy at a specific scale (period) and time, and for the Morlet wavelet function that is complex, the WPS is also complex. The WPS (also called a scalogram or wavelet periodogram) is defined as the squared modulus of the CWT expressed here as:

$$W_T = |\check{T}\psi(s, t)|^2 \quad (2.11)$$

where  $W_T$  is the WPS of the transformed time series  $\check{T}\psi$ .

The  $W_T$  is then plotted as a contour map where dominant modes of variability (such as inter-seasonal, inter-annual and even inter-decadal) occurring in a time series can be inferred from the cycles (periodicity) realised in a WPS map (Sen and Ogrin, 2015).

### ***Significance testing of dominant frequency features (periodicities)***

To determine the level of significance of the dominant frequency features in a  $W_T$ , an appropriate background spectrum is chosen. I assumed that different attainments of CWT process will be randomly distributed about this mean background and the actual spectrum can be compared against this random distribution. The appropriate background chosen for temperature is the red noise. I chose the red noise background because the temperature data

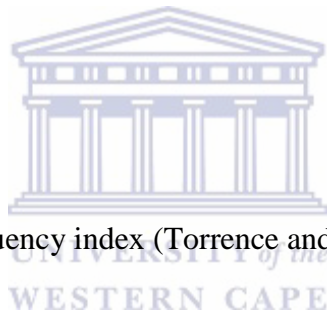


was found to approximate to normal distribution which is a criterion of choosing this background. To construct this background, I first modelled the time series as a lag-1 autocorrelation (AR(1)) process. Thus:

$$T_{AR}(t) = \alpha T_{t-1} + Z_t \quad (2.12)$$

where  $T_{AR}(t)$  is the modelled time series,  $Z_t$  is taken from a Gaussian white noise process (the white noise process assumes that data is random and the variance is evenly distributed among frequencies),  $\alpha$  is the estimated autoregressive coefficient and  $T_0=0$ . Then a local WPS ( $W_t$ ) defined as the vertical slice of the  $W_T$  at a given time, is expressed as:

$$W_t = \frac{1-\alpha^2}{1+\alpha^2-2\alpha\cos(\frac{2\pi k}{N})} \quad (2.13)$$



Where  $k=0,1,\dots,N/2$  is the frequency index (Torrence and Compo, 1998).

To establish the significance of a peak of a local wavelet spectra, I defined a null hypothesis by assuming that the time series has a mean power spectrum given by Equation (2.10) and if a peak in the  $W_T$  is significantly above this background power spectrum, then it is a true feature with a given percentage of confidence (in this case 95%). I used the  $\chi^2$  distribution to test for the significance of the  $W_T$  since it follows a chi-square distribution with two degrees of freedom (Torrence and Compo, 1998). The significant modes are then shown as contours in the wavelet power spectrum (WPS) map.

I performed the wavelet transform of temperature time series using the ‘biwavelet’ software package which uses the Morlet as the mother wavelet. The package is written in R language

by Gouhier and Grinsted, (2015) <http://github.com/tgouhier/biwavelet>), using the wavelet program written by Torrence and Compo (1998) and modified by Valeda et al. (2012).

To aid the interpretation of CWT results, Figure 2.2 illustrates a CWT analysed variable in which several frequency features are observed. In this figure, the wavelet power spectrum (WPS) shows periods in months in the vertical axis against time (years); short periods (high-frequency features) are presented at the top and long periods (low-frequency features) at the bottom of the y-axis. Several significant features are labelled in the diagram; the most dominant being the 4-8 months periodicities which represent the semi-annual cycles and 8-16 months periodicities representing quasi-annual cycles are spread throughout the time axis.

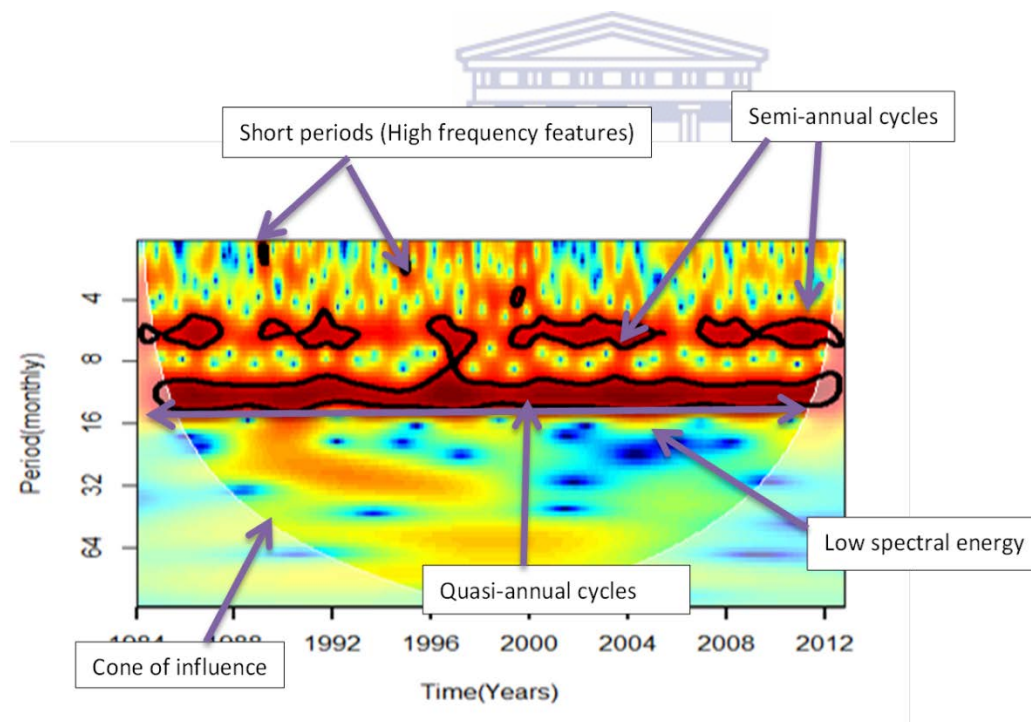


**Figure 2.2: An illustrative diagram(WPS map) of an output of a time series variable analysed using the CWT method (source: Author)**

## 2.4.2 Trend analysis

### *Simple linear regression and correlation methods*

A simple linear regression of a variable  $T$ , on time ( $t$ ) as a test for trend is written as:

$$T = \beta_0 + \beta_1 t + \varepsilon \quad (2.14)$$

where  $T$  is the temporally averaged variable [e.g., maximum ( $T_{\max}$ ) or minimum ( $T_{\min}$ ) temperature]  $t$  is the time in days, months, seasons or years,  $\beta_0$  and  $\beta_1$  are the y-intercept and slope respectively and  $\varepsilon$  is the random error. The null hypothesis for trend analysis is that the slope coefficient  $\beta_1 = 0$ , which means that no trend exists. Regression assumes that the data are normally distributed, and hence the time series was checked for normality before trend analysis was performed. The computation of  $\beta_1$  is as shown in Table 2.2. The t-test is used to test the null hypothesis that  $\beta_1 = 0$ , against the alternative  $\beta_1 \neq 0$ :

$$t = \frac{\beta_1}{\zeta / \sqrt{SS_T}} = \frac{r\sqrt{n-2}}{\sqrt{1-r^2}} \quad (2.15a)$$

where  $t$  represent the t-statistic,  $r$  is the correlation coefficient defined as:

$$r = SS_t / \sqrt{SS_T SS_t} \quad (2.15b)$$

and  $\zeta$  the variance defined as:

$$\zeta = \sqrt{(SS_T - \beta_1 SS_t) / n - 2} \quad (2.15c)$$

The terms in Equation (2.15) are defined in Table 2.3

$H_0$  is rejected if  $|t| > t_{crit}$  (at  $n-2$  degrees of freedom and at significant level  $\alpha= 0.05$ ).

**Table 2.3: Definition of terms and formulas used in computing regression and correlation coefficients;  $\bar{t}$  and  $\bar{T}$  are the arithmetic means of time and temperature respectively**

Name of term	Formula
Sums of squares of $t(SS_t)$	$\sum_{i=1}^n (t_i - \bar{t})^2$
Sums of squares $T(SS_T)$	$\sum_{i=1}^n (T_i - \bar{T})^2$
Sums of cross-product ( $SS_{tT}$ )	$\sum_{i=1}^n (T_i - \bar{T})(t_i - \bar{t})$
Estimate of $\beta_1$	$\beta_1 = \frac{SS_{tT}}{SS_t}$

### ***The Mann-Kendall test***

The Mann-Kendall test (Kendall, 1975) is a non-parametric test that detects the presence of a monotonic trend within a time series in the absence of any seasonal variation or other cycles (Biggs and Atkinson, 2011). This method has the advantages that, it is not affected by gross data errors and outliers, and has been widely used to test randomness against trend in hydrology and climatology.

The Mann-Kendall test can be stated generally as a test for checking whether the temperature random variable  $T(t)$  in a time series increase or decrease with time ( $t$ ). No assumption of normality is required but there must not be serial correlations in the  $T(t)$  data for the p-values

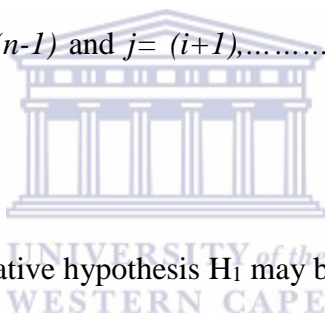
to be correct. The test is monotonic and hence invariant to power transformation (Helsel and Frans, 2006). The Kendall tau ( $\tau$ ) is computed by first ordering all data pairs (T,t) by increasing T. If no trend exist, the  $T$ -values will decrease and increase about an equal number of times. The test statistics is the Kendall  $S$  is computed by subtracting the number of ‘discordant pairs’,  $M$ , ( i.e. the number of (T, t) pairs where  $T$  decreases as t increases) from the number of ‘concordant pairs’  $P$  (i.e. the number of (T, t) pairs where  $T$  increases with increasing t).

$$S=P-M \tag{2.16}$$

Where  $P$ = number of pluses (concordant pairs)  $T_i > T_j$

$M$ = number of minuses discordant pairs  $T_i < T_j$

Where  $t_j > t_i$  for all  $i=1, \dots, (n-1)$  and  $j= (i+1), \dots, n$  and  $n$  is the number of data points.



The null hypothesis  $H_0$  and alternative hypothesis  $H_1$  may be stated as follows:

$$H_0: \text{prob } [T_i > T_j] = 0.5 \text{ where } t_j > t_i$$

$$H_1: \text{prob } [T_i > T_j] \neq 0.5 \tag{2.17}$$

If no trend exists (i.e.  $H_0$  is true), about half of the comparisons would be concordant and half discordant and  $S$  would be close to zero. If  $S$  is significantly different from zero, the data indicate that a trend in  $T$  occurs. Since there are  $\frac{n(n-1)}{2}$  possible comparisons made, among the  $n$  data pairs, then if all values of  $T$  increase along with  $t$  values, then:

$$S= \frac{n(n-1)}{2} = 1 \tag{2.18}$$

and if all values of  $T$  decrease with increase of  $t$ , then:

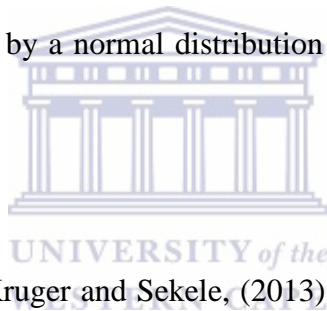
$$S = \left( \frac{n(n-1)}{2} \right) = -1 \quad (2.19)$$

The coefficient  $\tau$  measures the strength of the monotonic association between T and time (t) given by:

$$\tau = \frac{S}{n(n-1)/2} \quad (2.20)$$

where  $-1 \leq \tau \leq 1$

The significance of  $\tau$  is tested by comparing  $S$  to what it would be when  $H_0$  is true. The p-value summarizes the probability of getting the observed value of  $\tau$ , or one more extreme when  $H_0$  is true. When p-value is small ( $< 0.05$ ), the likelihood that there is either a positive (+  $\tau$ ) or negative (- $\tau$ ) trend is high and  $H_0$  is rejected. For larger sample sizes  $S$  is converted to  $Z$ , a statistic that is approximated by a normal distribution as described in Helsel and Frans, (2006).



An important observation from Kruger and Sekele, (2013) is that trend analyses of variables with magnitudes that have cyclic signature depend heavily on the analysis period and that in climate analysis with near decadal cycles, erroneous or exaggerated long-term trends may be inferred by the trend analysis. However, by using monthly and seasonally averaged time series, seasonal and annual cycles are minimized and only long-term (decadal) cycles may influence the trend result. Such cycles have not been established in the temperature of the EEA region.

## 2.5 Results and discussion

### 2.5.1 Spatial and temporal variations of temperature

Climatologically, temperature in Kenya exhibits spatial variability owing to the heterogeneity of the topography, presences of large water bodies as well as geographical location (Fig 1.2). Table 2.4 shows the long-term annual mean  $T_{\max}$  and  $T_{\min}$  for stations in the central highlands east of the Rift Valley (Nairobi), the coastal region (Mombasa), within the Rift valley(Nakuru) and over the highlands west of the Rift Valley (Kisumu). Generally, the stations over the highlands have lower mean temperature than those at the coastal region except Kisumu that has  $T_{\max}$  almost comparable to the coastal region due to its location close to Lake Victoria; Nakuru though higher in elevation than Nairobi has higher mean  $T_{\max}$  and much lower  $T_{\min}$  due to its location within the Rift Valley.

**Table 2.4** Variation of annual mean temperature with altitude

Region	Station	Altitude (mamsl)	$T_{\max}$ (°C)	$T_{\min}$ (°C)
Nairobi (central highlands)	NU	1679	25.1	14.1
	NR <sub>D</sub>	1798	24.0	13.6
	NR <sub>K</sub>	1820	23.3	13.2
	NR <sub>T</sub>	1549	25.7	14.1
Mombasa (coast)	MU	55	30.5	21.8
	MR <sub>Mt</sub>	20	30.0	22.6
	MR <sub>Ms</sub>	91	30.1	22.9
Kisumu (western highlands & Lake Victoria)	KU	1146	29.8	17.3
	KR	1493	25.6	15.4
Nakuru (Rift Valley)	NKU	1901	25.8	11.9

Descriptive statistics of long-term monthly means (Figure 2.3) further indicate that on average  $T_{\max}$  and  $T_{\min}$  over Nairobi are higher in the urban station than their neighbouring rural station while over the coast the urban area is cooler than the neighbouring rural areas. Over the western highlands, Kisumu is warmer than Kisii on average. Note also that: a)

$T_{max}$  over Nairobi is highest in February and  $T_{min}$  is highest in March (Fig 2.3 a&b)); b)  $T_{max}$  over Mombasa is highest in March and  $T_{min}$  in April (Fig 2.3 (c&d)), and; c) that temperature in Kenya has an annual cycle with a long hot season from September to April and a shorter cool season from May to August.

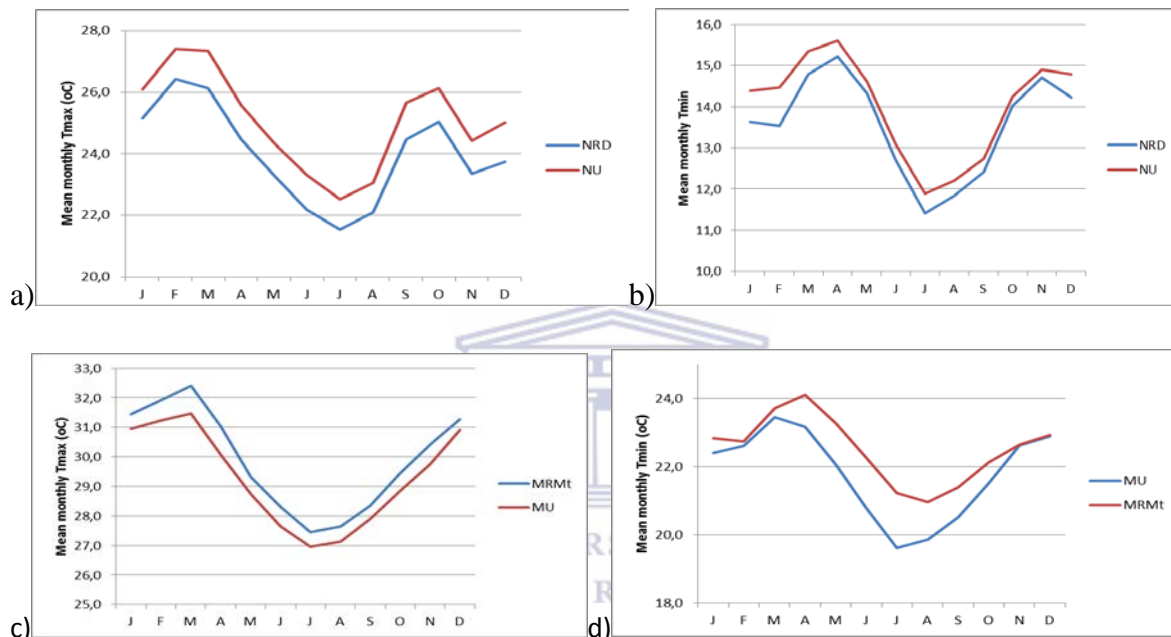


**Figure 2.3: Annual temperature cycle of the mean monthly  $T_{max}$  and  $T_{min}$  for urban and representative nearby rural stations for; a&b)Nairobi ; c&d Mombasa**

A number of factors that could account for the observed differences in long-term mean temperature in urban and neighbouring stations within the same climatic zone include:

- i) differences in elevation and geographical location; for instance KR station is about 300 metres above mean sea level (mamsl) higher than KU which could account for some of the temperature differences due to the lapse rate. NU and  $NR_T$  over Nairobi are lower in elevation than  $NR_D$  and  $NR_K$  and mean temperature differences are also notable and;



- ii) local and environmental factors such as the urban heat island effect due to urbanization, nearness of a station to forested land (cooling effect due to evapotranspiration) and nearness to water bodies (effects of land and sea breezes). The influence of urbanization on the temperature differences was investigated further in Chapter 4.

The temperature differences between seasons of  $T_{max}$  and  $T_{min}$  respectively are small in all stations. For instance, the temperature difference between the warmest (DJF) and coolest (JJA) seasons in a given station is  $<5^{\circ}C$  for both  $T_{max}$  and  $T_{min}$  which is a characteristic of temperatures of the equatorial regions. The lowest seasonal  $T_{min}$  was observed in Nakuru within the Rift Valley (Fig 2.4). The spatial variations of seasonal  $T_{max}$  and  $T_{min}$  are such that the coastal region (Mombasa) and Kisumu near Lake Victoria have mean  $T_{max}$  above  $25^{\circ}C$  in all seasons, while Nairobi, Nakuru, and Kisii have  $T_{max}$  of between  $20$  to  $25^{\circ}C$ . Likewise, the  $T_{min}$  is highest at the coast for all seasons ( $>20$  but  $<25^{\circ}C$ ) while all other stations  $T_{min}$  is between  $10$ , during the cold season, and  $15^{\circ}C$  during the warm season.

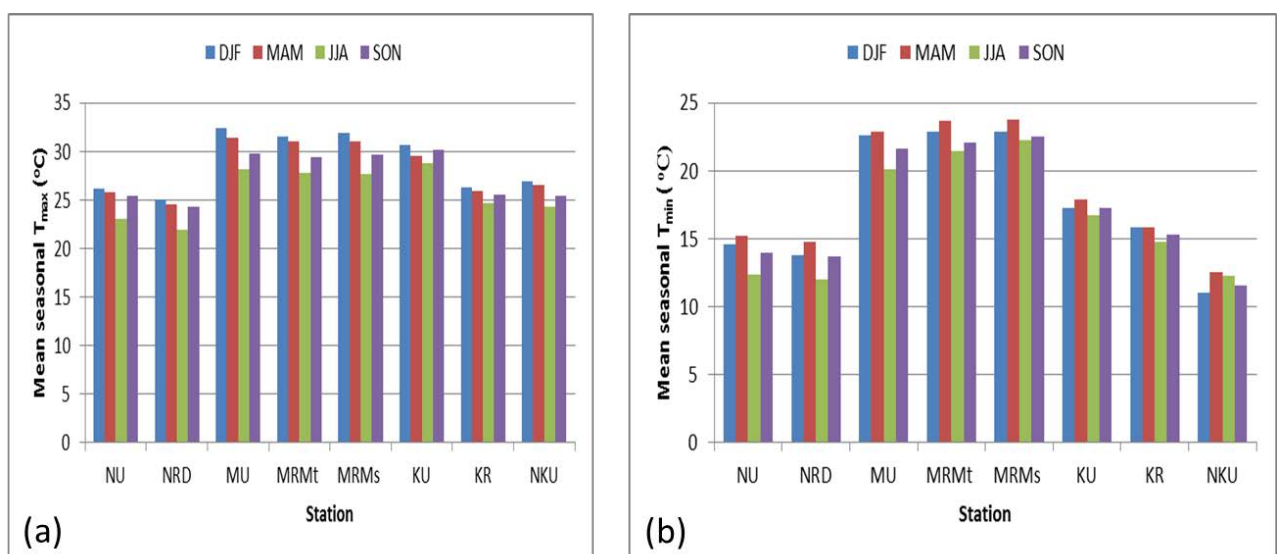


Figure 2.4: Spatial and temporal variations of the mean seasonal temperature for urban and rural stations; a)  $T_{max}$  ; b)  $T_{min}$

### 2.5.2 Continuous wavelet transform (CWT) analysis of temperature

To examine the variability of temperature, the monthly mean  $T_{\max}$  and  $T_{\min}$  time series were subjected to further exploration using time series plots and CWT analysis. In a CWT analysis, the temporal distribution of the frequency features of temperature signal was found by successively passing dilated and compressed functions of a Morlet wavelet according to Equation (2.4). The wavelet coefficients obtained were computed into the wavelet power spectrum (WPS) according to Equation (2.11) and plotted on a WPS contour map. The cone of influence (COI) on each WPS map was computed using Equation (2.10) and indicated on the map while areas of significant dominant frequency components (periodicities), at the 95% level of confidence against a red-noise background were determined (Equations 2.12 and 2.13). The corresponding time series of the monthly temperature were plotted alongside the WPS for each station. In each WPS plot the horizontal axis shows the time dimension (covering the analysis period) while the vertical axis shows the scales (periods in months in powers of 2) starting from high (at the bottom) to low periods (as illustrated in Figure 2.2). The spectral power representing regions of low (high) spectral energy is indicated by the colour code in such a way that the power ranges from blue (low power) to dark red (high power). The high spectral power regions that are circled with the black contour lines indicate the existence of significant periodicities and the region below the white U-shaped curve represent the cone of influence (COI) within which the edge effects become important and the results within this region are interpreted with caution (Torrence and Compo 1998). The results are given for each urban area.

#### *Nairobi area*

The comparative examination of the variability of  $T_{\max}$  (and  $T_{\min}$ ) within an urban station and its neighbouring rural stations from the wavelet power spectrum (WSP) and the corresponding

time series plots for two stations (urban (NU) and rural (NR<sub>D</sub>)) are presented in Figure 2.5. Considering  $T_{max}$ , the WPS plots for two stations are almost similar (Figure 2.5 (a&b)). The expected annual cycle is observed in both stations while semi-annual cycles (periodicities of 4-6 months) that covered groups of years and were more frequent before the year 2000 and became short in duration with long non-significant periods thereafter, are also prominent. The time series plots (Fig 2.5b&c) have no observable trends.

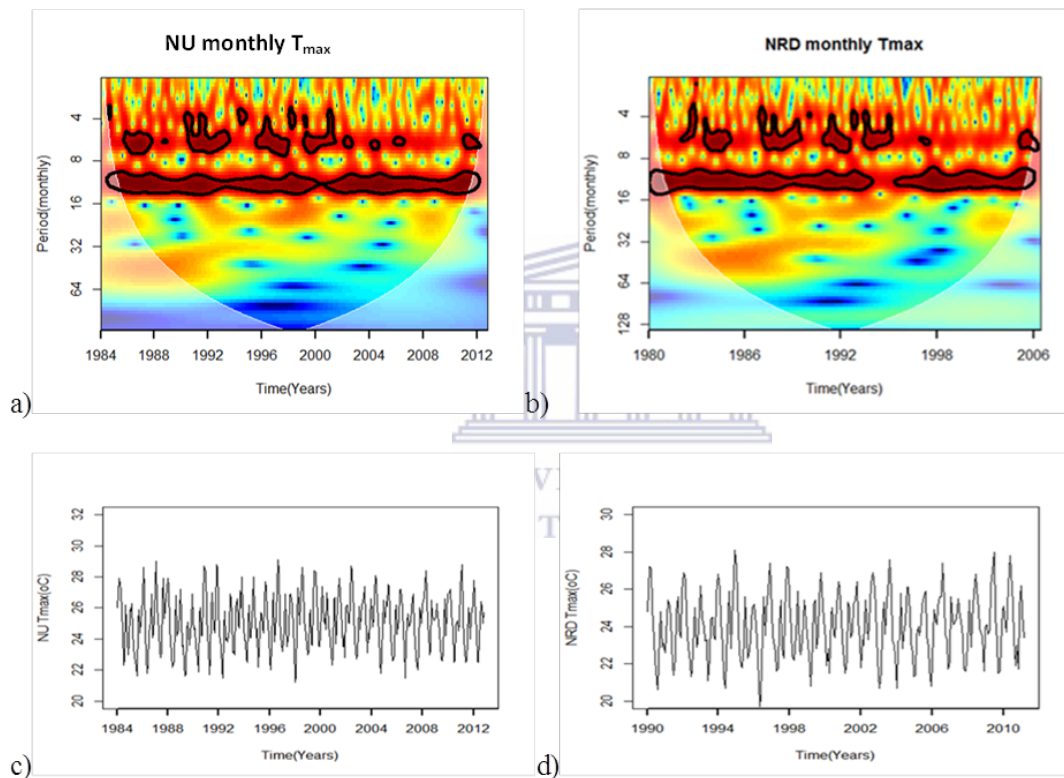


**Figure 2.5:**The wavelet power spectrum plots (WPS) of  $T_{max}$  over Nairobi; a) NU and; b) NR<sub>D</sub>; the dark red regions encircled by black contours in the WPS plots indicates the periodicities that are significant at the 95% level of confidence and the white U-curve marks the cone of influence (COI); the colour code is such that blue represent low spectral power and red is high power; c&d) show respectively the temporal variability of the monthly  $T_{max}$  of the same stations

To summarize the above observations,  $T_{\max}$  in Nairobi has a dominant quasi-annual cycle that varies between periodicities of 8-16 months (centred at 12 months). There were semi-annual cycles that were more common before 2000 than in later years in the two stations. The resultant effects of the occurrence of high-frequency features and the quasi-annual cycles are observed in the time series plots as high peak values. I particularly observed that when multiple periodicities occurred simultaneously higher temperature peaks were realized than when the quasi-annual cycle is the only dominant periodicity. For example in the time series plot, months in 1992, 1996 and 2012 have high peaks in both stations that are attributable to the simultaneous occurrence of the quasi-annual cycle with the 4-6 months periodicities. There was no observable increasing or decreasing trends in each of the time series. The quasi-annual cycle is also observed to vary with time in such a way that the significant periodicities cover more months (broad along the period axis) in some years than others (*e.g.*, in  $NR_D$  between 1995-1998 the annual cycle is not significant and low temperature were observed); these observations imply that  $T_{\max}$  over Nairobi exhibits high inter-annual variability that could be responsible for occurrence of high extremes in the time series plots. There are no cycles in the  $T_{\max}$  over Nairobi that is longer than 16 months.

Considering  $T_{\min}$  of the same stations (Fig 2.6 (a & b)), the semi-annual cycle is more dominant than in  $T_{\max}$ . *i.e.*, there are more periodicities of 4-8 months that are in isolated groups of years but present throughout the period (1980-2013) than were present in  $T_{\max}$ ; for example extended significant periodicities of 4-8 months were observed from 1998 to 2005 and between 2007 and 2013 in NU. Similar periodicities were observed for  $NR_D$  station from 2000 to 2013. The annual cycle was also dominant and more continuous for the urban station (NU) than rural ( $NR_D$ ), which has non-significant periods along the time axis. The semi-annual cycle in  $NR_D$  is also more dominant than the quasi-annual cycle. This would imply that local

influence on  $T_{\min}$  of  $NR_D$  is more than it is in  $NU$ . The time series plots indicate notable increasing trends in the  $T_{\min}$  series in each of the two stations (Fig 2.6 c&d).

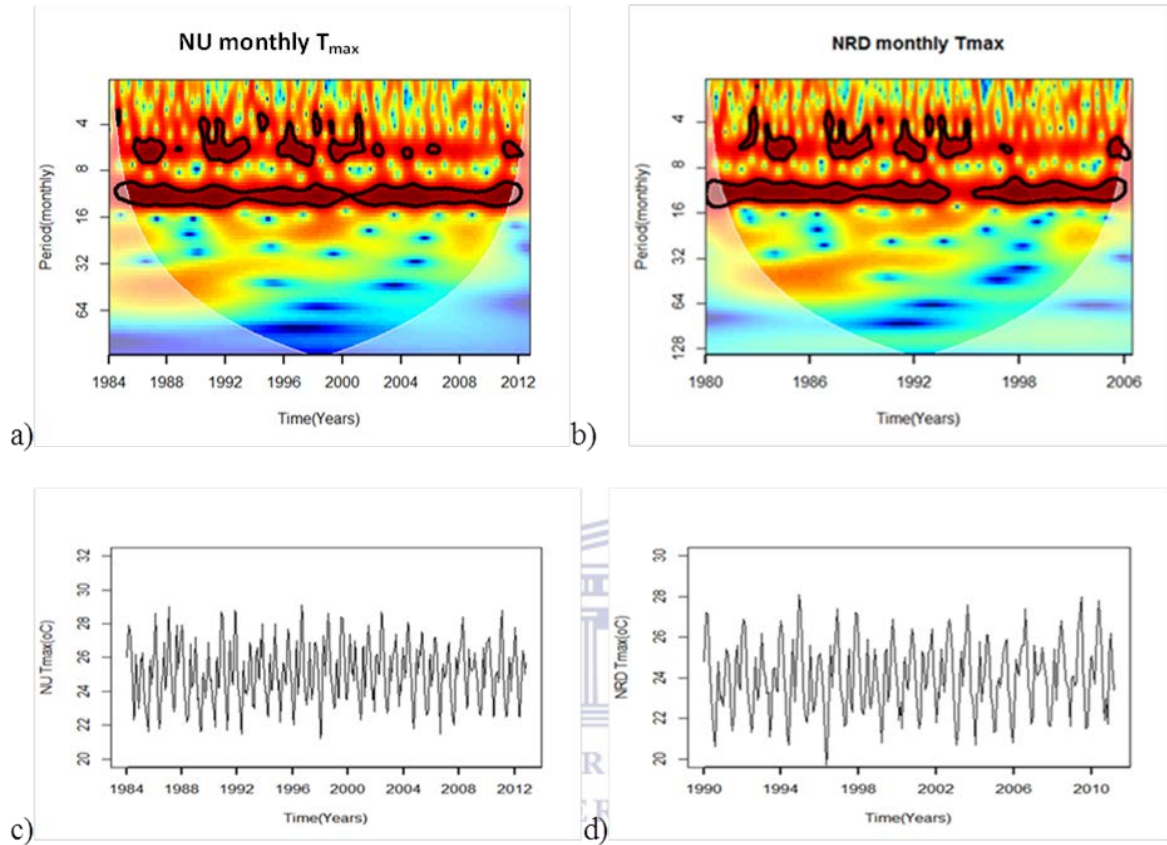


**Figure 2.6:**The wavelet power spectrum plots (WPS) of  $T_{\min}$  over Nairobi; a)  $NU$  and; b)  $NR_D$ ; the dark red regions encircled by black contours in the WPS plots indicates the periodicities that are significant at the 95% level of confidence and the white U-curve marks the cone of influence (COI); the colour code is such that blue represent low spectral power and red is high power; c&d) show respectively the temporal variability of the monthly  $T_{\min}$  of the same stations

Comparing CWT analysis of  $T_{\max}$  and  $T_{\min}$  over Nairobi, the difference in the variability of the  $T_{\min}$  compared to  $T_{\max}$  is clearly observed. For example,  $T_{\min}$  has notable increasing trends that can be attributed to the more frequent semi-annual cycles enhancing the annual cycle; note that the semi-annual periodicities were almost absent in  $T_{\max}$  after the year 2000. Also

spatial variability especially of  $T_{\min}$  was observed between the two stations; for instance the wavelet power spectrum of  $T_{\min}$  at NR<sub>D</sub> station has more high frequency features than NU, which would suggest that local effects are influencing  $T_{\min}$  more in the NR<sub>D</sub> station that could be attributed to urbanization through urban sprawl. Another notable observation was that both  $T_{\min}$  like  $T_{\max}$  had no significant periodicities beyond the quasi-annual cycle. This would imply that temperature in this region may not be influenced by the climate modes of variability (such as ENSO) that influence climate in the EEA region and have cycles beyond one year or the effects of such modes are superimposed in the annual cycle.

### ***Mombasa urban area***

Figure 2.7 (a&b) shows the variability of  $T_{\max}$  of two stations in the coastal region. For Mombasa urban station (MU) the WPS plot (Fig 2.7 (a)) have a dominant and broad quasi-annual cycle (8-16 months periodicities) with no periodicities beyond the 16 months and some isolated 1-5 and 1-3 months periodicities around 1992 and 2012 respectively. Consequently, the same pattern was observed in the WPS plot of the rural station MR<sub>M</sub>s (Fig 2.7 (b)) although in this station there were no other significant periodicities except the quasi-annual one. The time series plot of MU have no increasing or decreasing trend over the period from 1980-2013 (Fig 2.7(c)), while time series plot of the rural station exhibits an increasing trend especially observed after 1990 (Fig 2.7(d)).



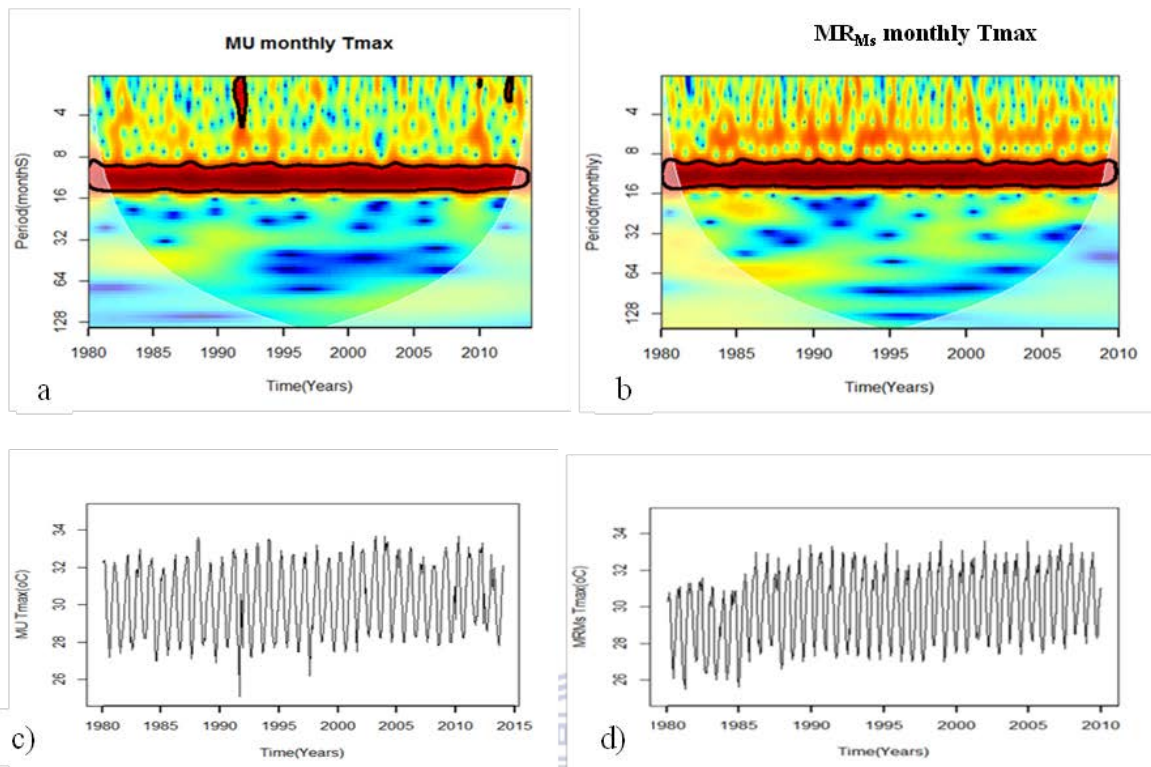


**Figure 2.7: The wavelet power spectrum plots (WPS) of the  $T_{max}$  over Mombasa; a) MU and; b)  $MR_{MS}$ ; the dark region regions encircled by black contours in the WPS plots indicate the periodicities that are significant at the 95% confidence level and the white curve marks the cone of influence (COI); the colour code is such that blue colour is low spectral power, and red is high power; c&d) show respectively the temporal variability of the monthly  $T_{max}$  of the same stations**

Comparing the urban and rural stations over Mombasa, the rural station has higher spectral energy throughout the 1980- 2013 period in the region of 4-6months periodicities (though not significant) that would be associated with the increasing trends in this station. These results indicate that high-frequency components (low periodicities) have almost no influence on the variability of  $T_{max}$  over the coastal region. Again there are no significant periodicities beyond the annual cycle implying that climate modes of variability that influence climate in EEA

has no influence on  $T_{max}$  at the coast over this period or such influence is embedded within the annual cycle.

Observations from the  $T_{min}$  depict observable differences from the  $T_{max}$  in that there are high-frequency modes of variability scattered along the time series and mainly at periodicities of 6-8 months for MU (Fig 2.8 (a)) and between 0-8 months for  $MR_{Ms}$  (Fig 2.8 (b)). However, the dominant periodicity is still the annual cycle. Considering the time series plots of  $T_{min}$ , MU indicate a decreasing trend between 1980 to 1995 followed by increasing trend from 1990 to 2013 (Fig 2.8(c)) and  $MR_{Ms}$  had an increasing trend throughout (Fig 2.8(d)).

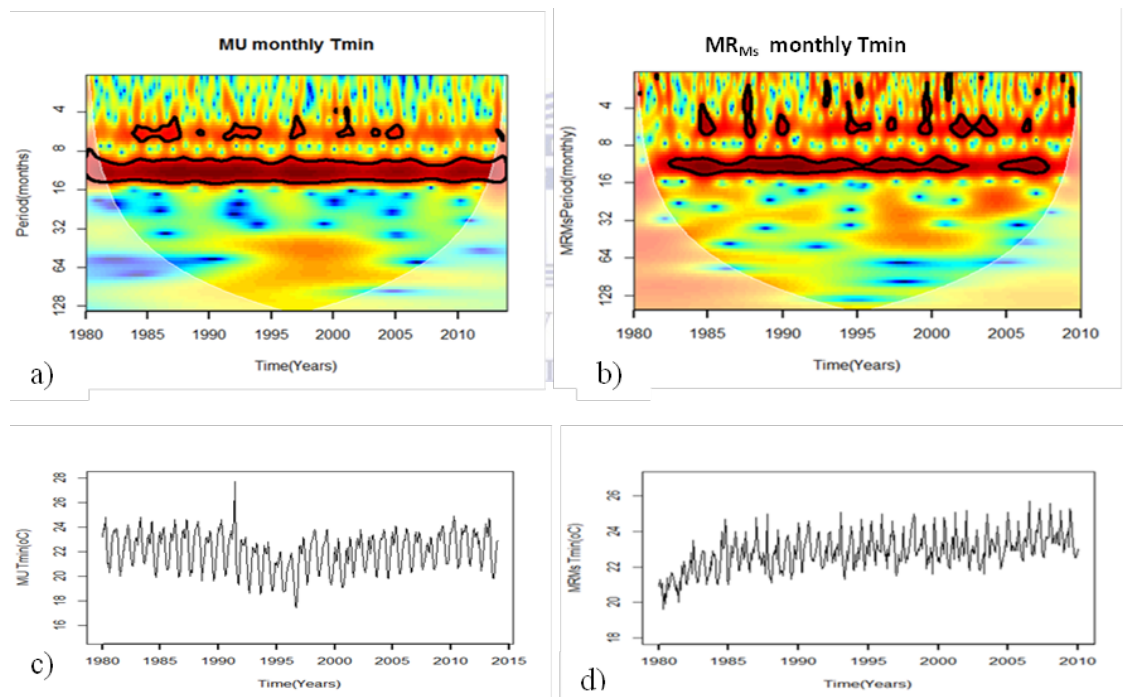


**Figure 2.8:**The wavelet power spectrum plots (WPS) of the  $T_{min}$  over Mombasa; a) MU and; b)  $MR_{Ms}$ ; the dark region regions encircled by black contours in the WPS plots indicate the periodicities that are significant at the 95% confidence level and the white curve marks the cone of influence (COI); the colour code is such that blue colour is low spectral power, and red is high power; c&d) show respectively the temporal variability of the monthly  $T_{max}$  of the same stations



The time series plot for MR<sub>Ms</sub> station indicates an increasing trend throughout the 1980-2013 periods. The implications of these results are that T<sub>min</sub> at the coast is being influenced by local factors such as urbanization and other forms of land cover changes, as well as global factors. It is worth noting that there are no high peaks in the time series plots especially for the T<sub>max</sub> for stations at the coast. This observation could be explained by the lack of multiple cycles occurring simultaneously like was observed over Nairobi. Some of the factors influencing temperature variability are explored further in Section (2.6.4) below.

In general, the results of rural areas at the coast of Kenya have indicated warming in both T<sub>max</sub> and T<sub>min</sub>, while in the urban station increasing trend was only observed in the T<sub>min</sub> and after 1990. Different factors could be influencing the warming of the T<sub>max</sub> and T<sub>min</sub>. For example, all the stations at the coast have a strong annual cycle but high-frequency components in the 0-6 month's periodicity were mainly found in the T<sub>min</sub>. These observations would imply that local factors are influencing T<sub>min</sub> while regional or global factors are influencing the T<sub>max</sub> more than local factors in rural areas. Further investigations to examine the significance of the trends in T<sub>max</sub> and T<sub>min</sub> were done statistically in the next Section (2.6.3) and later in Chapter 4, urban effects on temperature are explored.

### ***Kisumu urban area***

Kisumu (KU) and Kisii (KR) are stations in the western region of Kenya and close to Lake Victoria. Considering T<sub>max</sub> (Figure 2.9(a&b)), the annual cycle does not occur continuously over the whole time (1980-2013) but has significant isolated periodicities. For example during the periods 1980-85, 1990-95 and 2003-2007 in KU (Figure 2.9(a)), while KR (Figure 2.9(b)) had significant annual periodicities for isolated groups of years between 1980-1985 followed by a long period of non-significant periodicities. Significant periodicities

appeared again in KR between 1995 and 2013. For both stations, 4-6 months periodicities that are frequent but not continuous were observed after 1995. The time series plot depicts frequent high peaks of  $T_{max}$  at KU and no observable increasing or decreasing trend, while KR plot showed an increasing trend (Figure 2.9(c&d)).

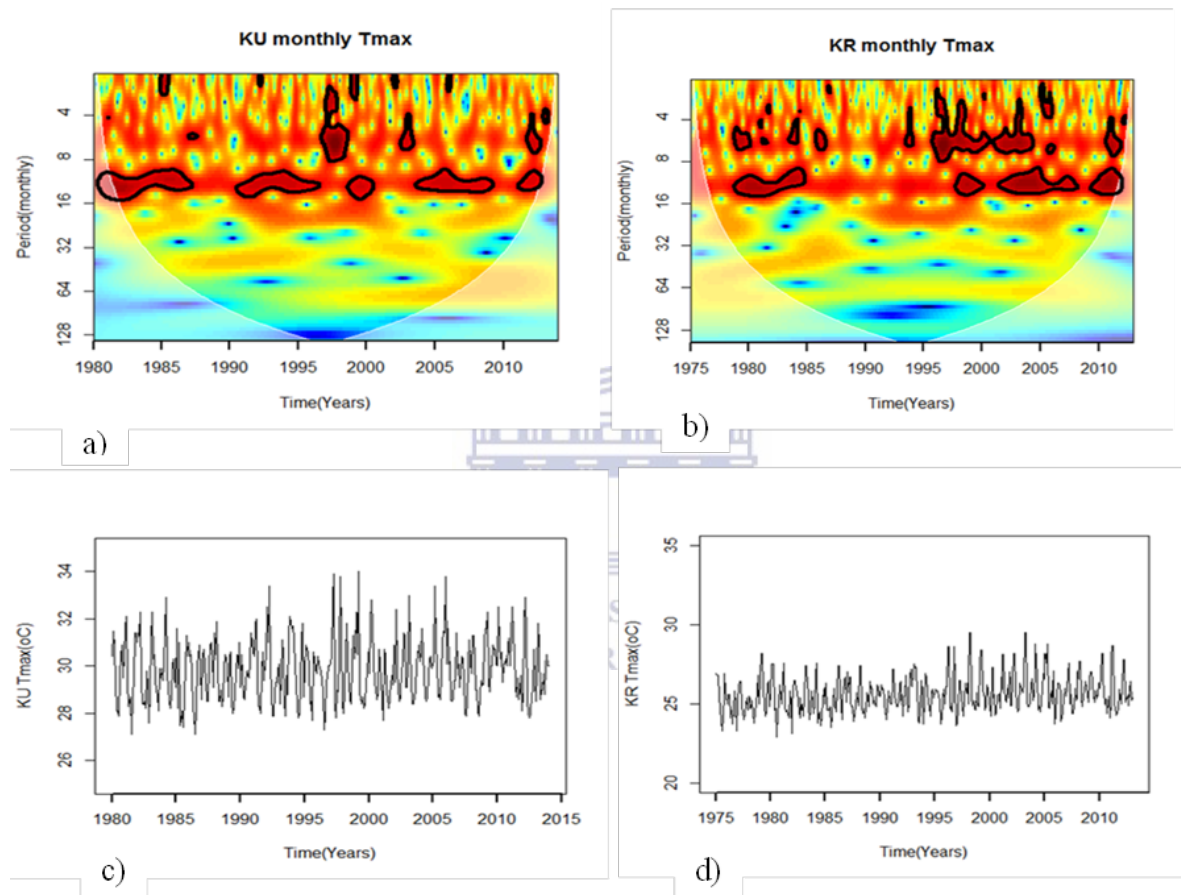


**Figure 2.9:**The wavelet power spectrum plots (WPS) of the  $T_{max}$  over the Lake region; a) Kisumu (KU) and; b) Kisii (KR); the black regions encircled by contours in the WSP plots indicates the periodicities that are significant at the 95% confidence level and the white curve marks the cone of influence (COI); the colour code is such that blue colour is low spectral power, and red is high power; c&d) show the temporal variability of the monthly  $T_{max}$  of the same stations respectively

For the  $T_{min}$  series, the high frequency component (4-6 months periodicities) are more dominant over KU than the annual cycle which only has a significant periodicity between 1980 and 1995 (Figure 2.10 (a) while in KR (Figure 2.10 (b)) the annual cycle is the dominant one with only a few isolated periodicities of 1-6 months. Notable also is the high spectral energy in the region of 32-64 months periods that were not in either Nairobi or Mombasa areas. Both stations showed increasing trends of  $T_{min}$ (Figure 2.10 (c&d)).

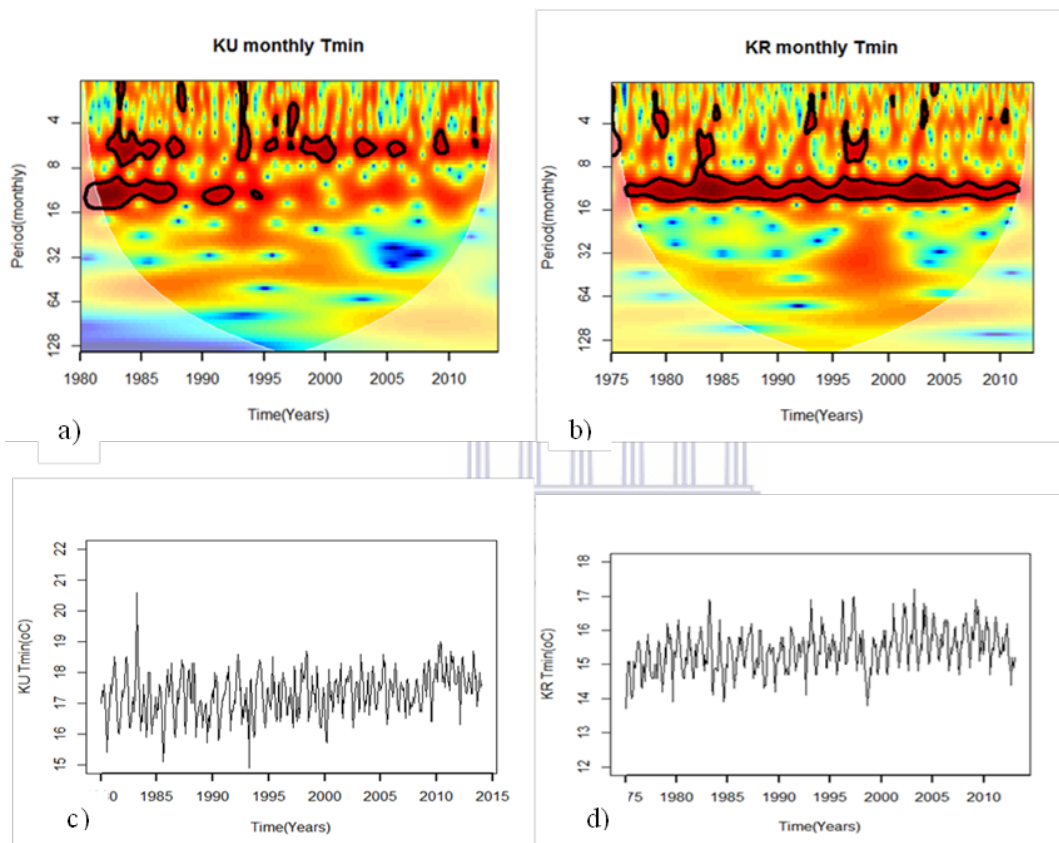


**Figure 2.10:**The wavelet power spectrum plots (WPS) of the  $T_{min}$  over the Lake region; a) Kisumu (KU) and; b)Kisii (KR); the black regions encircled by contours in the WPS plots indicates the periodicities that are significant at the 95% confidence level and the white curve marks the cone of influence (COI); the colour code is such that blue colour is low spectral power and red is high power; c&d) show the temporal variability of the monthly  $T_{min}$  of the same stations respectively

### *Nakuru urban area*

Nakuru(NKU) is the only station representing the urban area within the Rift Valley. The WPS, plot of  $T_{max}$ (Figure 2.11 (a), shows a dominant quasi-annual cycle (8-16 months periodicity) and isolated 1-8 months periodicities that were more frequently before the year 2000. The time series plot (Fig 2.11 (b))of the  $T_{max}$  has no trend between 1990 and 2005 after which a decline is observed from 2005-2013. High peaks of  $T_{max}$  values are observed especially between 1980 and 1990 when multiple periodicities are also observed in the WPS plot.

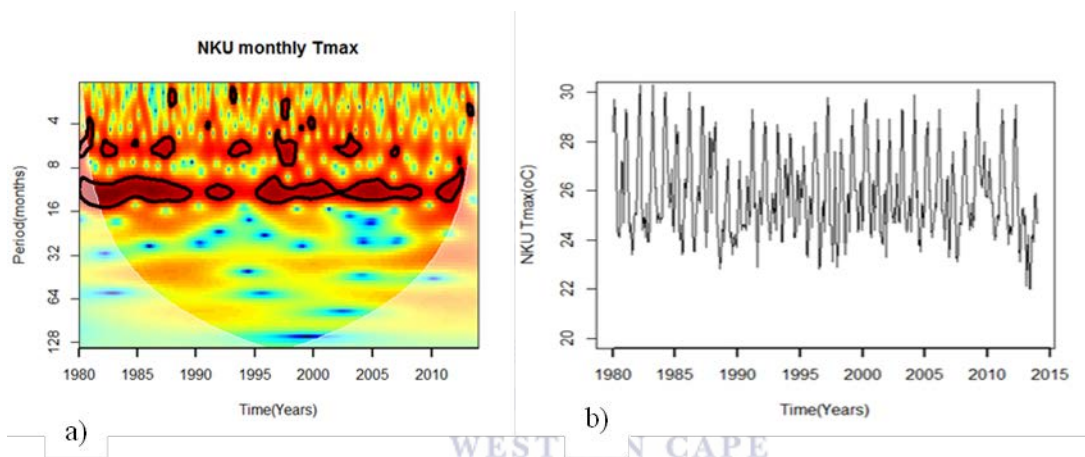


**Figure 2.11:** a) The wavelet power spectrum plots (WPS) of the  $T_{max}$  in Nakuru (NKU); the black regions encircled by contours in the WPS plots indicates the periodicities that are significant at the 95% confidence level and the white curve marks the cone of influence (COI); the colour code is such that blue colour is low spectral power, and red is high power; b) The temporal variability of the monthly  $T_{max}$  of NKU

The WPS plot of  $T_{min}$  for Nakuru station (Figure 2.12(a)) had spectral characteristics that were different from all other stations. For instance, the annual cycle is not common, and had high spectral energy in regions of periodicities of 8-32 months. The time series plot, however, depicts low and high peaks with an observable increasing trend (Figure 2.12(b)).

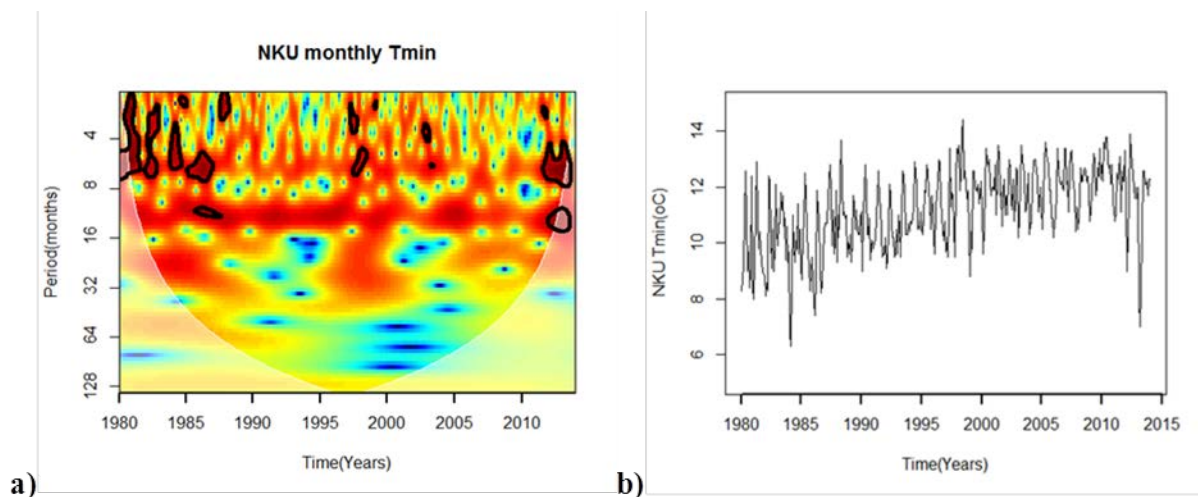
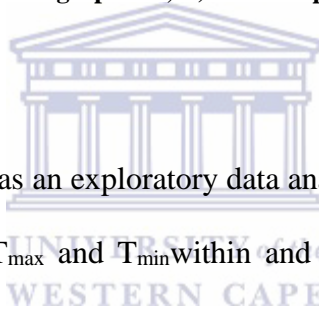


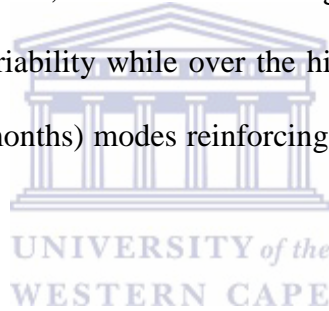
**Figure 2.12:** a) The wavelet power spectrum plots (WPS) of the  $T_{\min}$  in Nakuru (NKU); the black regions encircled by contours in the WPS plots indicates the periodicities that are significant at the 95% confidence level and the white curve marks the cone of influence (COI); the colour code is such that blue colour is low spectral power, and red is high power; b) The temporal variability of the monthly  $T_{\min}$  of NKU



The CWT applied in this section, as an exploratory data analysis tool to investigate the spatial and temporal variability of the  $T_{\max}$  and  $T_{\min}$  Within and in the neighbourhood of the four major urban areas of Kenya, brought about the following general observations:

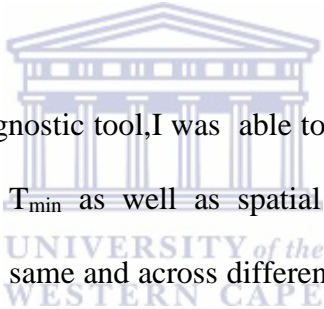
- i) The annual cycle of the  $T_{\max}$  and  $T_{\min}$  exhibited spatial differences across the the four regions. For instance, the annual cycle was the only dominant feature in the  $T_{\max}$  over the coastal region, while in Nakuru and the Lake Victoria region, the annual cycle was not continuously significant over the analysis periods and semi-annual cycles are more prominent.
- ii) The  $T_{\min}$  has high-frequency features (less than one-year periodicities) especially in urban stations, and in most of the stations, the  $T_{\min}$  time series had increasing trends in both urban and rural stations.

- iii) High peak temperature in the time series plots for a given station, across the analysis period, were observed when high and low-frequency features occurred simultaneously, while trends were observed when occurrence of multiple periodicities are continuous over a long period of time; as observed in  $T_{\min}$  series for most stations
- iv) There were spatial differences in the variability of  $T_{\max}$  and  $T_{\min}$  as observed from WPS plots; for instance a time series plot alone may not be able to show the significant difference between the temperature variability over the coastal region and central highlands i.e., over the coastal region the annual cycle is the only dominant mode of variability while over the highlands, there are high frequency (periodicities of 1-6 months) modes reinforcing the annual cycle in both  $T_{\max}$  and  $T_{\min}$ .
- v)  $T_{\max}$  and  $T_{\min}$  at monthly time scale had no significant periodicities longer than 16 months.



The observations in the CWT analysis indicates the existence of multi-temporal cycles in the temperature time series that would be interpreted to indicate that local factors and global factors are influencing the observed changes in temperature. However, the attribution of these factors would require further analysis to establish the factors that influence temperature at both local and global scales. The influence of global warming on urban and rural temperature was investigated in the next Section while in Chapter 4, the urban heat island (UHI) effect was investigated. However, a study by Prokoph and Patterson, (2004) using a similar method,

interpreted the inter-seasonal cycles to suggested that urban heat island effect was influencing temperature changes in Ottawa city (USA). Also land use changes and growth of towns in rural areas could be associated to some of the observed changes. For instance, Kisii stations showed significant change in both  $T_{\max}$  and  $T_{\min}$  after 1995 and was indicated in Mironga, (2005) to have undergone land use changes through draining of wetlands and increase of built-up areas of the Kisii town. Lack of significant cycles beyond one year would imply that the temperature within these locations is either not influenced by global modes of climate variability such as El-Nino Southern Oscillation (ENSO) and the Indian Ocean Dipole (IOD) which have cycles longer than one year, or their effects are superimposed within the annual cycles.



Using the CWT analysis as a diagnostic tool, I was able to establish important differences in the variability of the  $T_{\max}$  and  $T_{\min}$  as well as spatial differences (and similarities) in temperature variability within the same and across different climatic zones, and within urban and rural areas. These results agree with other studies that  $T_{\min}$  is increasing more than the  $T_{\max}$  in the EEA region (King'uyu, et al., 2000; Christy, et al., 2009; Omumbo, et al., 2011). However, the CWT analysis also revealed that, although  $T_{\max}$  showed no temporal trends in some stations, there were frequent occurrence of high values observed in time series plots that were resultant of simultaneous occurrence of the annual cycle and the high-frequency components. The frequent occurrence of high peaks is likely to introduce trends in the indices of extreme values of  $T_{\max}$ . However, CWT as a diagnostic tool would require the trend analysis methods to test for the significance of the observed changes. Trends analysis was carried out in the next section using the annual, seasonal and monthly time-scales of both  $T_{\max}$  and  $T_{\min}$ .



### 2.5.3 Trend analysis

Trend analysis at various time scales was carried out in this Section to confirm the exploratory observations. The outcome of the trend results would form foundation upon which the influence of temperature on rainfall (Chapter 5) would be investigated. The following variables were tested for trends in both  $T_{\max}$  and  $T_{\min}$  using the parametric linear regression and the non-parametric Mann-Kendall methods (Equations 2.14-2.20) including ; i) mean monthly values; ii) the means of the four seasons in each year (DJF, MAM, JJA and SON) and; iii) the mean annual values for each station. For each time-scale,  $T_{\max}$  and  $T_{\min}$  from all stations (Table 2.1) were tested for trends but only those whose  $\beta$  and  $\tau$  coefficients were significant (p-value < 0.05) were presented in the results.

#### *Trend analysis of $T_{\max}$*



Figure 2.13 shows linear regression coefficients ( $\beta$ ) for four stations whose  $T_{\max}$  had significant trends; Figure 2.13 (a) shows the trends of monthly  $T_{\max}$  while Figure 2.13 (b) shows the trends in the seasonal and annual means of  $T_{\max}$ . For instance, MR<sub>Ms</sub> station at the coast had trends in all months, all seasons and the annual mean, while the other stations had trends in some months and seasons and not in others. Notably, linear regression method detected trends in  $T_{\max}$  only in stations at the coast and KR in western Kenya, with the highest trend in annual mean recorded at MR<sub>Ms</sub> (0.044°C/year).



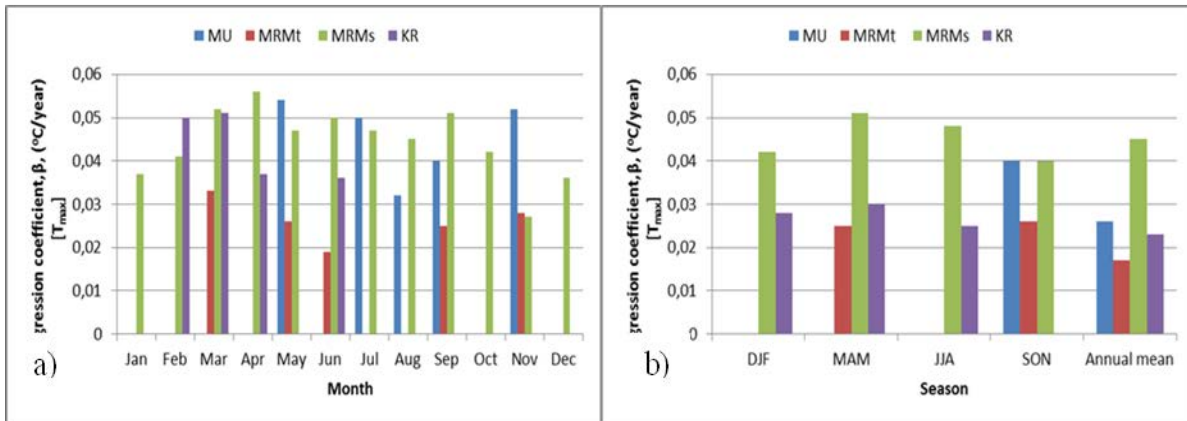


**Figure 2.13:**A summary of linear regression trend test results of  $T_{max}$ ; a) regression coefficients ( $\beta$ ) for the monthly  $T_{max}$  ; b)  $\beta$  of the seasonal and annual mean  $T_{max}$ ; note stations with no trends in  $T_{max}$  for any of the month, season or annual mean were not included in the summary; gaps in some periods for a given station indicate no trends (All the  $\beta$  values are significant at  $\alpha = 0.05$ ;  $p$ -values  $< 0.05$ )

Figure 2.14 (a&b) shows the summary of the Mann-Kendall coefficients ( $\tau$ ) for the period that a station had trends in  $T_{max}$ . Figure 2.14(a) shows the trend test results of all the stations where the coefficients of monthly  $T_{max}$  were statistically significant, while Figure 2.14(b) shows the same results for the seasonal and annual mean  $T_{min}$ . There were more trends detected by the Mann-Kendall method than with the linear regression method but all trends detected by the linear regression method were also confirmed by the Mann-Kendall method. For instance, MRMs has increasing trends in all months and NKU has negative trends in the months of September and October detected by Mann-Kendall but were not significant according to linear regression.

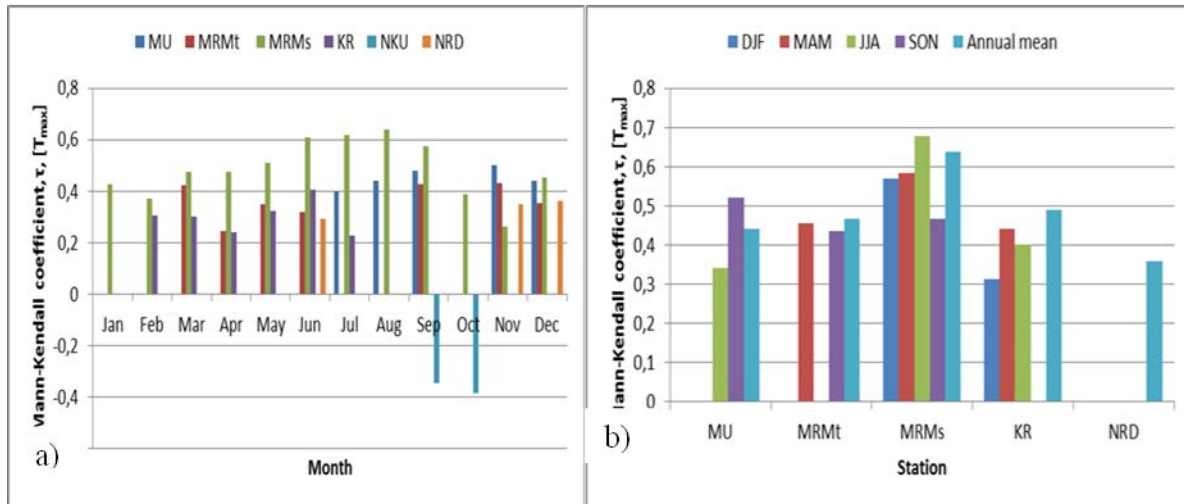
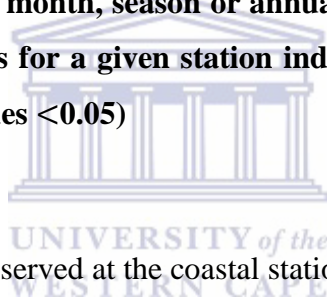


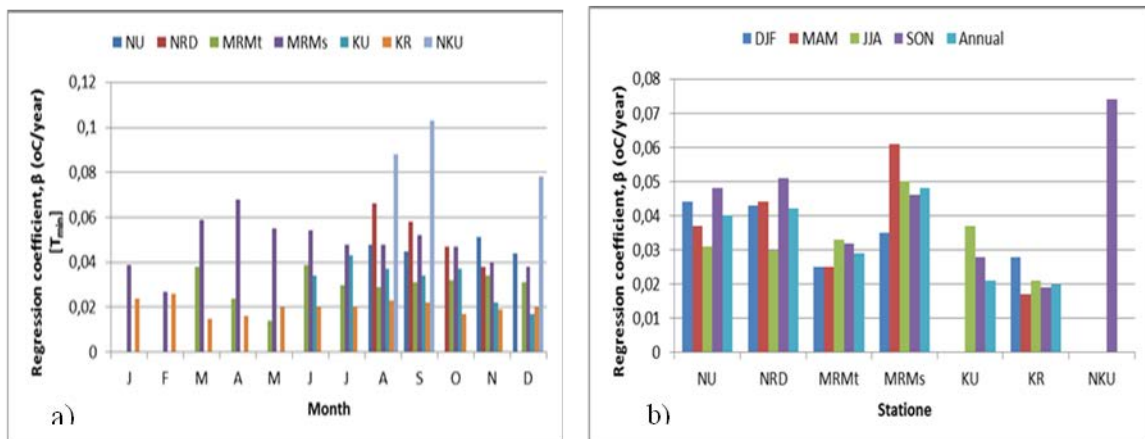
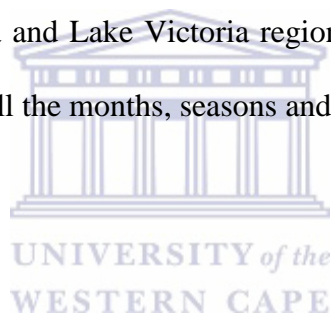
**Figure 2.14:** A summary of Mann-Kendall trend test results of  $T_{max}$ ; a) Mann-Kendall ( $\tau$ ) for the monthly  $T_{max}$ ; b)  $\tau$  for the seasonal and annual mean  $T_{max}$ ; note: stations with no trends in  $T_{max}$  for any of the month, season or annual mean were not included in the summary; gaps in some periods for a given station indicate no trends (All the  $\tau$  values are significant at  $\alpha = 0.05$ ;  $p$ -values  $< 0.05$ )



In general, positive trends were observed at the coastal stations and Kisii near lake Victoria. In particular Msabaha ( $MR_{Ms}$ ) which is about 90 km northeast of Mombasa town had increasing trends throughout the year. These results are consistent with the observations from the CWT analysis in some cases ( $MR_{Ms}$  and KR) while in other cases trends were not observed but have been detected through the statistical analysis at various scales (e.g., MU had increasing trends in JJA, SON and annual mean). Other studies that have reported trends in temperature in the EEA region include that of Christy, et al. (2009) who suggested that increasing  $T_{max}$  represent a significantly greater day-time connection to the deep atmosphere and hence may be proxy for global temperature change and Omumbo et al. (2011) who indicated that the increasing trends of local temperature were consistent with the global temperature change. Investigations of the influence of increasing global temperatures (global warming) to the local urban and rural temperatures were investigated in Section 2.6.5.

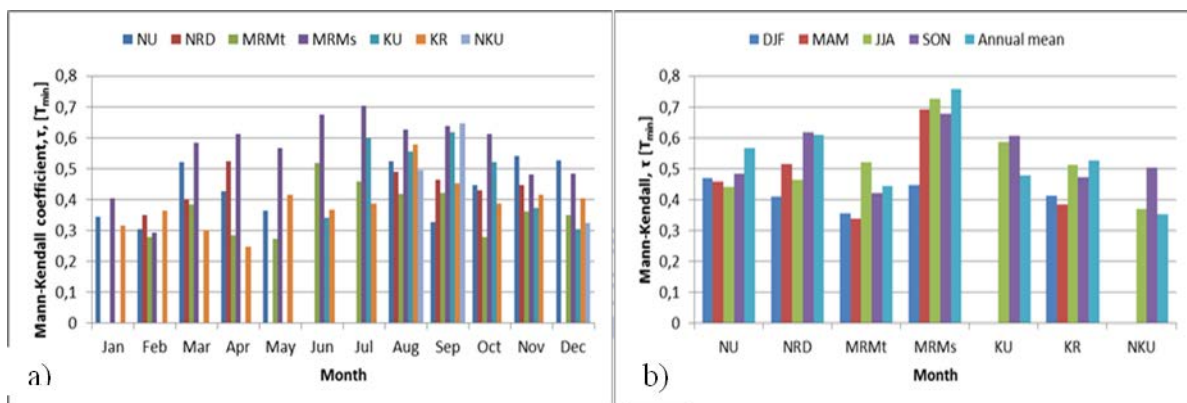
### Trend analysis of $T_{min}$

Figure 2.15 shows the linear regression results in which the  $\beta$  values were significant. Figure 2.15 (a) are the results for the monthly trends, while Figure 2.15 (b) are the results for the seasonal and annual means. NU and NR<sub>D</sub>(in Nairobi) had no trends in the months of January to July, and NKU (Nakuru) had no trends except in the months of August, September, December and the SON season which was the highest seasonal trend (0.074°C/year) among all stations. At the coastal region, MR<sub>M</sub>s had positive trends in all periods while MR<sub>M</sub>t has only January and February without trends. Note that MU had no trends for the whole period (1980-2013) which was attributed to the decline between 1980 and 1990 followed by an increase thereafter observed in the time series plot and the CWT analysis in the previous Section. Over the western Kenya and Lake Victoria region, Kisii(KR) station had weak but significant increasing trends for all the months, seasons and annual mean.



**Figure 2.15:**A summary of linear regression trend test results of  $T_{min}$ ; a) regression coefficients ( $\beta$ ) of the monthly  $T_{min}$  ; b)  $\beta$  of the seasonal and annual mean  $T_{min}$ ; (All the  $\beta$  values are significant at  $\alpha = 0.05$ ;  $p$ -values  $< 0.05$ )

The results of the Mann-Kendall trend test indicate showed more positive trends in each station than was found with regression method (Fig 2.16). For instance, NU had positive trends from January to May that were not significant with the regression method and NKU has more months (Fig 2.16(a)) and seasons (Fig 2.16(b)) with positive trends. The coastal stations had increasing trends in almost all months, seasons and the annual mean except MU that no trends. None of the stations had decreasing trends for the  $T_{min}$  series.



**Figure 2.16:** A summary of Mann-Kendall trend test results of  $T_{min}$ ; a) Mann-Kendall ( $\tau$ ) for the monthly  $T_{min}$ ; b)  $\tau$  for the seasonal and annual mean  $T_{min}$ ; note stations with no trends in  $T_{min}$  for any of the month, season or annual mean were not included in the summary; gaps in some periods for a given station indicate no trends (All the  $\tau$  values are significant at  $\alpha=0.05$  (with  $p$ -values  $<0.05$ ))

Although there is night-time warming over the coastal region throughout the year (as indicated by monthly positive trends),  $T_{min}$  at MU had trends only when analysed from 1990-2013. The increasing trends over this period may have been influenced mainly by local changes as suggested by the increase of the high-frequency components (4-6 months periodicities) WPS (Fig 2.7(a)) after 1995. It is worth noting that increasing trends of the  $T_{min}$  were observed in almost all stations and especially during the months of September to December and the SON season.

In summary, the trend analysis results corroborated those of King'uyu, et al. (2000), Christy, et al. (2009) and Omumbo, et al. (2011) who have reported increasing trends of the  $T_{\min}$  over the EA region and also confirm some of the observations of the CWT analysis. For instance, the cooling and warming of MU that makes trend results to apparently indicate lack of long-term change over time in  $T_{\min}$ .

The comparative analysis of rural and urban stations was important to establish the influence of both urbanization and global warming on local temperature. However trend analysis alone may be limited to show such differences. Combined with the CWT analysis which shows the high-frequency features associated with local changes, there is an indication that temperature is increasing due to both local changes (such as urbanization) and global warming. For example,  $T_{\max}$  at the coast has increasing trends although there were no significant high frequency (low periodicities) modes of variability thus implying that the warming is more global than local while the increasing trends in  $T_{\min}$  over Nairobi indicated more local influence than global.

### ***Trend analysis of extreme temperature indices***

The analysis of extreme indices of temperature was performed to establish if daily maximum values and other extreme indices from each of the four urban areas are undergoing changes over time. The aim of this analysis was to examine if the observed high (low) peak temperatures observed in the CWT analysis have long-term trends, that are likely to influence rainfall patterns. Four stations that had complete daily data were used to compute the temperature indices. A total of nine indices indicated in Table 2.2 were analysed for trends using the linear regression and Mann-Kendall methods.

Table 2.5 shows the results of the trends of annual series of each of the nine indices in each station. The diurnal temperature range (DTR) had significant negative trends in MU (coast) and NKU (Rift valley) stations implying that the annual mean daily difference between the  $T_{\max}$  and  $T_{\min}$  has declined over the last thirty years (1980-2013) at these two stations. This could be resulting from notable decreasing trends in the percentage of the days in a year when daily  $T_{\min}$  was less than the 10<sup>th</sup> percentile (i.e decreasing cool nights) and increasing trends in the percentage of the days in a year when daily  $T_{\min}$  was greater than the 90<sup>th</sup> percentile (i.e increasing warm nights) also in MU,  $\max T_{\min}$  and  $\min T_{\min}$  have significant increasing trends which are likely to influence negative trends in DTR. In general, all stations except NKU has increasing trends in the proportion of the time when  $T_{\max}$  was greater than the 90<sup>th</sup> percentile and when  $T_{\min}$  was greater than the 90<sup>th</sup> percentile while having negative trends in the proportion of the time when  $T_{\min}$  was less than the 10<sup>th</sup> percentile. Particularly in Mombasa and Nairobi, the minimum temperature is increasing as well as the proportion of time when  $T_{\max}$  exceeds the 90<sup>th</sup> percentile; i.e even when  $T_{\max}$  has no temporal trends, the number of hot days in a year is increasing.

These results agree with those of Omondi, et al. (2014) who reported that warm days and nights are increasing while cool nights are decreasing over the eastern African region. Kruger and Shongwe (2004) and New, et al. 2006 also reported the same for the southern and western African region respectively, and also reported that DTR does not show uniform increasing (or decreasing) trends across all regions.

**Table 2.5: Trend results of the extreme temperature indices of four stations; MU(Mombasa), NRD (Nairobi), NKU(Nakuru in Rift Valley) and KR (Kisii over the Western Kenya highlands); values in bold red are significant at  $\alpha=0.05$ ; the indices are described in Table 2.2**

Station Index	MU		NRD		NKU		KR	
	T	B	$\tau$	B	$\tau$	$\beta$	$\tau$	$\beta$
<b>DTR</b>	<b>-0.63</b>	<b>-0.09</b>	-0.04	-0.01	<b>-0.45</b>	-0.06	-0.09	-0.01
<b>MaxT<sub>max</sub></b>	-0.11	-0.03	0.27	0.03	0.06	0.02	<b>0.31</b>	<b>0.03</b>
<b>MaxT<sub>min</sub></b>	<b>0.46</b>	<b>0.1</b>	<b>0.48</b>	0.07	0.23	0.09	<b>0.35</b>	0.05
<b>MinT<sub>max</sub></b>	-0.06	-0.01	-0.12	-0.02	0.05	0.02	-0.17	-0.02
<b>MinT<sub>min</sub></b>	<b>0.58</b>	<b>0.13</b>	<b>0.38</b>	<b>0.11</b>	-0.03	-0.01	0.06	-0.06
<b>T<sub>max10p</sub></b>	-0.12	-0.01	-0.11	0.04	<b>0.19</b>	<b>0.47</b>	<b>-0.35</b>	<b>-0.12</b>
<b>T<sub>max90p</sub></b>	<b>0.47</b>	<b>0.52</b>	<b>0.44</b>	<b>0.46</b>	-0.15	-0.03	<b>0.35</b>	<b>0.24</b>
<b>T<sub>min10p</sub></b>	<b>-0.62</b>	<b>-1.0</b>	<b>-0.39</b>	-0.16	<b>-0.43</b>	<b>-0.38</b>	<b>-0.5</b>	-0.04
<b>T<sub>min90p</sub></b>	<b>0.7</b>	<b>0.63</b>	<b>0.69</b>	<b>0.83</b>	<b>0.62</b>	<b>0.42</b>	<b>0.44</b>	<b>0.37</b>

#### 2.5.4 Influence of global temperature anomalies

The CWT and trend analysis have shown that warming in and around urban areas is likely to be resulting from local (presence of periodicities few months in WPS plots) as well as global factors. To establish the influence of global warming on local urban and rural temperatures, correlation and regression analysis of the seasonal  $T_{max}$  and  $T_{min}$  respectively with the global mean (land and ocean) temperature anomalies (GT) was performed. Global warming is a term used to describe the gradual increase in the average temperature of the earth's atmosphere and oceans. GT has been used as an indicator of global warming since it represents the warming of the atmosphere across land and oceans (Hansen, et al., 2010). GT linear trend for the period 1880-2012 was used to report global warming in the Fifth Assessment Report of the IPCC (Stocker, (2013)).

The GT was averaged into seasonal and annual means using the monthly values with time corresponding to the length of time of temperature at the stations. Correlations were then



computed for each season and the annual mean. Figure 2.17 (a) shows the results of the correlations between the GT and  $T_{max}$  for the four seasons namely DJF, MAM, JJA and SON annual means. Results of  $T_{max}$  of NU, NRD and NKU showed no significant correlation with GT for all the seasons and MU has only weak correlations in JJA and SON. However, there were significant positive correlations in all seasons between GT and  $T_{max}$  of MR<sub>Mt</sub> and MR<sub>Ms</sub>. KR is also significantly correlated with GT except for the DJF season. These results imply that global warming is influencing the observed changes in  $T_{max}$  of the coastal and western rural areas of Kenya. The correlation between  $T_{min}$  and GT show higher positive correlations for all stations (Figure 2.17 (b)). NU, MU, KR had significant  $r$  in all seasons and MR<sub>Ms</sub> still has the highest correlation values in all seasons (all close to 0.8 except in DJF). These results corroborate the report of IPCC (Stocker, 2013) that global warming is influenced more by changes in  $T_{min}$  than  $T_{max}$ . Christy et al. (2009) suggested that the  $T_{max}$  and  $T_{min}$  should be treated as separate variables when evaluating temperature changes in climate change studies.

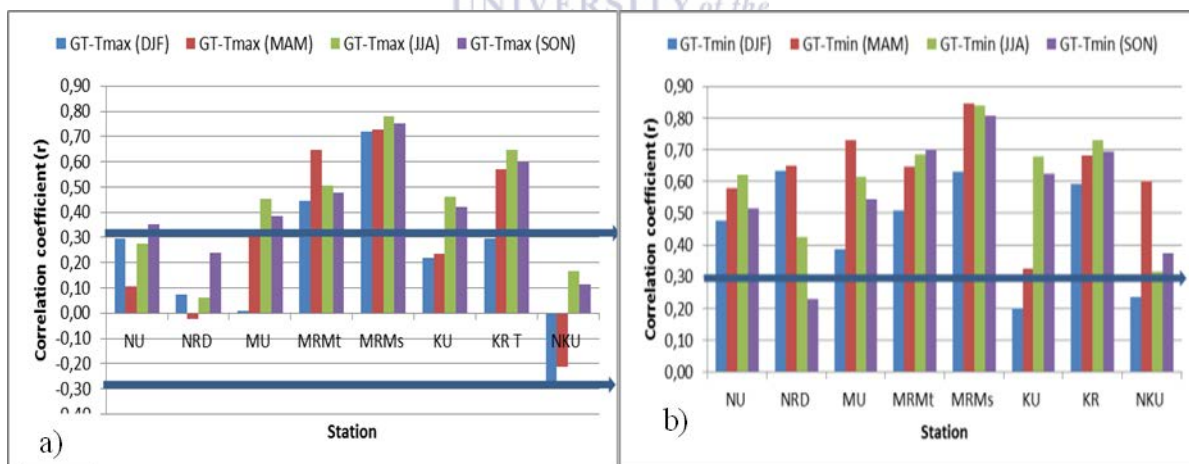


**Figure 2.17:** The association between global temperature anomalies (GT) and the urban and rural temperature for the four seasons (DJF, MAM, JJA and SON); a)  $T_{max}$  and; b)  $T_{min}$ ; the horizontal bar shows the value above (or below) which the correlations are statistically significant at  $\alpha=0.05$



Further analysis was carried out using linear regression to establish the proportion of variations of the annual mean  $T_{max}$  and  $T_{min}$  that could be explained by variations in the annual mean GT. Table 2.6 shows a summary of the proportions of variance of the station annual mean temperature that could be explained by the variance of the annual mean GT. In general, GT has more influence on the temperature of rural stations than the urban ones; e.g., GT explains 52% and 68% of the variance of MR<sub>Ms</sub>  $T_{max}$  and  $T_{min}$  respectively, and 41% and 56% of the variance of KR  $T_{max}$  and  $T_{min}$  respectively. Noted also was that although  $T_{min}$  at MU had a high annual rate of change over the last twenty years, only 36% of this change is accounted for by the GT; on the other hand, more than 50% of the variation of  $T_{min}$  at NU and NR<sub>D</sub> is accounted for by variation of GT.

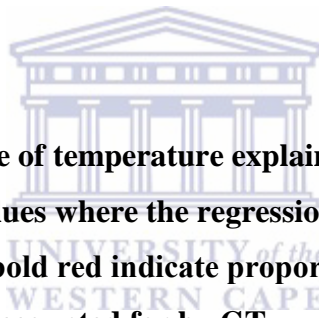


**Table 2.6: Proportion of variance of temperature explained by variation of global temperature (GT); \* indicate values where the regression coefficients were not significant at  $\alpha=0.05$ ; values in bold red indicate proportions where more than 50% of the variance of temperature is accounted for by GT**

		Station									
		NU	NR <sub>D</sub>	NR <sub>K</sub>	NR <sub>T</sub>	MU	MR <sub>Mt</sub>	MR <sub>Ms</sub>	KU	KR	NKU
Proportion (%)	GT- $T_{max}$	14	13*	35	40	22	43	<b>52</b>	13	41	08*
	GT- $T_{min}$	<b>54</b>	<b>54</b>	39	26	36	47	<b>68</b>	41	<b>56</b>	28

These results imply that global warming has more influence on  $T_{min}$  than  $T_{max}$  and influences temperatures more in rural than urban areas. Also noted was that although global warming has a significant influence on local temperature changes, it does not account for all the variations of  $T_{max}$  and  $T_{min}$  in each station which imply that other local factors such as urbanization have an effect on the observed changes. Urban effects on temperature are explored in Chapter 4.

### 2.5.5 Discussion

Temperature of the EEA region has not been subjected to rigorous analysis in relation to variability and change as global climate changes. With the emerging global warming and its expected influence on rainfall (Stocker, 2013), understanding temperature variability and change becomes important. The continuous wavelet transform (CWT) analysis brought about notable differences between the long-term variations of monthly mean  $T_{\max}$  and  $T_{\min}$  both in the urban and neighbouring rural stations. In general, from the four areas, the most dominant mode of temperature variability of  $T_{\max}$  is within the annual cycle, although higher frequency modes in  $T_{\max}$  were observed over the highlands, the Rift Valley, and the Lake region. For  $T_{\min}$  both the annual cycle and semi-annual cycles were common especially for the urban stations. I interpreted these results to imply local climate perturbations have more influence on the  $T_{\min}$  than the  $T_{\max}$  in Kenya. Similar suggestions were made by Christy, et al. (2009) who indicated that human development is responsible for the rising  $T_{\min}$ , while having little effect on  $T_{\max}$ . However at a small spatial scale, this study has established increasing trends of the  $T_{\max}$  at the coast (using rural stations) which could not have been apparent if Mombasa station alone was used for trend analysis; as is commonly the case in many climate studies (King'uyu, et al., 2000; Christy, et al., 2009; Omondi, et al., 2014). Other rural stations that are not commonly used in regional climate studies and had trends in  $T_{\max}$  included, Kisii in western Kenya, and Thika and Kabete near Nairobi. These observations suggest that a dense network of stations is required in studies of temperature variations and trends. Important observations was that, in general, the urban stations had no trends in  $T_{\max}$ , while many of the rural stations had. Further, global warming is influencing the temperature of the rural areas more than the urban areas. It is worth noting that the commonly used stations in most climate studies in EEA are those in and near urban areas, and so some of the changes observed here

have not been reported. Trend analysis of extreme temperature indices over the urban stations showed that, days when  $T_{\max}$  and  $T_{\min}$  exceeded the 90<sup>th</sup> percentile are increasing while cool nights are decreasing. Similar results were reported by Omondi, et al. (2014) for the Greater Horn of Africa (that includes Kenya). Even without trends in  $T_{\max}$ , increase of extremes could impact on rainfall especially in urban areas through enhancement of convective activities. Further, I have established that there exist significant relationships between the increasing trends in the station temperatures (especially  $T_{\min}$ ) and the global warming, thus corroborating other studies that the warming in the African region is consistent with global warming and is being influenced more by changes in  $T_{\min}$  than  $T_{\max}$  (Shongwe and Kruger, 2004; Christy et al., 2009; Omumbo et al., 2011; Stocker, 2013). The results also agree with the observations made by Prokoph and Patterson (2004) for Ottawa (Canada), Kruger and Shongwe (2004) for South Africa, and Christy et al. (2009) for EEA that the  $T_{\min}$  trends in and near urban centres are more influenced by the local urbanization processes than global climate change. In this regard, higher correlations between local temperature and global temperature (used as a proxy for global warming) were observed in rural stations. According to the IPCC (Stoker, 2013), the total global radiative forcing (RF) is positive which has led to increased uptake of energy by the climate system and accordingly, the mean global surface temperature has increased since the late 19<sup>th</sup> century. The global increase in surface temperature has been attributed mainly to increased concentrations of anthropogenic greenhouse gases that are mainly transparent to the incoming shortwave radiation and have the ability to absorb the outgoing long wave radiation and radiate in back into the atmosphere when the earth is cooler than the greenhouse gases, thus influencing the night-time temperature more than the day-time.

## 2.6 Summary

The aim of this Chapter was to investigate variability and possible changes of temperature of urban and rural stations in and around the four main urban areas of Kenya. Spatially the highest temperatures are experienced at the coast and Lake Victoria region while cooler temperatures are experienced over the highlands. Temporally the hottest period of the year in each region is December to April, while June and July are the coolest months. The non-stationarity of temperature was examined using the continuous wavelet transform (CWT) where semi-annual cycles (short periodicities) entrenched in the dominant annual cycles were observed. The short periodicity features were more frequent in  $T_{\min}$  than in  $T_{\max}$  for stations over Nairobi, Nakuru, and Lake Victoria regions while at the coast the annual cycle was dominant. The frequency of occurrence of the short periodicity was more in urban stations than rural stations. The concurrence of the annual and semi-annual cycles at a given time produced high peak of temperature values at that time. Trend analysis of monthly, seasonal and annual temperature in each of the stations further confirmed that  $T_{\min}$  has more increasing trends and that the urban stations have higher rates of increase of the  $T_{\min}$  than the rural stations. Trends of annual daily maximum temperature indices indicated that the percentage of the time when daily maximum and daily minimum temperature is greater than the 90<sup>th</sup> percentile is increasing while the percentage of the time when daily minimum temperature is less than the 10<sup>th</sup> percentile is decreasing; this implies that nights and days are warming while cool nights are decreasing. Further this study has shown that there exists significant relationships between the increasing trends in local temperatures (especially  $T_{\min}$ ) and the global warming and the relationship is stronger in rural areas than urban areas.

The implications of the observed trends and variability of temperature to urban design storms would be mainly through the influence of temperature on rainfall characteristics in urban

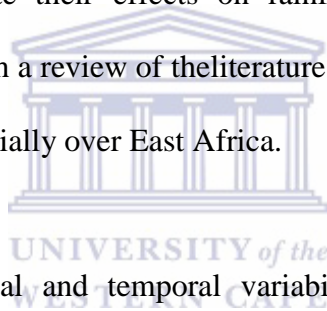
areas. Other factors such as the urban heat island (UHI) effect that could be influencing urban temperature were explored further in Chapter 4 and the effects of temperature changes (including UHI effect) on rainfall patterns in urban areas are investigated in Chapter 5.



### 3 CHAPTER 3: TEMPORAL VARIATIONS OF RAINFALL

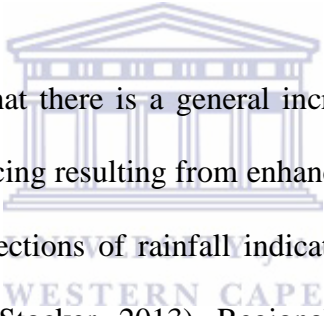
#### 3.1 Introduction

The aim of Chapter 3 is to investigate variability and possible changes over time of rainfall of urban and nearby rural areas. The comparative analyses of rainfall characteristics of urban and nearby rural areas form a basis upon which effects of temperature and urbanization on rainfall (Chapter 5), and the statistical analysis of extreme value were investigated (Chapter 6). In this part of my thesis, I used rainfall from sixteen (16) stations within urban areas of the four major towns (Nairobi, Mombasa, Kisumu, and Nakuru) and their rural neighbourhoods for analysis. The El Niño Southern Oscillation (ENSO) and the Indian Ocean Dipole (IOD) indices were used to investigate their effects on rainfall variability in the urban and rural areas. The Chapter starts with a review of the literature on spatial and temporal variations and changes of rainfall, and especially over East Africa.



The understanding of the spatial and temporal variability of rainfall is important for sustainable water resources as well as storm water management in both urban and rural areas. Studies have emphasized that global warming will increase rainfall variability and increase flood risks in many regions of the world (Jung, et al., 2011; Tabari, et al., 2012). Over the African region, studies have shown varied results in the changes of the variability of rainfall. For instance, Omondi, et al. (2014) analysed daily rainfall for the 1960-2006 period over the greater Horn of Africa (GHA) and reported a significant decrease in total rainfall for wet days (with rainfall more than 1mm), while New, et al. (2006) found mixed trends in rainfall extreme indices over the southern and western Africa region. From these studies, rainfall has mixed trend patterns over the African region with some countries having generally no trends in annual and seasonal rainfall. Most of the studies of rainfall characteristics in the EEA region are usually too coarse in spatial resolution (using only a few representative stations for

each country) and focused on trend analysis of indices of extreme daily rainfall. These results may not be directly applicable to storm water management at the urban area scale. Moreover, most of these studies did not indicate whether there were differences in rainfall variability between urban and rural areas although urbanization and other land use changes may cause such differences (Callejas, et al., 2011; Borges, et al., 2013). Again the response of the rainfall characteristics to climate change in urban and rural areas of the EEA needs to be understood for effective stormwater management. The comparative analysis of rainfall characteristics in urban and rural areas forms a basis for understanding possible changes in rainfall patterns that are important to modelling of urban design storm applicable instormwater management systems.



The fifth IPCC report indicated that there is a general increase in precipitation globally in response to the anthropogenic forcing resulting from enhanced moisture content in a warmer atmosphere, and that model projections of rainfall indicate an increase in extreme rainfall associated with global warming (Stocker, 2013). Regional studies on changes of climate extremes have confirmed that various indices of rainfall have changed particularly over the last four decades (New, et al., 2006; Anguilar et al., 2009; Donat, et al., 2014; Omondi, et al., 2014). Unlike the temperature extremes, precipitation has shown mixed regional trends with some regions showing increasing, others decreasing and even no trends. For instance Jhajharia, et al. (2012) reported mixed trends of total rainfall at monthly, seasonal and annual time scales over the northeast India, while Beguería, et al. (2011) reported no evidence of a generalized trend in extreme rainfall over northeast Spain. Mazvimavi, (2010) reported no significant change in annual rainfall over Zimbabwe.

Noticeable influence of human activities on rainfall patterns has been reported in some parts

of the world especially in urban areas; for example, Opija et al. (2007) found marked increase of heavy rainfall intensities attributable to anthropogenic changes over Nairobi (Kenya) area while Marengo et al. (2013) found increase in total and heavy rainfall and decrease in light rains over São Paulo metropolitan area (Brazil), and suggested that effects of urbanization were significant. However comparative studies on the spatial and temporal variations of rainfall within the fast growing urban and their neighboring rural areas of the equatorial EA region are limited. Such studies are important for understanding the challenges of urban storm water management taking into account local and global climate changes.

### **3.1.1 Climatology of rainfall over the EEA region**

Most of the annual rainfall over the tropics occurs within the tropical convergence zones such as the Inter-Tropical Convergence Zone (ITCZ) over the Pacific, Atlantic and Africa equatorial belt, the South Pacific convergence zone (SPCZ) over central south Pacific, and the South Atlantic Convergence Zone (SACZ) over southern America and southern Atlantic (Asnani, 1993). Over the equatorial African region, the beginning and end of the rainy seasons coincide with the arrival and the withdrawal respective of the ITCZ, which is mainly responsible for the inter-annual and intra-seasonal variability of rainfall (Bowden and Semazzi, 2007; Gitau, et al., 2014). The different scales of variability (diurnal, seasonal, annual and decadal) of rainfall in this region have mainly been linked to changes in the sea surface temperatures (SST) of the Indian and Atlantic oceans (Mukabana and Pielke, 1996), and the El Nino Southern Oscillation (ENSO) anomalies (Giannini, et al., 2001). However Marchant, et al. (2007) indicated that the dominant driver of the EA rainfall variability is the variation of the Indian Ocean sea surface temperatures (SSTs); the main feature being the Indian Ocean dipole (IOD). The IOD has been shown to influence rainfall through either



anomalous low-level easterly flow of moist air into the continent (Shongwe, et al., 2011), or a weakening of the low level westerly flow over the northern Indian Ocean that carries moisture away from the continent (Black, et al 2003). The effect of the IOD is more evident in the OND rainy season than in MAM although William and Funk, (2011) suggested that a reduction of MAM rains over Kenya and Ethiopia could be a response to a warmer Indian Ocean SSTs. In the EA region, other climate systems that drive the inter-annual variability are the monsoon winds, the relative positions and intensities of the pressure gradients of the equatorial low pressure (in the ITCZ), and the subtropical high pressure zones, that determine the areas of convergence between the south-easterly and north-easterly monsoon winds (Okoola, 1999). The SSTs of the adjacent oceans determine the moisture content the monsoons winds bring to the EEA region (Manatsa, et al., 2013). The interaction between the large scale flow and the localized circulations of thermal and orographic origins largely govern the spatial distribution of rainfall. The climatological large scale systems control the inter-annual and intra-seasonal variability of rainfall over Kenya, while the meso-scale and the local circulations mainly control spatial and diurnal variability (Mukabana and Pielke, 1996; Indeje, et al., 2000). Studies done in the EEA region have not considered the urban effects on rainfall characteristics that are likely to affect storm water management systems. I therefore undertook to investigate variability and possible changes of rainfall characteristics at daily, monthly, seasonal and annual time scales within and in the neighbourhood of the four major towns of Kenya. The Chapter form the foundation upon which the effects of enhanced temperature (observed in Chapter 2) on rainfall in urban areas were investigated (Chapter 5).

### 3.2 Data types and sources

Daily and monthly total rainfall time series for some urban and rural stations around the four main towns of Kenya (Nairobi, Mombasa, Kisumu and Nakuru) were collected from the Kenya Meteorological Department (KMD). From rainfall data, various variables were prepared for each station for the comparative analysis of urban and rural rainfall variations. The variables included: i) annual total rainfall; ii) seasonal total rainfall for MAM, JJA and OND; iii) monthly total rainfall, and; iv) daily extreme rainfall indices as defined by Expert Team on Climate Change Detection Monitoring and Indices (ETCCMDI) (Table 3.1) and prepared using the RClimDex software (Zang and Yang, 2004) described in Chapter 2, Section 2.6.4.

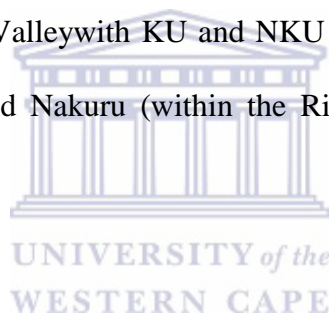


**Table 3.1: Indices of daily rainfall extremes used in this study**

Index	Index Name	Index definition	units
<b>RX1day</b>	Max 1-day rainfall amount	Monthly maximum 1-day rainfall	mm
<b>RX5day</b>	Max 5-day rainfall amount	Monthly maximum consecutive 5-day rainfall	mm
<b>SDII</b>	Simple daily intensity index	Ratio of daily amount to the number of wet days ( $\geq 1 \text{ mm}$ )	mm/day
<b>R10</b>	Number of heavy rainfall days	Annual count when rainfall $\geq 10 \text{ mm}$	days
<b>R25</b>	Number of heavy rainfall days	Annual count when rainfall $\geq 25 \text{ mm}$	days
<b>CDD</b>	Consecutive dry days	Maximum number of consecutive days when rainfall is $\leq 1 \text{ mm}$	days
<b>CWD</b>	Consecutive wet days	Maximum number of consecutive days when rainfall is $\geq 1 \text{ mm}$	days
<b>R95p</b>	Very wet days	Annual total rainfall $>95\%$ percentile	mm
<b>R99p</b>	extremely wet days	Annual total rainfall $>99\%$ percentile	mm
<b>PRCPTOT</b>	Annual total wet day rainfall	Annual total rainfall from days $\geq 1 \text{ mm}$	mm

### 3.2.1 Description of rainfall stations

The heterogeneous terrain of Kenya makes the country to have diverse climatic zones where localized circulations of thermal and orographic origin greatly influence the rainfall and thus creating significantly different rainfall patterns from one region to the other. Indeje, et al. (2000) delineated zones according to inter-station annual rainfall correlations with the highly correlated stations in a given region forming a homogeneous zone (Fig 3.2). Using Indeje, et al. (2000) classification, rainfall stations in my Thesis (Table 3.2) fell into the following categories: a) the stations over the coastal region, with Mombasa (MU) representing the urban station of Mombasa urban area, are in Zone I; b) stations over the central highlands of Kenya with Wilson airport (NU) as the urban station are located in zone III; and; c) stations located in the western region and the Rift Valley with KU and NKU representing the urban stations in Kisumu (near Lake Victoria) and Nakuru (within the Rift Valley) towns respectively are located in Zone VI.



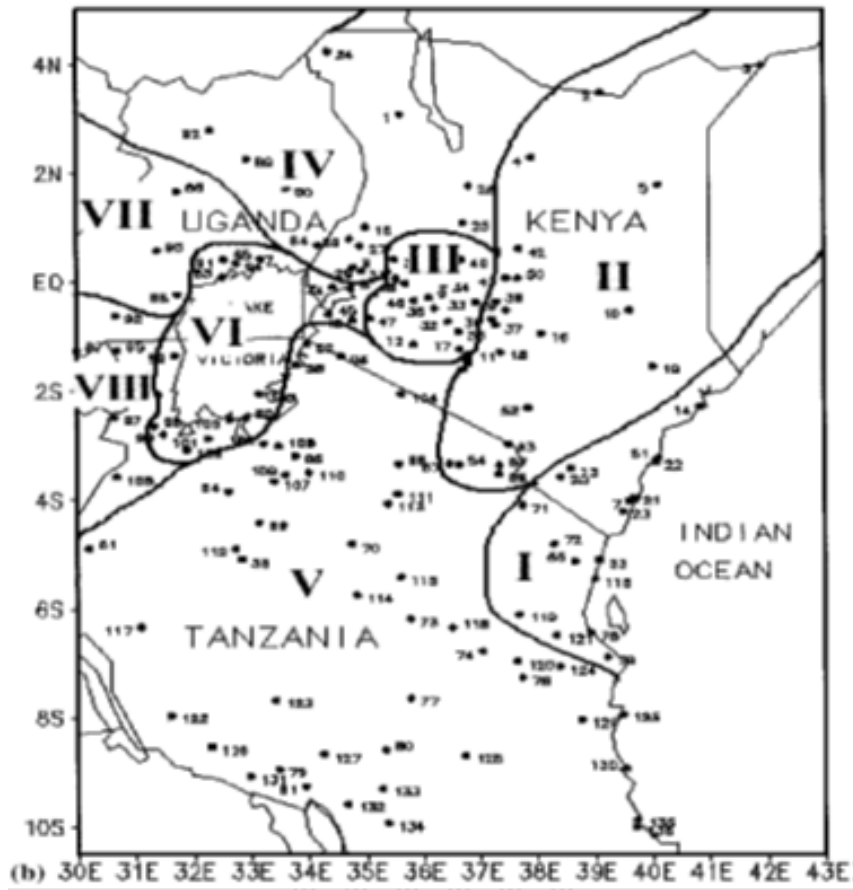


Figure 3.1: The eight homogeneous rainfall zones of East Africa (adopted from Indeje, et al., 2000)

**Table 3.2: Stations used for analysis of rainfall**

Meteorological Station Number	Station name	Station acronym	Latitude °S(-) /°N (+)	Long. (°E)	Altitude (m)	Length of rainfall data
9136130	Wilson	NU	-1.32	36.82	1679	1961-2013
9136164	Dagoretti	NR <sub>D</sub>	-1.30	36.70	1798	1961-2013
9137048	Thika	NR <sub>T</sub>	-0.98	37.07	1549	1961-2013
9138050	Nyeri	NYR	+0.43	36.97	1815	1970-2008
9034021	Mombasa	MU	-4.03	39.18	55	1961-2013
9339036	Mtwapa	MR <sub>Mt</sub>	-3.93	39.73	20	1961-2013
9340007	Msabaha	MR <sub>Ms</sub>	-3.27	40.05	91	1961-2013
9237000	Makindu	MKD	-2.28	37.83	1000	1961-2008
9338001	Voi	VOI	-3.70	38.57	560	1961-2008
9340008	Malindi	MLD	-3.23	40.10	20	1961-2008
9240001	Lamu	LAM	-2.27	40.90	30	1961-2008
9135001	Narok	NRK	-1.13	35.83	1890	1961-2008
9034025	Kisumu	KU	-0.10	34.70	1146	1961-2013
8334096	Kakamega	KKM	+0.28	34.75	1580	1961-2008
9034088	Kisii	KR	-0.68	34.73	1493	1963-2013
9036261	Nakuru	NKU	-0.27	36.12	1901	1970-2013

### 3.2.2 ENSO and IOD data

Rainfall variability in the EEA region has been associated with several modes of climate variability mainly ENSO and IOD. The El Niño tends to cause above average rainfall during the OND season, and the La Nina results in depressed rainfall during the same season. Positive IOD mode is associated with above normal rainfall (Indeje, et al., 2000; Clark, et al., (2003); Nicholson, 2014; Nicholson, 2015). As such, I used these two indices to examine their influence on the urban and rural rainfall characteristics in different climatic zones. ENSO in this study was represented by the NINO 3.4 SST index which is sea surface

temperature anomalies over the central equatorial Pacific (5°N-5°S and 120°-170°W). The mean monthly standardized values of this variable were obtained from the National Oceanic and Atmospheric Administration (NOAA) database (<http://www.cpc.noaa.gov/data/indices/CPC>). Mean monthly standardized indices of the Indian Ocean dipole (IOD) index were obtained from the Japanese agency for Marine-Earth Science and Technology (<http://www.jamstec.go.jp/frsgc/research/d1/iod/>); the IOD index is defined as the standardized anomalies of the difference between the sea surface temperature (SST) in the western (50°-70°E and 10°N/S) and eastern (90°-110°E and 10°N/S) equatorial Indian Ocean. The two variables were computed into seasonal and annual variables according to the corresponding rainfall variables.



### **3.3 Data quality control and methods of analysis**

Climatological records often contain errors, missing values, and other inconsistencies that should be checked before analysis. The missing rainfall values were estimated using correlation and regression methods described in Chapter 2 Section 2.5. The data were then tested for homogeneity using mass curves.

Rainfall was analysed to establish spatial and temporal variations at different time scales for stations within urban and neighbouring rural areas of the major urban areas of Kenya. Temporal and spatial variability and possible trends of monthly, seasonal and annual rainfall totals and daily rainfall indices were investigated using various methods that included the quantile regression; Mann-Kendall trend tests and the continuous wavelet transform (CWT). CWT is a valuable tool that is applied on rainfall data to discriminate temporal and spatial

variability of rainfall (Nakken, 1999; Nicholson, 2015). The CWT method interprets a rainfall time series by extracting the relevant information from the series as frequency components through transforming without changing it (Torrence and Compo 1998; Adamowski, et al., 2013). The strength of the wavelet transform method is in its ability to detect multiple cycles in a time series and how these cycles vary with time. Such cycles may influence results of trend tests when assumed absent.

The detailed description of the linear regression and Mann-Kendall trend test methods were presented in Chapter 2 (Section 2.5) and will be applied in this Chapter for rainfall analysis, since the methods are also suitable for testing trends in rainfall time series and have been widely used in rainfall analysis (Mazvimavi, 2010; Kruger and Sekele 2013; Omondi, et al., 2014). CWT method was also discussed in detail in Chapter 2 (Section 2.5) and will be applied in this Chapter by substituting the temperature variable  $T(t)$  in equations of transformation with the rainfall variable  $Y(t)$ . Some of the analyses methods not discussed in Chapter 2 and are used in the analysis of rainfall are discussed below.

### **3.3.1 Quantile regression**

Quantile regression (QR) is a method of estimating the relationships between one or more covariates and the conditional quantile of the response variable. It was developed in the 1970s as an extension of the linear model for approximating rates of change (Koenker and Bassett, 1978). The QR parameter estimates the change in a specified percentile of the response variable produced by a change in the predictor variable. Unlike the linear regression that assumes that the response is only affected by location (50<sup>th</sup> percentile) of the distribution, the QR provides a complete picture of the conditional distribution of the response variable when both the lower and the upper or all the quantiles are of interest. In the analysis of

change of rainfall characteristics, all quantiles of the rainfall variable are important; particularly, changes in the upper quantiles of rainfall in urban areas that would enhance flooding. The parameters estimated are semi-parametric since no parametric distribution is presumed for the random error part of the model, although a parametric form is presumed for the deterministic portion. The conditional quantiles denoted by  $Y(\kappa|t)$  are the inverse of the conditional cumulative distribution function of the response variable  $Y^{-1}(\kappa|t)$  where  $\kappa \in [0,1]$  signifies the quantiles. The QR estimates are an ascending sequence of planes that are above an increasing segment of sample observations with increasing value of the quantiles ( $\kappa$ ).

The linear function of rainfall variable  $Y(t)$  is given by:

$$Y(\kappa|t) = \beta_0(\kappa) + \beta_1(\kappa)t + \varepsilon \quad (3.1)$$

where,  $Y(\kappa|t)$  is the conditional quantile of rainfall,  $Y(t)$  is the rainfall time series of interest (e.g., annual or seasonal) and  $t$  is the time (the independent variable or covariate); the  $\kappa$  indicates that the parameter are for a specified quantile  $\kappa$  ( $0 < \kappa < 1$ );  $\beta_0$  and  $\beta_1$  are the intercept and slope respectively, and  $\varepsilon$  is the random error of the QR model.

To detect the presence of trend for any given percentile in the rainfall time series, the  $\beta_1(\kappa)$  was evaluated. A positive (negative)  $\beta_1(\kappa)$  that is significantly different from zero at a given level of significance (5% in this case) would be an indicator of increasing (decreasing) trend of the time series in quantile  $\kappa$ . I used the “quantreg” software developed by Koenker (2006) and written in R language (<http://www.r-project.org>) to evaluate the coefficients of the quantile regression model (Equation 3.1) applying the rank inverse method. With this software I also estimated the standard error, the t-statistic, the p-value and the confidence intervals of the coefficients. The advantage of the QR over the simple linear regression is that it is able to



describe the response of both variables with constant slope in all quantiles and those with varying slopes from one quantile to another (Mazvimavi, 2010). The 10<sup>th</sup> 20<sup>th</sup> and 30<sup>th</sup> quantile were considered to designate low rainfall while the 70<sup>th</sup> 80<sup>th</sup> and 90<sup>th</sup> are heavy rainfall percentiles.

### **3.4 Results and discussion**

#### **3.4.1 Estimating missing values and homogeneity test**

The method of inter-station correlations of neighbouring stations discussed in Chapter 2, Section 2.4 was used to estimate missing values in the monthly rainfall time series. The complete time series was then checked for errors and other inconsistencies.

Lack of homogeneity in data may occur due to station relocations, equipment changes, equipment drifts, changes in the method of data collection, and changes in the general surroundings of a station. The rainfall data underwent homogeneity testing to identify any breakpoints which may have resulted from non-climate factors. The data for the sixteen rainfall stations were fairly homogeneous as indicated by results of mass curves of some stations (Figure 3.2).

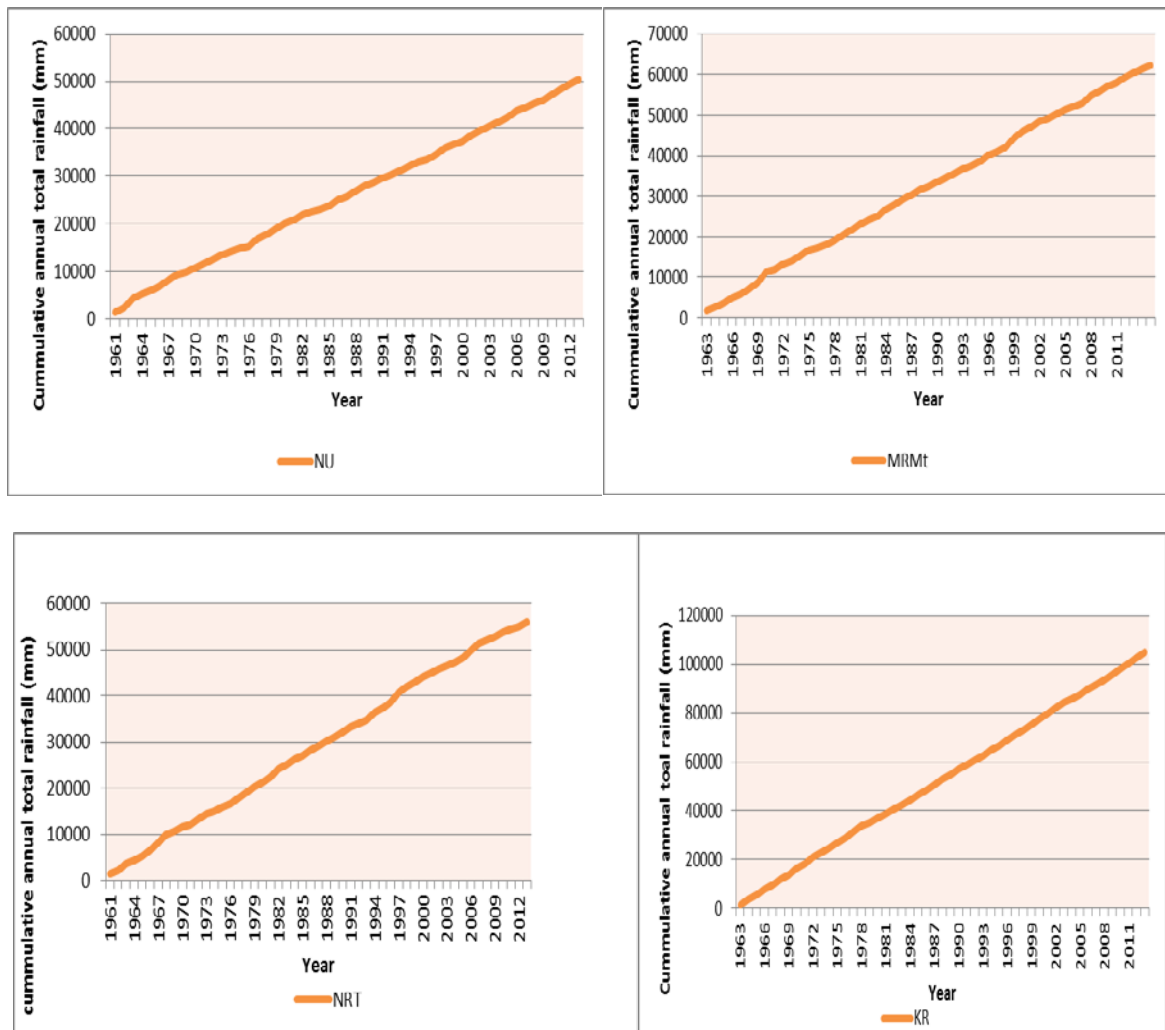


**Figure 3.2: Mass curves of rainfall of some stations showing rainfall homogeneity**

### 3.4.2 Spatial and temporal variability of rainfall

The mean total annual rainfall for the stations within and close to the four major towns of Kenya ranges from 500 to 2000 mm/year (Fig 3.3(a)). MKD and VOI stations are situated in the lowlands between the central highlands and the coastal plains and have the lowest mean annual rainfall in the range of 500-600mm/year. Over the central highlands (NU, NR<sub>D</sub>, NYR and NR<sub>T</sub> stations) and Rift valley (NKU), the mean annual rainfall ranges between 900 and 1000 mm/year, while the coastal region receives mean annual rainfall ranging between 1000 to 1200 mm/year. The western region of Kenya has the highest mean annual rainfall; KR and KKM stations have mean annual rainfall of 1800 and 2000mm/year respectively. The seasonal

variations follow the same pattern, with the MAM season providing almost half of the annual total rainfall at most stations. The rural stations have in general higher mean annual total rainfall than the urban ones; for example NR<sub>D</sub> (1065 mm/year) is higher than NU (948 mm/year), MR<sub>Mt</sub> (1276mm/year) is higher than MU (1056 mm/year) and KR (2060 mm/year) is much higher than KU (1379 mm/year).

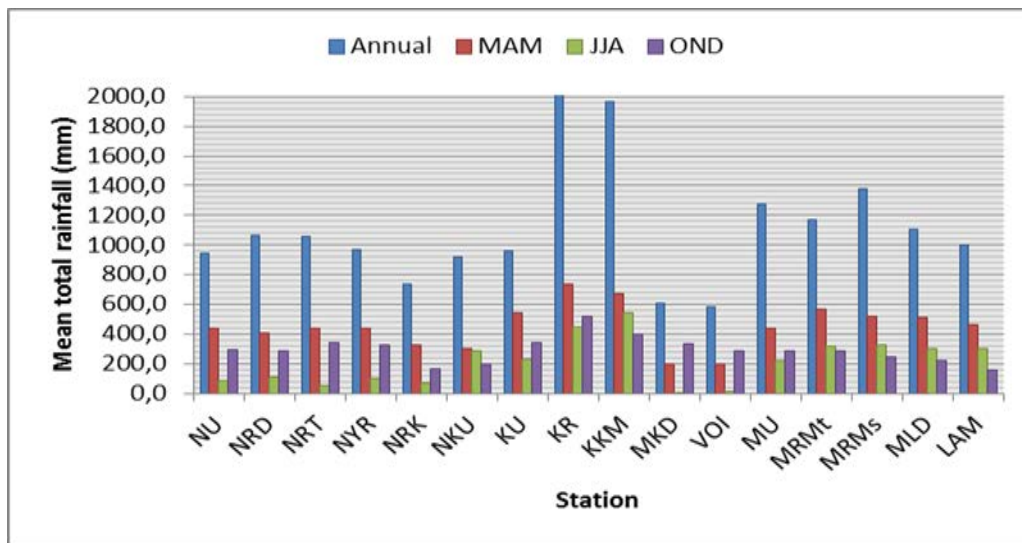


**Figure 3.3: Spatial variation of the mean annual and seasonal rainfall**

The spatial difference between the urban and rural stations could however not be attributed to effects of urbanization alone since other factors, such difference in altitude between the urban and rural stations could also play a part. Opija, et al. (2007) suggested that the spatial variability of rainfall over Nairobi result from forest distribution in the less built-up areas enhancing the humidity field conducive for convective activities, while Mukabana and Pielke, (1996) attributed spatial variability to differences in altitude. The mean annual rainfall is mainly contributed by the two rainy seasons that occur during the transition of the monsoon wind circulations. During MAM, the ITCZ moves slowly over the EEA region with resultant heavy rainfall for a longer period (Okoola, 1999). On the other hand during the OND

season, the ITCZ migrates rapidly southwards and the season is characterized by heavy rains of relatively short duration as illustrated in Figure 3.4.

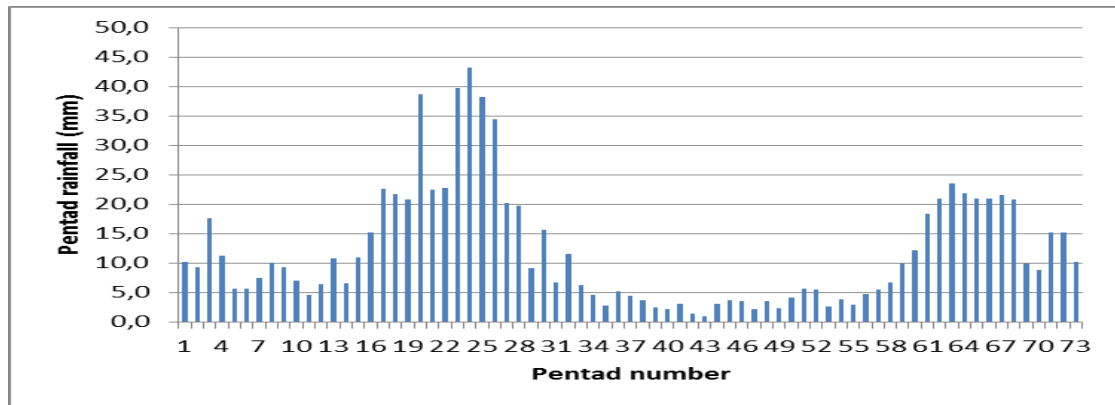


**Figure 3.4:**An example from NU station showing the mean pentad distribution of rainfall within a year. (MAM spread from about the 13<sup>th</sup> to the 30<sup>th</sup> pentad while OND is from pentad 58 to 70); mean 5-day rainfall total

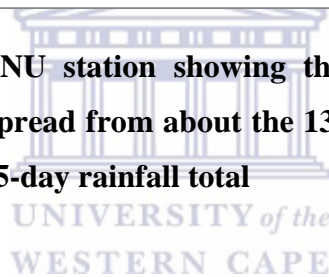
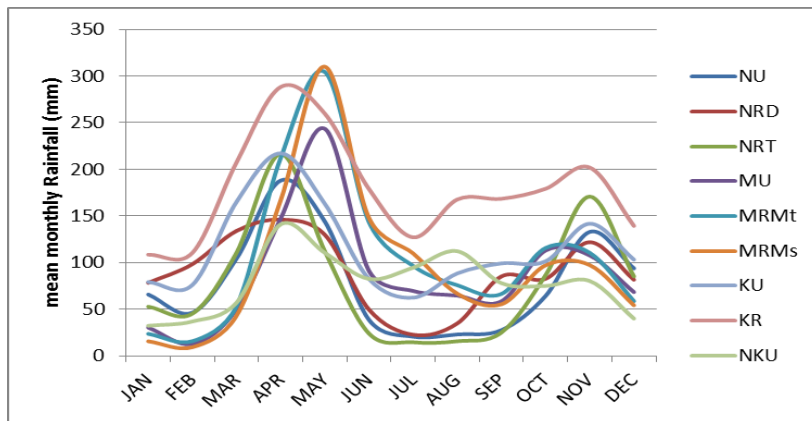
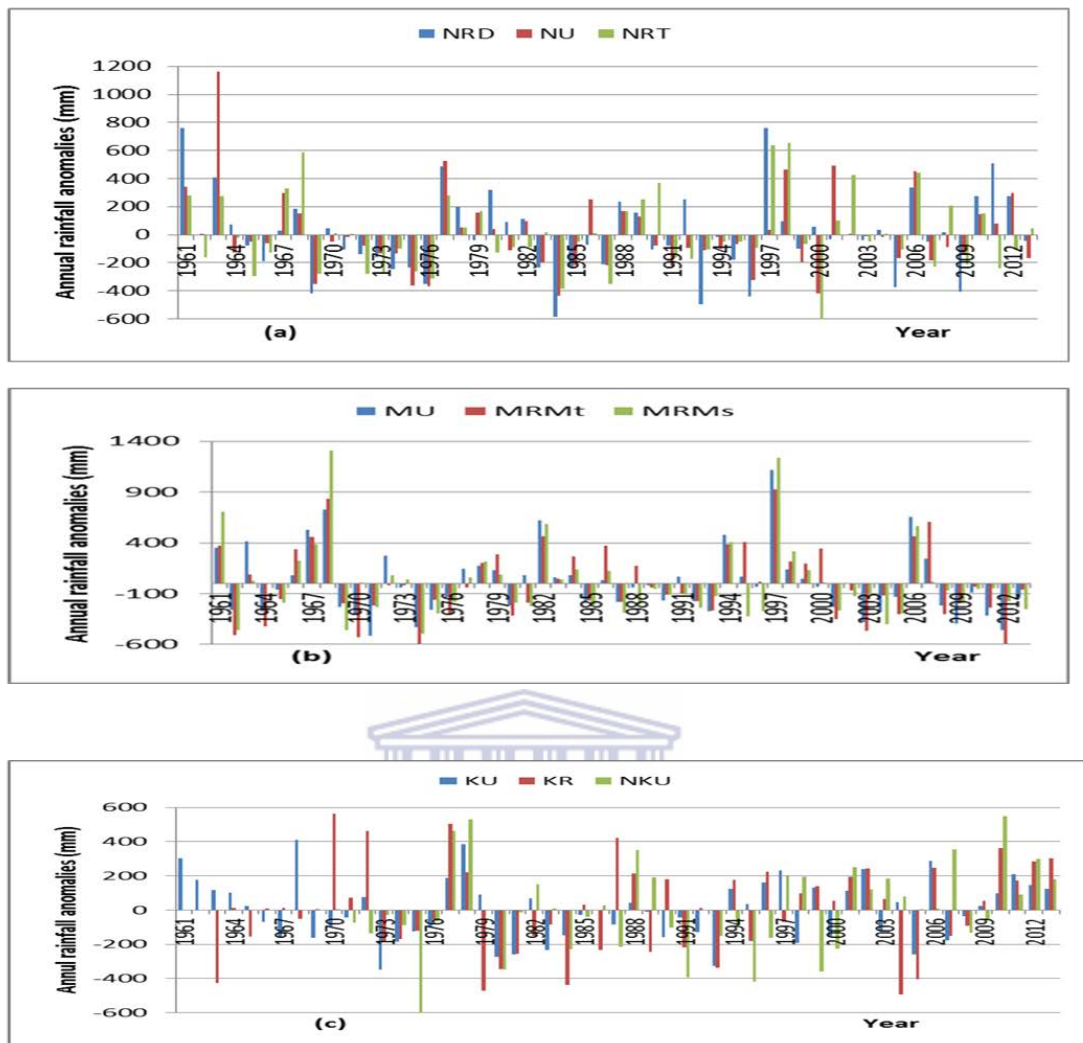


Figure 3.5 depicts the mean spatial variations of the monthly rainfall showing when peak rainfall is received at stations in different climate zones. The stations over the central highlands (NU, NR<sub>D</sub> and NR<sub>T</sub>), the Rift Valley (e.g., NKU) and the western Kenya highlands (e.g., KU and KR) have a first peak rainfall in April (with the highest amount received in the western Kenya region). The coastal stations (e.g. MU, MR<sub>Mt</sub> and MR<sub>Ms</sub>) receive their first peak in May (with highest totals of about 300mm/month in MR<sub>Ms</sub> and MR<sub>Mt</sub>); the second peak in the year is in November for all stations. Some stations over the coastal and the Rift Valley regions have significant amounts of rainfall during the months of June, July and August that forms the JJA season.



**Figure 3.5: Spatial variability of the mean monthly rainfall depicting the bimodal rainfall characteristics and seasonal peak months of some stations from each climatic zone**

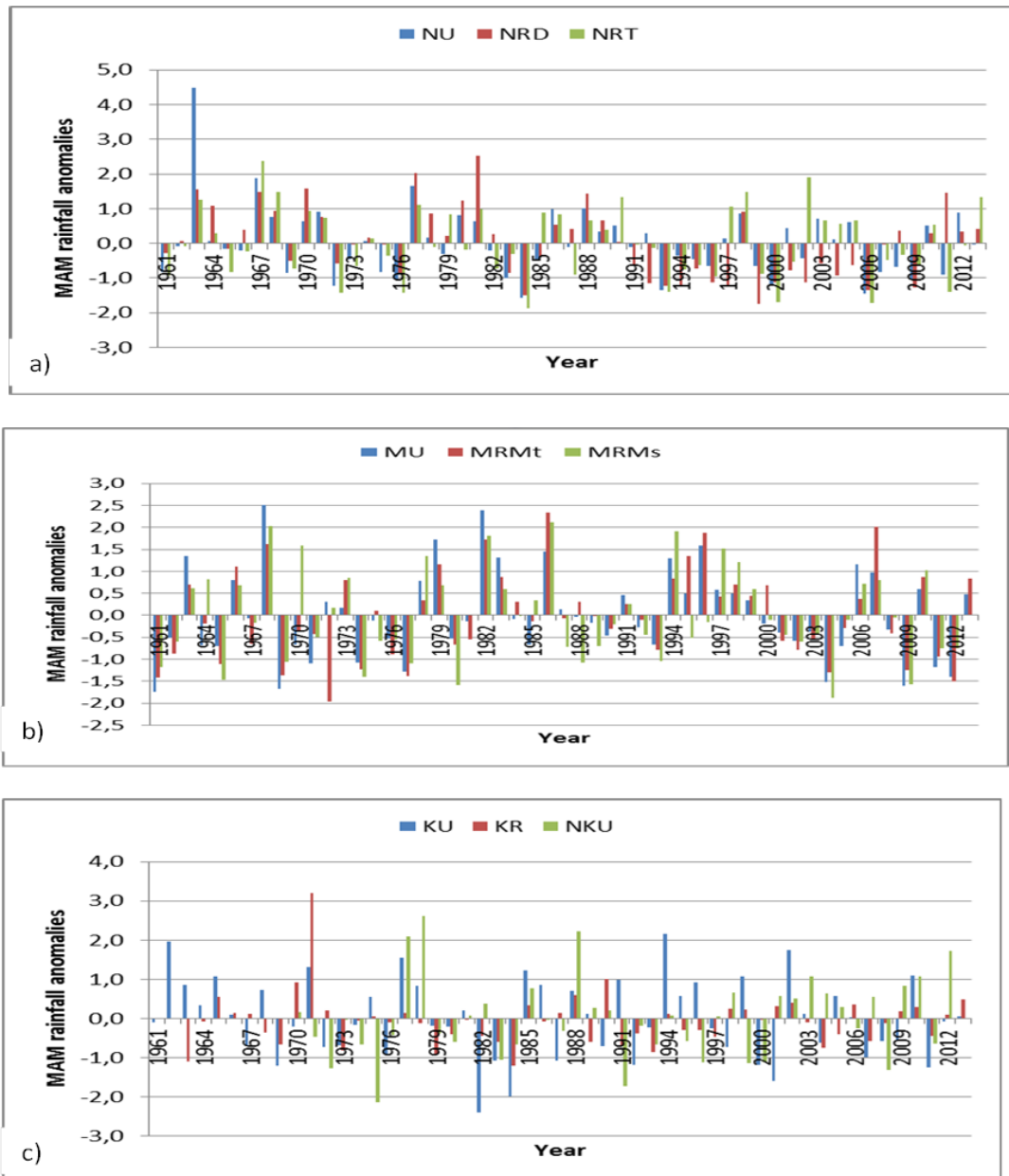
Apart from the spatial variability, rainfall over the EEA region has high inter-annual variability. Anomalies of annual total rainfall showed that there were a group of years with annual rainfall above (below) the mean for each station (Fig 3.6(a-c)). For example, annual rainfall between 1970 and 1976 was below the mean at all stations, while 1979-1987 annual rainfall was below the mean over the western highlands and 2001-2006 and 2008-2013 the coastal stations annual rainfall was below average. On the other hand, the coastal region between 1996 and 2000, western highlands from 2009 to 2013 and central highlands from 2008 to 2012 had above average rainfall. Inter-annual variability of the seasonal rainfall influences the annual rainfall outcome.



**Figure 3.6: Temporal variability of annual total rainfall for urban and rural stations over; a) central Kenya highlands; b) coastal region; c) Lake Victoria region and the Rift Valley**

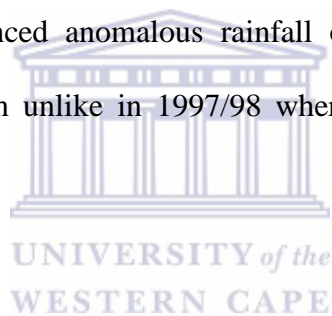
Figure 3.7 shows the inter-annual variability of seasonal rainfall received in MAM at stations representing the different climatic zones. Over the central highlands of Kenya, some years had rainfall that was more than two standard deviations ( $2\sigma$ ) above the mean e.g., 1963 (NU), 1967 (NR<sub>T</sub>), 1978 and 1981 (NR<sub>D</sub>). However, from 1982-2013, no year had seasonal rainfall equal to or more than  $2\sigma$  for all stations within the central highlands. Over the coastal region, 1967, 1981, 1986 and 1998 had rainfall of  $2\sigma$  above the mean, but in none of the years was

seasonal rainfall anomalies lower than  $-2\sigma$ . Over western Kenya, very few years had rainfall above or below  $2\sigma$ ; e.g., KU in 1967 & 1994 and NKU in 1978 and 1988 had rainfall equal to or more than  $2\sigma$  above the mean.



**Figure 3.7: Temporal variability of MAM seasonal rainfall for urban and rural stations; a) central highland; b) Coastal region and; c) western Kenya and Rift Valley; the mean and standard deviations were calculated from the whole length of the time series (1961-2013)**

Considering the OND season, over the central highlands and the coast region, high rainfall values exceeding  $3\sigma$  above the mean were observed in several years (Fig 3.8). For example, 1961 over the central highlands, and 1997 over the coast; the seasonal rainfall was close  $5\sigma$  above the mean. The western Kenya had rainfall of close to  $3\sigma$  above the mean in 1961 and 1997. No year in the three regions had rainfall in OND of  $2\sigma$  below the mean for the period considered (1961-2013). What I observed to be unusual was that the coastal region had the lowest values of the standardized anomalies compared to stations from the central and western Kenya highland in 1961 (Fig 3.8(ii)); the year which has been documented in literature to have had the worst floods in EEA in recent times. This observation would suggest that factors that influenced anomalous rainfall of 1961 over the EEA had less influence over the coastal region unlike in 1997/98 where anomalously high rainfall was recorded at the coast.





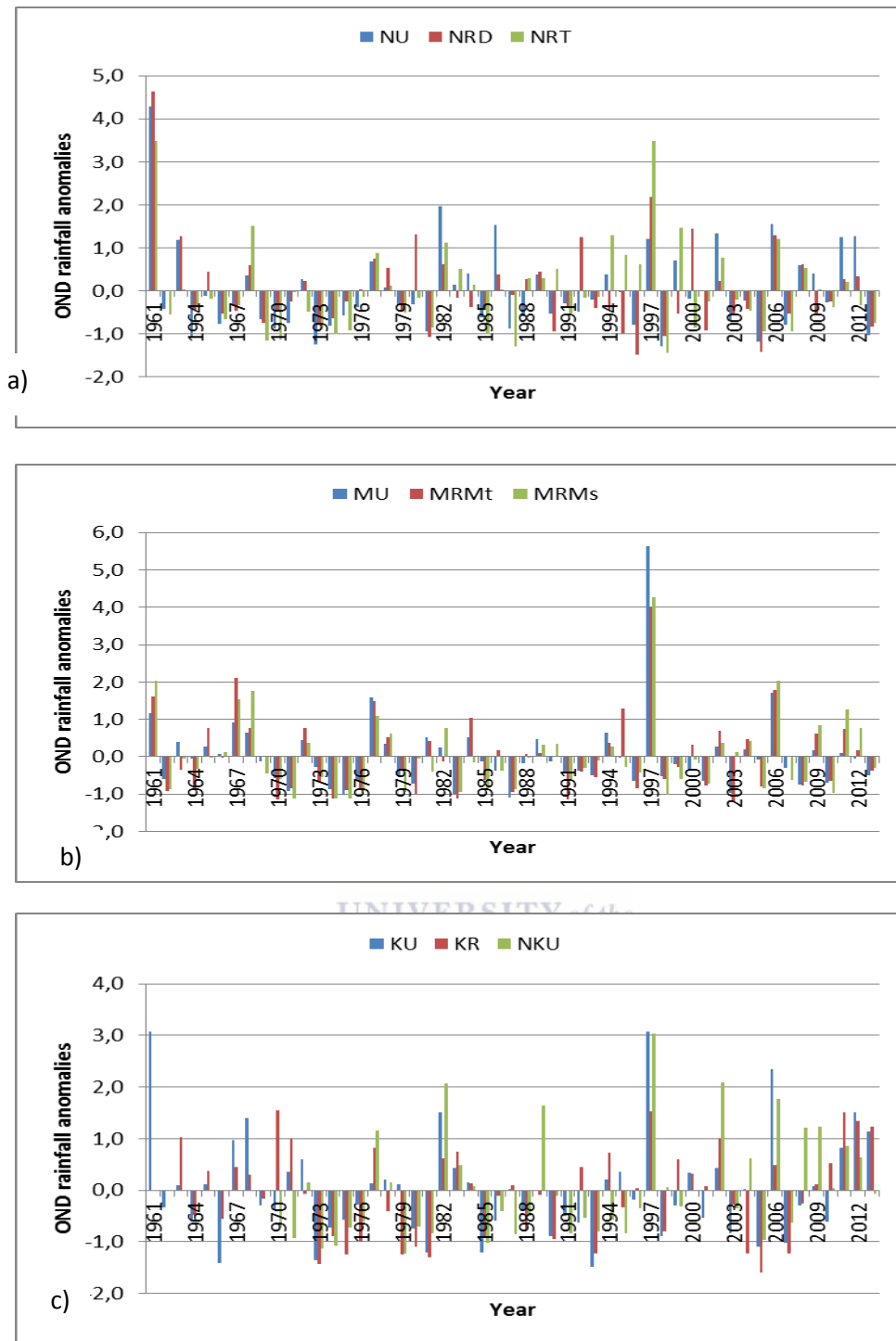


**Figure 3.8: Temporal variability of OND seasonal rainfall for urban and rural stations; a) central highland; b) coastal region and; c) western Kenya and Rift Valley**

From the observed temporal behaviour of the annual and seasonal rainfall, further analysis using the continuous wavelet transform CWT analysis of monthly rainfall was done to examine the persistence and the cyclic behaviour of the observed variabilities.

### **3.4.3 Exploring rainfall variability using CWT**

The basic aim of the CWT analysis is to determine the dominant frequency components (periodicities) at a given time and the characteristics of these components over time in order to ascertain the nature and persistence of the modes of rainfall variability. I subjected the monthly rainfall totalsto the CWT analysis using one-month time step and scales (periods) of powers of 2. As discussed in detail in Chapter 2, Section 2.5, the CWT maps the spectral characteristics of the time series onto a time-frequency (time-period) plane from which the significant dominant periodicities can be observed and related to rainfall variability. The temporal distribution of the frequency components of the rainfall time series signal was found by successively passing stretched and compressed functions of a Morlet wavelet according to Equation (2.2) as described in Chapter 2, Section 2.5.

#### ***CWT analysis of monthly rainfall in and around Nairobi***

Figure 3.9 (a) are the WPS plots showing the variability of spectral power of monthly rainfall time series at an urban (NU) and a nearby (NR<sub>D</sub>) station respectively, while Fig 3.9 (b) are the time series plots of monthly rainfall at the same stations. The general similarities of the features of the WPS plots of these two stations are an indication that they belong to same rainfall homogeneous zone and hence the rainfall is controlled by the same large-scale climate systems. The most dominant periodicities are semi-annual cycles (4-6 month) that represent the seasonality of rainfall. Quasi-annual cycles (8-16 months periodicities) were also observed in each WPS plot which would imply the inter-annual variability of rainfall caused by climate

modes of variability that influence the EEA rainfall. Other less common features are the high-frequency cycles (1-4 months periodicities) and an isolated low-frequency cycles (32-64 months periodicities) that are observed in both stations between 1995 and 1998. Particularly notable was the high peak rainfall observed in years when there was simultaneous occurrence of multiple periodicities (particularly the annual and semi-annual cycles). For instance in 1961, 1967, 1978, 1998 had high rainfall peaks. However, there were no observable trends in the monthly rainfall time series plots Fig 3.9 (b). The spatial differences in rainfall variability between the urban and rural stations were mainly observed in occurrence of the high frequency cycles, but were not conspicuous.

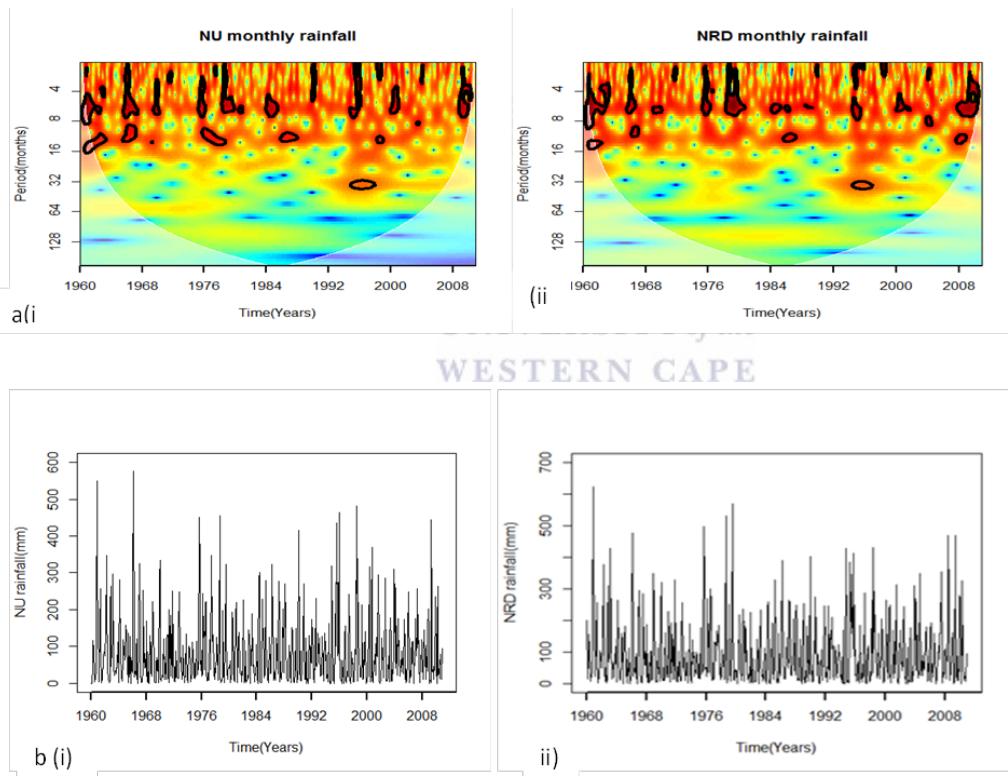


**Figure 3.9:** a) The wavelet power spectra of rainfall time series of; i) NU and; ii) NR<sub>D</sub> stations; the black contours mark the significant periodicities at 95% confidence level while the white U-shaped curve marks the COI. The colour code is such that blue is for low spectral energy and red is high energy; b) The variability of monthly rainfall total over time of; i) NU and; ii) NR<sub>D</sub>

### *CWT of monthly rainfall in and around Mombasa*

Figure 3.10 (a) shows the spectral power variance of rainfall time series of an urban (MU) and nearby rural ( $MR_{Mt}$ ) station near Mombasa town. The general observations of rainfall variability at the coast are the dominant semi-annual cycles (4-6 months periodicities) representing the seasonality of rainfall and a few periodicities of 8-16 months that only appeared after 1963. The high-frequency features (periodicities of 1-4 months) were also frequent at both the urban and rural stations implying local effects on rainfall probably as a result of land-seas breezes. Inter-station differences were observed in the WPS plots such that MU has quasi-annual cycle only between 1980 and 1981 with high rainfall peak (Fig 3.9(b)) while  $MR_{Mt}$  has more frequent annual cycles, especially between 1980 and 2000. Again a low-frequency feature (periodicities of 16-32 months) was observed in the WPS plot of MU between 1995 and 2000 and not in the other stations (although the spectral energy is also high). The infrequent occurrence of the quasi-annual cycles would imply that the mode of climate variability that influences the inter-annual variability of rainfall over the coastal region is less common than over the central highlands. For instance, 1961-1962 had significant annual cycles over the highland that are conspicuously absent from the coast. High monthly rainfall peak values in the time series plots (Fig 3.10(b)) were observed when multiple cycles occurred simultaneously; for example, in 1997 to 2000, and from 2006 to 2008 in both stations. However, no temporal trends were observable in the rainfall time series plots.

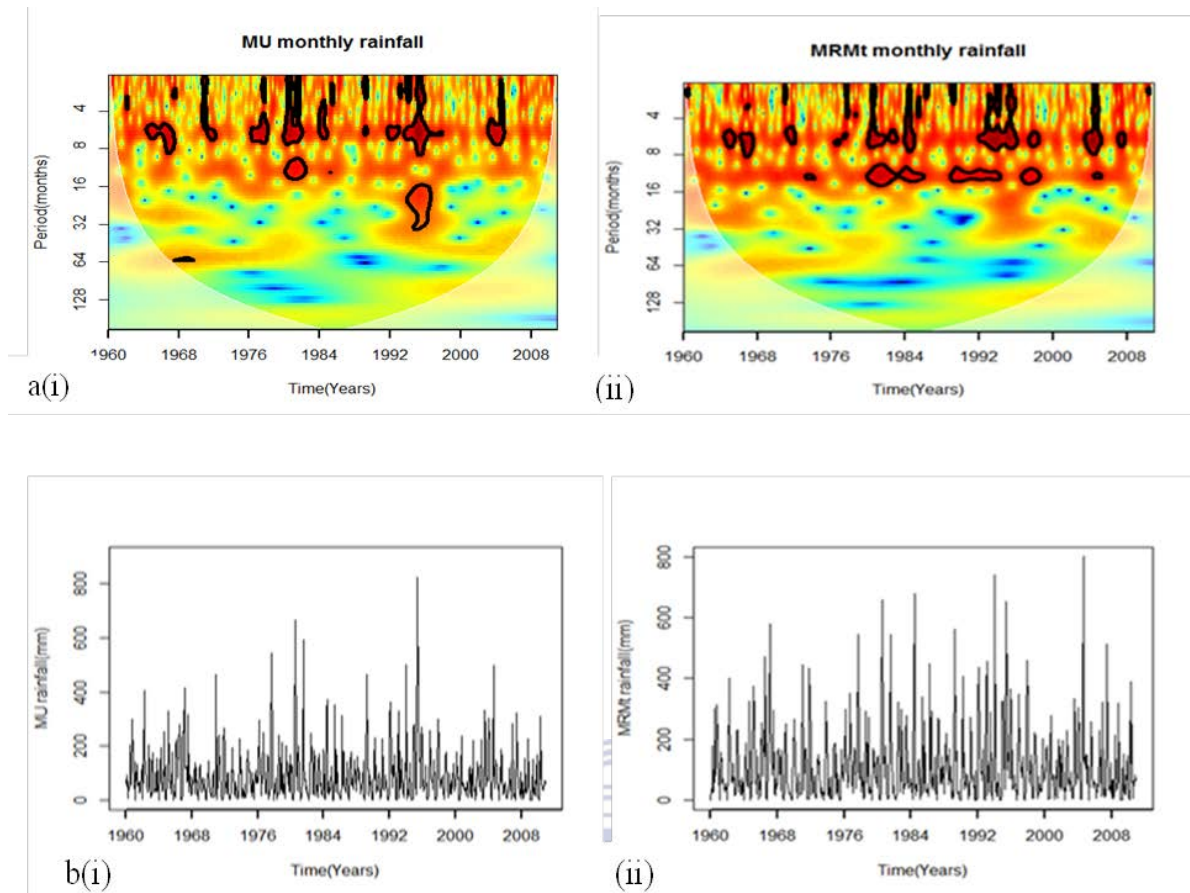


**Figure 3.10:** a) The wavelet power spectra of rainfall time series of; i) MU and; ii)  $MR_{Mt}$  stations; the black contours mark the significant periodicities at 95% confidence level while the white u-shaped curve marks the COI. The colour code is such that blue is for low spectral energy and red is high energy; b) The variability of monthly rainfall total with of; i) MU and; ii)  $MR_{Mt}$

These observations suggest that the rainfall variation is influenced by both local factors and other modes of climate variability (such as positive phases of ENSO and IOD). Notable was the lack of significant quasi-annual cycles from 1970-1976 and from 2000-2005 with resultant low rainfall in the time series plots. Depressed rainfall at the coast during these periods was also observed in the preliminary exploration of the annual and seasonal rainfall in the previous Section.

### *CWT analysis of monthly rainfall for Nakuru and Kisumu*

Figure 3.11 shows the spectral energy variation for Nakuru rainfall within the Rift Valley. From the WPS plot (Figure 3.11 (a)), only isolated high-frequency components (1-8 months periodicities) that are punctuated by long periods of low energy were observed. The low spectral energy of the WPS is an indication of lower rainfall received at this station than over the central highlands or the Lake Victoria region in western Kenya. The low rainfall over Nakuru station is also depicted in the time series plots. A notable feature in this station, however, is the occurrence of low-frequency features (periodicities of 32-64 months) observed in 1978 and also from 1992 - 1995. The concurrence of the high frequency features, the annual cycle and the low frequency feature (periodicities of 1-6, 8-16 and 32- 64 months) in 1978 resulted in high peak rainfall observed in the time series plot (Figure 3.11 (b)), which was also observed in the annual rainfall anomalies in the previous Section. The semi-annual cycles at Nakuru from 1970-2013 are separated by long periods of low spectral energy. For example, 1970-1975, 1976-1986 and from 1987-2002 had low spectral energy, and were observed as periods with low rainfall in the time series plots. This observation would imply that seasonal rainfall within the Rift Valley has long periods of low rainfall, and high rainfall is observed when multiple frequency components occur simultaneously. There were no observable trends in the monthly rainfall time series.

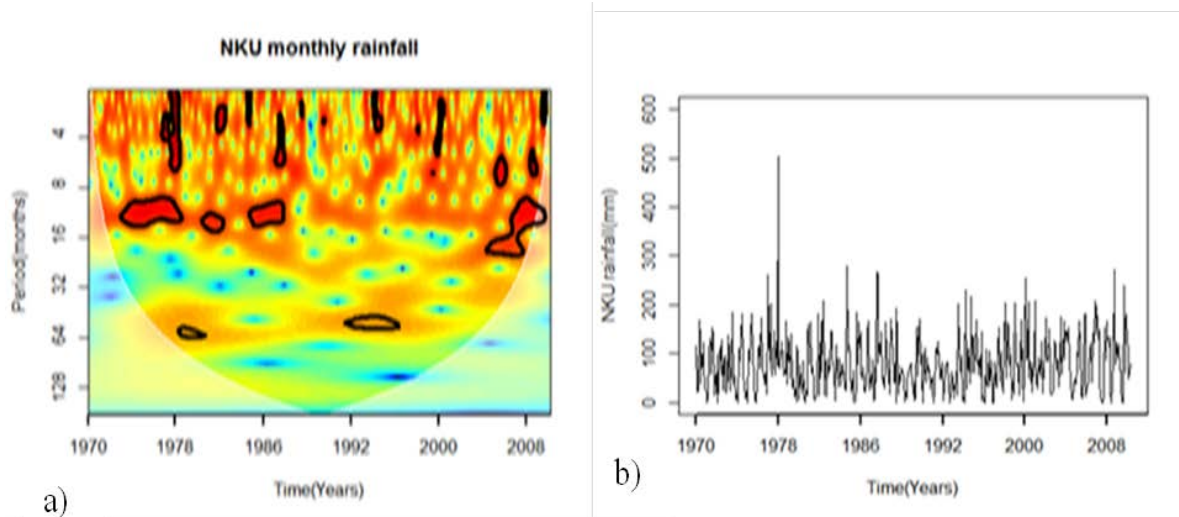


**Figure 3.11: a) The wavelet power spectrum of rainfall time series of Nakuru (NKU); the black contours mark the significant periodicities at 95% confidence level while the white U-shaped curve marks the COI. The colour code is such that blue is for low spectral energy and red is high energy; b) the variability of monthly rainfall total with time of NKU**

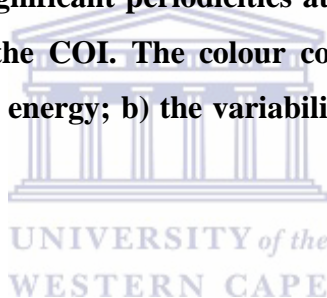
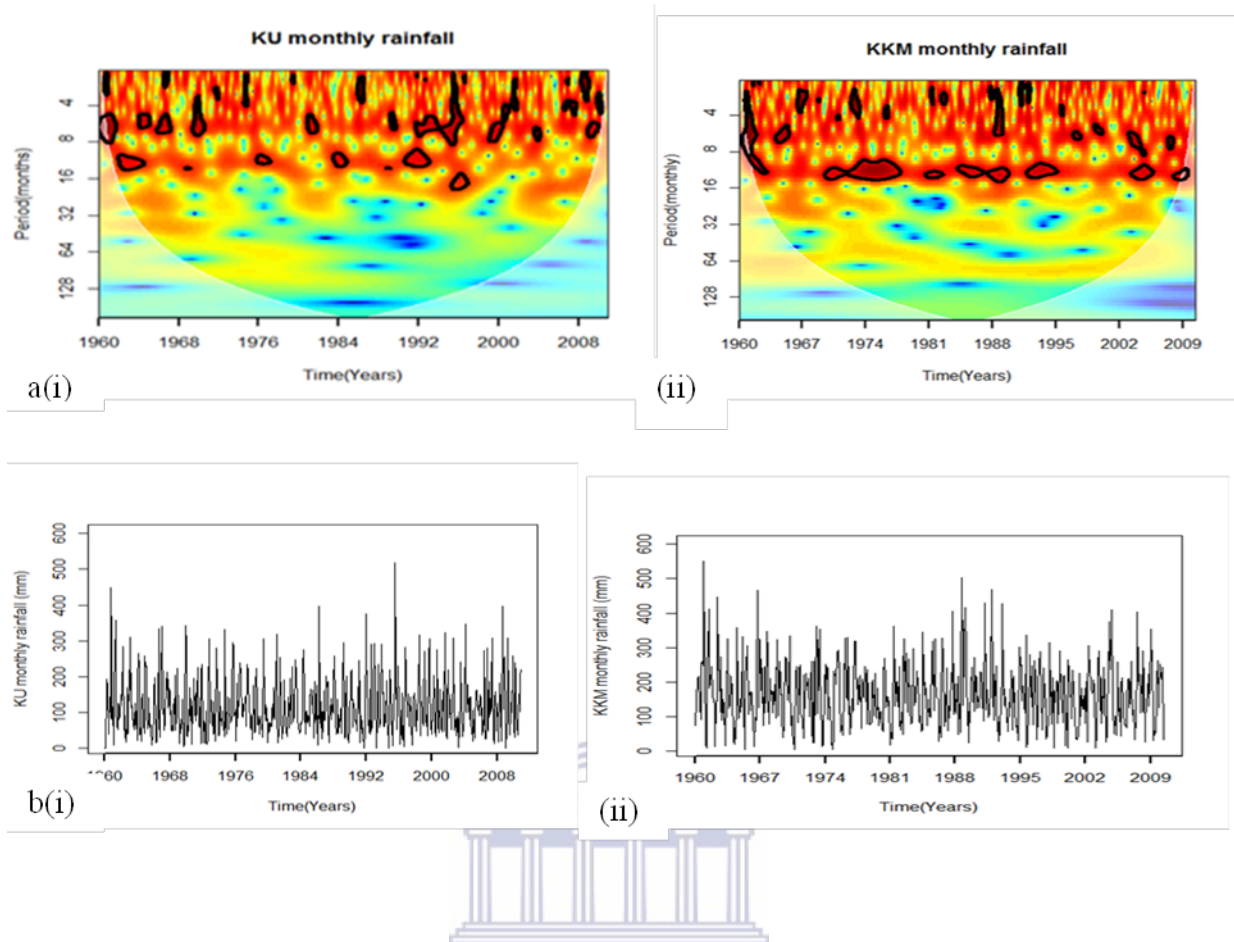


Figure 3.12 shows the spectral power variance of rainfall over the western highlands of Kenya. The common frequency features observed at Kisumu (KU) and Kakamega (KKM) are the annual (8-16 months periodicities) and semi-annual (4-8 months) cycles; high-frequency cycles (1-4 months periodicities) are also observed (Figure 3.12 (a&b)). Particularly noted was that annual cycles at KKM (Figure 3.12 (b)) had major breaks from 1964 to 1970 and from 1995 to 2002 with a significant reduction in monthly rainfall during these periods (Figure 3.12 (c&d)). Similar annual periodicities were observed in KU but less frequent and only appeared before 1992.



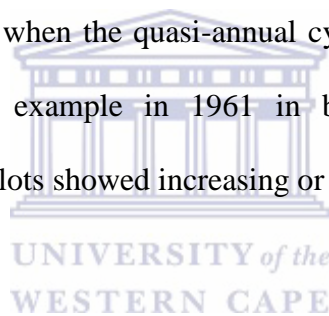


**Figure 3.12:**a) The wavelet power spectra of rainfall time series of; i) Kisumu (KU) and; ii) Kakamega (KKM) stations; the black contours mark the significant periodicities at 95% confidence level while the white U-shaped curve marks the COI. The colour code is such that blue is for low spectral energy and red is high energy; b) The variability of monthly rainfall total with of; i) Kisumu and; ii) Kakamega

Another observable difference between KU and KKM WPS plots was that after 1990, KU had frequent and significant high-frequency components (1-8months' periodicities) while in KKM the annual cycles were more common. For both stations, there were no frequency components beyond the periodicities of 16 months.



The observations of rainfall variability over Kisumu and Kakamega suggest that although the two stations are in the same rainfall homogeneous zones, the factors influencing rainfall variability are different. Kakamega has more inter-annual variability than Kisumu, as indicated by the frequent occurrence of the quasi-annual cycles in Figure 3.12 (a(ii)). On the other hand, local factors appear to influence the variation of Kisumu rainfall more than in Kakamega. These variances could be attributed to the urban and lake breeze effects on rainfall in Kisumu, which is near Lake Victoria. The higher spectral energy of the WPS of KKM is attributable to the higher amount of rainfall than in Kisumu. None of the two stations had low-frequency components beyond the annual cycle; thus suggesting that low-frequency modes of climate variability have little influence on rainfall in this region. High rainfall peaks observed in the time series plots occurred when the quasi-annual cycle occurred simultaneously with the high-frequency cycles; for example in 1961 in both stations and 1997-1998 in Kisumu. None of the time series plots showed increasing or decreasing trend.



From the CWT analysis of the variability of monthly rainfall, multiple spectral cycles (semi-annual, intra-annual and inter-annual) were observed in all the stations considered in this study. Results showed that time periods that had unusually high rainfall amounts were associated with the simultaneous occurrence of multiple periodicities over a given year (or group of years). In Kenya rainfall has high temporal and spatial variability, the main features observed from the CWT analysis include:

- Multiple cycles were observed in each time series; the common ones are high frequency, semi-annual and the quasi-annual cycles that were associated with the factors that influence rainfall at local, seasonal and inter-annual time scales.

- Simultaneous occurrence of multiple cycles was observed to cause high rainfall amounts. For example, the concurrence of the semi-annual (1-8 months periodicities) and the annual cycles (8-16 months periodicities) in 1961-1963 caused high rainfall over the central and western highlands of Kenya; simultaneous occurrence of the semi-annual, annual cycle and 32-64 months periodicities in 1965-1967, 1995-1998, 2005-2007 caused resultant high rainfall total over the coastal region and the central highlands of Kenya.
- Lack of significant simultaneously occurring cycles in the 1970s in all regions and from 2008 to 2013 at the coast caused resultant depressed rainfall in the regions.

Similar methods of the CWT analysis were used by Turki, et al. (2016) who reported multiple cycles of rainfall in Marrakech (Morocco) and noted that high (low) spectral power appeared during wet (dry) periods and Li, et al. (2015) observed a dominant annual (1-year) cycle in the monthly rainfall of Huangtupo (China) which was associated with the monsoons of Asia. These observations agree with Nicholson, (2015) who indicated that several factors appear to act jointly to produce the very wet years.

#### **3.4.4 Effects of ENSO and IOD on rainfall variability**

ENSO and IOD modes of climate variability have been shown to influence rainfall variability at annual and seasonal time scales in the EEA region (Indeje, 2000, Clark, et al., 2003; Black, et al., 2003; Nicholson 2014; Nicholson 2015). However, the influence of these modes of climate variability on rainfall at a small spatial scale is not yet fully established. From the previous Section, western Kenya region did not have high rainfall in 1997-98 periods, which has been documented as a period when ENSO coupled with IOD to produce widespread

rainfall anomalies during the OND season. Likewise, the coastal region did not have anomalous rainfall in 1961 as was observed in the other regions, and 1961 have been documented to have had a positive IOD mode (Clark, et al., 2003). These observations prompted me to examine relationships of these two modes of climate variability with rainfall.

Figure 3.13 shows the spectral variance of the annual NINO3.4 and IOD indices respectively. NINO 3.4 had significant cycles of 3-4 year periodicities between 1967 and 1970 followed by a long period of low spectral energy until about 1980. Between 1980 and 2000 there was an extended 3-6 year periodicity. In comparison, the IOD was continuously significant from 1961 to 2000 with periodicities between 4-6 years that changed from 1985 to 2000 to 3-4 year periodicities.

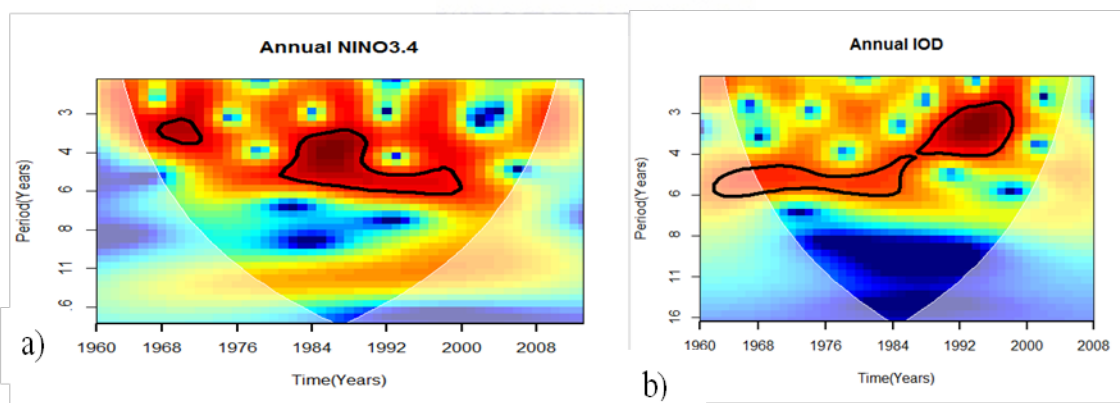
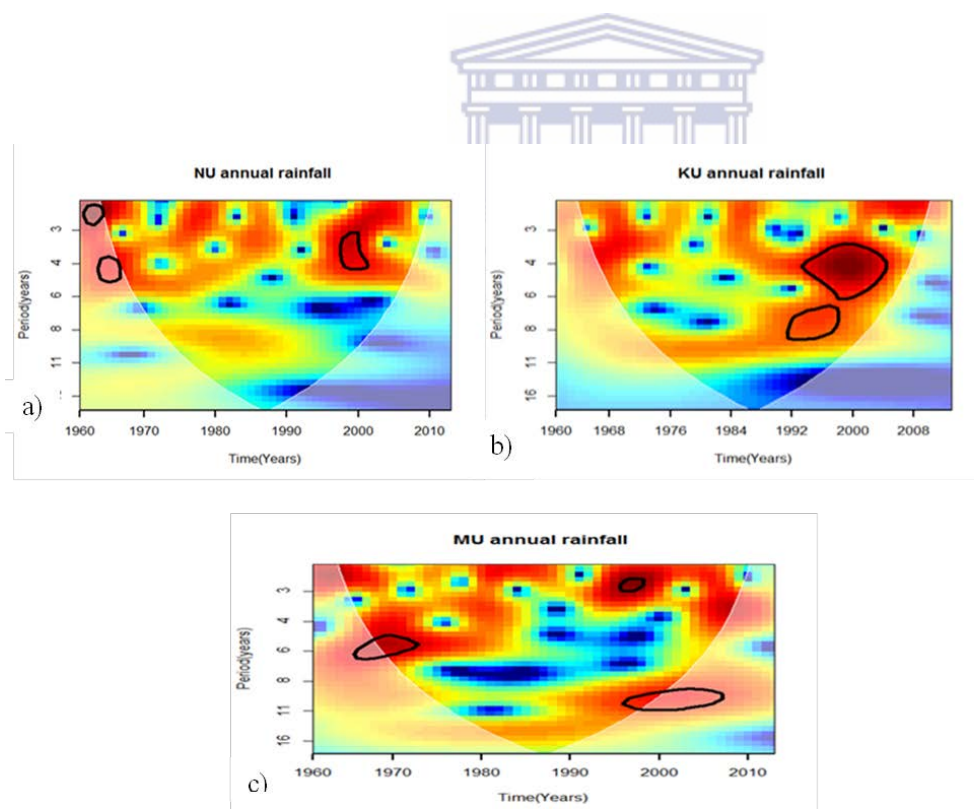


Figure 3.13: The wavelet power spectra of the annual time series of; a) NINO3.4 and; b) IOD indices; the black contours mark the significant periodicities at 95% confidence level while the white U-shaped curve marks the COI. The colour code is such that blue is for low spectral energy and red is high energy

To compare the variability of ENSO and IOD with annual rainfall at local level, CWT analysis was carried out on the annual rainfall time series. Figure 3.14 shows some representative results from each region. A 3-6 years periodicity was dominant in all regions between 1995 and 2000. This time coincides with the simultaneous occurrence of significant periodicities of ENSO and IOD. In addition, an 8-11 years periodicity was dominant at the coast and lake region from 1995-2000; thus implying that not all the annual rainfall variability in 1997-98 could be explained by the variability of ENSO and IOD. Worth noting was that not all regions had significant periodicities in the rainfall time series during 1961-1962 (*e.g.*, coastal region); thus implying that positive mode of IOD does not influence rainfall variability equally in all parts of Kenya.



**Figure 3.14:**The wavelet power spectra of annual rainfall of stations in; a) Nairobi; b) Mombasa; c) Kisumu; the black contours mark the significant periodicities at 95% confidence level while the white U-shaped curve marks the COI. The colour code is such that blue is for low spectral energy and red is high energy

These observations corroborate partly the results of Clark et al., (2003) and Black, et al., (2003) who indicated that the widespread anomalous rainfall of 1997-1998 resulted from a positive ENSO coupling with an IOD event. However, the occurrence of significant 8-11 periodicity cycle at the coast and Kisumu suggests that another low-frequency climate system was also responsible for the rainfall anomalies at the coast and western Kenya during the 1997-98 periods. These observations agree with Nicholson, (2014) and Nicholson (2015) who indicated that ENSO and IOD are not totally responsible for the occurrence of anomalous rainfall in Kenya.

Further analysis was carried out to examine the statistical relationships between the ENSO and IOD respectively with seasonal and annual rainfall of the various urban areas that come from different climatic zones. Linear correlations between the anomalies of annual and seasonal rainfall and NINO 3.4 and IOD respectively (Figure 3.15) showed that there were more stations whose annual rainfall were significantly positively correlated with mean annual IOD indices than the NINO 3.4 indices (Figure 3.15(a)) and that the OND seasonal rainfall was more positively correlated with either seasonal NINO 3.4 or IOD at any given station than the MAM season.

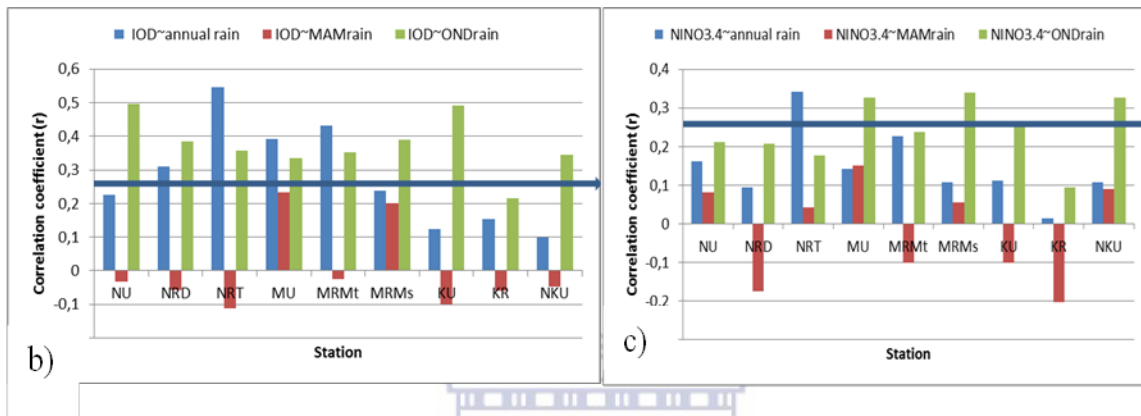
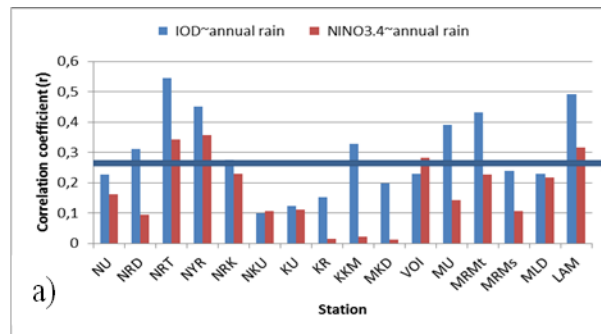


**Figure 3.15: Linear correlations between; a) annual rainfall with NINO 3.4 and IOD indices respectively; b&c) seasonal rainfall with IOD and NINO 3.4 indices; the horizontal bar in each plot marks the point ( $r= 0.27$ ) above which the coefficients are significant at  $\alpha=0.05$**

The deductions from the correlations between rainfall and ENSO and IOD were that:

- i) The influence of ENSO and IOD on rainfall at seasonal and annual time scales is spatially different. For instance, the western Kenya region has almost no significant correlations at annual time scale with either NINO 3.4 or IOD, and had only a few positive correlations between IOD and OND rainfall.
- ii) IOD has more positive correlations with annual and OND rainfall than NINO 3.4 in each region; meaning that rainfall in each region is influenced more by the

variability of sea surface temperature over the Indian Ocean than in the anomalies in the Pacific

- iii) The MAM rainfall has no significant correlations with either NINO 3.4 or IOD in all regions.

These results collaborates those of the CWT analysis, and Black, et al. (2003) who observed that there have been above average rainfall during every positive IOD mode from 1960-2001, compared to only during four out of nine El-Niño years, and that the five seasons with highest OND rainfall during the 1960-2001 period occurred during a positive IOD mode. These observations also agree with results of Camberlin et al. (2009) who indicated that MAM rainfall depends on a combination of unrelated factors and are only weakly correlated with ENSO. Nicholson (2014) and Nicholson (2015) also indicated that two or more factors act in each season simultaneously to produce anomalously wet years and that ENSO alone is weakly associated with rainfall anomalies over the EEA region.

#### **3.4.5 Trend analysis of rainfall**

After examining rainfall variability and the possible factors that influence occurrences of high seasonal rainfall, it is also important to examine if there have been long-term trends in rainfall at various time scales in and around the major towns to inform better decisions in the designs of urban stormwater management systems. Parametric (linear and quantile regression) and non-parametric (Mann-Kendall) methods of trend analyses were used to investigate trends in the monthly, seasonal and annual rainfall in all the stations.

### Results from quantile regression

Considering the MAM season, the most notable trends were in NR<sub>D</sub> (Dagoretti Corner in Nairobi) station which had decreasing trend from the 20<sup>th</sup> to the 60<sup>th</sup> percentile (Table 3.3). The other station with trends in MAM rainfall is Nakuru (NKU) with increasing trend in the 60<sup>th</sup> percentile. Figure 3.16 gives a graphical representation of some of the trend results.

**Table 3.3: Quantile regression trend results of MAM seasonal rainfall**

	MAM					
station	NR <sub>D</sub>					NKU
n <sup>th</sup> Quantile	20	30	40	50	60	60
$\beta(\kappa)$ (mm/year)	-0.6	-0.5	-0.5	-6.3	-5.6	4.2

note: only quantiles with significant coefficients at  $\alpha = 0.05$  ( $p < 0.05$ ) were presented; -  $\beta(\kappa)$  values signifies decreasing trends and  $\beta(\kappa)$  is for increasing trends

Rainfall in the JJA season had increasing trends over Nairobi; in particular, NR<sub>D</sub> station which had increasing trends in the 20<sup>th</sup>, 30<sup>th</sup> and 90<sup>th</sup> percentile (Table 3.4) thus implying an increase of light rains as well as heavy rains during this season; increasing trends were also observed in Kisumu rainfall in the 90<sup>th</sup> percentile, while Nakuru had increasing trends in the 90<sup>th</sup> percentile and decreasing trend in the 10<sup>th</sup> percentile. Other decreasing trends during this season were detected in Mombasa where both MR<sub>Mt</sub> and MR<sub>Ms</sub> had respectively decreasing trends in the 50<sup>th</sup> and 60<sup>th</sup> percentile.

**Table 3.4: Quantile regression trend results of JJA seasonal rainfall**

	JJA Season									
station	NR <sub>D</sub>			MR <sub>Mt</sub>		MR <sub>Ms</sub>		KU	NKU	
n <sup>th</sup> percentile	20	30	90	50	60	50	60	90	10	90
$\beta(\kappa)$ (mm/year)	0.8	9.7	3.8	-2.4	-0.3	-3.7	-2.8	3.2	-3.1	2.6

note: only quantiles with significant coefficients at  $\alpha = 0.05$  ( $p < 0.05$ ) were presented; -  $\beta(\kappa)$  values signifies decreasing trends and  $\kappa$  is for increasing trends

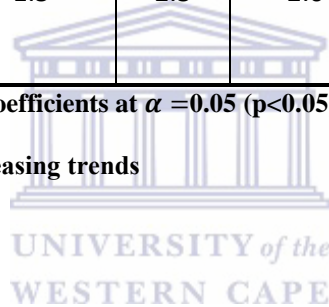


During OND season, only  $MR_{Mt}$  and  $MR_{Ms}$  had an increase in light rains (10<sup>th</sup> percentile) and Nakuru also had increasing trends in several percentiles (Table 3.5(a)). The trend resultsshowed that there were no significant changes in the annual total rainfall in all the stations except). Nakuru(NKU), that had an increasing trend in the 10<sup>th</sup>percentile (Figure 3.16(b)).

**Table 3.5:Quantile regression trend results ofOND seasonalrainfall**

	OND Season					
station	$MR_{Mt}$	$MR_{Ms}$	NKU			
nth percentile	10	10	20	30	40	60
$\beta(\kappa)$ (mm/year)	2.0	1.5	2.3	2.0	2.2	3.0

**note: only quantiles with significant coefficients at  $\alpha =0.05$  ( $p<0.05$ ) were presented; -  $\beta(\kappa)$  values signifies decreasing trends and  $\beta(\kappa)$  is for increasing trends**



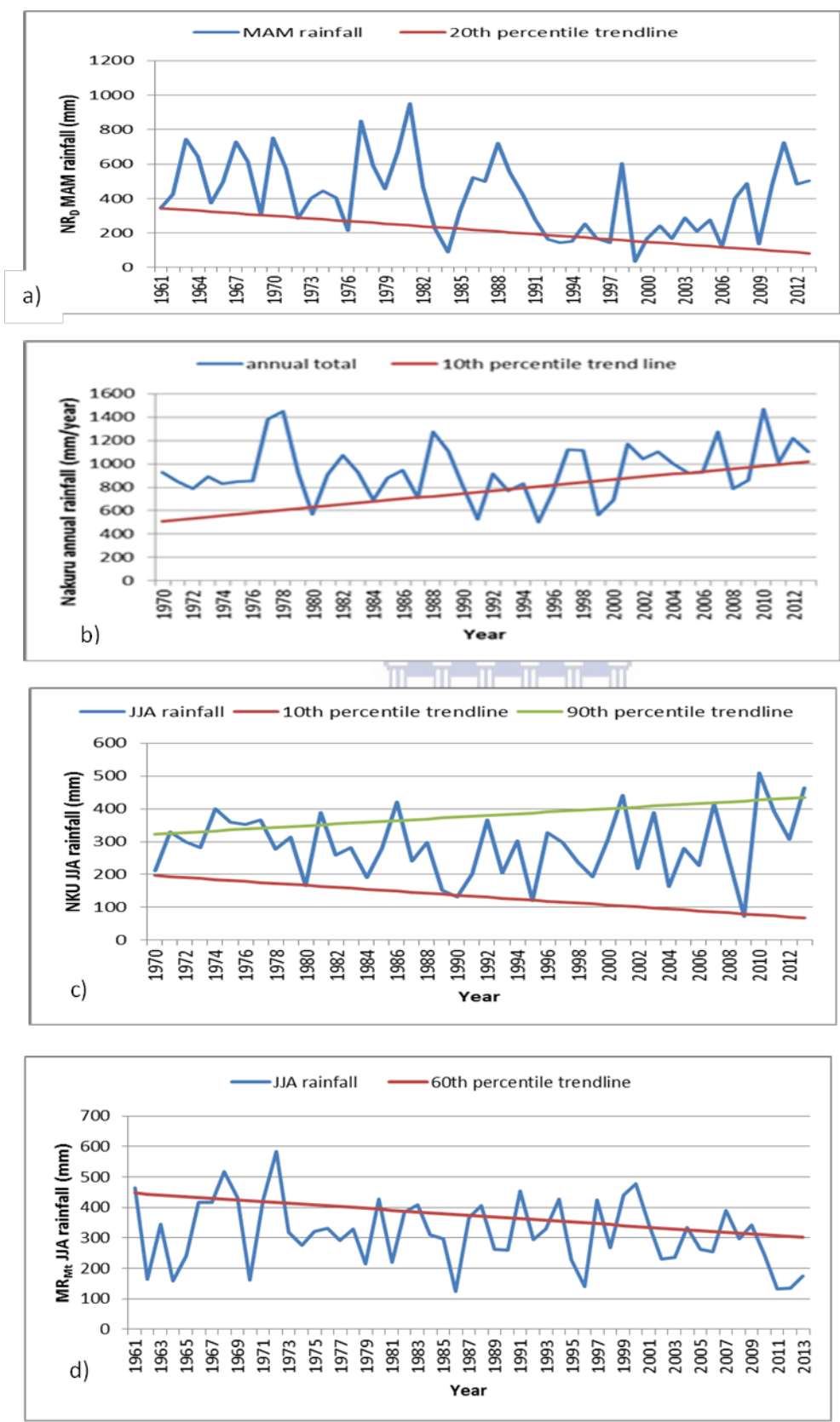


**Figure 3.16:Quantile regression analysis for; a) MAM rainfall at NR<sub>D</sub> ; b) annual rainfall at Nakuru; c) JJArainfall at Nakuru and; d) JJA rainfall at Mtwapa (MR<sub>Mt</sub>)**

**Results from linear regression and Mann-Kendall**

Trends observed in monthly rainfall are given in Table 3.6. The stations with trends in the monthly rainfall detected either by the linear regression or the Mann-Kendall methods were found to be those mainly from the stations that had trends in one quantile or another in the quantile regression analysis of the seasonal rainfall. For instance, NR<sub>D</sub> had most trends in which, in some months rainfall was increasing ( e.g., June, July, September) and decreasing in others (April, May, and November) thus confirming the increase in JJA and decrease trends in MAM seasonal rainfall. The Mann-Kendall test of the seasonal rainfall also confirmed a decrease of MAM and an increase of JJA rainfall in NR<sub>D</sub> as well as an increase of OND rainfall in Nakuru (Table 3.4(b)).



**Table 3.6: Trend analysis of monthly and seasonal rainfall from Mann-Kendall ( $\tau$ ) and linear regression ( $\beta$ )**

a)	NRD							NU	NKU	KU	KR
Station	Feb	Apr	May	Jun	Jul	Sep	Nov	Apr	Nov	Sep	Feb
Month	Feb	Apr	May	Jun	Jul	Sep	Nov	Apr	Nov	Sep	Feb
MK( $\tau$ )	0.24	-0.37	-0.26	0.20	0.21	0.32	-0.23	-0.17	0.2	0.23	-0.25
LR( $\beta$ ) mm/yr	2.1	-1.5	-----	0.6	2.3	1.5	-1.6	-----	-----	1.2	4.5

b)	NRD		NKU
Station	NRD		NKU
Season	MAM	JJA	OND
MK, ( $\tau$ )	-0.24	0.24	0.29

Note: only for stations where the coefficients were significant at  $\alpha = 0.05$  ( $p < 0.05$ ); ---- signifies months when trends were not detected by one of the methods

The different methods used to investigate trends in rainfall showed that out of the sixteen stations, the only stations with significant changes in rainfall are Dagorreti (NR<sub>D</sub>) in Nairobi, stations at the coast (MR<sub>Mt</sub> and MR<sub>Ms</sub>) near Mombasa town and NKU station in Nakuru town; these stations are either in urban or rural areas near the towns. Worth noting is that most

rural stations away from the major towns had no temporal trends. The observed trends could be resulting from changes in local circulation patterns as a result of changes in heat flux resulting from the expansion of built up area and urban development and or changes of regional temperature especially at the coast (observed in Chapter 2). For instance, NR<sub>D</sub> is situated on the outskirts of Nairobi downwind of the central business district (CBD) and have been undergoing environmental changes as the city expands (Mundia and M. Aniya 2006), which is likely to affect rainfall characteristics on a small spatial scale. Influence of Changes in local factors on urban rainfall was explored further in Chapter 5.

### ***Trend analysis of daily indices of extreme rainfall***

Analysis of annual daily rainfall indices of extremes described in Table 3.2 showed no trends in most of the indices in almost all the stations except in Nakuru (NKU); in this station, PRCPTOT (annual total wet day rainfall), R25 (annual count of days when rainfall was more than 25mm), and R95p (annual rainfall total greater than the 95<sup>th</sup> percentile) indices had weak increasing trends detected only by the MK tests (Figure 3.17). These results were consistent with those of the quantile regression analysis that indicated an increase in heavy and annual rainfall in Nakuru station.

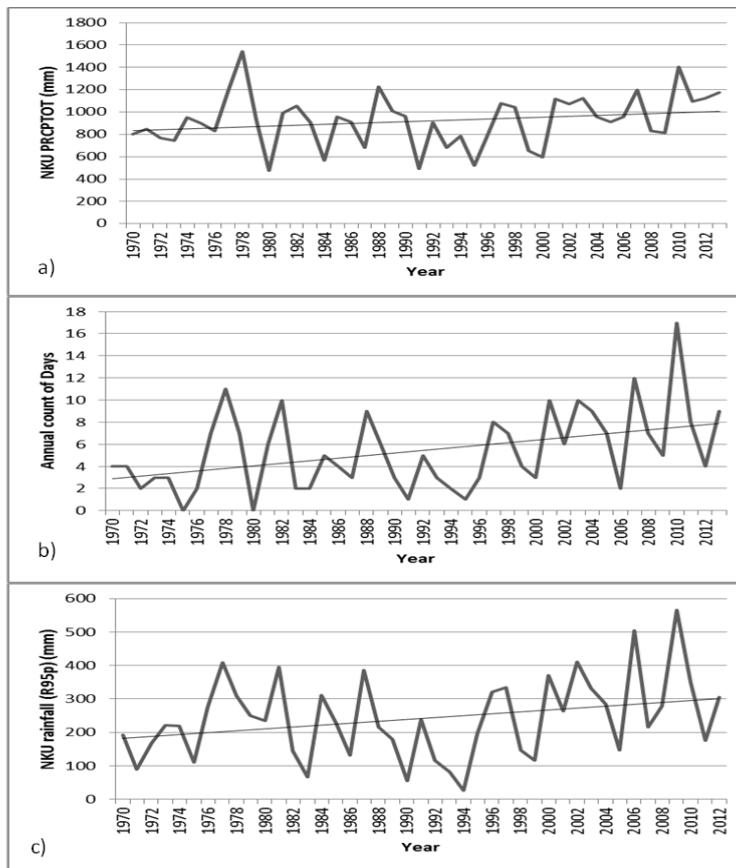


**Figure 3.17: Temporal variation of indices of rainfall extreme at Nakuru station depicting weak positive trends; a) PRCPTOT-annual total wet day rainfall; b) R25- annual count of days when rainfall  $\geq 25$ mm; c) R95p - annual precipitation total  $> 95^{\text{th}}$  percentile.**

### 3.4.6 Discussion

#### *Rainfall variability*

Variability and possible changes of rainfall at stations in and nearby each of the four urban areas of Kenya used in my Thesis was thoroughly investigated using exploratory data analysis, CWT and statistical methods. The temporal variability of the seasonal rainfall in each climatic zone has spatial differences, although rainfall occurs mainly within the MAM and OND season. The spatial differences imply that rainfall variability in each climatic zone responds differently to the modes of climate variability that influence rainfall over the EEAs was also indicated in Camberlin, et al. (2009), Hastenrath et al. (2010) and Nicholson, (2015).

The spatial and temporal variabilities were observed more clearly from the CWT analysis of monthly rainfall time series in which the significant spectral variance of the rainfall was observed in the dominant periodicities of the WPS plots. The concurrent of multiple periodicities signify the different modes of climate variability that influence the outcome of rainfall at a given time as was indicated by Li, et al. (2015). Over the EEA the high-frequency features were observed that were attributable to local factors such as the breezes (at the coast and Lake Victoria regions) and other thermal circulations such urban effects. It was noted that the stations at the coast and in urban areas had more of the high-frequency cycles (1-4 months periodicities) than those in rural areas and away from water bodies. The semi-annual cycles were associated with the two rainfall seasons (MAM and OND) that are influenced by the bi-annual convergence of the monsoon winds in the ITCZ within the EEA region, while the quasi-annual cycles and other higher periodicities (e.g., a common periodicity of 32-64 months observed in all regions except western Kenya in 1997-98), were associated with synoptic systems that influence rainfall in EEA. For instance coupled positive ENSO/ IOD anomalies were suggested to have caused the rainfall anomalies of 197-98 (Clark, et al., 2003; Black, et al., 2003). Other observations from the CWT analysis showed that 1982-1994 had no significant periodicities and rainfall was depressed at the coast and, the highest monthly peak rainfall occurred between 1995 and 2000 in most stations. These results corroborate statistical observations by Clark, et al., (2003) that IOD and ENSO correlations with the coastal OND rainfall were weak between 1983 and 1993 with resultant depressed rainfall, and strong between 1994 and 2000 with resultant increased rainfall. Spatial variabilities within the same climatic zones were mainly observed from differences in spectral energy in the WPS plot and common occurrence of high frequency features (1-4 month periodicities); thus implying that the differences were as a result of local factors rather

than from large-scale climate systems. Notable was that rainfall at Nakuru, within the Rift Valley, had different characteristics than the station to the east and to the west of the Rift Valley. Rainfall variability at this station is influenced more by the quasi-annual cycles than the seasonal cycle. This observation may be explained by the statistical results which indicated that Nakuru rainfall during the OND season is significantly correlated with ENSO and IOD indices. The results from the CWT analysis in this study agree with Nakken, (1999), Adamowski, et al. (2013) and Nicholson (2015) who indicated that changes in hydro-meteorological time series are not controlled by a single factor and that occurrence of many factors produce extreme events.

Statistically, the relationship between rainfall variability and ENSO and/or IOD was shown in this study to differ according to region and season. In particular, ENSO is weakly associated with seasonal rainfall, especially in central and western highlands of Kenya. IOD is more strongly associated with OND rainfall than with MAM rainfall and mainly over the central highlands and the coast than the western Kenya region. Individually the associations of IOD or ENSO with OND rainfall is weak ( $r < 0.5$ ) in all regions. From the CWT analysis, however, the urban effect on rainfall could not be discriminated since other factors such as altitude and presence of water bodies could also bring about the observed differences. For the first time in the studies of rainfall variability over Kenya, important spatial and temporal variabilities have been established using the CWT analysis at small spatial scales. Further analysis to examine the influence of urbanization on rainfall was explored in Chapter 5.

### ***Rainfall trends***

Trends of annual, seasonal and monthly rainfalltime series together with extreme daily rainfall indices from sixteen stations were carried out. The quantile regression was particularly useful in investigating if there are trends in other percentiles,since the Mann-Kendall method tests trends around the median (50<sup>th</sup> percentile). Most stations had no trends for the annual, seasonal or monthly rainfall totals and also in most of the daily rainfall extreme indices. However, there were few cases where trends were detected by either of the methods or both. While the methods in most cases agreed, there were a few cases where trends of a particular seasonal rainfall were not detected by the Mann-Kendall tests but showed trends in some percentilese.g., in JJA rainfall of  $MR_{Mt}$  and  $MR_{Ms}$  ,respectively showed negative trends in 50<sup>th</sup> and 60<sup>th</sup> percentile which were not detected by the Mann-Kendall tests. The stations that showed consistent increasing and decreasing trends were only  $NR_D$  (in Nairobi city) and  $NKU$  (in Nakuru town). Therefore, from the stations considered in this study, which were drawn from the highland west and east of the Rift valley and the coast of Kenya(in the neighbourhoods of the four major urban areas),rainfall generally had no trends at annual and seasonal time scales over the last fifty years. The indices of extremes also generally had no significant change over time.The few isolated trends were thereforeattributed to local anthropogenic influence on rainfall rather than large-scale forcing of the climate systems. Similar conclusions were made in Clark, et al. (2003) for rainfall at the coast of Kenya,while Mazvimavi (2010) found no significant changes in seasonal and annual rainfall overZimbabwe.

### 3.5 Summary

The aim of this Chapter was to investigate variability and possible changes of rainfall, in and around the four major urban areas of Kenya. The spatial-temporal variations and trends of daily, monthly, seasonal and annual rainfall were examined using exploratory data, CWT,and



trend analysis methods for sixteen stations drawn in and around the towns. The four major towns of Kenya are situated in three different rainfall homogeneous zones. All the stations receive varying mean annual amounts of rainfall ranging from 600mm/year in the lowlands, 900 mm/year over the central highlands and 1200-2000mm/year over the western and coastal regions. Although most of the stations had no temporal trends in rainfall series at all the time-scales considered, the high inter-annual variability with frequent occurrences of high daily (and seasonal) amounts could be a challenge in urban stormwater management.

In conclusion, therefore, I have established that inter-annual variability of rainfall at various time scales in Kenya is more important in water resources management than temporal trends. While a number of years have had anomalous seasonal rainfall, only a few stations near to urban areas had increasing or decreasing trends. This observation suggests that in urban storm water management, the factors that influence rainfall variability should be well understood. The study further showed that temporal and spatial variability of the factors influencing rainfall (observed as dominant periodicities from the CWT analysis) are important since they influence the occurrence of extreme rainfall events. The years that had anomalous rainfall were observed to have high and low-frequency features that are indicative of different forcing factors occurring simultaneously. However, there is need to understand the nature of these factors that force extreme rainfall events. For instance, I established that although ENSO and IOD influence rainfall variability at inter-annual time scales (either individually or together), their influence individually is weak and has spatial disparities. Understanding of non-stationarity of rainfall variability at small spatial scale is therefore important in water resource management in the diversely heterogeneous climate zones of EEA. Challenges of storm water management in urban areas of Kenya are therefore likely to be experienced due to changes in rainfall variability (forced at a given time by different factors) rather than

through long-term temporal trends. Further investigations of the influence of local factors (urbanization and temperature) on urban rainfall were investigated in Chapter 5, while the suitable extreme value models for producing design storms applicable in storm water management systems were explored in Chapter 6. However, in the next Chapter (4), I explored the possible existence of the urban heat island whose effect is likely to influence urban rainfall.



## 4 CHAPTER 4: URBAN HEAT ISLAND

### 4.1 Introduction

From the analyses of temperature and rainfall in Chapters 2 and 3 respectively, I have established that local factors are influencing temperature changes that could also be influencing rainfall changes in areas close to the towns. The aim of this Chapter is to explore if UHI, as one of the local factors likely to have influenced temperature changes, exist in the fast growing cities of Kenya. The outcome of this Chapter, together with the outcomes of Chapters 2&3, form a basis for which the influence of temperature on urban rainfall is investigated (Chapter 5). Temperature from weather stations within and near Nairobi and Mombasa, and land surface temperatures (LSTs) over each city were used to investigate UHI and determine its intensity. The choice of these two cities was motivated by the fact that they are the largest in Kenya by population and spatial extent and they have a network of weather stations with temperature data of sufficient time length that represent urban and rural temperature characteristics adequately. The Chapter starts with reviewing the relevant literature on UHI and its determination in various parts of the world. Methods used for determination of UHI and the challenges encountered are also highlighted.

The United Nations (UN Habitat, 2008) estimate that, about half of the world's population is living in urban areas, and this proportion may reach 70% by the year 2050. This rate of urbanization is currently the key driver of the climate change mainly because intense and fast urbanization has resulted in human-induced land use/land cover changes that impact on the climate system through changes in urban heat fluxes (McCarthy, et al., 2010; Zhang, et al., 2014). Such changes are likely to influence changes in rainfall patterns over urban areas which are likely to impact on storm designs used in storm water management systems.

Human activities such as urbanization, intense use of land, deforestation, burning of fossil fuels among others, usually modify the planetary boundary layer (PBL) through changes in local air circulations. The PBL is that part of the troposphere that is directly affected by the presence of the earth's surface and acts in reaction to the surface forcing on time scales of hours or less; such forcings include frictional drag, evaporation, and transpiration, pollutant emissions, terrain-induced flows, *etc.*). The surface-atmosphere interactions play an important role in the earth's climate system since the PBL transport heat, momentum, and humidity within it (Gross, 2014; Barlow, 2014). In urban areas, the PBL is modified into the urban boundary layer (UBL) which has a roughness layer (depending on the building height and density), inertia layer and the outer layer. UBL is much deeper than the PBL (Fig 4.1) (Barlow, 2014). The heterogeneous surface heat fluxes between urban and rural environments produce positive temperature differences over the urban and negative over the rural areas; a phenomenon termed as the urban heat island (UHI) effect.

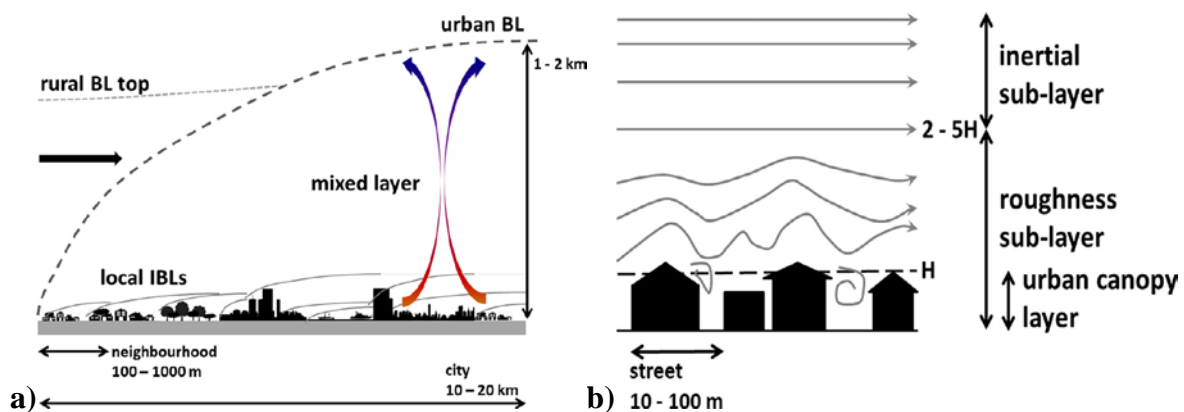
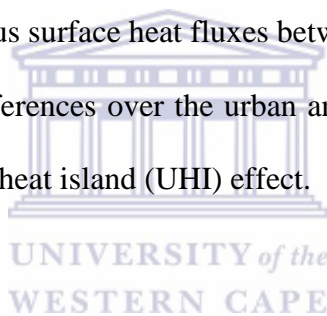


Figure 4.1: Schematic diagram of daytime convective UBL with wind flowing from left to right. Dashed lines indicate the top of rural and urban boundary layers; solid lines indicate local internal boundary layers; (b) Schematic diagram of roughness and inertial sub-layers; grey arrows indicate streamlines; dashed line indicates mean building height (adopted from Barlow (2014)).

### 4.1.1 Generation of UHI

The urban area alters the boundary layer processes mainly by the creation of a UHI. A typical example of rural and urban surface energy fluxes is given in Figure 4.2 after Shepherd (2005). Surface heat budget equation may be represented as:

$$q_{sw} + q_{lw} + q_{sh} + q_{le} + q_g + q_a = 0 \quad (4.1)$$

where  $q_{sw}$  represent the net shortwave irradiance,  $q_{lw}$  is the net long-wave irradiance,  $q_{sh}$  is the surface sensible heat flux,  $q_{le}$  is the latent turbulent heat flux,  $q_a$  is the anthropogenic heat input, and  $q_g$  represents ground heat conduction. A typical example (Figure 4.2 (a)) shows the apportioning of solar radiation in an urban and rural environment. The incident solar radiation,  $q_i$ , of  $7.6 \text{ kW h m}^2 \text{ day}^{-1}$  is received in both locations since they obtain solar radiation of equal intensity. In the rural forest, with an albedo of 0.25 typical of a rural ecosystem, the reflected solar radiation,  $q_R$ , is  $1.9 \text{ kW h m}^2 \text{ day}^{-1}$  and in the city where the albedo is much lower, the reflected radiation is  $0.4 \text{ kW h m}^2 \text{ day}^{-1}$ . This illustration shows that the urban environment has a capacity to absorb more of the sun's energy than the rural environment and thus increasing its surface temperature as shown in Figure 4.2 (b). The differences in the reflected solar radiation, anthropogenic heat, latent heat, and outgoing infrared terms lead to heat islands and result in urban island thermal circulations (Shepherd, 2005; Stewart and Oke 2012).

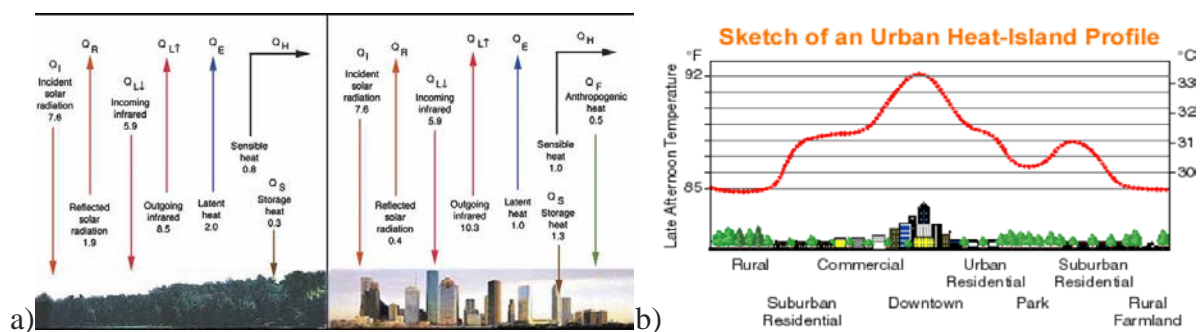


Figure 4.2: A typical rural and urban surface energy balance (the values are in units of  $\text{kW h m}^2 \text{ day}^{-1}$  (Shepherd 2005)); b) day-time urban heat island profile (from World Resource Centre)

The anthropogenic heat enters the environment directly while only a part of the solar radiation heat up the environment directly. As the earth's surface gets replaced with concrete buildings, asphalt pavements and tarmac roads in an urban setting, higher solar radiation is retained through greater thermal conductivity, while the ability to release the energy at night (stored mainly during the day), becomes low due to the sky view factor; defined as the ratio of the amount of sky hemisphere visible from ground level to that of an unobstructed hemisphere ( Grimmond,2007; Stewart and Oke, 2012), and low albedo which results in high heat retention within the building structures. Reduced vegetation cover reduces cooling through evapotranspiration,while high roughness reduces the amount of convective heat removal and transfer by winds. Increased human activities especially in transport and industries add aerosols and gaseous pollutants which increase greenhouse gas effect (*i.e.*, absorption of outgoing long wave radiation and re-radiating it back at night when the earth's surface is cooler than the air above it).Direct heat from combustion of fuels and other thermal sources of heat also increases heat ejected into an urban environment. The overall effect is a warmer urban environment as compared to the surrounding rural environment and thus theUHIphenomenon.

The strength of the UHI formed in a given city is influenced by natural and anthropogenic factors. For instance, winds help to regulate temperature by cooling down the hot urban air with the cooler air of surrounding rural areas. In cities and heavily built up areas, the wind speed is lower with frequent gusts experienced in urban canyons (Ongoma, et al., 2013) hence lowering the mixing of warm and cool air. The varied urban morphology results in increased frictional drag on the air flowing over the urban terrain, and the thermal convergence created by the UHI slows down wind. The limited air circulation and low wind speeds tend to retain heat and pollutants in the urban area thus strengthening the UHI.

Increase in cloud cover reduces the solar heat intensity and hence reduces the radiative cooling at night, while calm days and clear skies maximize the amount of radiation received (Memmon, et al 2007). From an anthropogenic perspective, urban populations influence UHI through direct heat release through metabolism, and indirectly through heat-generating activities such as domestic heating, automobiles, power plants, and air conditioners among other sources (Stewart and Oke, 2012). Other factors such as building design and building materials of the urban fabrics play a role in the amount of heat absorbed and emitted in an urban area; the balance of which forms the UHI (Figure 4.3).

Over coastal cities, the UHI interact with the ocean breeze and the prevailing synoptic wind systems to produce a unique circulation system that is largely dependent on the strength of the ocean breezes, the intensity of the UHI and the speed and direction of the prevailing winds (Freitas, et al., 2007). During the day, this interaction intensifies the sea breeze circulation and hence a chain flow is created that is able to transport pollutants and heat away from the urban area and may create urban cool islands within the city (Ohashi and Kida, 2002).

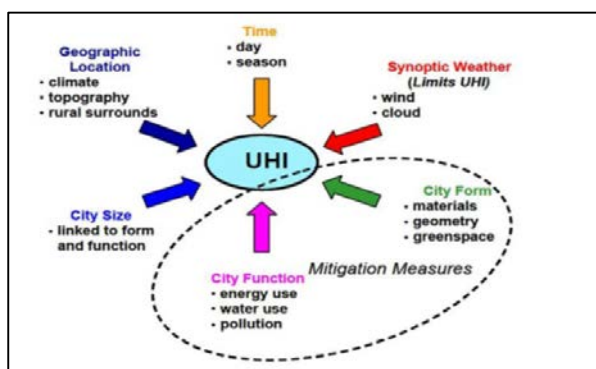


Figure 4.3: Factors that influence the generation of Urban Heat Island (Oke, 2010).

#### 4.1.2 Determination of UHI intensity

The UHI intensity (UHII) has been measured as the surface air temperature difference between an urban area and a neighboring rural area. Studies have shown that UHII phenomenon is common in cities regardless of the climatic region and is manifested more strongly at night-time than daytime. UHII is stronger in winter than summer in temperate regions, and also in dry than wet season in the tropical regions (Murphy et al., 2011; Peng et al., 2011; Vardoulaski et al., 2013; Ahmed et al., 2014). UHII has been shown to be more apparent when winds are weak and skies are clear (Shepherd, 2005). The UHII can exhibit diurnal and seasonal cycles, is modulated by wind and cloud conditions and its magnitude is proportional to the size of a city (Karl, et al., 1988; Shepherd 2005; Peng, et al., 2011). Various methods have been used to determine UHII ranging from trend analysis of long-term temperature data (Makokha and Shisanya 2010; Efe and Eyefia 2014), direct measurement of temperature differences in urban and rural locations for a given period of time, and use of satellite thermal imagery (Cheng, et al., 2006; Kloog, et al., 2012; Cheval and Dumitrescu, 2015).

Some of the assumptions made in determining UHI intensity from weather station data are that the landscape effects on both stations are insignificant and the rural station has insignificant urban effects. However there are limitations of choice of such urban and rural stations because, in many areas, the rural stations close to urban areas are also facing urbanization as urban populations increase (Arnifield, 2003; Barlow, 2014), there are inadequate meteorological stations especially in the rural areas that have not been influenced by urbanization, and the limited time in which data are available (Hart and Sailor 2009). These limitations give rise to underestimation or overestimation of the UHI effect that makes allogical comparison between studies difficult (Stewart and Oke, 2012).



According to the World Meteorological Organization (WMO, 2008), urban and rural stations should monitor the areas which give the largest and least impacts respectively to a city. However, UHIs have been determined using a range of different methods; such as the temperature difference between a well-developed urban area and least developed area (Murphy, et al., 2011), or between two differently built up areas (Dixon and Mote 2003). The methods of data collection for determining UHI in different cities all over the world are also varied in terms of the type, time scale of data collected as well as spatial coverage of the urban and rural areas.

Lack of standard methods of characterizing urban and rural sites in urban climate studies and the problem of urban sprawling into rural areas, make it difficult to adequately define urban and rural sites for such studies. It also becomes difficult to compare the representativeness of urban and rural sites within an urban area and across urban areas of other regions. To address this problem, Stewart and Oke (2012) proposed a climate based classification system for describing the physical conditions around the temperature measuring sites; the system is referred to as a Local Climate Zone (LCZ) classification scheme. The LCZs are defined by regions of uniform surface cover, structure, materials and anthropogenic activities that extend hundreds of meters to a few kilometres in the horizontal scale, upwind of the temperature sensor. Each LCZ has a typical screen-height temperature. The LCZ types are categorized by their measurable physical properties such as the sky view factors, building surface fraction height, and proportion of roughness elements (Figure 4.4). In this classification framework, the intra-urban UHI intensity is defined as the temperature difference between two LCZs that have different urban characteristics rather than the common urban-rural temperature gradients used in most studies (Stewart and Oke, 2014; Caseo, et al., 2014). Although this scheme would adequately represent intra-urban UHI intensity in a city, it requires a dense network of

temperature sensors to adequately represent different characteristics of urban morphology that may not be available in most urban areas. Most of the weather stations have sensors that measure temperature that represent a number of different LCZs (Savic, et al., 2013).

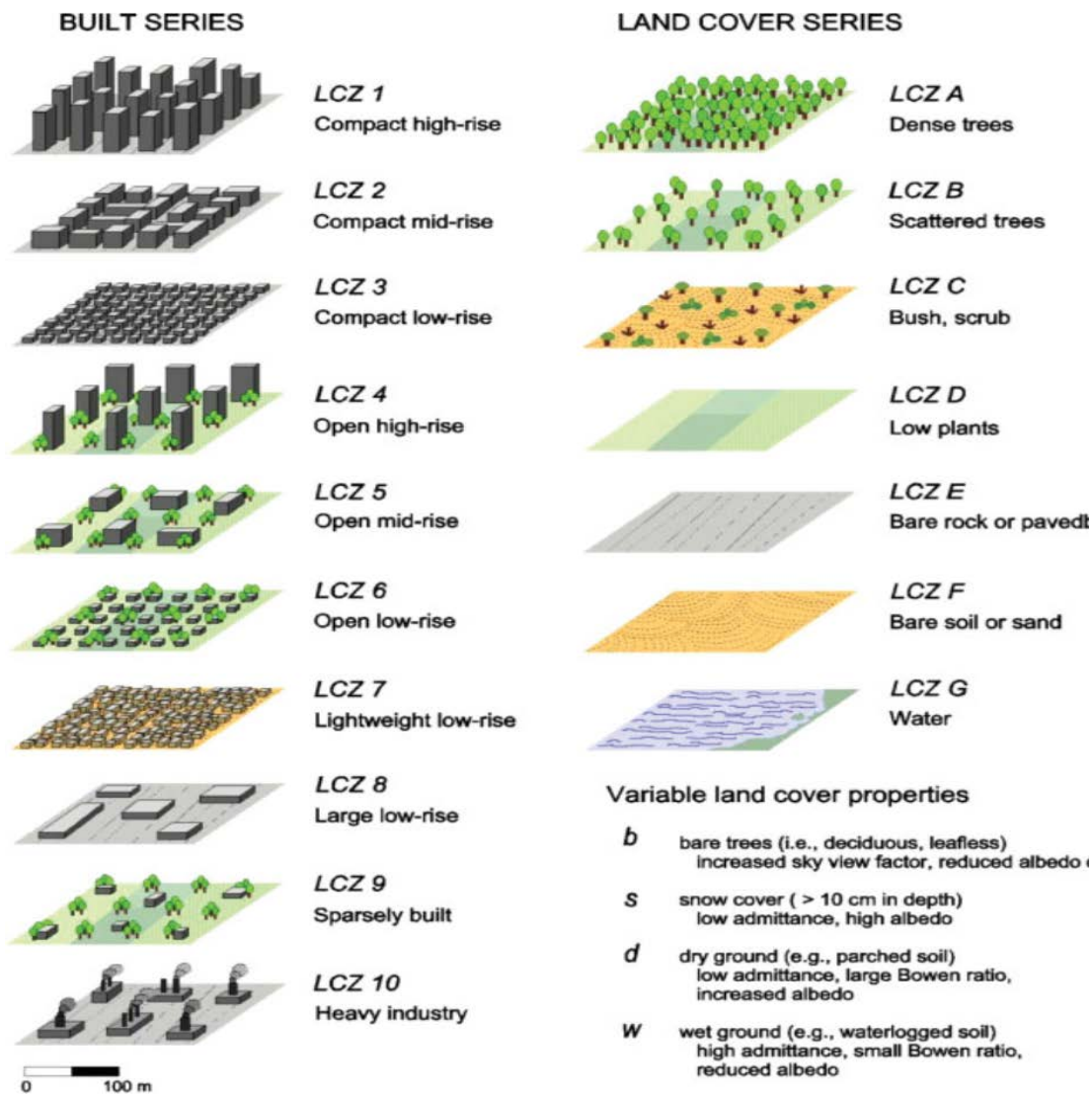


Figure 4.4: The 'Local Climate Zone' (LCZ) classification scheme and its 17 standard classes (from Stewart and Oke, 2012).

Due to the scarcity of a dense network of weather stations within urban areas, intra-urban temperature differences, including UHI have also been studied using land surface temperature (LST) data retrieved from various earth observing satellite data (Kloog, et al 2012; Cheval and Dumitrescu 2015). The remote sensing of LST is based on Plank's theory of

electromagnetism, which relates the radiative energy of a black body to its temperature. According to this theory, a black body has an emissivity of one ( $\varepsilon = 1$ ); however, most natural objects are non-black bodies with emissivity ranging between 0 and 1 ( $0 < \varepsilon < 1$ ) for a given wavelength ( $\lambda$ ) of radiation (Dash, et al., 2002). The spectral emissivity  $\varepsilon(\lambda)$  is the ratio between the radiance released by an object at a given  $\lambda$  and that emitted by a black body at the same temperature. The Planck's function for non-black body may be expressed as:

$$R(\lambda, T) = \varepsilon(\lambda) B(\lambda, T) = \varepsilon(\lambda) \frac{c_1 \lambda^{-5}}{\pi (\exp(c_2 / \lambda T) - 1)} \quad (4.2)$$

where  $B(\lambda, T)$  is the spectral radiance of a black body ( $W M^{-2} \mu m^{-1} sr^{-1}$ );  $R(\lambda, T)$  is the spectral radiance of a non-black body;  $\lambda$  is the wavelength in meters;  $\varepsilon(\lambda)$  is the emissivity at that wavelength;  $T$  is the brightness temperature in Kelvin (K), and  $c_1$  and  $c_2$ , are universal constants (Dash, et al., 2002). The temperature,  $T$ , is computed from the radiance measured at the top of the atmosphere (TOA) and can be obtained by inverting the Planck's function.

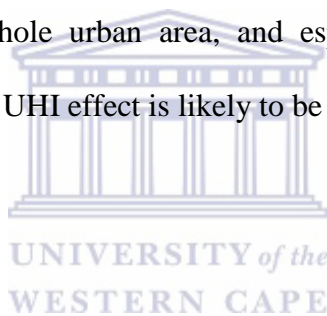
Thus:

$$T = \frac{c_2}{\lambda \ln \left[ \frac{\varepsilon(\lambda) c_1}{\pi \lambda^5 R} + 1 \right]} \quad (4.3)$$

where all the terms are as given in Equation 4.2.

The TOA brightness temperature is usually lower than the surface temperature due to atmospheric effects that attenuate the radiance energy as it passes through it, and spectral emissivity due to roughness properties of the land surface (Kloog, et al., 2012). The LST is therefore retrieved from  $T$  using various algorithms that account for the atmospheric effects.

One such algorithm is the generalised split-window that is used to retrieve Moderate Resolution Imaging Spectral radiometers (MODIS) data that was used in this study (described later). A limitation of the thermal remote sensing technique is the requirement of clear skies in order to derive accurate readings. Hence clear skies observations are obtained using cloud masking algorithms in MODIS data. The MODIS land surface temperature data has been found to have an accuracy within the limits of 1°C in the -10 and 50°C, as was validated by the MODIS land team validation (MODIS land team 2011) (Cheval and Dumitrescu, 2015). However, due to the limited time that MODIS LST data is available, it is not sufficiently long for climate studies and have been used in this study to complement the surface air temperature data from the meteorological stations. LST data are ideal since they have spatial coverage of the whole urban area, and especially over the central business districts (CBD) where the greatest UHI effect is likely to be felt and have no weather stations.



## **4.2 Methodology**

Nairobi and Mombasa (Fig 4.5) were used to investigate the existence of UHI since they have adequate temperature measuring sites within and outside the urban areas necessary for long-term temperature differences analysis (Table 4.1). The physical and climatological description of these cities was given in Chapter 1.

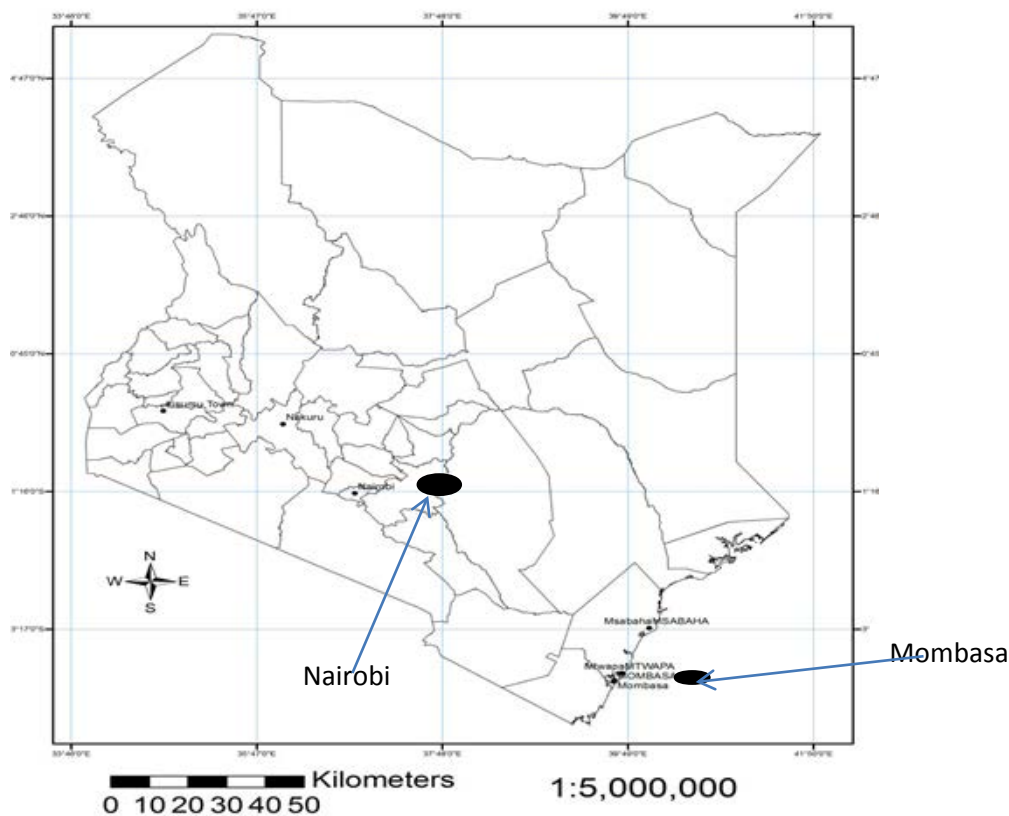


Figure 4.5: Map of Kenya showing the locations of Nairobi and Mombasa; Nairobi urban area in central highlands of Kenya and Mombasa is a coastal town

#### 4.2.1 Description of urban and rural temperature measuring stations

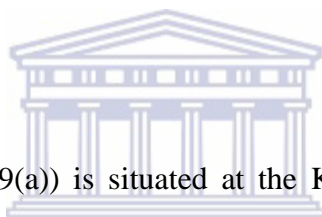
According to WMO (2011), guidelines on selection of sites for the assessment of urban effects on weather and climate (such as the UHI effect), urban and rural stations should be selected such that they are likely to sample air drawn across relatively homogeneous terrains and thus representative of a single climate zone. However due to variation in topography in Kenya, microclimate effects between the network of stations is likely to be experienced. To reduce these effects in the assessment of the UHI intensity in this study and following the study of Tyanc and Toros, (1997) and Elagib, (2011), the temperature differences are analysed for trends to examine if continued urbanization has an effect on UHI intensity.

The existing weather stations may not be described completely as a Local Climate Zone (LCZ) following the scheme proposed by Stewart and Oke (2012). However certain aspects of this scheme were used in this study in describing the land-use/cover types around each of the station designated to represent “urban” and “rural” sites. Over Nairobi for example, NR<sub>D</sub> designated as rural station for Nairobi in this study is located in the outer fringes of the Nairobi urban area and therefore have suffered urban sprawl over the years; however, it represents an area with natural vegetation and less built-up area relative to the city centre, and hence considered as a rural station. The UHI intensities were defined as the temperature differences between two sites designated as  $\Delta T(u - r)$ ;  $u$  and  $r$  representing the urban and rural stations respectively. Table 4.3 shows the description of the locations and elevations of the seven stations used for UHI investigations; of which four are within and near Nairobi (NU, NR<sub>D</sub>, NR<sub>K</sub> and NR<sub>T</sub>) and three in coastal region of Kenya (MU, MR<sub>Mt</sub> and MR<sub>Ms</sub>). Note that I used the same acronyms in Chapter 2&3, and that MU and NU represents the urban(U) sites, while all the other sites are designated as rural(R) with reference to the urban site. Description of each site is aimed at bringing out the differences between the land use/cover types in sites designated as urban and rural since some of the rural sites may have some urban characteristics due to urban sprawling into rural areas.

### ***Temperature measuring sites over Nairobi***

The distribution of meteorological weather stations around the city makes it ideal for intra-urban UHI studies using historical temperature data. Figure 4.9 (a) shows the land use types around three of the four stations used my Thesis. The rural and urban stations for Nairobi were described using information from field visits and from the Google earth maps as follows:

i) **NU** station (marked 4 in Figure 4.9 (a)) is stationed at the Wilson airport 4 km south of the CBD, about 2 km northeast of the main industrial area and borders the Nairobi Nation Park to the south. The type of land use upwind of **NU** station is mainly high-density habitation of compact mid-rise buildings with scattered trees (e.g., Fig 4.9(b)) that can be described as an LCZ2<sub>D</sub> in Stewart and Oke (2012), and an industrial area comprising of low-rise and mid-rise industrial structures described as an LCZ10 (Fig 4.4). Since wind direction over Nairobi is predominantly north-easterly (Ongoma, et al., 2013) and a temperature sensor records air temperature a few kilometres upwind of the station (Stewart and Oke 2012), **NU**, therefore, represents the air temperature of the built up areas to the east and south-east of the station including from the industrial area.



ii) **NR<sub>D</sub>** (marked 2 in Fig 4.9(a)) is situated at the Kenya Meteorological Department (KMD) headquarters, 8 km west of the CBD along Ngong Road. The immediate neighbourhood upwind of the station comprises of low-density habitation with a combination of open high-rise building types with scattered trees (LCZ4<sub>B</sub>) and woodland. This area could have urban effects due to its location downwind of the Nairobi CBD.

iii) **NR<sub>K</sub>** (marked 1 in Fig 4.9(a)) is an agro-meteorological station situated at the University of Nairobi (Kabete Campus) about 20 km northwest of the CBD. The station is in a rural environment such that the area upwind of the station is a low-density habitation of medium built-up areas to the south and open agricultural areas to the east that can be described by LCZ6<sub>B</sub>. The temperature sensor at this site



samples air mainly from the surrounding agricultural land areas thus has less urban effect than **NR<sub>b</sub>**.

- iv) **NR<sub>r</sub>** (outside the urban area) is an agro-meteorological weather station housed at Kenya Research Institute (KARI) in Thika district, and about 50 km North-east of Nairobi. The type of land use upwind of this station is agricultural, that can be described as LCZD.

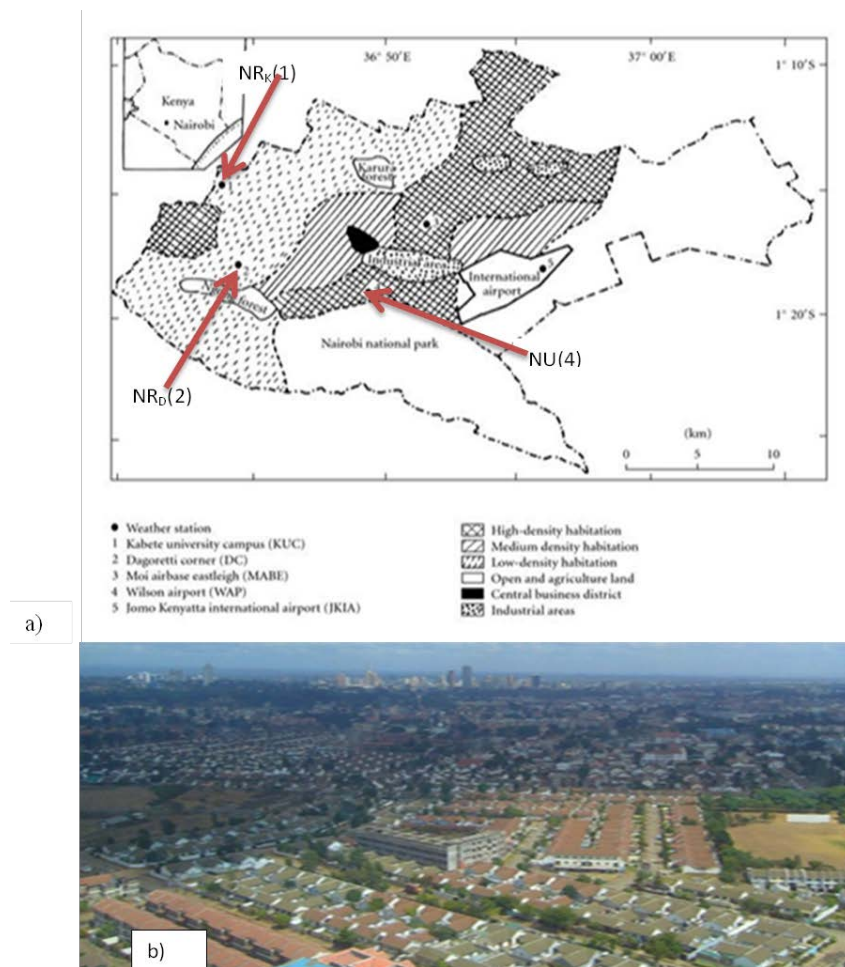


**Figure 4.6:**a) Location of three of the four weather stations used to study UHI in Nairobi (adopted from Makokha and Shisanya 2010 and modified for clarity ); b) An aerial image of Nairobi built-up areas south of the CBD close to Wilson airport (NU) (source: World Resource Institute, 2014)



### *Temperature measuring sites at the coast of Kenya near Mombasa*

The stations used to investigate UHI in Mombasa city (Fig 4.7) are as follows:

- i) **MU** station is about 10 km west of Mombasa Island. The Island accommodates the main administrative centre, the CBD, and main industrial area of Mombasacity. The land uses upwind of **MU** include dense mix of midrise buildings with few trees and mostly concrete paved land cover that can be described as an LCZ2B close to the airport, and (LCZ10) near the industrial area according to Stewart and Oke (2012) . The area is partly surrounded by ocean water from the creeks described as an LCZG (Fig 4.4). The predominant winds over Mombasa are south-easterlies (Ongoma, et al., 2013) and hence **MU** station records air temperature mainly from the areas to the east and southeast of the airport including from the main town on the Island. The temperature would also be influenced by the surrounding water from the creeks and from the ocean to the east.
- ii) **MR<sub>Mt</sub>** is a station on the outskirts of Mombasa town located at KARI (Kilifi) about 16 km northeast of Mombasa Island and a few kilometres north of the Mtwapa town. The area to the east of the station is predominantly agricultural while compact low rise buildings dominating the southern part that can be described by LCZ6 and LCZB. The area upwind of **MR<sub>Mt</sub>** station is partly from open agriculture land, partly from the town to the south-east and from the ocean since the winds are predominantly south-easterlies.

iii)  $MR_{Ms}$  is also an agro-meteorological station about 90 km northeast of Mombasa Island; the station is located in a region that is predominantly agricultural with bushes, shrubs and, woody trees; land cover is mostly pervious (bare soil) that can be described by LCZC. The area upwind of the station is completely ‘rural’ with no urban influence but open to the ocean.

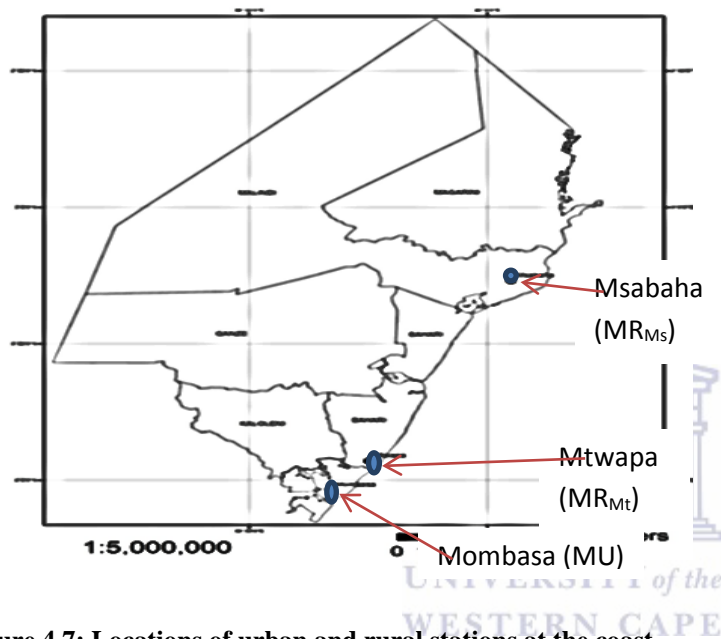


Figure 4.7: Locations of urban and rural stations at the coast

Table 4.1: Urban and rural stations used to investigate UHI

Station No.	Station name	Acronym	Lat. (°S)	Long. (°E)	Altitude (m)	Length of Temperature data
9136130	Wilson	NU (Urban)	1.38	36.82	1679	1980-2013
9136164	Dagoretti	NR <sub>D</sub>	1.30	36.70	1798	1980-2013
9136208	Kabete	NR <sub>K</sub>	1.27	36.75	1820	1980-2012
9137048	Thika	NR <sub>T</sub>	0.98	37.07	1549	1980-2012
9334021	Mombasa	MU (Urban)	4.03	39.60	55	1980-2013
9339036	Mtwapa	MR <sub>Mt</sub>	3.93	39.73	21	1980-2013
9340007	Msabaha	MR <sub>Ms</sub>	3.27	40.05	90	1974-2013

#### 4.2.2 Data and methodology

Temperature data taken from the seven stations described in the previous section were used to investigate long-term temperature differences between the urban and rural stations and consequently the existence of UHI in the two major towns of Kenya. The approach I used to investigate UHI from the surface air temperature was to compute the monthly, seasonal and annual UHI intensities and analyse their trends. Land surface temperature (LST) data for the last twelve years were also obtained from remote sensing using the MODIS data (MOD11A2) taken at a spatial resolution of one (1) km and temporal resolution of eight(8)days. The LST data were averaged into monthly means and used as an alternative set for investigating urban temperature variations and the existence of UHI.

##### *Computations of UHI from air temperature*

In my thesis, the urban heat island intensity (UHI) is defined as the temperature difference between the urban and rural station, symbolically given as:

$$\Delta T_{\max}(u-r) = \theta_{uT_{\max}} - \theta_{rT_{\max}} \quad (4.4a)$$

$$\Delta T_{\min}(u-r) = \theta_{uT_{\min}} - \theta_{rT_{\min}} \quad (4.4b)$$

where  $\Delta T_{\max}(u-r)$  [  $\Delta T_{\min}(u-r)$  ] is the temperature differences between the urban and rural stations respectively and  $\theta_{uT_{\max}}$  ( $\theta_{rT_{\min}}$ ) are the urban and rural  $T_{\max}$  [  $T_{\min}$  ] respectively. The urban-rural pairs of stations used are shown in Table 4.2. The mean monthly  $T_{\max}$  and  $T_{\min}$  from the urban and rural stations were used to compute the monthly  $\Delta T_{\max}(u-r)$  and  $\Delta T_{\min}(u-r)$  respectively, while the seasonal temperature differences were computed as the average monthly differences for December, January and February (DJF), March, April and May (MAM), June July August (JJA) and September, October and November (SON). These seasons correspond to the hot and dry (DJF); warm and wet (MAM); cool and cloudy (JJA) and; warm and wet (SON) seasons respectively of the equatorial East Africa (EEA) region.

Variables computed from the station data were the monthly, seasonal and annual  $\Delta T_{\max}$  (u-r) and  $\Delta T_{\min}$  (u-r) for each pair of stations over Nairobi and Mombasa urban areas. The time series for the monthly  $\Delta T$ (u-r) variables were computed by subtracting the rural monthly  $T_{\max}$  ( $T_{\min}$ ) from the corresponding urban value for each month thus:

$$\Delta T_j^i(u-r) = \theta_{ju}^i - \theta_{jr}^i \quad (4.5)$$

where  $\Delta T_j^i$  is the temperature difference of  $T_{\max}$  (or  $T_{\min}$ ) of month  $i$  and year  $j$ ;  $\theta_{ju}^i$  and  $\theta_{jr}^i$  are the point temperature data of month  $i$  and year  $j$  for urban and rural station respectively. Note that for each year  $j$  there are twelve values ( $i=1, \dots, 12$ ) and  $j$  will depend on the length of data i.e.,  $j=1, \dots, n$  where  $n$  is the time length of data. For the seasonal and annual means for year  $j$  were computed as:

$$\text{Seasonal mean } [\Delta T_{jk} (u - r)] = \frac{\sum_{i=1}^3 \Delta T_j^i}{3} \quad (4.6)$$

Where  $k$  is the season of three months in each year and  $j=1, \dots, n$

$$\text{Annual mean } [\Delta T_j(u-r)] = \frac{\sum_{i=1}^{12} \Delta T_j^i}{12} \quad (4.7)$$

The computations yielded twelve (12) time series for the monthly temperature differences for each pair of stations, four (4) for the seasonal values and one (1) for the annual values and each variable had time length  $n$ .

**Table 4.2: Urban-rural pair of stations used to compute temperature differences ( $\Delta T(u-r)$ )**

Urban area	Station pairs	Length of temperature data
Nairobi	NU-NR <sub>D</sub>	1980-2013
	NU-NR <sub>K</sub>	1980-2013
	NU-NR <sub>T</sub>	1980-2013
Mombasa	MU-MR <sub>Mt</sub>	1990-2013
	MU-MR <sub>Ms</sub>	1990-2013

The computed  $\Delta T_{\max}$  (u-r) and  $\Delta T_{\min}$  (u-r) were used to explore temporal and spatial long-term variations of UHI intensity for each urban area and if there have been trends in the UHI. Thus trend analysis using the Mann-Kendall and linear regression methods was done on each variable and results tested using the t-test at  $\alpha=0.05$ . The hypothesis for the trend analysis was that UHI intensity would have positive trend if the temperature of the urban station has increased over time due to urban effects and hence imply the strengthening of UHI. The assumption was that none of the rural stations has decreasing trends (in this case supported by results of Chapter 2). The methods of trend analysis of time series applied in this Chapter were discussed in detail in Chapter 2 (Section 2.5).



### *Determination of UHI from land surface temperature*

The advantage of the land surface temperature (LST) remote sensed data is in their ability to represent large area whose temperature is synchronously observed. LST data have been used in many UHI studies to supplement or as alternative to weather station data (Chen, et al., 2006; Schwarz, et al., 2011; Cheval and Dumitrscu 2015). LST data for Nairobi and its environs, between the latitudes 1.10°S and 1.52°S and longitudes 36.51°E and 37.21°E, and for Mombasa and its environs, between the latitudes 3.85°S and 4.19°S and longitudes 39.51°E and 39.82°E were retrieved from the Moderate Resolution Imaging Spectroradiometer (MODIS) ([modis.gsfc.nasa.gov/data/dataproduct/dataproducts](http://modis.gsfc.nasa.gov/data/dataproduct/dataproducts)). The MODIS product MOD11A2 is obtained using the generalized split-window algorithm (Wan and Dozier, 1997). Generalized Split Window algorithm is used to execute corrections of the atmospheric effects based on the differential absorption of infra-red (IR) bands next to each other and within one atmospheric window. The algorithm requires land surface emissivity as the input data (Wan and Dozier, 1997).

According to the split window algorithm, LST is retrieved from the equation given as:

$$LST = b_0 + \left( b_1 + b_2 \left( \frac{1-\varepsilon}{\varepsilon} \right) + b_3 \frac{\Delta\varepsilon}{\varepsilon^2} \right) \frac{T_i - T_j}{2} + \left( b_4 + b_5 \left( \frac{1-\varepsilon}{\varepsilon} \right) + b_6 \frac{\Delta\varepsilon}{\varepsilon^2} \right) \frac{T_i - T_j}{2} \quad (4.8)$$

where  $\varepsilon$  and  $\Delta\varepsilon$  are the mean and differences of emissivity in the wavelength bands 31 and 32 and  $i=31$  and  $j=32$ ;  $T_i$  and  $T_j$  are the top of the atmosphere brightness temperature of each band computed from Equation 4.3; the coefficients  $b_0, b_1, \dots, b_6$  depend on viewing zenith angle, atmospheric surface temperature and water vapour, and are derived using regression analysis of radiative transfer simulation data of surface air temperature (Wan, 2014). The MOD11A2 comprises of LST data for day-time and night-time taken at a spatial resolution of 1 km and temporal resolution of 8 days and computed as monthly mean values at each co-ordinate “X”, “Y”; where “X” represents the longitude and “Y” the latitude. Twelve years of monthly mean LST was available for analysis (2004-2015). Kloog, et al., (2012) using data for Massachusetts (USA) indicated that there is a high correlation ( $R^2 = 0.85$ ) between air temperature and LST especially for the night-time values and hence comparisons of UHI from LST and air temperature data would be appropriate.

In my Thesis, LST data was used to:

- a) examine the variations of day-time and night-time temperature across Nairobi and Mombasa urban areas. Here, two transects (North-south (N-S) and west-east (W-E)) that traverse the heavily built-up areas (CBDs) in each city were drawn and LST along each transect used to investigate surface UHI. The transects were drawn using the Google Earth maps and city land use maps, traversing the CBD and the heavily built up areas of each city (Figure 4.8). Thus; i) N-S transect for Nairobi was located along the longitude 36.81°E and the latitudes varied from 1.09°S (rural areas

to the north of the CBD) to 1.41°S (National park and rural areas south of the CBD). The W-E transect passed through the latitude 1.28°S and the longitudes varied from 36.64 °E (low-density residential areas) to 37.10°E (high density residential and open land) (Fig 4.8(a&b)). Day-time and night-time monthly LST for pixels along longitude 36.81°E ( for N-S)and latitude1.28°S (for W-E)were then plotted against the latitude (longitude) so as to observe the temperature profile of Nairobi urban area for both day-time and night-time and thus locate the UHI; ii)The N-S and W-E transects for Mombasa were drawn passing through Mombasa Island which formsthe main part of the city (Figure 4.8(c&d)). The N-S transect was located along the longitude 39.64°E and the latitudes varied from 3.85°S (rural areas to the north of the Island) to 4.18°S (rural areas south of the Island). The W-E transect passed through the latitude 4.05°S and the longitudes varied from 39.48°E (west of Port Rietz) to 37.10°E (rural land to the east of the Island) (Fig 4.8(c&d)).Note that the main city of Mombasa is surrounded by water, and thetransects pass through the water both in the N-S and W-E directions. Day-time and night-time LST for pixels along longitude39.64°E ( N-S)and latitude 4.05°S (W-E) were then plotted against the latitude (longitude) so as to observe the temperature profile of Mombasa Island for both day-time and night-time and thus locate the UHI. For each urban area, the LST data used for analysis included mean temperature for the cold season (represented by July), hot season (represented by January) and the annual mean for each year; a mean for the twelve years for the same months and annual mean were also computed and plotted in order to examine the long-term mean temperature profiles. The results of this analysis are presented in the next Section.



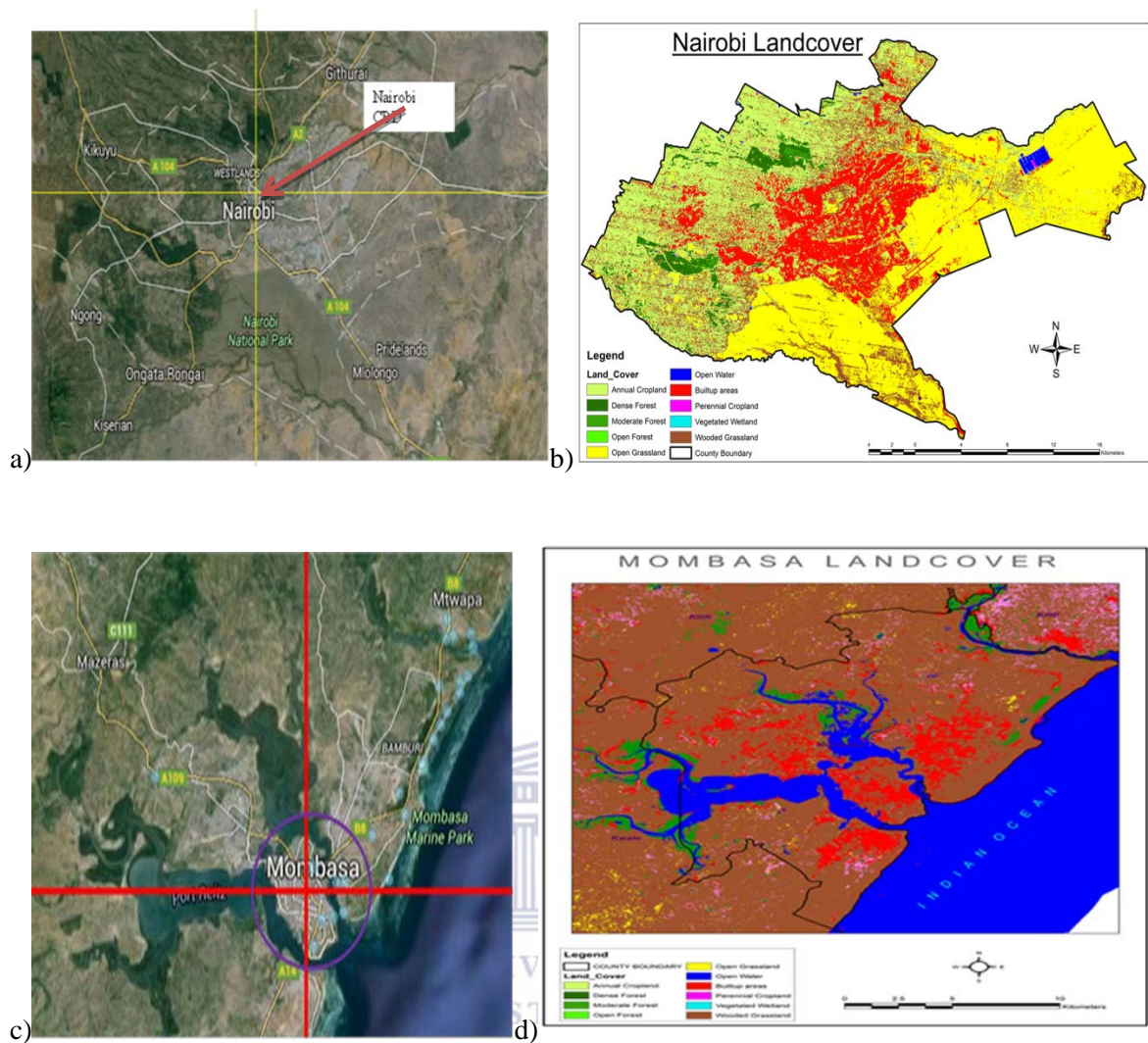


Figure 4.8: a) Google Earth map showing the N-S (along 36.81 °E) and W-E (along 1.28°S) transects (marked yellow) used to compute temperature profiles for Nairobi; b) Nairobi land use Map; c) Google Earth map showing the N-S (along 39.64°E) and W-E (along 4.05°S) transects (marked red) used to compute temperature profiles for Mombasa; d) Mombasa land use map (both land use maps adopted from survey of Kenya, 2014)

b) Surface temperature maps of the mean monthly LST data were constructed for each urban area to examine the spatial distribution of the LST. The LST MODIS images are typically distributed as HDF (Hierarchical Data Format) 10 by 10 tiles, projected in sinusoidal projection. This type of projection is not supported in many geographical information systems (GIS). The data was first processed into a GIS usable format and

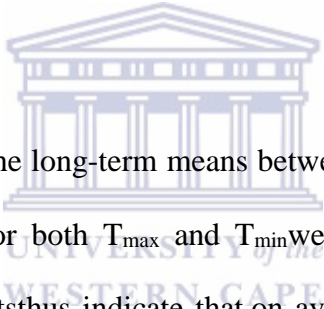


plotted into surface temperature raster maps. A base maps showing the administrative boundaries of each urban area were then overlaid on the LST raster maps.

### 4.3 Results and discussion

#### 4.3.1 The difference of means of $T_{\max}$ and $T_{\min}$ in urban and rural stations

The long-term means of  $T_{\max}$  and  $T_{\min}$  of the urban and rural stations over Nairobi and Mombasa were computed (Table 4.3) and differences of means tested for significance ( $\alpha = 0.05$ ) for the period of 1980-2013 (Table 4.4). The hypothesis here was that significant positive (negative) differences in the long-term means of the urban and rural temperatures would infer possible existence of UHI (urban cool island(UCI)) in the urban areas.



Over Nairobi, the differences in the long-term means between  $NU-NR_D$ , and  $NU-NR_K$  for all seasons and the annual mean, for both  $T_{\max}$  and  $T_{\min}$  were positive (positive t-values) and statistically significant. The results thus indicate that, on average, the urban station is warmer than the rural stations. The relative warmth of the urban station could be as a result of micro-climatic factors or the existence of the UHI. Further investigations were therefore carried out in next section to establish if this difference is due to UHI.

Over Mombasa urban area; i) the  $T_{\max}$  differences of means between MU and the rural stations was significant and t-values were positive except for DJF season which was negative (Table 4.4). Positive difference indicates that the urban station is on average warmer than rural stations while negative values indicate that the rural station is warmer; for instance  $MR_{Mt}$  and  $MR_{Ms}$  (rural stations in Mtwapa and Msabaha) are significantly warmer than Mombasa airport during DJF season; ii) the difference of means for the  $T_{\min}$ , for the two pairs

of stations (MU-MR<sub>Mt</sub> and MU-MR<sub>Ms</sub>), are all negative and significant except DJF season which is not significant; thus implying that it is warmer in the rural areas at night than in urban area.

**Table 4.3: The long-term mean of seasonal and annual T<sub>max</sub> and T<sub>min</sub> of selected stations in and near Nairobi and Mombasa**

Season	NU		NR <sub>D</sub>		MU		MR <sub>Mt</sub>		MR <sub>Ms</sub>	
	T <sub>max</sub>	T <sub>min</sub>	T <sub>max</sub>	T <sub>min</sub>	T <sub>max</sub>	T <sub>min</sub>	T <sub>max</sub>	T <sub>min</sub>	T <sub>max</sub>	T <sub>min</sub>
<b>Mean temperature (°C)</b>										
<b>DJF</b>	26.2	14.6	25.1	13.8	32.4	22.6	31.6	22.9	31.9	22.9
<b>MAM</b>	25.8	15.2	24.6	14.8	31.4	22.9	31.0	23.7	31.0	23.8
<b>JJA</b>	23.0	12.4	21.9	12.0	28.2	20.1	27.8	21.5	27.7	22.3
<b>SON</b>	25.4	13.9	24.3	13.7	28.8	21.7	29.4	22.0	29.6	22.4
<b>Annual</b>	25.1	14.1	24.0	13.6	29.3	21.8	29.9	22.5	30.0	22.9

**Table 4.4: Analysis of difference of mean of T<sub>max</sub> and T<sub>min</sub> between urban and rural stations over Nairobi and Mombasa for each season and the annual mean; t-value represent the t-statistic; \* indicate t- values that are not significant at a  $\alpha = 0.05$**

Nairobi			Mombasa			
	T <sub>max</sub>	T <sub>min</sub>	T <sub>max</sub>	T <sub>min</sub>	T <sub>max</sub>	T <sub>min</sub>
	NU-NR <sub>D</sub>	NU-NR <sub>D</sub>	MU-MR <sub>Mt</sub>	MU-MR <sub>Mt</sub>	MU-MR <sub>Ms</sub>	MU-MR <sub>Ms</sub>
<b>DJF</b>						
<b>t-value</b>	6.1	4.9	-8.3	-1.4*	-2.8	-1.5*
<b>MAM</b>						
<b>t-value</b>	7.0	2.7	3.4	-4.6	-0.4*	-3.8
<b>JJA</b>						
<b>t-value</b>	7.3	3.1	5.0	-7.5	3.5	-10.8
<b>SON</b>						
<b>t-value</b>	8.9	1.5	3.5	-3.1	0.2*	-5.1
<b>ANNUAL</b>						
<b>t-value</b>	4.5	3.8	6.5	-4.7	2.4	-5.8

In general, the differences in the means between the urban and rural stations were positive over Nairobi for both  $T_{\max}$  and  $T_{\min}$  which (in the absence of the spatial differences) would be an indicator of UHI. Over the coastal areameans of  $T_{\min}$  (and in some cases even  $T_{\max}$ ) was higher in the rural stations than the urban which is a pointer to the existence of an urban cool island (UCI). Further investigations were carried out in next sections to confirm these observations.

#### **4.3.2 UHI over Nairobi**

##### *Temperature trends for Nairobi urban area*

To further examine the existence of UHI over Nairobi, the rates of warming in the urban and rural stations for the seasonal  $T_{\min}$  were compared using the linear regression coefficients ( $\beta$ ) which are statistically significant at  $\alpha= 0.05$  (Fig 4.9). The proposition here was that if urban areas have higher rates of warming than the rural areas, then UHI exists since in the absence of the urban effects the temperature within Nairobi would be influenced by similar climate factors and relatively change at the same rate (note that from Chapter 2,  $T_{\max}$  had no trends over Nairobi and hence not used here).  $NU$  and  $NR_D$  have comparatively equal rates of change in all seasons while  $NR_K$  has the lowest except in JJA season.

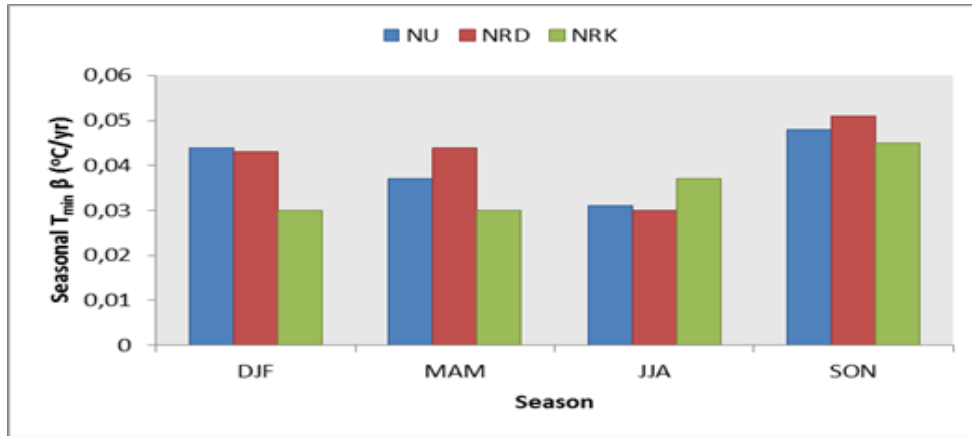


**Figure 4.9: Comparison between the rates of change of seasonal  $T_{\min}$  between urban and rural stations in Nairobi area. (all the regression coefficients ( $\beta$ ) are significant at  $\alpha=0.05$ )**

The observed significant warming of  $T_{\min}$  in the three stations could be attributed to urbanization as well as global warming effects (as established in Chapter 2). However, UHI could not clearly be inferred from the trends between NU and NR<sub>D</sub> since the stations have almost equal rates of change of  $T_{\min}$  over time. However, there is a considerable difference between the urban station and NR<sub>K</sub>. Therefore there is a possibility that UHI exists in the urban area whose intensity is stronger between NU and NR<sub>K</sub> than between NU and NR<sub>D</sub>. In the next section, temperature differences were used to examine the UHI intensity between the urban and rural stations and its temporal variability.

***Temporal variability and trends of temperature differences ( $\Delta T(u-r)$ )***

Figure 4.10(a,b&c) shows the temporal variability of the of the annual mean  $\Delta T_{\max}(u-r)$  and  $\Delta T_{\min}(u-r)$  for NU-NR<sub>D</sub>, NU-NR<sub>K</sub> and NU-NR<sub>T</sub> pairs of stations respectively. Figure 4.11 shows the long-term mean seasonal and annual values of the  $\Delta T_{\max}(u-r)$  and  $\Delta T_{\min}(u-r)$  of the same station pairs.

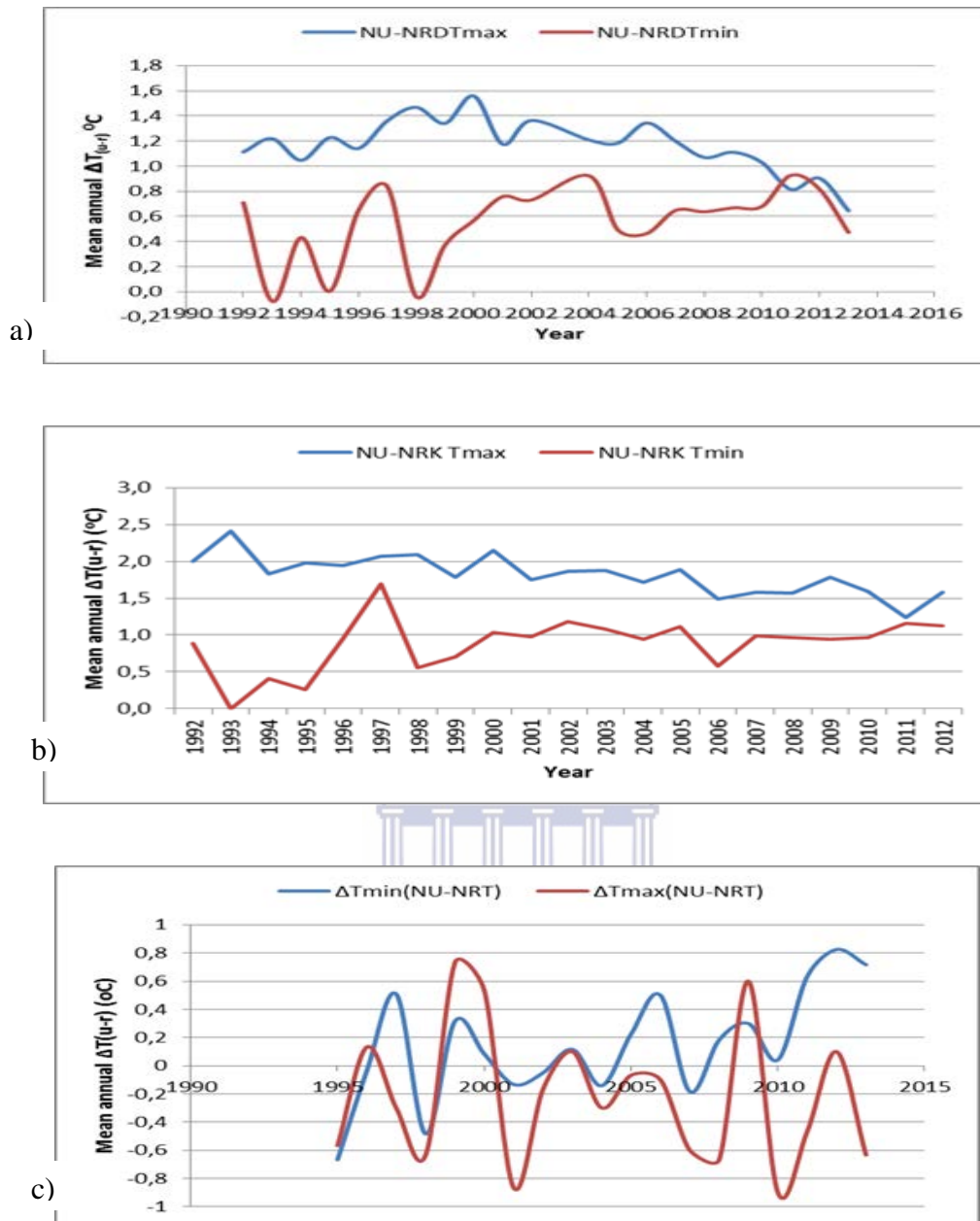


**Figure 4.10: Temporal variations of annual  $\Delta T_{\text{max}}(u-r)$  and  $\Delta T_{\text{min}}(u-r)$  for urban-rural pair of station in Nairobi; a) NU- NR<sub>D</sub>, b) NU- NR<sub>K</sub>, and c) NU- NR<sub>T</sub>**

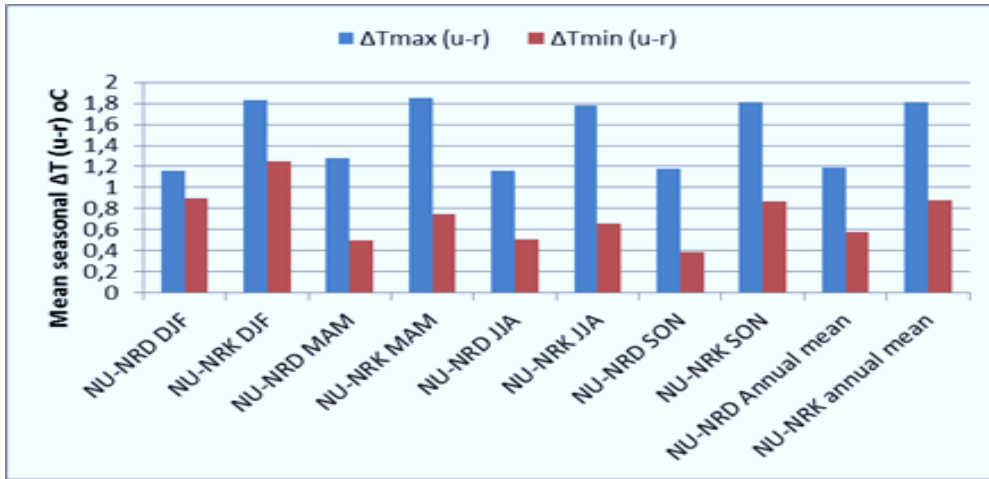


**Figure 4.11: Seasonal and annual mean values of  $\Delta T_{\max} (u-r)$  and  $\Delta T_{\min} (u-r)$  over Nairobi (for the temperature differences between urban station**

The observations I made from the above results were that; i) higher temperature differences between the urban and rural areas over Nairobi on average occur during the day; *i.e.*, the  $\Delta T_{\max} (u-r)$  of each pair of stations are higher than the  $\Delta T_{\min} (u-r)$ . The  $\Delta T_{\max} (u-r)$  values were however observed to be decreasing with time. For example, annual mean  $\Delta T_{\max} (u-r)$  for NU-NRD and NU-NRK was 1.6°C and 2.3°C respectively in the year 2000 and has decreased to about 0.8°C and 1.1°C respectively by 2013. Note that the annual mean  $\Delta T_{\max} (u-r)$  for NU-NRT (Fig 4.9 (c)) had no observable trend and the variability does not suggest consistent UHI intensity while  $\Delta T_{\min} (u-r)$  showed an increasing trend; ii) the  $T_{\min}$  annual mean temperature differences are increasing although they are lower than the day-time for each pair of stations and; iii) seasonally,  $\Delta T_{\min} (u-r)$  are lower compared with those of  $\Delta T_{\max} (u-r)$  in each season. Higher values of  $\Delta T_{\min} (u-r)$  were observed in the dry season (DJF) than in warmer seasons. Seasonal values of  $\Delta T_{\max} (u-r)$  and  $\Delta T_{\min} (u-r)$  are relatively much lower for NU-NRD than the NU-NRK pair in all seasons.

These observations indicate that positive temperature gradients exist between the highly built up areas around the Wilson Airport (NU) and the rural stations in the outer fringes of the city. The differences for  $T_{\max}$  are however decreasing with time being higher in the 1990s than in recent years (2013) and are fairly constant in all seasons, while for  $T_{\min}$ , the differences are increasing and are higher during the warm seasons than the colder season. Since the stations are within the same climatic zone and the difference in elevation is minimal (<150m), temperature differences could be attributed to the UHI effect and their values represent the UHI intensity between the urban and the rural area. The UHI intensity was tested for trends to ascertain if the changes observed in the exploratory time series were statistically significant.

Table 4.5 shows the result of the trend analysis in which negative trends for  $\Delta T_{\max}(u-r)$  and positive trends for  $\Delta T_{\min}(u-r)$  were realised.



**Table 4.5: Assessment of temporal trends of  $\Delta T(u-r)$  for Nairobi using linear regression; results are only for those seasons that trends were significant at  $\alpha=0.05$**

Season	Station pair	t-statistic	$\beta$ ( $^{\circ}\text{C}/\text{year}$ )	p-value
JJA $\Delta T_{\max}(u-r)$	NU-NR <sub>K</sub>	-4.8	-0.06	0.000
SON $\Delta T_{\max}(u-r)$	NU-NR <sub>K</sub>	-5.2	-0.05	0.001
SON $\Delta T_{\min}(u-r)$	NU-NR <sub>K</sub>	2.0	0.03	0.042
Annual $\Delta T_{\max}(u-r)$	NU-NR <sub>K</sub>	-5.6	-0.03	0.000
Annual $\Delta T_{\min}(u-r)$	NU-NR <sub>K</sub>	2.1	0.03	0.043
Annual $\Delta T_{\max}(u-r)$	NU-NR <sub>D</sub>	-2.8	-0.02	0.011
Annual $\Delta T_{\min}(u-r)$	NU-NR <sub>D</sub>	2.2	0.02	0.040
MAM $\Delta T_{\min}(u-r)$	NU-NR <sub>T</sub>	4.7	0.05	0.034
JJA $\Delta T_{\min}(u-r)$	NU-NR <sub>T</sub>	2.3	0.03	0.024
SON $\Delta T_{\min}(u-r)$	NU-NR <sub>T</sub>	5.1	0.05	0.025
Annual $\Delta T_{\min}(u-r)$	NU-NR <sub>T</sub>	3.0	0.02	0.005

From the trend results, the following observations were made:

- i. There are Significant negative trends in the  $\Delta T_{\max} (u-r)$  seasonal and annual series especially in the NU-NR<sub>K</sub> pair; thus implying that the day time UHI intensity between Wilson airport and Kabete has declined over the years. Note that NU-NR<sub>D</sub> pair had a negative trend only in the annual  $\Delta T_{\max}(u-r)$  and NU-NR<sub>T</sub> had no trends in  $\Delta T_{\max}(u-r)$ .
- ii.  $\Delta T_{\min} (u-r)$  series had significant positive trends in all pairs; In particular, NU-NR<sub>T</sub> pair has increasing trends in all seasons except DJF, while NU-NR<sub>K</sub> had positive trends in SON and annual  $\Delta T_{\min} (u-r)$  and NU-NR<sub>D</sub> had positive trends only in the annual mean  $\Delta T_{\min} (u-r)$ .

The existence of a positive trend in night-time UHI intensity would imply that temperature in the urban station has been increasing, or temperature in the rural station has been decreasing. Since the latter is not the case (from Chapter 2) then, positive UHI trends imply strengthening of the night-time UHI over time in the city. On the other hand, decreasing trends of day-time UHI would imply a number of possibilities; i) that the rural temperature is increasing more than in the urban (which was observed for Kabete station  $T_{\max}$  in Chapter 2) and/ or; ii) that temperature is decreasing in the urban areas. Since  $T_{\max}$  of NU had no temporal trends, there is a high possibility that the weakening of UHI would be due to the increasing  $T_{\max}$  in the rural areas.

To examine if indeed increasing  $T_{\max}$  of the rural areas is associated significantly with decreasing  $\Delta T_{\max} (u-r)$ , I correlated the annual mean  $\Delta T_{\max}(u-r)$  with the rural stations' annual  $T_{\max}$ . The results (Figure 4.12) showed negative relationships that were statistically significant. The relationship is stronger between NU-NR<sub>K</sub> than NU-NR<sub>D</sub>. The negative



correlations imply that the increasing trends in  $T_{\max}$  in rural areas are to some extent influencing the decline in temperature gradient between the urban and rural areas and thus lowering the UHI.

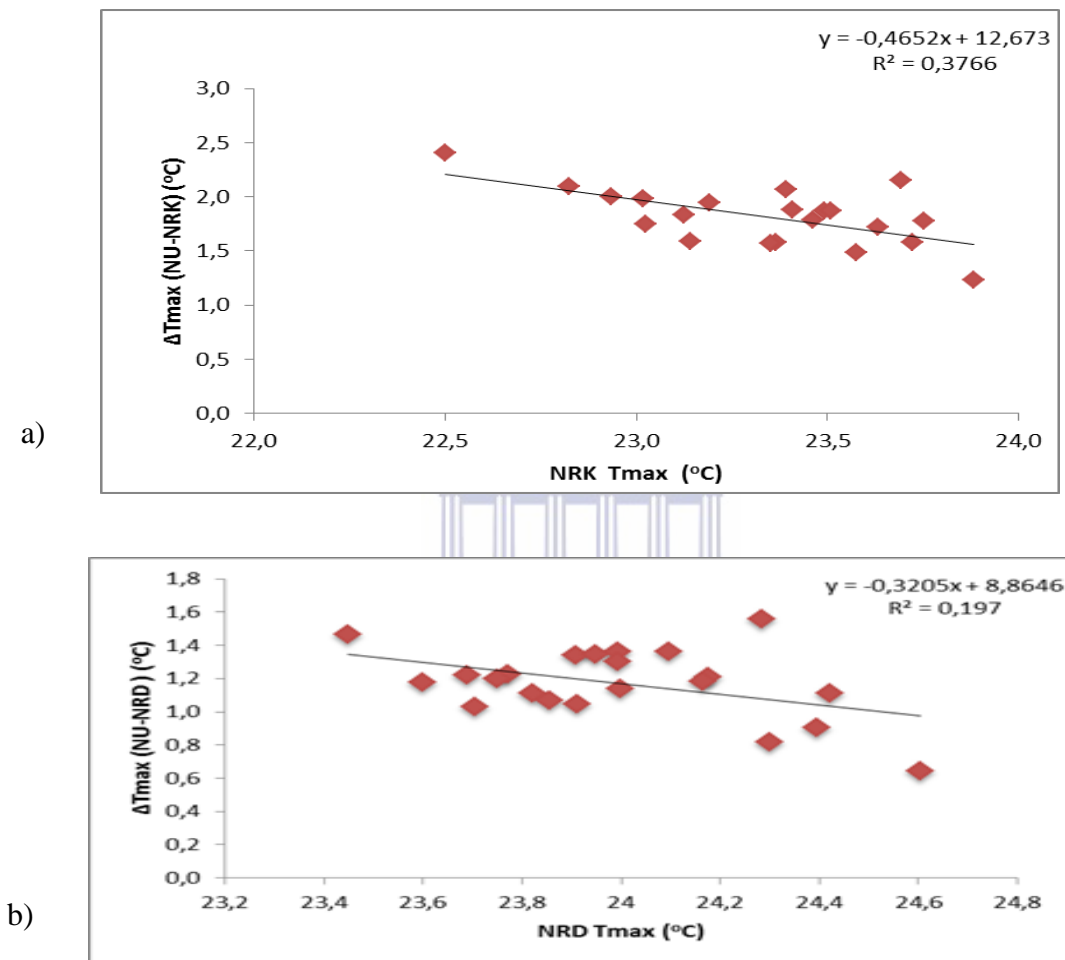


**Figure 4.12: Linear relationships between  $\Delta T_{\max}(u-r)$  and the rural  $T_{\max}$  over Nairobi depicting the influence of increasing rural  $T_{\max}$  on UHI intensity; a)  $\Delta T_{\max}(u-r)$  for NU-NR<sub>K</sub> and  $T_{\max}$  at NR<sub>K</sub>; b)  $\Delta T_{\max}(u-r)$  for NU-NR<sub>D</sub> and  $T_{\max}$  at NR<sub>D</sub>**

The relationship between UHI and temperature also reported in Camillon and Baros (1997) who indicated that negative correlations between UHI and rural temperature suggest that UHI intensity is partially dependent on temperature itself. Thus increasing trends of rural

temperature would diminish the urban-rural temperature gradients. However, considering the weak correlations, other factors could also be influencing that change. Further investigations of UHI were done using the land surface temperature in the next Section.

The conclusions drawn from the analysis of the temperature differences between urban and rural areas over Nairobi were that; i) a stronger day-time than night-time UHI exist in Nairobi whose intensity relative to the rural stations is diminishing partly due to increasing  $T_{\max}$  in rural stations; ii) A night-time UHI also exists whose intensity relative to rural stations is increasing partly due to higher rate of increase of  $T_{\min}$  in the urban area. However, due to the lack of a dense network of weather stations, the conclusions only hold for the part of the urban area where the urban station is located and only relative to the rural areas considered here. UHI intensity has been shown to be dependent not only on the location of the urban station in the city but also the land use type of the rural area(s) used to compute the UHI (Cheval and Demistrescu, 2015). To expand more on the existence of UHI over Nairobi, and considering that the urban station used in this section was not within the CBD, land surface temperature data was used.

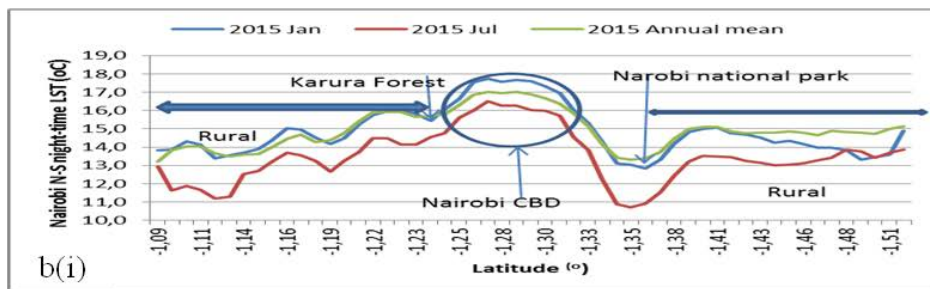
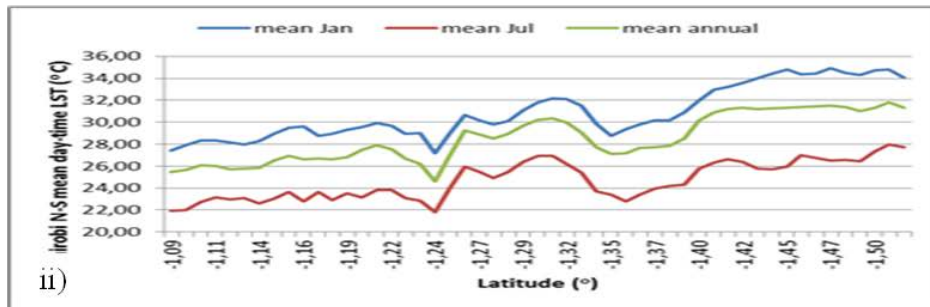
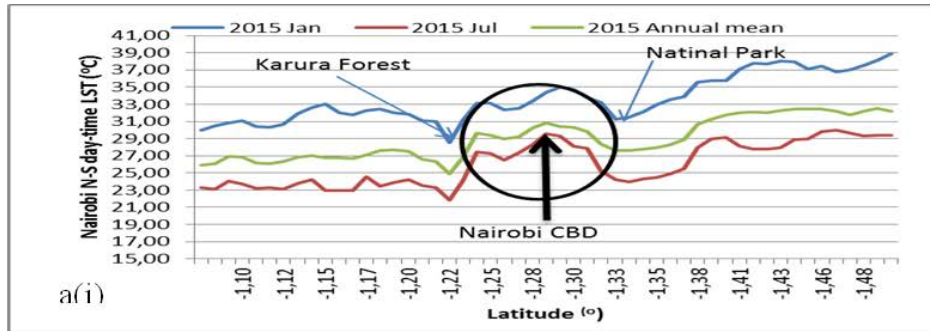
### *Analysis of UHI from LST over Nairobi*

Lack of a dense network of stations in and around Nairobi to represent different land use types, necessitated the use of LST data to assess the spatial variation of UHI in Nairobi. The gridded monthly LST data dating from January 2004 to December 2015 were used. Day-time and night-time LST for a north-south (N-S) transect, along the longitude 36.81°E, and west-east (W-E) transect, along the latitude 1.28°S, both passing through the CBD were used.

Latitude (longitude) was plotted against temperature for each year showing the variation of LST during the hot season (represented by January), cool season (represented by July) and the annual mean LST for each year; also the long-term average SLT for each month and each year (averaged for the period 2004-2015), was plotted against the longitude (latitude) to show the mean profile. The aim of this analysis was to observe if temperature profiles (for both day-time and night-time) of the transects passing through the heavily built-up areas of the city will show the urban heat island and the spatial characteristic of its intensity when the city is approached from rural areas with different land use/cover types.

Figure 4.13(a) shows the N-S variation of day-time, and night-time LST for the year 2015, and the mean profile. Figure (4.13a(i)) shows a plot for the year 2015 showing the location of the CBD and the land use types to the North and south of the CBD; Figure (4.13a (ii)) shows the same information but for the mean LST profile. Figure 4.13(b) shows the N-S variation of the night-time temperature for the same periods. Note that the profiles were labelled using the land use and Google Earth maps shown in Fig 4.8(a).

Figure 4.14(a) shows the W-E variation of day-time, and night-time LST for the year 2015, and the mean profile for the twelve years (2004-2015). Figure (4.14a (i)) shows a plot for the year 2015 showing the location of the CBD and the land use types to the west and east of the CBD; Figure (4.14a (ii)) shows the same information but for mean LST profile for the period (2004-2015). Figure 4.14(b) shows the W-E variation of the night-time temperature for the same periods.



WESTERN CAPE

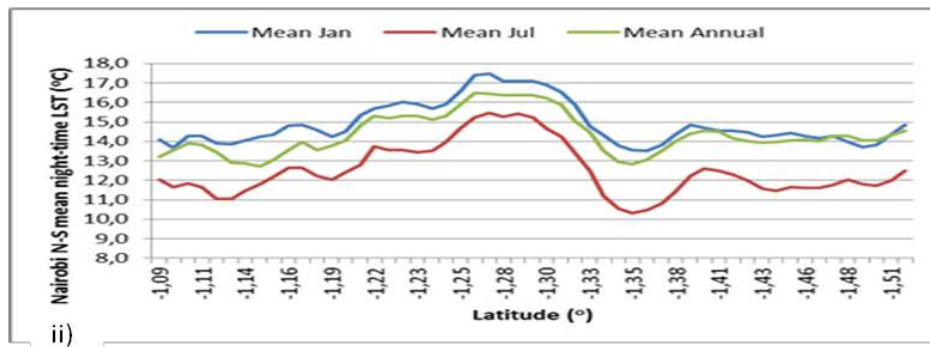


Figure 4.13: N-S land surface temperature profiles (along longitude 36.81) showing; a) day-time; b) night-time temperature variability between the CBD and rural area to the north (Karura forest) and south (woodland in the Nairobi National Park); each profile shows temperature variability for the warm (January) and cool (July) months and the annual mean for; i) 2015; ii) long-term average (2004-2015); note Nairobi UHI is observed clearly within the CBD(1.25-1.30°S) for both day and night-time profiles

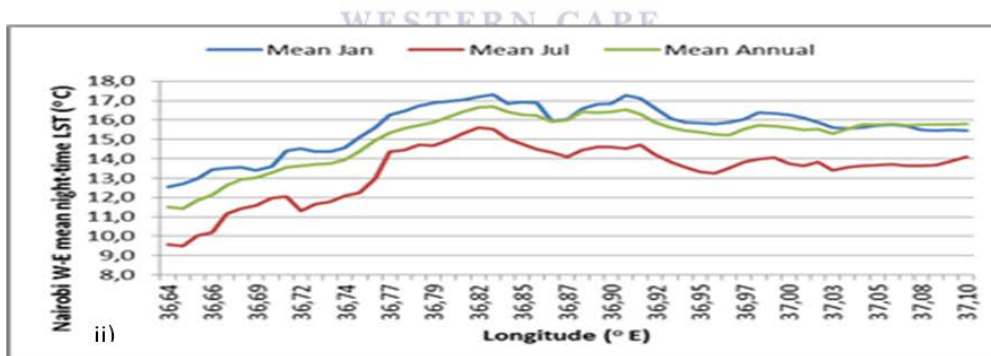
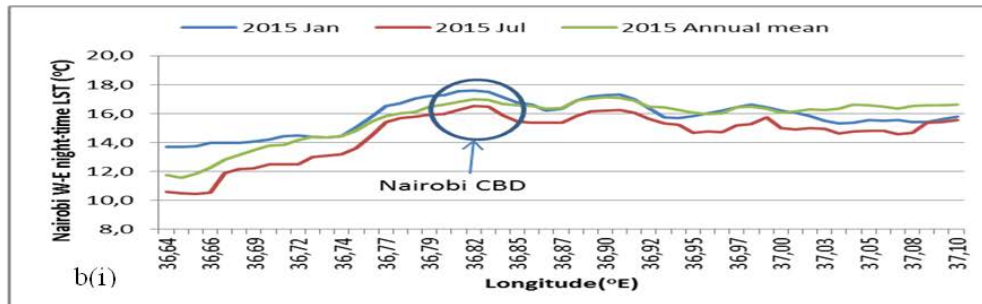
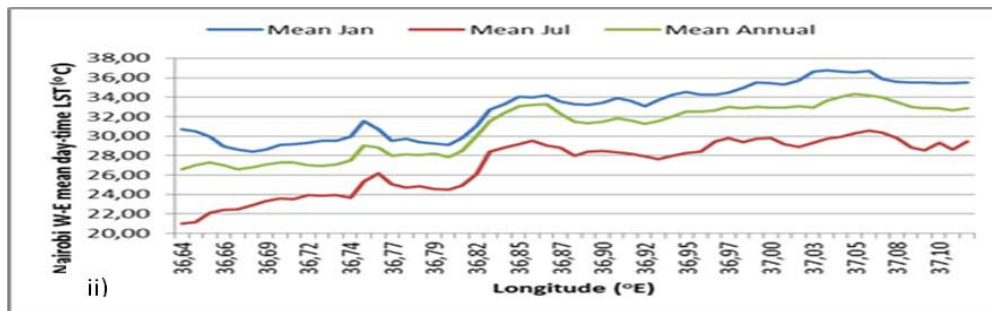
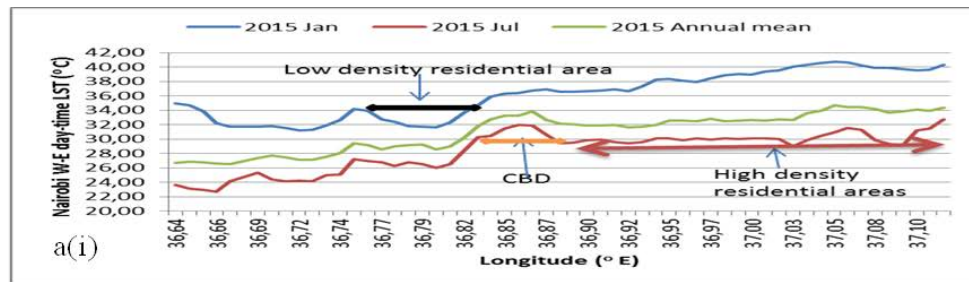
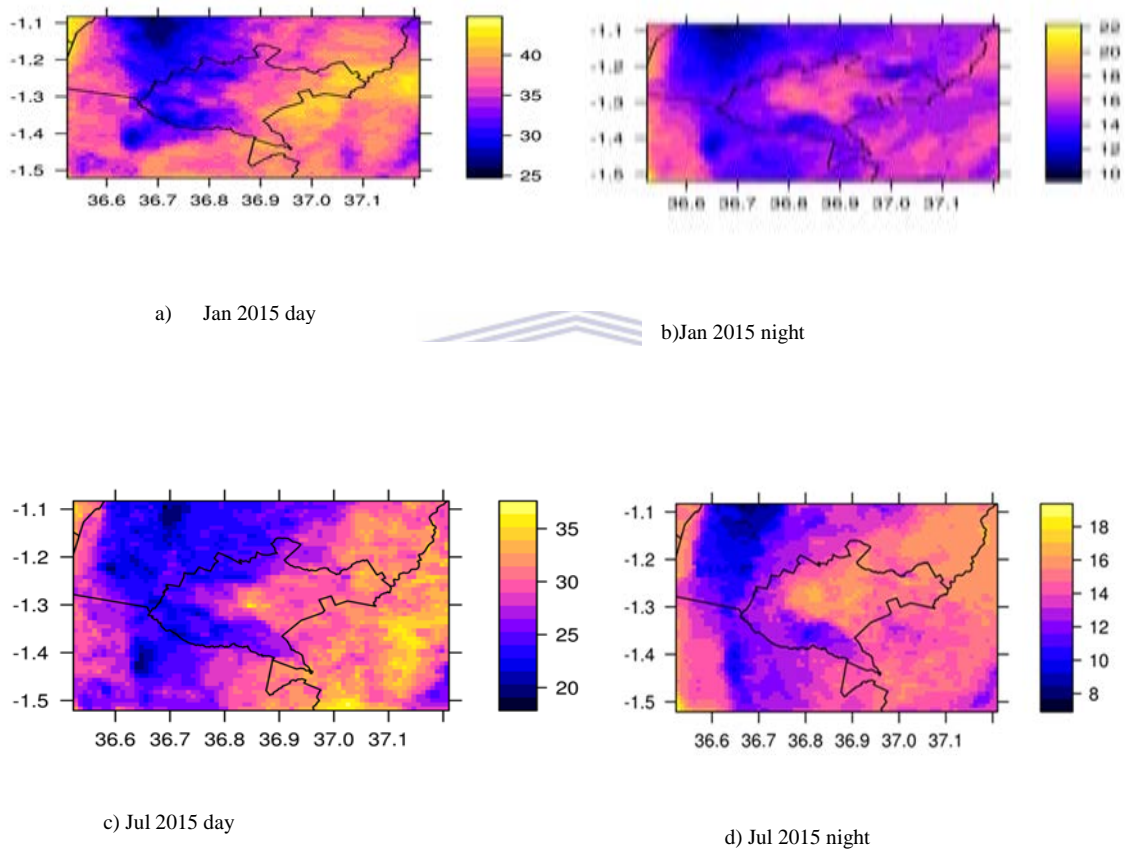


Figure 4.14: W-E land surface temperature profile (along Latitude 1.28°S) showing a) day-time; b) night-time temperature variations between the City CBD and low-density residential area to the west and high-density residential areas to the east; each profile shows LST variability for the warm (January) and cool (July) months and the annual mean for i) 2015; ii) long-term average (2004-2015); note Nairobi UHI is observed within the CBD (between longitude 36.81-36.87°E) in the night-time profile

Figure 4.15 shows maps of monthly mean land surface temperature for Nairobi during a hot month (January) and a cool month (July) for some years. The maps show that the eastern side of Nairobi is warmer than the western side during both day and night. The night-time UHI is also observable in most maps



**Figure 4.15: Mean monthly distribution of land surface temperature for 2015; a) January day-time; b) January night-time; c) July day-time and; d) July night-time; the horizontal axis represents the Longitudes(°E) and the vertical axis represents latitudes (°S); the CBD is located approximately 1.28-1.29°S and 36.81-36.84°E; The vertical bar in each map shows the range of temperature in °C**



From the analysis of LST over Nairobi, the following observations were made:

- a) From the temperature profile for the N-S transect, day-time temperature difference between the forested area to the north (Karura Forest) and the CBD is about 4°C (using the long-term annual mean profile) and between woodland area (National Park) and the CBD is about 3°C. The forest is much cooler during the day which is attributed to the latent heat flux via evapotranspiration.
- b) For the night-time profile of the N-S transect, the temperature differences were much lower (about 1 °C on average) between the CBD and the forested areas whereas there was a sharp drop between the CBD to the coolest point in the woodland to the south of about 4°C on average. This observation implies that land in the Park, which mainly has shrubs, bushes, and bare ground, cools much more at night than in the deciduous forest to the north, and that the intensity of surface UHI depends on the land cover of the rural environment. Noted also was that in the night-time LST profile, changes of temperature from one land cover type to another occur gradually unlike for the day-time where changes are abrupt. Another observation between day-time and night LST was that temperature remained lower outside the CBD for the night-time LST, which was not the case for the day-time profile.
- c) The W-E transect depicts an LST day-time profile that has a different pattern with the areas east of the CBD having relatively higher temperature than the west. On average the temperature difference between the low-density residential areas to the west and the CBD is about 6°C, while the temperature difference between the CBD and the high-density residential areas to the east is about -2°C. However, unlike the N-S profile, the UHI of the CBD from the W-E profile is not distinguishable from the

higher temperatures to the east. The pattern could be attributed to the rapid growth of high-density residential houses and increased road networks to the east.

- d) From the night-time LST profiles of the W-E transect, there is a steady rise in temperature from west to east with highest being within the CBD and a fall thereafter. The temperature difference between the low-density residential areas and CBD is about 2°C. Beyond the CBD eastwards temperatures are slightly lower than within the CBD which implies that the high-density residential areas cool faster than the CBD although the difference is minimal immediately out of the CBD, and becomes more pronounced in the rural areas (beyond 36.95°E).

The LST over Nairobi suggests that UHI exists within the highly built-up areas of the city (especially within the CBD). The intensity of the UHI is more prominent in the N-S direction than the W-E due to the existence of natural land cover in the forested area to the north and the bush land to the south; implying the dependency of surface UHI intensity on the land cover of the rural environment. The UHI within the CBD is stronger during the day but easily distinguishable from the night-time temperature profile. The day-time land surface temperature maps clearly depict the relative warmth of the eastern side of Nairobi city than the western side. Seasonally the UHI is more pronounced during the hot season than the cold season.



### 4.3.3 UHI over Mombasa

#### *Temporal trends of minimum temperature over Mombasa*

The same investigations that were carried over Nairobi were done for Mombasa. Further analysis to confirm the preliminary results obtained in Section 4.4.2, were carried out to establish the nature of UHI over Mombasa. The rates of warming in the urban and rural stations for the  $T_{\min}$  were compared using the linear regression coefficients ( $\beta$ ) that were statistically significant at  $\alpha = 0.05$  (Chapter 2). The hypothesis here was that if urban areas have higher rates of warming than the rural areas then UHI exists; assuming that in the absence of the urban effects the temperature within Mombasa would be influenced by similar climate factors and change at relatively the same rate.  $T_{\min}$  was used since it had increasing trends in all stations for the period between 1990 and 2013.

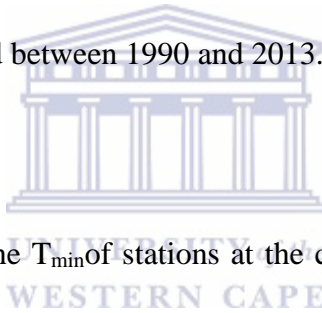
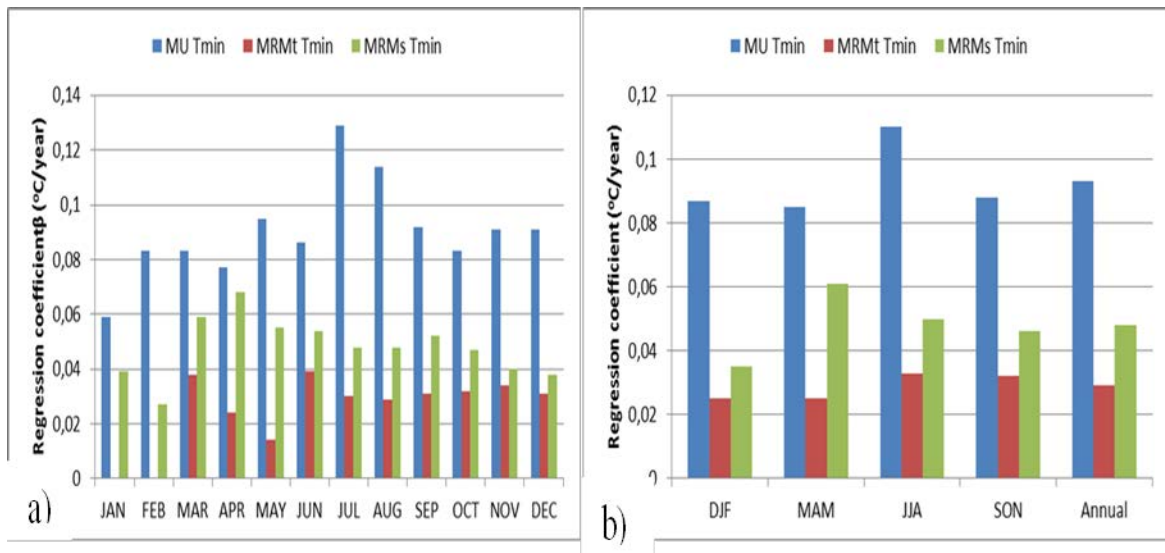


Figure 4.16 shows the trends of the  $T_{\min}$  of stations at the coastal region near Mombasa. The urban station (MU) had increasing trends that were higher than in the rural stations in all months (Figure 4.16(a)). The trends in MU were especially high during the cool season of JJA (Figure 4.16(b)).



**Figure 4.16: Comparison of the rates of change of  $T_{min}$  between the urban station and the rural stations for; a) monthly trends and; b) seasonal and annual trends; all the coefficients were statistically significant at  $\alpha=0.05$ .**

### *Temporal variability of temperature difference ( $\Delta T(u-r)$ )*

The temperature differences between the urban and rural stations over Mombasa revealed different scenarios from that observed over Nairobi area. Figure 4.17 shows the temporal variations of the annual  $\Delta T_{max}(u-r)$  and  $\Delta T_{min}(u-r)$ . The temporal variability of  $\Delta T_{max}(u-r)$  for both pairs of stations showed that the values were close to zero with only a mean value of slightly more than  $1^{\circ}\text{C}$  in 2004 in the MU-MRMt pair. On the other hand,  $\Delta T_{min}(u-r)$  values for both pairs of stations were less than zero (i.e., negative) over the whole period but are increasing with time. For instance, for  $\Delta T_{min}(u-r)$  between MU and MRMt, the lowest difference ( $\sim -2^{\circ}\text{C}$ ) recorded in 1994 has progressively increased to  $\sim -0.5^{\circ}\text{C}$  by 2010 (Figure 4.17 (a)), also  $\Delta T_{min}(u-r)$  between MU and MRMs has a similar pattern except that the negative values of  $\Delta T_{min}(u-r)$  were much lower in the 1990s ( $\sim -3.0^{\circ}\text{C}$ ) and has progressively increased to about  $-1^{\circ}\text{C}$  by 2010 (Figure 4.17(b)).

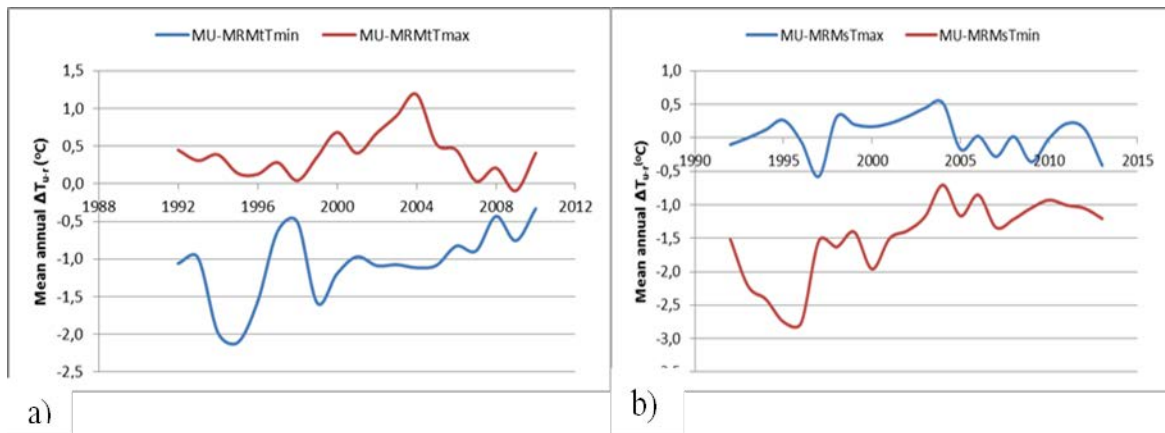


**Figure 4.17: Temporal Variation of annual mean temperature differences ( $\Delta T_{\max}(u-r)$  and  $\Delta T_{\min}(u-r)$ ) over Mombasa for; a) MU-MR Mt and, b) MU-MR Ms**

Figure 4.18 shows the long term mean monthly and seasonal  $\Delta T_{\max}(u-r)$  and  $\Delta T_{\min}(u-r)$ . For both pairs of station, low positive values of  $\Delta T_{\max}(u-r)$  were observed. Accordingly, the mean monthly and seasonal values of the  $\Delta T_{\min}(u-r)$  from both pair of stations, were all negative and lowest in the cool months from April to September with a peak in July, while seasonally the lowest values were in JJA ( $\sim -2.5^{\circ}\text{C}$ ) and highest in DJF ( $\sim -0.5^{\circ}\text{C}$ ) (Fig 4.18).

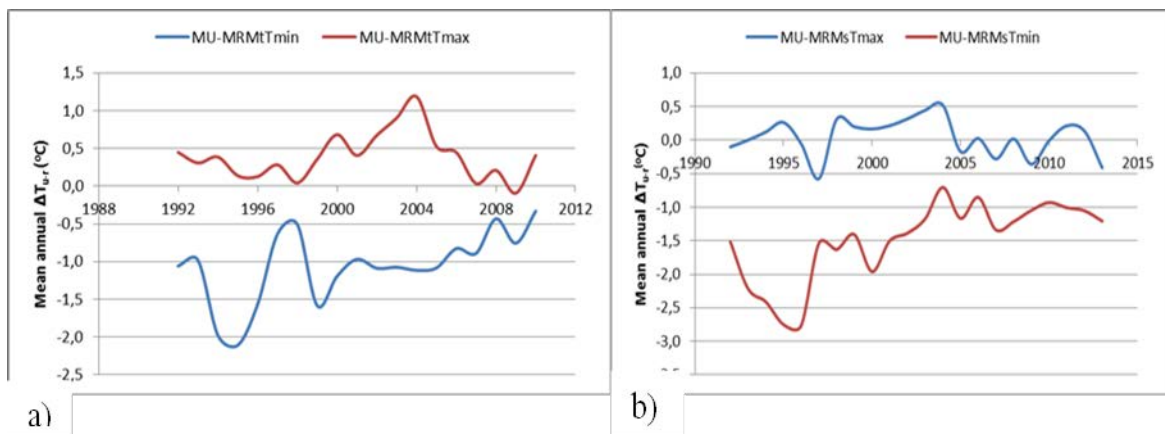


**Figure 4.18: Long-term mean monthly and seasonal values of  $\Delta T_{\max}(u-r)$  and  $\Delta T_{\min}(u-r)$  for; a) MU-MR Mt, and b) MU-MR Ms**

From the long-term variations of  $\Delta T$  (u-r), day-time UHI intensity in Mombasa relative to the two rural stations, is almost non-existent, while the night-time UHI intensity is negative. The negative values of  $\Delta T_{\min}$  (u-r) suggest the existence of an urban cool island (UCI) over Mombasa whose intensity is diminishing with time.

To further examine if the observed trends in the temperature differences were statistically significant, trend analysis was performed on the seasonal and annual means of both  $\Delta T_{\max}$  (u-r) and  $\Delta T_{\min}$  (u-r) for MU-MR<sub>Mt</sub> and MU-MR<sub>Ms</sub> pair of stations. As expected, the  $\Delta T_{\max}$  (u-r) series in both pair of stations had no trends in any season or even in the annual mean (results not shown). Positive trends were found in all seasons and the annual mean for the  $\Delta T_{\min}$  (u-r) (Table 4.6). The important thing to note from these results is that the positive trends are from the negative temperature differences between the urban and the rural stations towards positive differences; implying the UCI intensity is diminishing with time.

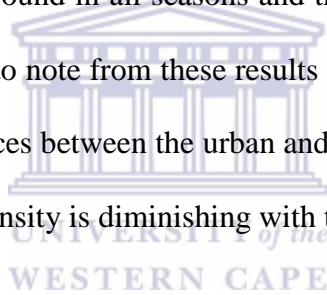


**Table 4.6: Temporal trends of temperature differences between Mombasa urban and rural stations; all the  $\beta$  values are significant at  $\alpha=0.05$**

Season	$\Delta T_{\min}(\text{u-r})$	t-stat	$\beta(^{\circ}\text{C}/\text{year})$	p-value
<b>DJF</b>	<b>MU-MR<sub>Mt</sub></b>	3.67	0.04	0.003
	<b>MU-MR<sub>Ms</sub></b>	2.76	0.06	0.011
<b>MAM</b>	<b>MU-MR<sub>Mt</sub></b>	2.45	0.05	0.023
	<b>MU-MR<sub>Ms</sub></b>	1.93	0.03	0.005
<b>JJA</b>	<b>MU-MR<sub>Mt</sub></b>	4.05	0.06	0.000
	<b>MU-MR<sub>Ms</sub></b>	3.24	0.07	0.004
<b>SON</b>	<b>MU-MR<sub>Mt</sub></b>	3.32	0.06	0.003
	<b>MU-MR<sub>Ms</sub></b>	3.74	0.06	0.001
<b>ANNUAL MEAN</b>	<b>MU-MR<sub>Mt</sub></b>	4.22	0.05	0.000
	<b>MU-MR<sub>Ms</sub></b>	3.67	0.05	0.001

Since the  $T_{\min}$  of the urban station in Mombasa was found to be increasing at a higher rate than in the rural stations, the influence of  $T_{\min}$  at MU on  $\Delta T_{\min}$  (u-r) for each pair of stations was examined. Fig 4.19 shows that there exist significant positive relationships between  $\Delta T_{\min}$  (u-r) and  $T_{\min}$  for MU with  $R^2$  values  $\approx 0.7$  for each pair of stations.

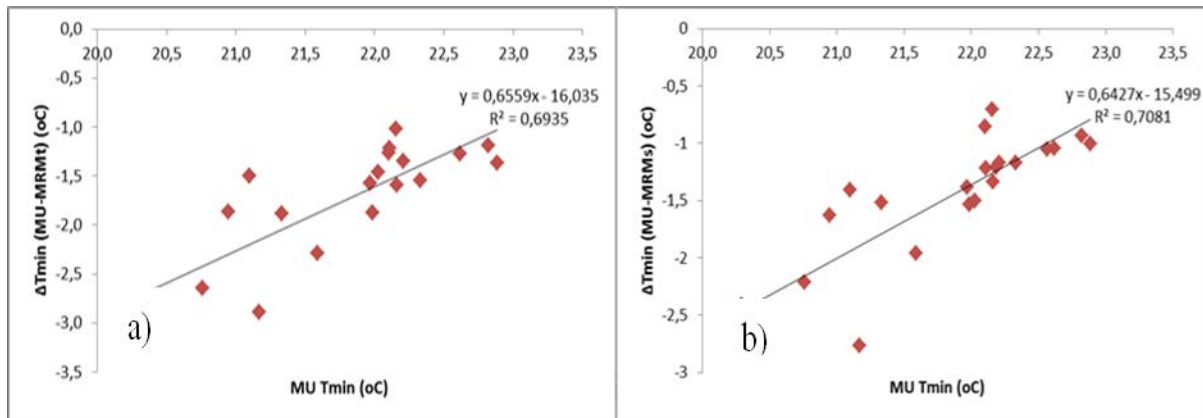


**Figure 4.19: Linear relationships between urban-rural temperature differences and the urban  $T_{\min}$  over Mombasa; a)  $\Delta T_{\min}$  (MU-MR<sub>Mt</sub>) and MU  $T_{\min}$ ; b)  $\Delta T_{\min}$  (MU-MR<sub>Ms</sub>) and MU  $T_{\min}$**

The regression results confirm that higher rate of increase of the  $T_{\min}$  at MU than in the rural stations is partly attributing to the weakening of negative temperature differences between urban and rural areas at the coast. Hence Mombasa town within the airport area is tending towards becoming an urban heat island. The deductions from the analysis of the urban-rural temperature differences for Mombasa were that:

- A day-time UHI over Mombasa could not be established from the urban and rural weather stations. Further investigations were done in the next Section using remotely sensed land surface temperature.

- For the night-time temperature, negative temperature differences suggest urban cool island (UCI) intensity in Mombasa city around the airport (location of the urban station) whose intensity has weakened over time. The existence of negative UHI intensities was attributed to the nearness of the rural stations to the Indian Ocean, since oceans are warmer during the night than land, while the diminishing negative intensities were fairly strongly associated with the increasing  $T_{\min}$  of the urban station.

### *Analysis of UHI from LST in and around Mombasa*

To further examine UHI over the coastal city of Mombasa, LST data described in Section 4.3.2 were used. Particular attention was given to the temperatures of Mombasa Island where the main city buildings (including the central business district (CBD) and industrial area) are situated. Monthly data of LST for 2004-2015, covering the area enclosed by latitudes 3.85°S - 4.02°S and longitudes 39.5°E - 39.82°E, and retrieved at a spatial resolution of 1 km were used. For each year, I analysed LST along two transects, (north-south (N-S) and west-east (W-E)). I used the N-S temperature values at each pixel along the longitude 39.64 and varying from latitudes 3.85°S to 4.02°S to examine the N-S temperature variations. The choice of this longitude was motivated by the fact that it passes through the heavily built-up urban area including the industrial area within the Island. A temperature profile of N-S transect was then plotted for the mean monthly LST data at each latitude and along the fixed longitude (see Figure 4.8) for the hot season (DJF), the cool season (JJA) and for the annual mean (average for all months in one year); a mean profile comprising of long-term averages of the monthly and annual LST at each latitude and along the fixed longitude was also plotted.

Fig 4.20 (a&b) shows the profiles depicting N-S variations of the day-time and night-time mean LST for January, July and annual mean of; i)2005 and; ii) the mean profile for the whole period (2004-2015). Fig 4.20 (c) shows a rotated strip of a Google Earth map indicating the different land cover types (the rural areas, the urban areas, and ocean water) whose temperature is represented in the profile.

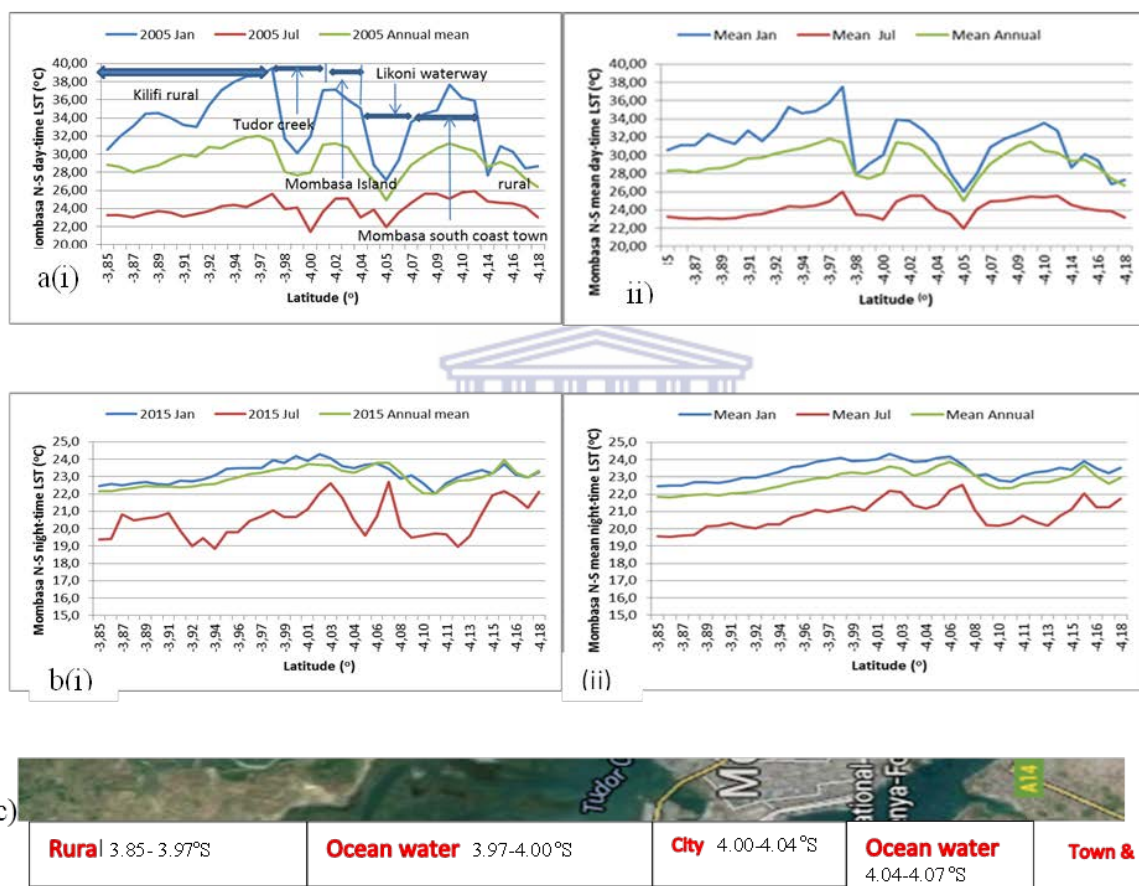


**Figure 4.20:** N-S land surface temperature profiles (along longitude 39.64°E) showing; a) day-time; b) night-time LST spatial variability between the Mombasa Island town and rural area to the north and south; each profile shows temperature variability for the warm (January) and cool (July) months and the annual mean for; i) 2015; ii) long-term average (2004-2015) for the same months and annuals; c) a rotated N-S strip of Google Earth map of Mombasa showing the different types of land cover traversed by the temperature profile from the north (left) to south (right).



The main observations here are that; i) the day-time profile have sharp drops in temperature from the north rural areas to the Tudor Creek, which then increases sharply from the creek to in the city within the Island. From the Island, the temperature drops again within the Likoni waterway, then rises over the mainland town, and drops in the rural areas further south. The temperature drops are more pronounced in the hot season (January) than in the cold season (July); ii) the night-time profile depicts a different pattern in which temperature rises gradually from the rural area to the north, across the Tudor creek and the Island town and decreases slightly over the Likoni Waterway and then rises over the mainland town. Note that from the north, the temperature of the Tudor Creek and the Island town is not distinguishable but between the Island and the Likoni Waterway the difference is noticeable. The difference could be attributed to the depth of the ocean; Likoni waterway is deep sea while Tudor is shallow sea.

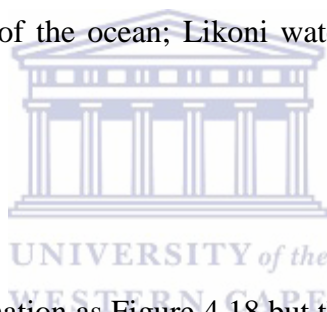


Figure 4.21 shows the same information as Figure 4.18 but the profile depicting W-E variation of January, July and annual mean day-time and night-time LST. Figure 4.19 (c) shows a strip of a Google earth map indicating the different land cover types traversed by the W-E transect whose temperature profile is presented. An almost similar pattern with the N-S profile is observed here. For the day-time profile, the temperatures are high in rural areas east of the Island and drop sharply over the Port Rietz water-way (deep sea). The temperature then rises sharply over the town before dropping slightly over the Tudor Creek (shallow sea). Note that Port Rietz is an extension of the Likoni waterway. For the night-time profile, the temperature between the Island and water is hardly distinguishable especially during the hot season.



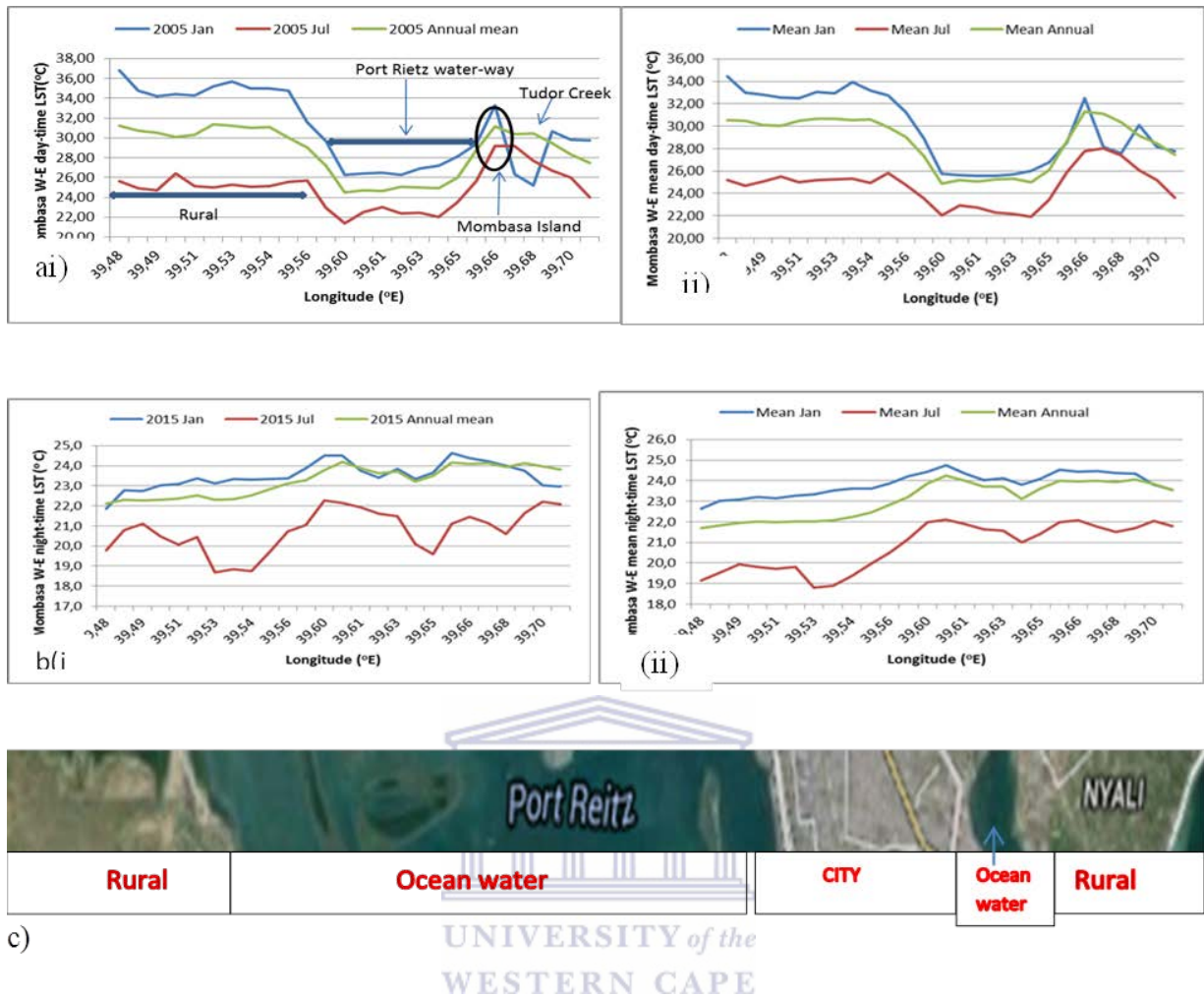
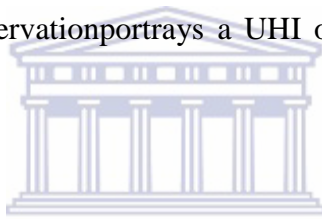


Figure 4.21: W-E land surface temperature profiles (along latitude 4.05°S) showing; a) day-time; b) night-time LST variability between the Mombasa Island town and rural area to the west and east; each profile shows temperature variability for the warm (January) and cool (July) months and the annual mean for; i) 2015; ii) long-term average (2004-2015); a W-E strip of Google earth map showing the different land cover types traversed by the W-E profile from the west to the east.

The following deductions were made from the spatial and temporal analysis of LST over Mombasa:

- a) The temperature profile over Mombasa is greatly influenced by the neighbouring water bodies. During the day, the N-S and W-E profiles showed higher

temperatures over the rural areas that decreased sharply over the water bodies and rose sharply over the city. On average, the day-time temperature in the city was lower than in the rural areas. These observations imply that there are day-time negative LST differences between the city and the rural land in the neighbourhood. The negative LST differences would imply an urban cool island over the Island town relative to the rural land areas; however, the town is warmer than the adjacent water bodies. For instance for the N-S profile, the average LST difference between the urban area and the rural land areas is about  $-2^{\circ}\text{C}$  and in absolute terms is higher during the hot season than the cold season. Noted also was that in the N-S direction, the day-time temperature increased after passing Likoni waterway towards the south similar to that observed over the Island. This observation portrays a UHI of the urban sprawl in the coastal mainland area.



- b) On average, the night-time LST profiles showed gradual changes in temperature across the different land cover types. Temperatures in rural areas are lower than those of both the water and the town. Worthwhile noting also was that, there is almost no difference between the temperature of water and the neighbouring urban land in the night-time profile, and temperatures to the east of the Island are higher than to the west which is quite opposite of the day-time profile. The UHI is clearer during day-time than during night-time profiles.
- c) The Mombasa airport and surrounding areas are relatively cooler than the Island with about  $1^{\circ}\text{C}$  (averaged over the period 2004-2015). Similar observations were made using the land surface temperature maps (Figure 4.22). The area around the Mombasa airport areas is also cooler at night than rural areas close to the ocean. This observation is likely to explain the existence of night-time negative air temperature

gradients between Mombasa airport and the two stations along the coast (Mtwapa and Msabaha) (considering that, I found a positive correlation between air temperature and LST of  $\sim 0.6$  in both urban areas).

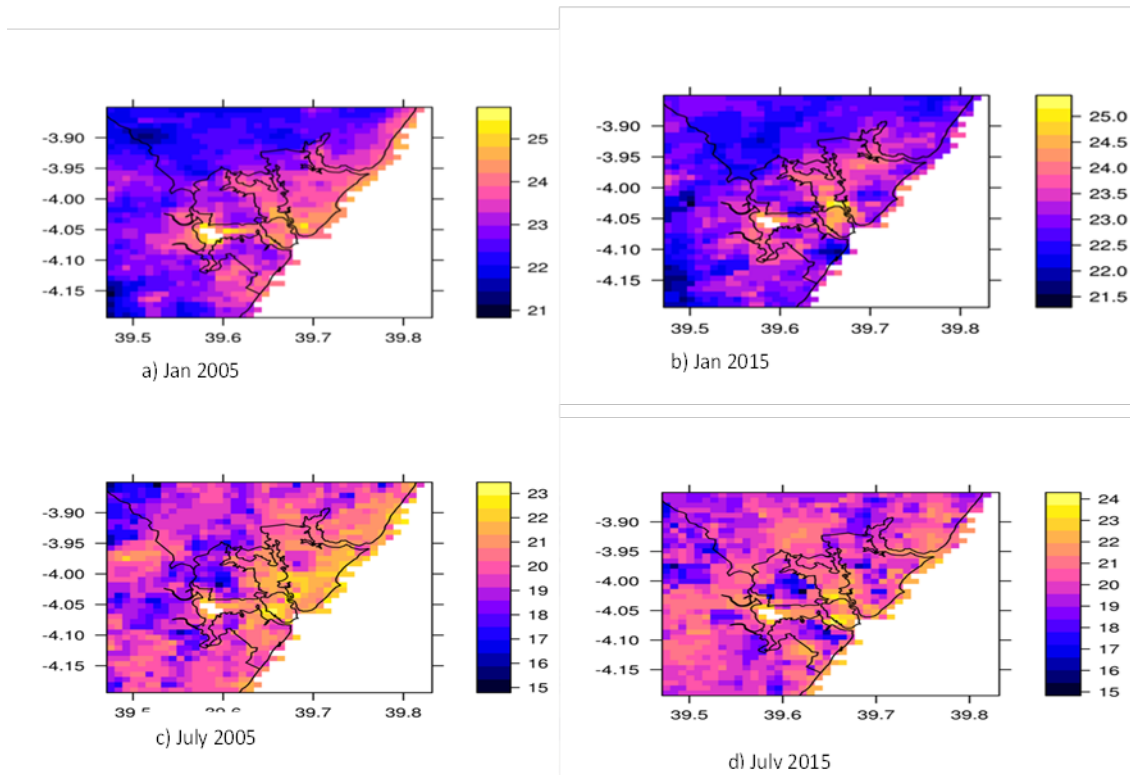


**Figure 4.22: Mean monthly distribution of night-time LST of 2005 and 2015 January and July showing the cool areas around the airport and higher temperature in the city, the water-ways and the areas near the ocean; the horizontal axis represents the Longitudes( $^{\circ}$ E) and the vertical axis represents latitudes ( $^{\circ}$ S); the vertical bar in each map shows the range of temperature in  $^{\circ}$ C; Mombasa airport is located at approximately  $4.04^{\circ}$ S,  $39.6^{\circ}$ E.**

The LST results showed that in general; i) Mombasa Island town is cooler than neighbouring rural land areas but warmer than the adjacent water bodies during the day; ii) Mombasa town is only slightly warmer than its surrounding at night; iii) the urban area close to the Mombasa airport is cooler than the more urbanized Island, and also than the areas close to the ocean during the night. The weak UHI in Mombasa city (within the Island) and the sprawling

towns in the mainland, was observed in night-time LST; iii) the ocean-land temperature contrast both during the day and at night influences the temperature profiles of Mombasa and thus modulates the UHI.

#### 4.3.4 Discussion

##### *Nairobi UHI*

Temporal variability and trend analysis of day-time and night-time air temperature differences at monthly, seasonal and annual timescales, between urban and rural stations showed that UHI exists over Nairobi. The day-time UHI was found to be stronger than the night-time but its intensity has decreased over time. The decline of the day-time UHI intensity was significantly associated with increasing trends in  $T_{\max}$  of rural areas. The increasing  $T_{\max}$  was attributed partly to global warming (Chapter 2) and effects of urban sprawl as was indicated in Makokha and Shisanya (2010) who reported that urban sprawl into rural areas close to the CBD has influenced temperature increase in these areas. The use of remote sensed land surface temperature (LST) greatly strengthened the conclusion of existence of UHI observed from station data. The N-S transects passing through the CBD of Nairobi showed that temperatures increased steadily towards the CBD and decreased out of the CBD; thus showing a well formed UHI especially for the night-time profile. However, the day-time UHI in the W-E transect was diffuse with higher temperatures in the eastern side of the CBD than over the CBD. The higher temperatures to the east were attributed to the development of high-density residential buildings, and effects of urban sprawl. This increase of LST on the eastern side of the CBD was also reported by Muthoka and Mundia, (2014) who associated the increase to the conversion of natural vegetation to built-up land. Cheval and Demitrescu (2015) used a similar method to study UHI over Bucharest (Romania), and indicated that the type of landcover in an area exerts a strong influence

on the LST and hence on the relative UHI intensity. The observed day-time UHI both in air temperature and LST could be associated with land use/cover changes and increase in population. For instance Land cover/use change studies over Nairobi area reported that built up areas have increased significantly over the last three decades (Mundia and Aniya, 2006; Muthokha and Mundia, 2014) and urban population in Nairobi has also increased from about half a million people in the 1960s to more than 3.1 million (KNBS 2010). Government reports also indicate that, apart from the residents living in Nairobi, commuters from other parts of the country who work in Nairobi usually push the daytime population to over four million people. The increase in population and economic activities have increased anthropogenic sensible heat in Nairobi especially during the day and also pollutants that have greenhouse gas effect (Opija et al., 2008; Hart and Sailor, 2009) thus increasing the heat energy flux in the urban environment.



The UHI intensities over Nairobi have seasonal characteristics; for instance, the night-time UHI from the air temperature data was strongest during the DJF season and weakest in JJA season. The DJF season is the hottest period of the year when dry continental north easterlies dominate the EEA region. The sky also is mainly cloudless during this season thus maximum radiation is received during the day and the urban fabric would absorb more heat during the day and release at night. These results agree with those of Murphy et al., (2011), Vardoulaski, et al. (2013) and Ahmed, et al. (2014) who indicated that UHI in the tropical cities is highest during the dry season. However from the LST, night-time UHI over Nairobi CBD has almost the same intensity for the hot and cold season.

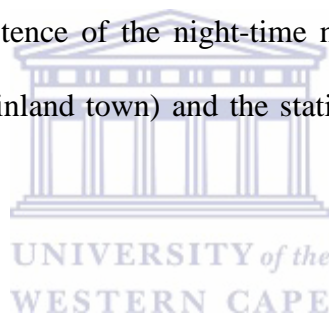
### *Mombasa UHI*

From the analysis of air temperature data, the day-time temperature difference between Mombasa town (around the airport) and rural areas to the northeast near the coastline, were close to zero. However, from the LST analysis, the day-time N-S and W-E transects traversing the Mombasa Island showed interesting temperature profiles in which the different land cover types were easily distinguishable. The day-time LST profile showed that the rural areas are warmer than Mombasa Island (city centre) while the areas covered by inshore water from the Indian Ocean are much cooler than the Island. Therefore, relative to the rural land areas, the Island have negative UHI intensity, while relative to the inshore water, the UHI intensity is positive during the day. The influence of water bodies on UHI was also reported in Cheval and Demitrescu (2015) for the city of (Bucharest) Romania.



The night-time air temperature differences between Mombasa Airport station and the rural areas to the northeast were found to be negative. The trends of these urban-rural temperature differences were increasing thus implying decreasing of the urban Cool Island (UCI) intensity. The decreasing UCI intensity was attributed to the increasing trend of  $T_{\min}$  at the Mombasa airport station. The night-time LST along the N-S and W-E transects showed profiles in which temperature changed gradually from one land cover type to another. The rural areas were on average cooler than the city at night. Interestingly, it was not possible to distinguish the inshore water from the urban area in the night-time profiles; the temperature gradually increased to a maximum over the city and then decreased. Considering the night-time LST, a weak UHI was detected in Mombasa Island, and also in the mainland towns close to the Island.

The temperature profiles over Mombasa are however more complex than over Nairobi mainly due to the presence of the ocean and the inland waterways. For instance, the surface temperature maps showed that night-time LST is higher over the land closer to the ocean than away from the coast. This phenomenon is expected climatologically since oceans are cooler than land during the day and warmer at night. The presence of the sea-land breezes during the day and land-sea breezes during the night complicates the radiative processes of a coastal city (Emmanuel and Johansson, 2006). Freitas, et al. (2006) showed that the presence of a city at the coast increases sea breeze propagation into the centre of the city; a phenomenon that could be used explain the relative coolness of Mombasa Island compared to the inland rural areas. Further, the influence of the ocean-land temperature contrast at night observed in the LST maps could explain the existence of the night-time negative air temperature gradients between Mombasa airport area (inland town) and the stations along the coast (Mtwapa and Msabaha).

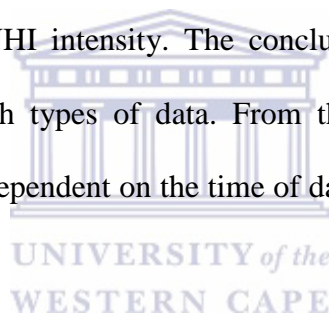


Studies have shown that Indian Ocean SSTs close to the Kenyan coast have been increasing since the mid-20<sup>th</sup> Century (Deser et al., 2010; Roxy, 2014; Roxy, et al., 2014) which could also influence temperature differences between Mombasa inland town and the rural areas close to the ocean. Wind speeds in Mombasa were reported to have significantly reduced in the last twenty years (Ongoma et al., 2013). Reduction in wind speed would affect the effective mixing of cool and warm air and also the transport of pollutants thus enhancing the night time temperature over Mombasa as indicated by Giannaros and Melas, (2012).



#### 4.4 Summary

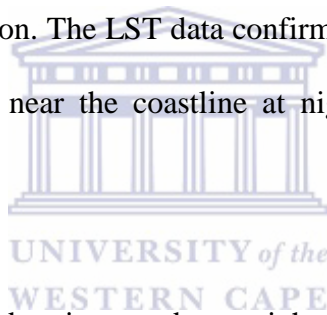
In this Chapter, I aimed at establishing if UHIs exist in Nairobi and Mombasa cities. The results from this Chapter formed a basis upon which investigations of the influence of urban temperature on rainfall in the next Chapter is based. The use of the air temperature and LST were complementary in the establishment of UHI over Nairobi and Mombasa. The data from the limited weather stations were not adequate alone to make firm conclusions of UHI mainly because none of the weather station is situated within the CBD of either town. On the other hand, LST data from MODIS allowed for a more spatial evaluation of the UHI particularly with respect to the heavily built-up town centres and their immediate environs. However, the data was only available for the last twelve (12) years and could not be adequately used to investigate long-term trends in UHI intensity. The conclusions thus arrived at were made stronger through the use of both types of data. From the two cities, UHI was observed. However, its intensity is highly dependent on the time of day and land cover types of the rural areas considered.



There were important differences of the UHI and its intensity between Nairobi and Mombasa cities; 1) Over Nairobi, the day-time UHI intensity from the air temperature data was found to be stronger than the night-time one. The day-time air temperature UHI had decreasing trends that were found to be significantly negatively correlated with the  $T_{\max}$  at the rural stations. The decreasing trends of UHI were partly attributed to the effects of global warming that is influencing rural temperature more than urban temperature and effects of urban sprawling into rural areas. The night-time UHI from air temperature was much lower than the day-time but its intensity had increased over time. From the LST, both day and night UHIs over Nairobi were distinguishable within the CBD from the temperature profiles especially for the N-S transects that traversed rural areas with natural vegetation. The night-time UHI was more



conspicuous and regularly formed than the day-time one. The LSTUHI intensity was also much lower during the night-time than day-time. Seasonally, UHI was higher during hot months than the cold months: 2) Over Mombasa urban area, there was no significant day-time UHI intensity from the air temperature between the Mombasa Airport and the stations in Mtwapa and Msabaha along the Kenyan coast. However, the day-time LSTs within Mombasa Island were lower than in the rural land areas, but higher than the adjacent water bodies. From the night-time surface air temperature, negative temperature differences indicative of an urban cool island (UCI) was observed between Mombasa airport area and rural stations along the coast. The UCI intensities were on average higher during cool months than the warm months. The UCI intensity had decreasing trends that were associated with the increasing of  $T_{\min}$  at the Mombasa Airport station. The LST data confirmed that the area around the airport is on average cooler than areas near the coastline at night and thus the reason for UCI intensities.



The main implication of the day-time and or night-time UHI effect to stormwater management in urban areas would be through UHI circulation influencing the formation of convective clouds and hence increase rainfall intensities especially in the downwind areas of the CBDs. If rainfall intensities or duration of wet spells are enhanced due to the UHI effect, the urban design storms that are used in storm water management systems would be affected, and undue urban flooding could be experienced in the urban areas and/or their downwind neighbourhoods. The effects of enhanced urban temperatures on rainfall were investigated in Chapter 5.

## 5 CHAPTER 5: EFFECTS OF TEMPERATURE ON URBAN RAINFALL

### 5.1 Introduction

The continuing conversion of natural land cover to urban land is altering the surface energy balance, and consequently increases sensible heat at the expense of the latent heat (Lamprey, 2010). The difference between the relative warmth of a city and the surrounding rural area is due to the changes in the surface energy budget in the city arising from anthropogenic heat released from buildings, greater absorption of incoming shortwave radiation resulting from urban canyon geometry and urban building materials, decreasing outgoing long wave radiation due to reduced sky view factor by canyon geometry, and increased pollution as discussed in Chapter 4. The result of the differential thermal heating in an urban environment is greater day-time storage and night-time release of solar energy and increased convective heat due to reduced latent heat flux from impermeable surfaces (Shepherd 2005). This modification of the natural environment, affects thermal stratification of the air above the urban area, the local heat balance, the hydrologic cycle as well as the micro and meso-scale circulation patterns (Molders and Olson, 2004). The high aerodynamic roughness and surface heterogeneity of a city affect the speed of the wind (Ongoma, et al., 2013), low-level convergence, transport of suspended pollutants and increase vertical mixing through changes in the urban boundary layer (UBL).

Energy flux changes resulting from urbanization have the potential of modifying rainfall patterns in terms of amount, spatial distribution, and /or intensity. The urban-induced changes of the natural precipitation could result from the modification of the atmosphere through formation of urban heat islands (UHIs), modification of microphysical and dynamical processes in passing clouds through addition of condensation nuclei from industrial

pollutants, increase in low level mechanical turbulence from urban created obstacles, and modification of low level atmospheric moisture content by accumulations of industrially generated plumes from cooling towers (Huff and Changnon, 1972; Zhong and Yang, 2015). Changes in rainfall intensity and or distribution in an urban environment have the potential to influence the urban hydrologic response especially in the way stormwater is generated.

### **5.1.1 Effects of urban temperature on urban precipitation patterns**

The Metropolitan Meteorological Experiment (METROMEX) was one of the early studies that took place in the 1970s in the United States to investigate the modification of meso-scale and convective rainfall by major cities (Changnon, et al., 1977). The results from these studies indicated that urban effects lead to increased precipitation during summer months of these regions which was found to occur 50-75 km downwind of a city. The areal extent and the magnitude of the urban and downwind precipitation anomalies were related to the size of the city. Baik et al. (2001) showed that even weak heat islands result in surface sensible heat flux convergence and buoyancy that influence rainfall development. Shepherd, (2006) indicated that the prevailing flow of wind interacts with the UHI to enhance urban precipitation downwind of the city. Other regional studies that have suggested correlations between rainfall intensities and UHI include Jauregui and Romales (1996) over the Mexico City (Mexico), Shepherd, et al. (2010) over a coastal city in USA and Fujibe, (2003) over major cities in Japan. Biazeto, (2012) and Marengo, et al. (2013) suggested that changes in rainfall regime in the urban areas had a strong correlation with urbanization. Efe and Eyefia, (2014) observed that in the city of Benin in Nigeria, the precipitation amount and intensity had increased due to urbanization and the presence of the UHI. Shepherd et al. (2002) studied four cities in the USA using rainfall rates from the Tropical Rainfall Measuring Mission (TRMM) and corroborated Bornstein and Lin (2000) that there is a bias towards

greater rainfall enhancement in the downwind region of the urban area with minimal enhancement directly over or upwind. Kishtawal, et al. (2010) assessed the urbanization impact on the heavy rainfall climatology of Indian summer monsoon and observed an increasing trend in the frequency of heavy rainfall over urban regions during the monsoon season.

UHI circulation would interact with the meso-scale and large-scale circulations in a region to influence rainfall patterns not only in the neighbourhood of the urban area but further downwind. Miao, et al. (2009) investigated the influence of the urban temperature on the urban boundary layer (UBL) using both observations and numerical simulations over the city of Beijing (China) and found that the UHI modified the local mountain/valley circulations. Yang et al. (2013) and Zhang et al. (2014) showed that UHI circulations influence local lake breezes. Wang, (2008) showed that an isolated UHI might enhance horizontal wind speed over an urban area. Opija and Mukabana (2004) using dynamical simulation over Nairobi area, suggested that urban-rural circulations forced by the difference in temperature between cities and their surrounding and sustained by frictional drag over the urban built-up areas enhanced the development of convective rainfall and may alter rainfall patterns in and downwind of the urban area.

In a dynamical simulation to investigate the impacts of meso-scale circulations on rainfall over Kenya considering terrain induced circulations and land-water temperature contrast (excluding UHI effect), Mukabana and Pierlke (1996) indicated that the complex heterogeneity of the terrain, large inland and coastal water bodies together with the strong equatorial insolation generate strong meso-scale circulations with strong diurnal cycles which

interact among themselves and with the large scale monsoon flow to produce the observed rainfall patterns over Kenya. Opija and Mukabana (2004) suggested that the UHI in Nairobi urban area have a destabilizing effect on the monsoon flow which would enhance thermal and mechanical turbulence. Coupled with increased roughness within the city, the destabilized monsoon flow may result in enhanced rainfall downwind of the urban area. However, the effects of the interactions among the enhanced thermal circulations due to UHI and global warming, the meso-scale circulations and the large-scale monsoon circulations on rainfall distribution over urban areas of Kenya have not yet been established.

### 5.1.2 The mechanisms of temperature enhancement on urban rainfall

When land cover changes due to urbanization, the atmosphere responds to the perturbations in the lower boundary conditions through complex processes and responses that may influence rainfall patterns. The physical processes that link changes in the land surface with climate system include; a) the changes of local surface conditions in terms of temperature and humidity occasioned by the changes in the surface energy balance; a process driven mainly by changes in the surface albedo and surface emission of the earth's radiation, and b) the apportioning of the net surface radiation into sensible and latent heat fluxes which is driven by changes in moisture storage ability in the soil layer, and changes in surface roughness (Eltahir and Pal, 1996; Pielke, 2001). These changes are explained by considering the energy and moisture budget equations and their inter-dependence. The surface heat budget equation was expressed in Equation 4.1 (Chapter 4) as:

$$q_{sw} + q_{lw} + q_{sh} + q_{le} + q_g + q_a = 0 \quad (5.1)$$

where  $q_{sw}$  represent the net shortwave irradiance,  $q_{lw}$  is the net long-wave irradiance,  $q_{sh}$  is the surface sensible heat flux,  $q_{le}$  is the latent turbulent heat flux,  $q_a$  is the anthropogenic heat

input, and  $q_g$  represents ground heat conduction. By representing the net radiative fluxes ( $q_{sw} + q_{lw}$ ) as  $R_n$ , and assuming that  $q_a$  is negligible, Equation (5.1) is represented as:

$$R_n = q_g + q_{sh} + q_{le} \quad (5.2)$$

The moisture budget of the surface may be represented as:

$$P = E + T + R + I \quad (5.3)$$

where  $P$  is the total precipitation;  $E$  = evaporation;  $T$  = transpiration;  $R$  = runoff and;  $I$  = infiltration (see Figure 5.1 which show a schematic representation of the moisture budget in an urban and rural environment).  $E$  is a function of  $q_{le}$  (i.e.,  $E = f(q_{le})$ ) and;

$$q_{le} = R_n - (q_g + q_{sh}) \quad (5.4)$$

Thus surface changes affecting  $R_n$ ,  $q_g$ , or  $q_{sh}$  will affect  $E$ . Surface heat flux change in the absence of large-scale wind flow is related to change in temperature through the following thermodynamic equation:

$$\frac{\partial \theta}{\partial t} = \frac{\partial}{\partial z} \left( \frac{q_{sh}}{\rho c_p} \right) \quad (5.5)$$

where  $c_p$  is the specific heat capacity of air at constant pressure,  $\rho$  is the density of air,  $z$  is the vertical distance and  $\theta$  is the temperature; Equation (5.5) can be integrated and averaged (according to Pielke (2001)) to get:

$$\frac{\partial \bar{\theta}}{\partial t} = \frac{1.2}{\rho z_i c_p} q_{sh} \quad (5.6)$$

where  $z_i$  is the height of the boundary layer. In Equation (5.6), changes in sensible heat flux ( $q_{sh}$ ) at a given height of the boundary layer is directly related to the rate of change in

temperature if other conditions of the equation are kept constant; also  $z_i$  will depend on the rate of heating produced by a given amount sensible heat flux.

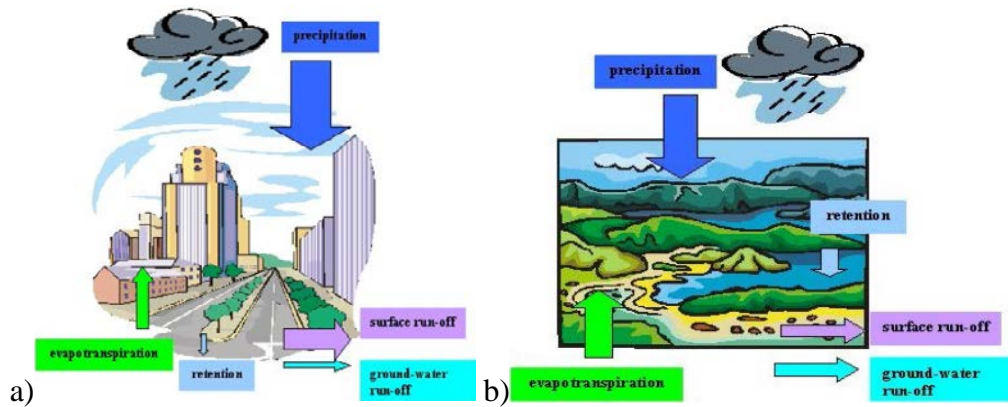


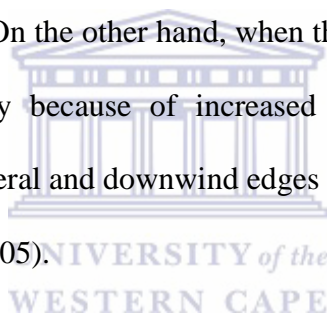
**Figure 5.1: A schematic diagram showing elements of precipitation in an (a) urban and; (b) rural area(adopted from Efe and Eyefia, 2014).**

Changing local temperature creates instability and rising air motions. The degree of local instability is characterized by convective available potential energy (CAPE) which is a function of temperature and humidity (Eltahir and Pal, 1996). The triggering mechanism leading to energy release and creation of rainfall in convective storms is a non-linear process prompted partially by surface conditions and partially by upper air conditions. Vertical motions can create convective thunderstorms that may produce rainfall in the city and mostly at night when the UHI intensity is strongest if there is enough moisture and winds are calm (Bornstein and Lin, 2000).

### 5.1.3 Influence of thermally induced motions on rainfall

The UHI circulation results from the interaction of the atmosphere and the horizontal temperature difference associated with gradients in sensible heat densities between urban and

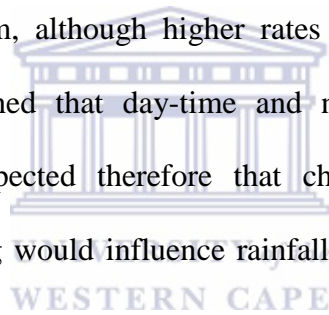
rural areas. The thermally created pressure gradients induce convergent motions towards the centre of a city in the lower levels with divergent motions in the upper levels. The surface heat flux in the rural area can be significant during the day and may develop into a mixed layer. However, the rural heat flux is lower than the urban equivalent because plants use up a large portion of the solar energy in evapotranspiration and the subsequent difference in the heat flux sets up the UHI circulation. The impact of the ambient wind strength causes the UHI circulation to become urban trails directed downwind of the city (Opija and Mukabana, 2004; Hidalgo, et al., 2009). According to Bornstein and Lin (2000), under calm regional wind flow, a relatively low pressure may be created over the city by the unusually high temperature of the UHI and cooler air rushes into the urban area causing warm air to rise, that may cause rainfall over the city. On the other hand, when the regional flow is unstable, winds tend to diverge around the city because of increased surface roughness thus creating maximum precipitation on the lateral and downwind edges of the city with a minimum located over the urban area (Shepherd, 2005).



Furthermore, studies have shown that thermally induced circulation in a given location could affect moisture convergence in far off regions (100s of kilometres) through the interaction with the meso-scale and synoptic scale systems of that region (Weaver and Avissar, 2001; Zhong and Yang 2015), and that the spatial structure of the surface heating can produce focused preferred regions for deep convection (Pielke, 2001). In the equatorial regions, insolation is usually strong for most parts of the year which encourage the convective type of rainfall. Various studies have suggested that there is a reasonably stable relationship governing the intensity characteristics of the convective type of rainfall with urban energy flux (Eltahir, and Pal, 1996; Opija and Mukabana, 2004). The interaction between urbanized landscapes and the overlying atmosphere influence the way heat and moisture move upwards



from the surface into the atmosphere. According to Dixon and Mote (2003), the effects of the UHI circulations on rainfall patterns have been best observed when the atmosphere is unstable but not enough to produce widespread rainfall and suggested that low-level moisture rather than UHI intensity is more important for UHI induced rainfall. Mukabana and Pielke, (1996) suggested that convective rainfall in Kenya only occurs when the synoptic monsoon wind system provides the necessary moisture; even in regions of strong meso-scale circulations such as the coast and Lake Victoria regions. UHI in Kenyan towns would, therefore, be expected to interact with the meso-scale and synoptic systems to influence rainfall patterns during the periods when the monsoon winds bring in moisture. In Chapter 2, I established that increasing trends in temperature are not only in urban areas but also in sub-urban and rural areas near them, although higher rates were observed within the urban stations. In Chapter 4, I established that day-time and night-time UHI exist in Nairobi and Mombasa. It would be expected therefore that changes in energy fluxes due to urbanization and global warming would influence rainfall patterns in and around the urban areas.



Due to the heterogeneity of topography and presence of water bodies, the EEA region experiences different scales of atmospheric motions which interact to produce the observed weather and climate patterns. Figure 5.2 shows a schematic representation of the various spatial and temporal dimensions of such atmospheric motions which include; a) the micro-scale horizontal motions which are mainly caused by small-scale air disturbances covering a few metres to a few kilometres and takes seconds to a few hours to dissipate (they are referred to as local circulations in this study *e.g.*, UHI circulations and other local thermally induced motions); b) the meso-scale motions that are larger and covers from tens to about 1000 km, and persist for days to weeks (*e.g.*, land and sea breezes and mountain and valley

winds) and; c) the synoptic scale motions that are sometimes referred to as the planetary motions(*e.g.*,Figure 5.3). Using dynamical simulations, Mukabana and Pielke, (1996) suggested that the ocean breeze at the Kenyan coast not only influences rainfall at the coast but also interacts with the upslope winds from the walls of Rift Valley to influence convergence over the central highlands. Weaver and Avissar (2000) indicated that by changing the scale and properties of naturally occurring land surface elements (such as in urbanization), human influence can significantly change local (and regional) weather and climate through changes in air circulation patterns, and Kang, et al. (2012) suggested that local surface heterogeneity at scales of 10s to 100s of km might create changes in low-level horizontal wind speed thus influencing vertical motions and rainfall patterns. Further, Hildago, et al. (2009) indicated that UHI circulation is affected by background wind field and demonstrated that when the background winds increase, the surface convergence over a city decreases and the UHI circulation moves downwind of the city. These observations suggest that the effects of enhanced temperature in one location are likely to be experienced not only at that location but in locations of 100s of kilometres further downwind depending on the prevailing climatic conditions and surface heterogeneity.

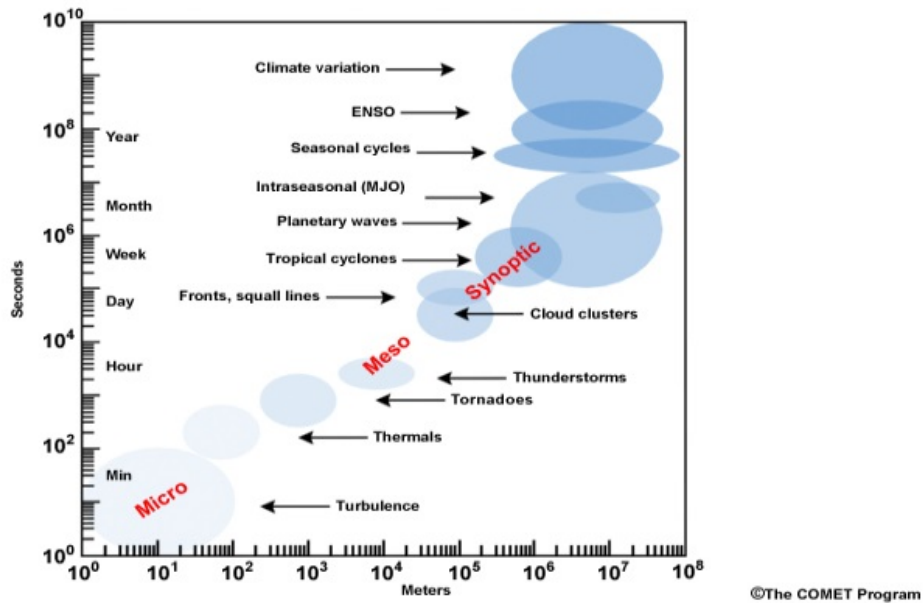


**Figure 5.2: Temporal and spatial extent of different scales of atmospheric motions**  
 (Source:<http://www.comet.ucar.edu/>)

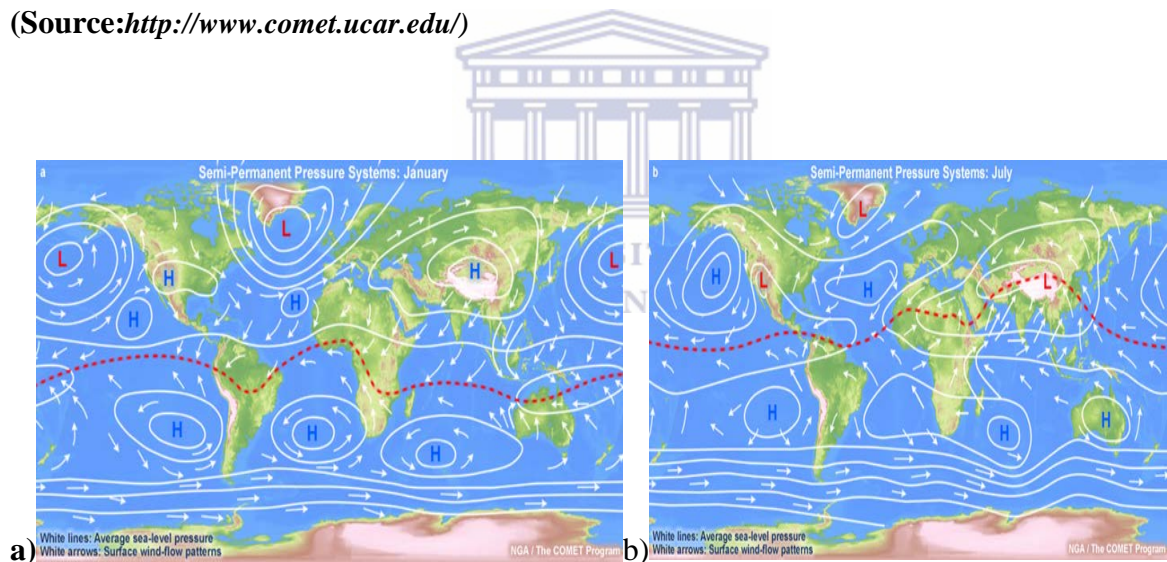


**Figure 5.3: Mean westerly and easterly winds and pressure systems across the globe in**  
 a) January and; b) July depicting synoptic scale motions (red dashed line shows the  
 equatorial low-pressure belt; referred to as the ITCZ over African continent) (Source:  
<http://www.comet.ucar.edu/>)

The major urban areas of Kenya are situated within regions of naturally occurring strong meso-scale circulations. For instance; a) Mombasa at the coastal and Kisumu near Lake Victoria are urban areas that experience land (sea) breeze circulations; with the coastal sea

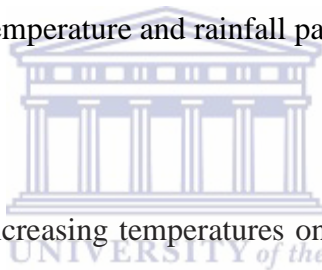
breeze relative to the town being an easterly flow and the Lake Victoria breeze a westerly flow and; b) Nakuru experiences valley/mountain circulations induced by the floor and the escarpments east and west of the Rift, and land/lake breezes from Lake Nakuru within the town. The interactions among the synoptic-scale, meso-scale and the local circulations induced by UHI effect and regional warming are likely to influence rainfall patterns locally and regionally.

Trend analysis of rainfall in Chapter 3 showed that only some stations within and near urban areas had long-term temporal trends in seasonal rainfall amounts. Using statistical methods in this Chapter, I investigated the effects of the UHI and regional warming (especially over the coastal region) on the rainfall patterns over urban areas locally, and whether the interactions of the different scales of atmospheric motion as suggested in Weaver and Avissar, (2000) and Pielke, (2001) would influence changes in rainfall across the varied climatic zones that these urban areas are found.

## **5.2 Materials and methods**

The aim of this Chapter is to establish if increasing temperatures in and around the major urban areas of Kenya, and the existence of UHI in the urban areas, (that were established in Chapter 2 and 4 respectively), have influenced seasonal rainfall characteristics in urban areas. Chapter 2 showed that increasing temperatures are being experienced in both urban and neighbouring rural areas. Chapter 3 established that only a few stations within and close to urban areas had temporal trends (positive and negative) in monthly and seasonal rainfall during the 1961-2013 period. This Chapter links with results from Chapter 2, 3&4 and I hypothesised that the trends observed in the rainfall in and close to urban areas(Chapter

3) have been influenced by the increasing temperature and the UHI effect. I used Statistical methods to investigate; i) if there have been any significant urban effects on seasonal rainfall by comparing rainfall at the urban station with rainfall at the neighbouring rural stations; ii) if there exist statistical relationships between the UHI intensities and rainfall at the urban and nearby rural stations and; iii) if enhanced temperature within and around urban areas in one climate zone influences changes in rainfall in urban areas of other climate zones in the diversely inhomogeneous terrain of Kenya that produces varied scales of atmospheric motions. The Chapter starts with a review of the literature on the influence of urbanization (including UHI) on urban rainfall patterns, effects of enhanced thermal circulation on the convective type of rainfall and the various methods that have been used to determine relationships between enhanced temperature and rainfall patterns.

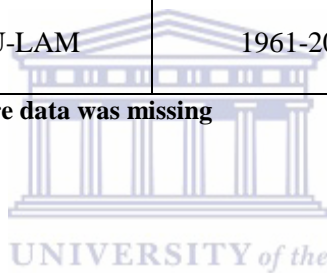


To investigate the influence of increasing temperatures on urban rainfall, rural stations close to the urban stations (NU and MU), were selected from the sixteen (16) stations used in Chapter 3 (Appendix 5.1). Inter-stations correlations (Appendix 5.2) were used to delineate the stations in and around each urban area that have the highest rainfall correlations with the urban station in each season and therefore have the least spatial climatological differences (Camberlin et al., 2009). Temperature data for the selected stations was retrieved from Chapter 2, and UHI data from Chapter 4. The rationale for using seasonal data is that rainfall and temperature in Kenya are seasonal and varies spatially according to climatic zones (Indeje, et al., 2000). Table 5.1 shows the urban-rural pairs of stations used for investigating the urban and UHI effect on rainfall.

**Table 5.1: Pairs of urban-rural stations used in investigating urban and UHI effects on rainfall**

Urban area	Station pair	Length of rainfall data	Length of temperature data
<b>Nairobi</b>	NU-NR <sub>D</sub>	1961-2013	1980-2013
	NU-NR <sub>K</sub>	1961-2013	1979-2013
	NU-NR <sub>T</sub>	1961-2013	1984-2013
	NU-NYR	1961-2008	.....
<b>Mombasa</b>	MU-MR <sub>Mt</sub>	1961-2013	1980-2013
	MU-MR <sub>Ms</sub>	1961-2013	1980-2013
	MU-VOI	1961-2008	.....
	MU-LAM	1961-2008	.....

Note: “.....” indicate that temperature data was missing



Seasonal rainfall differences between an urban and rural station (designated in my Thesis as  $\Delta R_{U-R}$ ) and logarithmic values of the ratio of urban to rural seasonal rainfall (designated in this study as  $\log(U/R)$ ) were then computed as time series for each season as:

$$\Delta R_{jU-R}^i = R_{jU}^i - R_{jR}^i \quad (5.7)$$

$$\log(U/R) = \log\left(\frac{U_j^i}{R_j^i}\right) \quad (5.8)$$

Where  $\Delta R_{jU-R}^i$  is the rainfall difference in mm for season  $i$  and year  $j$ ,  $R_U$  and  $R_R$  are seasonal rainfall totals for the urban and rural stations respectively, and  $\log(U/R)$  is the logarithm of the ratio of urban  $U_j^i$  to rural  $R_j^i$  seasonal rainfall of season  $i$  and year  $j$ . A time series from each method, and for each season (MAM, JJA and OND) is created whose length is

from  $j=1, \dots, j=n$ ;  $n$  is the number of years in the rainfall time series. The two variables were then used to:

- a) Investigate the changes over time that may have occurred between seasonal rainfall in an urban and a neighbouring rural station. To achieve this, exploratory time series plots and trend analysis of the  $\Delta R_{U-R}$  and  $\log(U/R)$  time series were used. The trend analysis was done using the linear regression and Mann-Kendall methods discussed in Chapter 2. The hypothesis here was that the presence of trends in the long-term series of  $\Delta R_{U-R}$  and or  $\log(U/R)$  implies changes in rainfall have occurred as a result of urban effects influencing seasonal rainfall characteristics; otherwise, no trends would mean the variability is due to micro-climatic differences between the urban and rural station. A similar method was used in Tayanc and Toros, (1997) to investigate the urban effect on rainfall over Turkey.
- b) Correlations between the seasonal  $\Delta R_{U-R}(\log(U/R))$  and the corresponding seasonal UHI intensity (computed in Chapter 4) for each urban and rural pair of stations were computed. The hypothesis to be tested here was that existence of the UHI has influenced urban seasonal rainfall.

Other investigations to establish influence of enhanced temperature on rainfall in urban areas included:

- c) Correlations of UHI intensity with the individual urban and rural rainfall time series of each season in order to examine the influence of UHI on the urban and rural rainfall separately.



d) Correlations between seasonal rainfall and temperature at each station, and inter-station correlations of rainfall with the temperature at other stations in the neighbourhood, and in other climatic zones. My hypothesis here was that increasing temperature in and nearby urban areas in one climatic zone could influence urban rainfall at that station and/ or at stations in other zones through enhanced thermal circulations interacting with the synoptic monsoon and other meso-scale circulations as suggested by Mukabana and Pielke (1996). In this analysis,  $T_{\max}$  and  $T_{\min}$  (from Chapter 2) of the corresponding seasons with rainfall were used. The rationale to use seasonal  $T_{\max}$  and  $T_{\min}$  was that each of these temperature variables was observed to have increasing trends in most stations in and around the urban areas (Chapter 2).

Since temporal dependence between rainfall and temperature is likely to influence the significance of correlation coefficients (Zhao and Khalil 1992), the t-test statistics was computed by considering the effective number of degrees of freedom for each paired sample. The effective degrees of freedom ( $\nu$ ) were computed following Davis (1976) as:

$$\nu = \frac{N\Delta t}{\eta} \quad (5.9)$$

where,

$$\eta = (1 + 2 \sum_{i=1}^N C_{RR}(i\Delta t)C_{TT}(i\Delta t))\Delta t \quad (5.10)$$

$N$  is the number of the paired data points,  $\Delta t$  is the time step  $C_{RR}$  and  $C_{TT}$  are the auto-correlation coefficients of rainfall and temperature respectively. The computed values of  $\nu$  were then used to compute the t-test statistics and the significant values at 5% level were identified.



## 5.3 Results and discussion

### 5.3.1 Urban and UHI effects on rainfall

Spatial and temporal variability of seasonal  $\Delta R_{U-R}$  and  $\log(U/R)$  were examined in order to establish if continued urbanization has influenced changes in rainfall of the urban station. The rainfall time series of Nairobi and Mombasa and their respective neighbouring stations runs from 1961-2013; a period when both cities have been rapidly developing (refer to Chapter 1&4).

Time series plots of seasonal  $\Delta R_{U-R}$  and  $\log(U/R)$  from each of the urban-rural pair of stations indicated that  $\Delta R_{U-R}$  had changed during some periods as shown in Figure 5.4 for Nairobi and Figure 5.5 for Mombasa. For instance; i)  $\Delta R_{U-R}$  of MAM season between NU and NR<sub>D</sub> changed from being near zero to positive from 1985 to about 2005 (Figure 5.4(a)), and within this period, the positive difference is observed to be increasing with time. The positive values imply that rainfall at the urban station during this period was higher than rainfall at the rural station, while the two stations were receiving relatively equal amounts of rainfall between 1961 and 1985. These results are consistent with the results of Chapter 3 which showed decreasing trends in MAM rainfall at NR<sub>D</sub> during MAM season; ii)  $\Delta R_{U-R}$  of JJA season between NU and NR<sub>D</sub> had observable decreasing trends especially from 1990 onwards (Figure 5.4(b)). This observation implies that the rural station was receiving more rainfall than the urban station. The observation is consistent with results of Chapter 3 that indicated that JJA seasonal rainfall at NR<sub>D</sub> had increasing trends while NU had no trends.

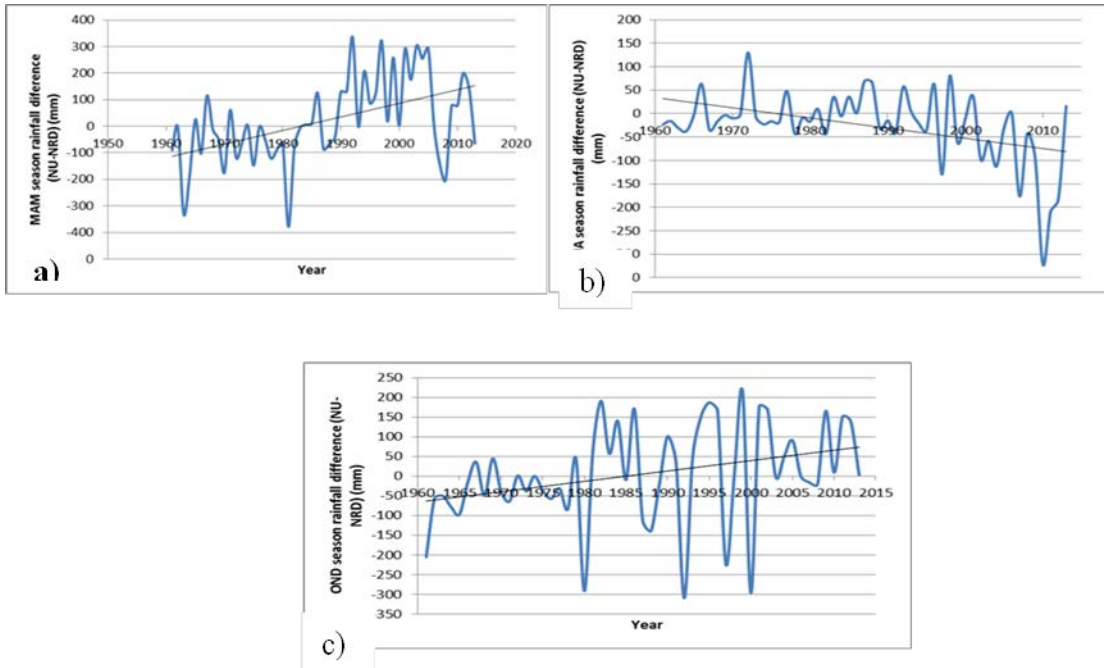
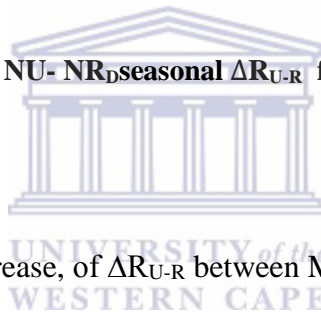


**Figure 5.4: Temporal variability of NU- NR<sub>D</sub>seasonal  $\Delta R_{U-R}$  for a) MAM, b) JJA and c) OND**



In Mombasa, there is notable decrease, of  $\Delta R_{U-R}$  between MU and MR<sub>Mt</sub> during MAM season, and increase of  $\Delta R_{U-R}$  from the year 2000 during the JJA season (Fig 5.5(a&c)). Other  $\Delta R_{U-R}$  time series between Mombasa and the rural stations had no observable changes over the analysis period (1961-2013).

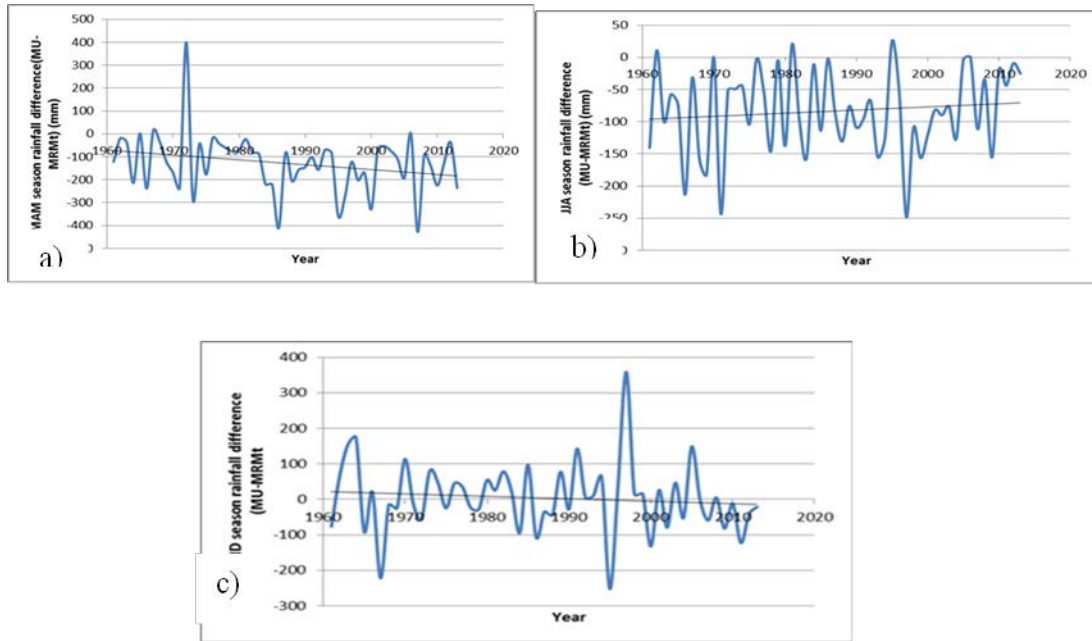


**Figure 5.5: Temporal variability of MU- MR<sub>M</sub>, seasonal ΔR<sub>U-R</sub> of; a) MAM, d) JJA and c) OND**

Theurban-rural rainfall differences were further investigated for long-term temporal trends using linear regression and Mann-Kendall methods and the results tested at  $\alpha=0.05$ . Only  $\Delta R_{U-R}$  and  $\log(U/R)$  of NU-NR<sub>D</sub> pair of stations during the JJA season showed significant negative trends from both methods (with p-values<0.05) (Fig5.6) all other pairs had no long-term temporal trends.

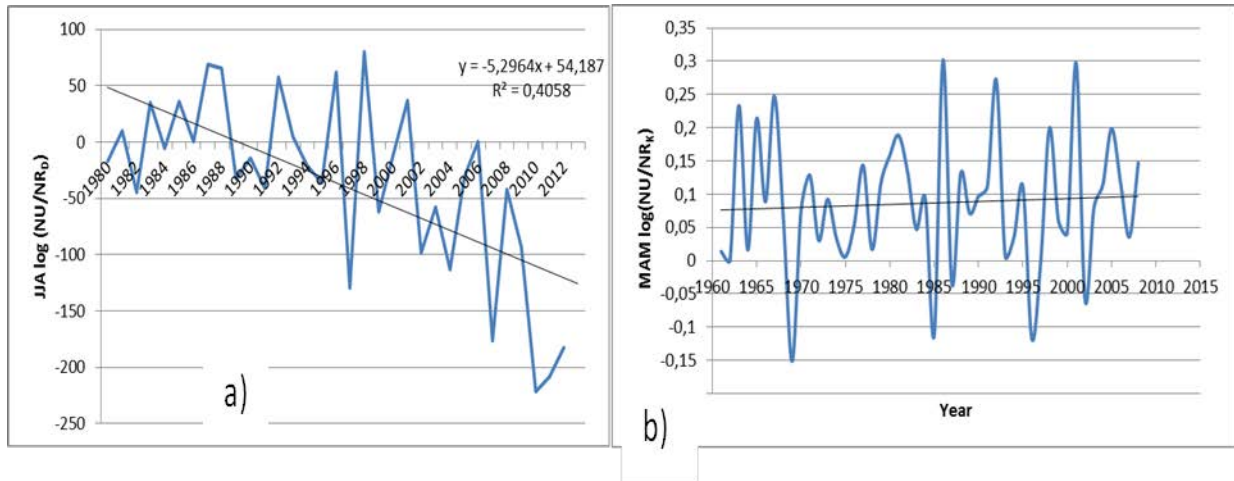
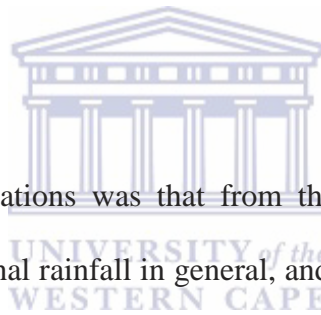
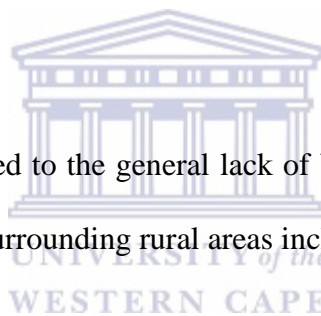


**Figure 5.6: Trends of log (U/R) between; a) NU and NR<sub>D</sub> JJA rainfall; the decreasing trend was significant ( $\tau = -0.31$ , p-value= 0.01;  $\beta = -5.3$ , p-value= 0.01); b) NU and NR<sub>K</sub> MAM rainfall showing no trend**



The implication of these observations was that from the long-term rainfall series, urban effects have not influenced seasonal rainfall in general, and especially in Mombasa. However in Nairobi, changes of rainfall in NR<sub>D</sub> were observed in MAM and JJA. These changes imply that either rainfall at the urban station was increasing or that rainfall in the rural station was decreasing for the MAM season. From trend analysis in Chapter 3, NU had no temporal trends in MAM rainfall while NR<sub>D</sub> had negative trends. A similar conclusion was made for the JJA season in which NR<sub>D</sub> had increasing trends for JJA seasonal rainfall. A decline in MAM, increase in JJA and no trend in the annual total rainfall at NR<sub>D</sub>(Chapter 3), suggests a shift of rainfall from MAM towards JJA at this station. Note that rainfall in NR<sub>D</sub> had negative trends for April and May and positive trends for June and July months (Chapter 3). NR<sub>D</sub> is about 10 km downwind of the Nairobi city centre and it is likely that these changes are resulting from the UHI effect from the city. To ascertain if this is the case further analysis was carried out.

First, correlations between the seasonal  $\Delta R_{U-R}$  (and  $\log(U/R)$ ) and UHI intensity of each urban and rural pair of stations were carried using both the UHI intensities ( $\Delta T_{\max}(u-r)$  and  $\Delta T_{\min}(u-r)$ ) respectively as defined in Chapter 4. Then UHI intensities were correlated with the urban and rural station rainfall respectively. The results showed that all the urban-rural station pairs had no significant correlations with UHI, and rainfall at individual stations was not significantly correlated with UHI (results not presented). These results indicate that the local UHI effect is either not strong enough to induce the observed changes or is masked by the synoptic and other meso-scale systems; for example,  $NR_D$ ,  $NR_K$  stations are downwind of the Nairobi CBD. UHI had no significant correlations with  $\Delta R_{U-R}$  (or  $\log(U/R)$ ) or with the rainfall.



Several reasons could be attributed to the general lack of UHI effects on seasonal rainfall in the Kenyan urban areas and the surrounding rural areas including:

- a) Dependence of rainfall over the EEA on the large scale synoptic systems (mainly ITCZ and monsoon winds). These systems which have been suggested in Shepherd and Burian, (2003) to diminish thermal differentiation between urban and surrounding rural areas. The effects of urbanization are likely to be diffused in the rainfall of the main seasons (MAM and OND); for instance Kaufmann, et al. (2007), indicated that the urban effect on rainfall in the Pearl River Delta (China) was more apparent during winter when the large-scale summer monsoon was not dominating the area. The results of the rainfall difference between  $NU$  (urban) and  $NR_D$  rural station downwind of the Nairobi CBD during the JJA season would suggest urban effects of on rainfall. However, lack of significant correlation of the rainfall differences (or rainfall at each station) with UHI would imply that the observed change could be resulting from the

interaction of the UHI over Nairobi with the synoptic monsoon system. For the coastal region rural areas close to the town that would be expected to have higher rainfall owing to the existence a negative UHI intensity had no significant correlations. The complex interaction between the negative temperature gradients' circulation, the land/sea breezes and the synoptic flow is likely to advect moisture further downwind towards the urban areas over the highlands owing to landscape heterogeneity and the thermal gradient between the coastal region and the highlands as suggested by Weaver and Avissar (2000).

- b) Another reason why urbanization may not have a direct influence on seasonal rainfall could be due to lack of enough moisture to cause moist convection during periods when UHI is strong; for example UHI in Nairobi is strong during the hot and dry season of DJF while atmospheric moisture is lowest and hence resulting in dry convection. Dixon and Mote (2003) showed that availability of low-level moisture rather than UHI intensity was more important for urban-induced rainfall.
- c) Apart from the meteorological and thermodynamic conditions, urban effects on rainfall patterns have been attributed to the size of the city (Shepherd 2005). In this study, the rainfall differences were computed for a period of over fifty (50) years over which rapid urbanization have been taking place. However, there was no significant change in rainfall difference in most of the urban-rural pair of stations except between NU and NR<sub>D</sub> during JJA season which was not significantly correlated with the UHI. The results, therefore, imply that the growth of the cities has not directly influenced the observed long-term trends in rainfall amounts at the seasonal time scales. To

examine further, the effects of enhanced temperature on rainfall, correlations of temperature and rainfall on a region scale were computed as described in Section 5.2.

### **5.3.2 Spatial influence of temperature on urban rainfall**

In the previous Section (5.3.1), UHI intensity was not significantly associated with urban or the neighbouring rural seasonal rainfall. However, in Chapter 3, the few temporal trends in rainfall were established for stations in and close to the urban areas. In this Section, it is hypothesized that increasing temperature ( $T_{\max}$  and  $T_{\min}$ ) at a given station will influence rainfall changes at that station, in the neighbouring stations, and in stations in other climatic zones. The rationale of this hypothesis is that Kenya has a heterogeneous topography that produces diverse atmospheric circulations of thermal and orographic origin. These motions have been shown to interact with each other and with the monsoon system, and control areas of convergence of rainfall in Kenya (Mukabana and Pielke, 1996). Enhanced temperatures due to UHI and global warming are expected to influence changes in rainfall through enhanced thermal circulations. These circulations interact with the other atmospheric circulations to influence changes in rainfall in other climatic zones. To establish if the hypothesis is true, station and inter-station correlation analyses were done between seasonal rainfall and the corresponding seasonal mean  $T_{\max}$  and  $T_{\min}$  for seven stations which had temporal trends in rainfall (Chapter 3), and are in different climatic zones. To minimize chance correlations, the resulting correlation coefficients were tested for effective significance using Equations (5.8) and (5.9). In most samples, the auto-correlations of rainfall and temperature respectively were zero, and therefore the degrees of freedom used in the t-test was equal to the number of data points for the samples being correlated.

Tables 5.4-5.6 show results of the correlations of rainfall and temperature of the three rainfall seasons (MAM, JJA, and OND), and Figure 5.8 shows some examples of regression plots. In Table 5.4, the correlations between MAM seasonal rainfall with mean  $T_{\max}$  and  $T_{\min}$  of MAM season respectively showed that:

- For the  $T_{\max}$ , significant negative correlation between station rainfall and temperature during this season was observed at MU (Table 5.4 (a)). However, MU rainfall was also negatively correlated with  $T_{\max}$  of the two neighbouring stations ( $MR_{Mt}$  and  $MR_{Ms}$ ). Inter-station positive significant correlations were observed between; i) rainfall at  $NR_D$  (in Nairobi area) with  $T_{\max}$  at  $MR_{Mt}$  (at the coast); ii) rainfall at NKU (within the Rift Valley) with  $T_{\max}$  at  $MR_{Mt}$  and  $MR_{Ms}$  respectively (at the coast).
- For the  $T_{\min}$ , significant positive correlations between station rainfall and temperature during MAM season were observed at  $NR_D$  and NKU respectively (Table 5.4 (b)). Rainfall at  $NR_D$ , and at NKU was also respectively significantly positively correlated with  $T_{\min}$  of a number of stations in other climatic zones. Only  $MR_{Mt}$  rainfall is significantly negatively correlated with MU  $T_{\min}$  ( $r=-0.45$ ), while NU, KU, and MU rainfall was not significantly correlated with  $T_{\min}$  at the station or any other station.



**Table 5.2: Correlations coefficients of MAM rainfall and mean MAM temperature**

a)		MAM $T_{max}$						
		NU	NR <sub>D</sub>	NKU	KU	MU	MR <sub>Mt</sub>	MR <sub>Ms</sub>
MAM rainfall	NU	-0.37	0.00	-0.22	-0.31	-0.14	0.00	0.00
	NR <sub>D</sub>	-0.29	0.00	-0.21	0.28	0.00	<b>0.55</b>	0.32
	NKU	0.00	0.13	0.00	0.00	0.16	<b>0.65</b>	<b>0.54</b>
	KU	-0.38	-0.29	-0.13	<b>-0.56</b>	-0.22	0.00	0.00
	MU	-0.33	<b>-0.45</b>	-0.26	0.00	<b>-0.55</b>	-0.33	-0.33
	MR <sub>Mt</sub>	-0.25	-0.29	-0.16	0.00	<b>-0.48</b>	-0.28	-0.16
	MR <sub>Ms</sub>	-0.22	-0.32	0.18	0.00	<b>-0.48</b>	-0.34	0.00

b)		MAM $T_{min}$						
		NU	NR <sub>D</sub>	NKU	KU	MU	MR <sub>Mt</sub>	MR <sub>Ms</sub>
MAM rainfall	NU	0.33	0.26	0.39	0.26	0.20	0.20	0.00
	NR <sub>D</sub>	<b>0.43</b>	<b>0.61</b>	-0.14	<b>0.46</b>	0.25	0.25	<b>0.47</b>
	NKU	<b>0.46</b>	0.39	<b>0.43</b>	<b>0.54</b>	<b>0.47</b>	<b>0.62</b>	<b>0.55</b>
	KU	-0.16	0.00	0.00	0.20	-0.22	0.17	0.00
	MU	-0.19	0.00	-0.21	-0.32	-0.37	-0.37	-0.4
	MR <sub>Mt</sub>	-0.18	0.00	-0.17	-0.34	<b>-0.44</b>	-0.31	-0.31
	MR <sub>Ms</sub>	0.00	0.00	0.00	-0.28	-0.15	-0.27	0.00

Note: all values in bold red ( $r > \pm 0.42$ ) are significant at  $\alpha=0.05$ ; the stations highlighted in blue /yellow has positive/negative trends in MAM rainfall (Chapter 3)

Table 5.5 shows the correlations between JJA seasonal rainfall and JJA mean  $T_{max}$  and  $T_{min}$  respectively.

- Considering the correlations of JJA rainfall with  $T_{max}$  (Table 5.5 (a)); i) negative correlations between station rainfall and  $T_{max}$  were observed at NKU, KU, and MU; ii) for the inter-station correlations, only rainfall of NR<sub>D</sub> was significantly positively

correlated with  $T_{\max}$  of the coastal stations (MU ( $r=0.54$ ),  $MR_{Ms}(r=0.45)$   $MR_{Ms}(r=0.59)$ ), and rainfall at  $MR_{Mt}$  and  $MR_{Ms}$  stations was negatively correlated with  $T_{\max}$  of MU.

- From the correlations between JJA rainfall and  $T_{\min}$  (Table 5.5(b)), significant correlations between station rainfall and temperature were only observed at NU and  $NR_D$  which had positive correlations. Other inter-station correlations between rainfall in one station and temperature at another station were observed. For example; i) NU rainfall was positively correlated with  $T_{\min}$  at  $MR_{Ms}$  station ; ii) rainfall at NKU was positively correlated with  $T_{\min}$  at KU and; iii)  $NR_D$  rainfall was positively correlated with  $T_{\min}$  of all the other stations except NKU with particularly high correlations with the  $T_{\min}$  at coastal and Lake region stations (e.g., correlation between rainfall at  $NR_D$  and  $T_{\min}$  at  $MR_{Mt}(r= 0.60)$ ;  $MR_{Ms}(r = 0.83)$  and; KU ( $r=0.73$ ). There were no significant negative correlations between any pair of stations with  $T_{\min}$  during this season.

**Table 5.3: Correlations coefficients of JJA rainfall and mean JJA temperature**

(a)		JJA T <sub>max</sub>						
		NU	NR <sub>b</sub>	NKU	KU	MU	MR <sub>Mt</sub>	MR <sub>Ms</sub>
JJA rainfall	NU	-0.12	0.00	0.00	0.00	0.14	0.30	0.33
	NR <sub>b</sub>	0.21	0.41	0.00	0.33	<b>0.54</b>	<b>0.45</b>	<b>0.59</b>
	NKU	-0.37	0.00	<b>-0.43</b>	-0.12	0.15	0.00	0.34
	KU	0.00	0.11	0.00	<b>-0.43</b>	0.26	-0.27	0.00
	MU	0.10	0.00	0.13	-0.17	<b>-0.44</b>	-0.15	<b>-0.52</b>
	MR <sub>Mt</sub>	0.24	0.00	0.25	0.00	<b>-0.60</b>	-0.17	-0.38
	MR <sub>Ms</sub>	0.00	-0.23	0.25	0.00	<b>-0.53</b>	-0.29	-0.41
(b)		JJA T <sub>min</sub>						
		NU	NR <sub>b</sub>	NKU	KU	MU	MR <sub>Mt</sub>	MR <sub>Ms</sub>
JJA rainfall	NU	<b>0.56</b>	0.41	0.00	0.37	0.13	0.00	<b>0.49</b>
	NR <sub>b</sub>	<b>0.64</b>	<b>0.47</b>	0.10	<b>0.73</b>	<b>0.53</b>	<b>0.60</b>	<b>0.83</b>
	NKU	0.40	0.32	0.20	<b>0.58</b>	0.11	0.00	0.22
	KU	0.11	0.26	-0.14	0.20	0.15	0.00	0.00
	MU	-0.14	0.00	0.00	-0.32	0.00	0.00	-0.25
	MR <sub>Mt</sub>	0.00	-0.17	-0.17	-0.34	-0.23	0.00	-0.31
	MR <sub>Ms</sub>	0.00	0.15	0.00	-0.28	-0.19	-0.42	-0.36

Note: all values in red ( $r > \pm 0.42$ ) are significant at  $\alpha = 0.05$ ; the stations highlighted in blue /yellow had positive/negative trends in JJA rainfall (Chapter 3)

The correlations between OND seasonal rainfall and T<sub>max</sub> and T<sub>min</sub> respectively are as shown in Table 5.6. During this season only KU had a significant negative correlation between station rainfall and T<sub>max</sub>(Table 5.5(a)). From the correlations between rainfall of OND and T<sub>min</sub> (Table 5.6(b)), there were no significant correlations between station rainfall and T<sub>min</sub> except for NKU which was also consistently positively correlated with almost all other

stations. Other stations where rainfall had significant inter-correlations with  $T_{\min}$  are shown in the Table.

**Table 5.4: Correlations coefficients of OND rainfall and mean OND temperature**

a)		OND $T_{\max}$						
		NU	NR <sub>d</sub>	NKU	KU	MU	MR <sub>Mt</sub>	MR <sub>Ms</sub>
OND rainfall	NU	-0.30	-0.24	0.00	-0.25	0.00	0.00	0.00
	NR <sub>d</sub>	-0.16	-0.38	0.13	0.11	0.18	-0.35	0.00
	<b>NKU</b>	0.00	-0.18	0.00	0.1	-0.13	0.00	0.00
	<b>KU</b>	-0.13	0.00	0.00	<b>-0.45</b>	0.00	0.00	0.00
	MU	-0.22	-0.41	0.00	0.28	-0.4	0.39	0.00
	MR <sub>Mt</sub>	-0.28	<b>-0.43</b>	0.00	0.14	-0.37	0.31	0.00
	<b>MR<sub>Ms</sub></b>	0.00	0.00	-0.13	-0.29	-0.12	0.00	0.00

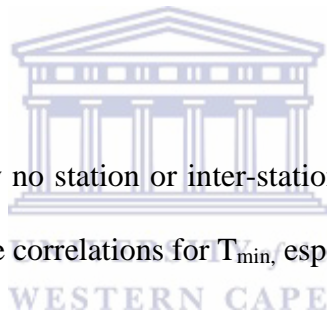
UNIVERSITY of the  
WESTERN CAPE

b)		OND $T_{\min}$						
		NU	NR <sub>d</sub>	NKU	KU	MU	MR <sub>Mt</sub>	MR <sub>Ms</sub>
OND rainfall	NU	0.35	<b>0.47</b>	<b>0.59</b>	0.10	0.35	0.2	0.17
	NR <sub>d</sub>	0.00	0.00	0.23	0.10	0.00	0.00	0.00
	<b>NKU</b>	<b>0.46</b>	<b>0.52</b>	<b>0.56</b>	<b>0.56</b>	<b>0.43</b>	-0.24	0.24
	<b>KU</b>	<b>0.45</b>	0.35	<b>0.46</b>	0.35	0.12	0.00	0.17
	MU	0.13	0.23	0.13	0.10	0.00	0.15	0.00
	MR <sub>Mt</sub>	0.12	0.34	0.23	0.10	0.00	0.25	0.00
	<b>MR<sub>Ms</sub></b>	0.37	<b>0.49</b>	<b>0.44</b>	0.33	0.00	0.00	0.00

Note: all values in red ( $r \geq \pm 0.42$ ) are significant at  $\alpha = 0.05$ ; the stations highlighted in blue has positive trends in OND seasonal rainfall (Chapter 3); the stations highlighted in blue had positive trends in OND rainfall (Chapter 3)

The general observations from the rainfall-temperature correlations were that:

- a) Most stations did not have a significant relationship between rainfall and temperature at the same station in any of the seasons.
- b) Few significant negative correlations between station rainfall and temperature were mainly observed in areas of sea/land breeze circulations. For instance, MAM rainfall at Kisumu station was negatively correlated with  $T_{\max}$  at the station, and over the coastal region, urban rainfall is negatively correlated with both  $T_{\max}$  and  $T_{\min}$  within the station and with the nearby stations, especially during MAM and JJA seasons.
- c) Seasonal temperatures (especially  $T_{\min}$ ) over Mombasa and the neighbouring stations are positively correlated with rainfall over Nairobi and Nakuru, especially during MAM and JJA seasons.
- d) OND season had virtually no station or inter-station rainfall-temperature correlations for  $T_{\max}$  and a few positive correlations for  $T_{\min}$ , especially at Nakuru.
- e) Stations that had temporal trends in rainfall (Chapter 3) had significant station and inter-station rainfall-temperature correlations especially with the  $T_{\min}$ , e.g., NR<sub>D</sub> in Nairobi during JJA season, and NKU in Nakuru during OND season.



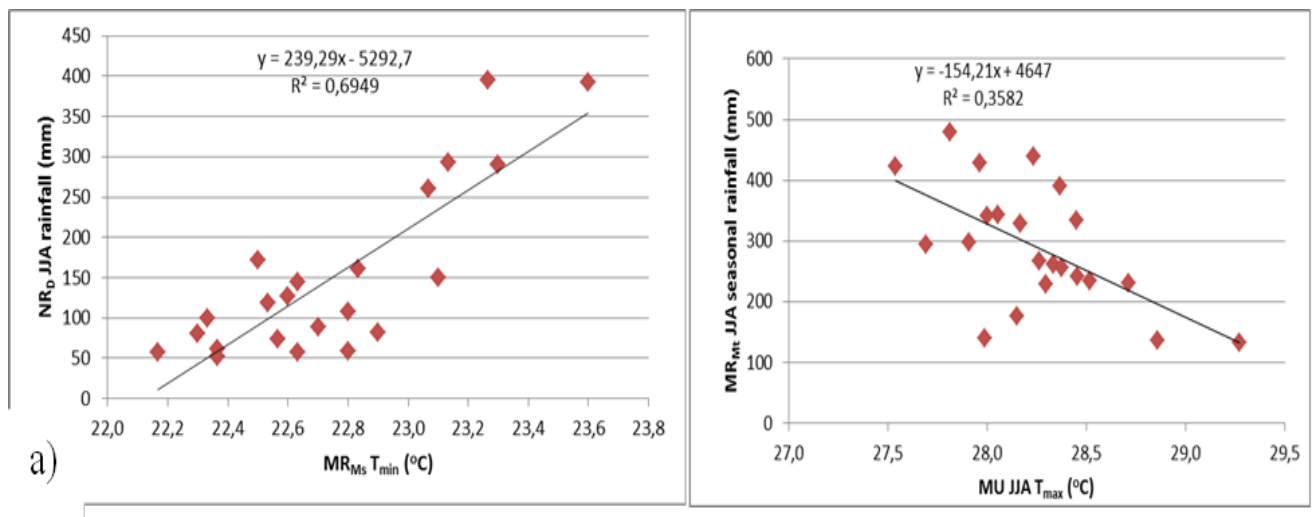


**Figure 5.7: Rainfall-temperature relationships; a) rainfall at Dagoretti in Nairobi and  $T_{min}$  at Msabaha near Mombasa for JJA season; b) rainfall at Mtwapa in Mombasa and  $T_{min}$  at Mombasa Airport.**

### 5.3.3 Discussion

The general lack of temporal trends in the urban-rural rainfall differences (and the logarithm of rainfall ratios) over Nairobi and Mombasa urban areas, indicate that urbanization effect has not significantly influenced changes in urban seasonal rainfall amounts. Particularly at the coast, no pattern or trends were detected in the seasonal rainfall difference. These results are similar to those of Tayanc and Toros (1997) who used the logarithm of rainfall ratios to investigate the influence of urbanization on rainfall urban areas of Turkey and found no urban influence on rainfall. An exception to these observations was found within Nairobi area where JJA seasonal rainfall difference between the urban and a neighbouring station (NU and  $NR_D$ ) had a significant negative trend in the rainfall differences (and log ratios). The negative trend was associated with increasing seasonal rainfall of  $NR_D$  during JJA (Chapter 3) implying that there is enhanced rainfall downwind of Nairobi CBD during this season. The lack of significant correlations between the rainfall differences (or rainfall total) and the UHI

intensity over Nairobi suggested that this observed change in JJA rainfall at NR<sub>D</sub> is not directly associated with UHI over Nairobi. Reasons for this would be that night-time UHI intensity during the cool months of JJA is weak, and the day-time UHI intensities are decreasing with time over the last thirty years (Chapter 4); thus active convection as a consequence of UHI effect would be weak.

The station and inter-station rainfall-temperature correlations were closely related to the results of the seasonal rainfall trends obtained in Chapter 3; positive (negative) rainfall-temperature correlations correspond, in most cases, with positive (negative) temporal trends in seasonal rainfall as observed in Section 5.3.2. These results suggest that changes in regional temperatures (including the UHI effect) have a positive/negative influence on seasonal rainfall not only within that urban area but also across urban areas in other climatic zones, and that  $T_{\min}$  has more positive influence on local and regional rainfall than  $T_{\max}$ . However, the observed rainfall-temperature relationships could be resulting from several different physical mechanisms including, changes in cloud cover, changes in rainfall, and changes in the heat budget due to UHI and global warming. Changes in rainfall may affect soil moisture which in turn may affect surface temperature by regulating the partitioning between the sensible heat and latent heat fluxes. In Chapter 2, I established that most urban and nearby rural stations had positive temporal trends in temperature (especially  $T_{\min}$ ), Chapter 3 established only very few temporal trends in seasonal rainfall in and close to urban areas, and in this Chapter (5), stations which had positive/negative trends in rainfall also had positive/negative rainfall-temperature relationships. I therefore concluded that the significant positive/negative rainfall-temperature relationships are as a result of changes in the heat budget of the urban areas and their environs. Changes in the heat fluxes caused by increasing temperatures due to urbanization and global warming (Chapter 2 and 4), especially at the

coast, are associated with changes in local thermal circulations. For example at the coast, the enhanced thermal circulations would interact with the meso-scale circulation (ocean/land breeze) to influence the convergence and divergence patterns of moist air brought in by the SE monsoon wind system (Mkabana and Pilke 1996; Weaver and Avissar, 2000). For instance, the widespread positive correlations between JJA rainfall at  $NR_D$  and  $T_{min}$  of the coastal and western Kenya region, and the subsequent increasing trends in rainfall could be explained to be a resultant of interaction of the enhanced thermal circulations with the synoptic and meso-scale systems. This interaction would enhance moisture convergence over Nairobi downwind of the city as was suggested by Opija and Mukabana, (2004). A possible mechanism that could explain the statistical relationships would be that the strong SE winds along the coast during JJA season would interact with warm, light and rising air due to enhanced temperatures (global warming and UHI effect) pushing it further downwind towards the highlands as suggested in Kitanda et al. (1997) and Hildago et al. (2009). The warm convective air in Nairobi due to its own UHI effect would further interact with the air from the coastal region influencing cloud formation downwind of the CBD (Shepherd, 2005). Weaver and Avissar, (2000) suggested that landscape heterogeneity is the main driving force of thermally induced motions and that their effect could be felt not only locally but in regions far away from the source. The moist cool air moving from the coast on the surface is replaced by a return flow from the highlands in the upper atmosphere subsiding over the coast. The subsiding air would be warmer than the cool south-easterlies at the surface and thus may create a stable atmosphere that is not conducive to cloud formation at the coast (Kitanda, et al., 1997). In this way, moist air would be shifted from the coast towards the highlands, active convection enhanced by Nairobi UHI downwind of the CBD, and rainfall gets depressed at the coast.

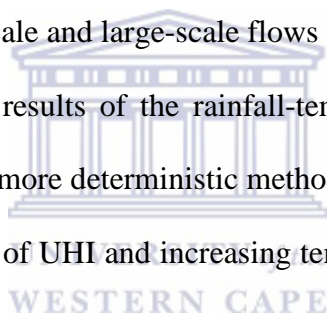


The positive rainfall-temperature relationship at Nakuru during the OND season would explain the increasing trend of seasonal rainfall. For instance, increasing  $T_{\min}$  within the station would enhance convergence of moist air from winds coming from the eastern and western highlands. Nakuru town has a more complex terrain than the other urban areas, with several meso-scale circulations interacting which include; i) the extended westerlies from Lake Victoria (sea breeze) and Congo air-mass (Mukabana and Pielke, 1996); ii) mountain/valley circulations induced by the escarpments (east and west) and floor of the Rift Valley and; iii) Lake Nakuru which is within the urban area south of the CBD setting up local land-lake (lake-land) breezes and; iv) the thermal circulations induced by the town's own UHI. From thermodynamic considerations, increasing  $T_{\min}$  would act to strengthen mountain/valley circulations at night (and weaken the land-breeze from Lake Nakuru) thus enhancing moisture convergence within the valley from the east and west of the valley. Increasing  $T_{\min}$  over the Lake Victoria region would further enhance convergence in Nakuru by weakening the land-lake breeze hence strengthening the westerly winds. This complex interaction of local and large-scale circulations could explain the positive association of rainfall with temperature at Nakuru town with resultant increasing trends in OND rainfall.

#### **5.4 Summary**

The aim of this Chapter was to establish if changing temperatures within and around urban areas (including UHI effect) have influenced changes in urban rainfall over the four major urban areas of Kenya. The conclusions made in this regard were that: a) in general, local urban and UHI effect have not significantly influenced changes in rainfall amounts at seasonal time scales; b) there exist positive relationships between urban rainfall and minimum temperature over Nairobi area and negative relationships over Mombasa; c) increasing

temperatures at the coast of Kenya is associated with increasing/decreasing of rainfall of JJA season over Nairobi/Mombasa, while increasing  $T_{min}$  over Nakuru, Kisumu and Nairobi are positively influencing rainfall of OND season over Nakuru. The effect of temperature on rainfall was attributed to interactions between local thermal circulations (induced by the changing temperature and UHI) with other meso-scale and synoptic-scale atmospheric processes. Notably, the four major urban areas used in my Thesis are in regions of strong meso-scale circulations even in the absence of urbanization, and hence changes in temperature in these urban and their surrounding areas not only affect the surrounding weather but also couple with the meso-scale and the large scale systems to influence temporal and spatial distribution of rainfall over larger areas. The possible interaction of UHI and regional warming with the natural meso-scale and large-scale flows of the Kenya's diverse topography was suggested by the statistical results of the rainfall-temperature relationships. However, I suggest that further studies using more deterministic methods be combined with the statistical method to improve on the effects of UHI and increasing temperatures on rainfall both locally and regionally.



Although urban effects including UHI have not locally influenced changes in urban rainfall amounts at seasonal time scales, rainfall may have changed in terms of the distribution of the daily rainfall over the hours of the day (i.e., hourly intensity) due to the increasing surface temperature caused by UHI and global warming (Chapter 2&4) which I did not investigate. Further investigations would be required to establish if intensities of individual storms have increased as a result of the increasing urban temperatures, especially over Nairobi where UHI is strong. Another important outcome was that rainfall in one location was observed to be influenced by changes of temperature of another location. This outcome was conspicuous during the JJA season and between Nairobi and the coastal region. There is a need for further

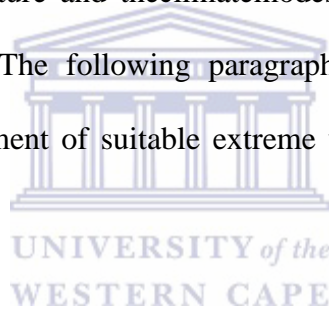
studies to document the physical factors and processes influencing such rainfall-temperature relationships. In the next Chapter (6), factors influencing the annual daily maximum rainfall series were investigated, and an extreme value model established for each of these four towns.



## **6 CHAPTER6: EXTREME VALUE DISTRIBUTION MODELS OF URBAN RAINFALL**

### **6.1 Introduction**

The aim of this Chapter is to establish suitable extreme value distribution models for each of the four urban areas of Kenya. I established in Chapter 3 that the annual rainfall maximum series had notemporal trends for the last 50 years and thatanomalously high values of daily rainfall were influenced by oceanic and atmospheric factorssuch as ENSO and IOD.In Chapter 5, local temperature was observed to influence rainfall at seasonal time scales. In this Chapter, it is hypothesized that there is non-stationarity in the extreme value distribution due to theinfluence of local temperature and theclimatemodes of variability (covariates)on the occurrence of extreme values. The following paragraphs provide the rationale and the literature related to the development of suitable extreme value distribution models and the theories involved.



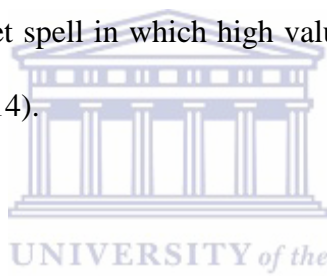
In many urban areas of the developing countries, storm water drainage is already a problem especially for short duration high peak rainfall intensities, and or heavy rainfall events prolonged for several days. Stormwater resulting from such events is likely to exceed the drainage capacity and cause urban flooding (Parkinson and Mark, 2005). In Kenya, like in many African countries, there is little literature on urban storm designs for water management systems (Parkinson and Mark, 2005). In particular very little literature exists on modeling of extreme rainfall in Kenya. Further, there are no design criteria manuals for urban drainage infrastructure in the Kenyan towns. According to the Nairobi City Council urban Master Plan (NCC, 2015), there are no usable technical data available with the city engineering department for carrying out design and maintenance of the storm water drainage at present;

a problem common in most urban areas of Kenya. The absence of such data makes it hard to manage the development and maintenance of stormwater drainage systems. The first step to effectively address the problem of flooding in Kenyan urban areas is to provide an adequate knowledge base on the characteristics of the distribution of extreme rainfall in urban each area.

Climate model projections indicate that urban flooding is likely to become more frequent especially in the developing countries as climate changes, and rapid urbanization continues (Zhang, et al., 2011; Stocker, 2013). Parkinson and Mark, (2005) suggested that potential climate change could be taken into account when planning the urban storm water management systems, while Milly et al. (2008) caution the use of stationarity of climate variables in urban infrastructure design. Mailhot and Duchesne, (2010) and Efrastratiadis et al. (2013) suggested changes in the methodologies used to create design storms for hydrological infrastructure and recommended that the design criteria should consider the projections of climate change. However without, the baseline surveys of the behavior of the extreme rainfall and its statistical distribution, such changes and future projections would not be possible.

Shongwe, et al. (2010) indicated that the frequency of anomalously high-intensity rainfall causing floods in East Africa (EA) has increased and that there has been an increase in the number of the reported hydro-meteorological disasters in this region. There is a perception that the increased flooding in urban areas of Kenya is from increased rainfall intensity as a result of climate change. However, Yang et al. (2011) suggested that the spatial pattern of urban development may also affect hydrologic regime of a catchment by influencing the

hydrologic connectivity of the urban area and flooding may occur even when rainfall intensity has not increased. In Chapter 3, trend analysis using the highest daily rainfall value for each year (annual block maxima) in each of the towns showed that there were no significant linear temporal trends of these extreme values for the period between 1961 and 2013, and the 95<sup>th</sup> percentile of rainfall in most stations did not have significant trends. However, due to high inter-annual variability of seasonal rainfall, there are years in the time series when daily values were extremely high; for example Mombasa recorded a daily rainfall value of 233 mm on the 19<sup>th</sup> October of 1997 during a wet spell that had other significantly high values (Okoola et al., 2008). Such extremes have been attributed to the inter-annual variability of ENSO/IOD (Chapter 3) and cause urban flooding especially because the extreme value comes within a wet spell in which high values are recorded for a consecutive number of days ( Gitau, et al., 2014).

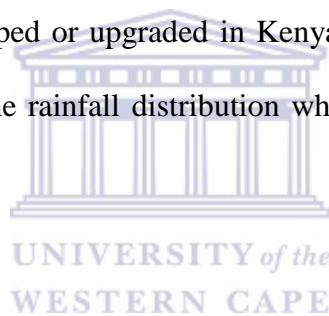


Although non-stationarity in extreme value analysis (EVA) of meteorological variables have been mainly associated with temporal trends in the model parameters (Coles 2001), studies have shown that non-stationarity may be also contributed by other large-scale modes of climate variability such as ENSO, IOD, SSTs and global temperatures influencing seasonal rainfall and or local factors such as mean (maximum or minimum) temperature (Cannon, 2010; Mondal and Mujumdar, 2015). Chapter 3 showed that anomalous seasonal rainfall is closely linked with different modes of climate variability occurring simultaneously and that there have been groups of years with high extreme values and others with low values. These observations suggest that the time series of extreme values may not be stationary with respect to these modes of climate variability. Nyeko-Ongiramoi, et al. (2013) indicated that over the Lake Victoria basin, the mean minimum temperature was positively correlated with extreme rainfall especially in the eastern side of the lake. Chapter 5 of this thesis also established

significant positive correlations between seasonal rainfall and temperature (especially with  $T_{\min}$ ) in urban areas. Several studies have shown that the statistical properties of the extreme values could change through time due to changes in other factors that directly or indirectly influences these variables (Cannon 2010; Mondal and Mujumdar, 2015). Cheng, et al., (2014) suggested that time-varying factors such as SSTs should be incorporated into the modelling of extreme values in order to improve the overall model fit and to investigate possible drivers of the extreme events. Mondal and Mujumdar, (2015) in a study of extreme rainfall over India, used ENSO (Nino 3.4 SST index), global and local air temperatures as covariates while Garcia-Aristzabal, et al.(2014) studied extreme values of rainfall and temperature for Dar Es Salaam (Tanzania) allowing for non-stationarity in time in the location parameter of the distribution model . It is, therefore, probable that even if the annual block maxima had no temporal trends (Chapter 3), other climate factors (referred to here as covariates) that are functions of time, and influence seasonal rainfall may influence the distribution of the extreme series. Such influence could render the methods for estimating flood designs used in the engineering of hydraulic structures, and other stormwater management systems developed for a stationary climate to be inappropriate, as was suggested by Mailhot and Duchesne, (2010).

The two rainfall seasons in Kenya within which the extreme events are experienced have different mechanisms that trigger their inter-annual variability. ENSO have been shown to strongly interact with climate dynamics of the Indian Ocean both in the monsoon season (JJA) and during the transition of the monsoon periods (MAM and OND) which coincides with the rainfall seasons in EEA (Mutai and Ward 2000; Camberlin and Philippon, 2002). Zonal sea surface temperature gradients over the equatorial Indian Ocean and the coupled IOD-ENSO events have been linked with some of the wettest periods in Kenya (e.g., in 1961, 1997 and 2006) which recorded high extreme values as was observed in Chapter 3 and

indicated in Black, et al.(2003) and Owiti, et al.(2008).Most of the anomalously high rainfall values, however, occur mainly during the OND season,and they form only a small fraction (about 10%) of the annual block maximum series.The bulk of the annual maximum values is recorded during the MAM season. The factors that influence the inter-annual variability of rainfall in the EEA have the potential to influence the extreme value distribution of rainfall. From the foregoing, both stationary and non-stationary extreme value distribution should be examined and compared for a given station in each of the four urban areas. The outcome of the extreme value analysis in this Chapter will form a foundation upon which the intensity-duration- frequency (IDF) curves used to design and/or upgrade flood protection structures in these urban areas can be based.This undertaking is important because the urban water structures proposed to be developed or upgraded in Kenya would require the knowledge of updated characteristics of extreme rainfall distribution which are not available in published literature at present.



The capacity of the existing urban drainage elements in many parts of the world has been defined through the statistical analysis of the recorded intense rainfall events. The extreme value theorem provides a framework for describing the statistical distribution of extreme rainfall events(Begueria, et al., 2011). The theorem was first introduced by Fisher and Tippet (1928) to study a series of independent and identically distributed variables under generalized conditions (Faranda, et al., 2011). There are two approaches used in performing the extreme value analysis. One approach uses a series of annual maximum upon which the generalized extreme value (GEV) is defined,andthe other utilizes partial duration series in which the generalized Pareto distribution (GPD) is based. The GDP analysis utilizes values above a certain threshold in a time series (Gilleland and Kartz, 2006;Gilleland and Kartz, 2013; Mondal and Mujumdar, 2015). The main challenge of the use of the GDP is the choice of



threshold, especially where there is a possibility of the data series having auto-correlations (Madsen, et al., 1997; Vasiliades, et al., 2014).

I used the GEV in this my Thesis by considering that rainfall over EEA is seasonal and exhibits intra-season variability with groups of wet and dry spells within a season (Gitau et al., 2014). Thus auto-correlation of extreme values makes the GPD method of extreme value analysis unsuitable. On the other hand, GEV analysis is robust when an annual maximum series is sufficiently long, and also allows for the inclusion of non-stationarity (Gilleland and Kartz, 2006).

## 6.2 Data sources

The daily rainfall data used in Chapter 3 were used. The highest daily rainfall recorded in each year for each station formed the annual maximum values (designated as  $\Omega(t)$  in my Thesis).  $\Omega(t)$  for Nairobi (NR<sub>D</sub>), Mombasa (MU), Kisumu (KU) and Nakuru (NKU) urban areas were used to fit the generalized extreme value (GEV) statistical model for each town (see the location of each town in Figure 1.3 in Chapter 1). The data period for each town is shown in Table 6.1.

**Table 6.1:Location of stations in each urban area with daily rainfall data used in GEV analysis**

City/ Town	Station acronym	Size of town in km <sup>2</sup>	Location (°S; °E)	Data period
<b>Nairobi</b>	NR <sub>D</sub>	689	1.3; 36.75	1961-2013
<b>Mombasa</b>	MU	230	4.03; 39.62	1961-2013
<b>Kisumu</b>	KU	417	0.1; 34.58	1961-2008
<b>Nakuru</b>	NKU	290	0.27; 37.07	1970-2013

Global indices that have been used as climate covariates included: a) NINO 3.4 and IOD Indices(described in Chapter 3);b) Southern Oscillation index (SOI);the SOI is defined as the standardized (or normalized) atmospheric pressure difference between Tahiti (India) and Darwin (Australia) over the western Pacific and was obtained from the National Centre for Environmental Prediction (NCEP) database (<ftp://ftp.ncep.noaa.gov/pub/cpc/wd52dg/data/indi>); c) global (air and ocean) temperature anomaly indices(described in Chapter2 ).

### 6.3 Data analysis

To assess if the common modes of climate variability that influence rainfall also influence the annual maximum value series, linear correlations were computed between the  $\Omega(t)$  series and the various global atmospheric and oceanic covariates.Zero- and time-lagged correlations were computed between the  $\Omega(t)$  series and the seasonal and annual series of the climate covariates . The rationale of using lag correlations was that according to several studies anomalies of the covariates usually lead seasonal rainfall anomalies. These covariatesaffect both the MAM and OND rainfall variabilitybut have more influence of the OND rainfall as

was established in Chapter 3 and reported in Indeje, et al. (2000), Camberlin and Philipon, (2002) and Nicholson, (2014). For each station, the covariate(s) that correlated with  $\Omega(t)$  at the 5% level of significance was (were) used in the extreme value analysis. Linear regression and correlation methods were discussed in detail in Chapter 2. The generalized extreme value (GEV) analysis is described in the next section.

### 6.3.1 Generalized extreme value (GEV) distribution

The GEV is a three parameter function in which the probability of occurrence ( $P_r$ ) of an extreme event, observed at any time ( $t$ ) can be described as:

$$P_r = \{y \leq z(t)\} = \text{GEV}(z(t); (\mu, \sigma, \xi)) \quad (6.1)$$

where  $\mu, \sigma$  and  $\xi$  are respectively the parameters of location, scale and shape;  $y$  and  $z(t)$  are the random variables of rainfall at time  $t$ . When the parameters in this distribution are time independent, the model is referred to as stationary in which it is assumed that the values of  $\mu, \sigma$  and  $\xi$  will remain the same during the next  $n$  years; the location parameter  $\mu$  specifies the centre of the distribution; the scale parameter  $\sigma$  determines the size of the deviations of  $\mu$ ; the shape parameter  $\xi$  shows how rapidly the upper tails decay ( $+\xi$  implies a heavy tail while  $-\xi$  implies a bounded tail and a limit of  $\xi \rightarrow 0$  implies an exponential tail) (Coles 2001).

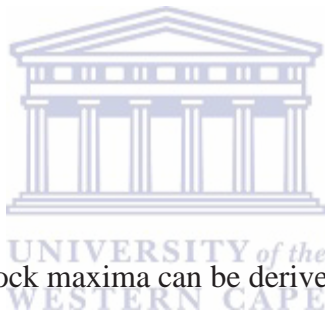
If a significant trend is detected in the annual maximum rainfall series or the annual maximum series varies with an independent covariate, which is also a function of time, the assumption that the probabilistic structure of this series is invariant does not apply (Coles, 2001; Blain, 2011; Liu, et al., 2013). Therefore under non-stationary climate conditions, the use of the stationary GEV model may underestimate or overestimate the probability of occurrence

associated with an extreme meteorological event (Milly, 2008; Blain, 2011). In that case, the non-stationary GEV model in which the parameters vary with time and or with a climate covariate (which is a function of time and does not come from the parent distribution of the extreme value series) could be fitted.

***The GEV theory***

Let  $Y_1, Y_2, \dots, Y_n$  be a series of independent and identically distributed random variables of rainfall of length,  $n$ , and having a common distribution  $F$ , then the distribution of the annual maxima may be presented as:

$$\Omega_n = \max\{Y_1, Y_2, \dots, Y_n\}, \tag{6.2}$$



in which the distribution of the block maxima can be derived as :

$$\Pr(\Omega_n < z) = \Pr\{Y_1 < z, \dots, Y_n < z\}, \tag{6.3}$$

and because of the independent property of  $Y_1, \dots, Y_n$  then,

$$\Pr(\Omega_n < z) = \Pr\{Y_1 < z\} \times \dots \times \Pr\{Y_n < z\} = \{F(z)\}^n, \tag{6.4}$$

$\Omega_n(t)$  can be normalized linearly by

$$\Omega_n^* = \frac{\Omega_n - b_n}{a_n} \tag{6.5}$$

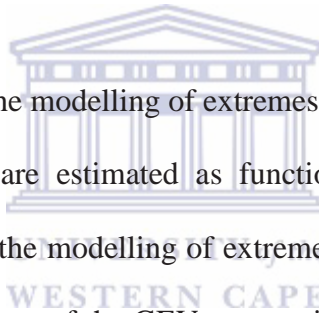
if there exists sequences of constants  $\{a_n < 0\}$  and  $b_n$  such that  $\left\{\frac{\Omega_n - b_n}{a_n} < z\right\} \rightarrow G(z)$ , as  $n \rightarrow \infty$ , then,  $G(z)$  is the generalized extreme value (GEV) distribution described as:

$$G(z) = \exp\left\{-\left[1 + \xi\left(\frac{z - \mu}{\sigma}\right)\right]^{-1/\xi}\right\},$$

(6.6)

and defined on  $\{z: 1 + \xi\left(\frac{z - \mu}{\sigma}\right) > 0\}$ , and  $-\infty < \mu < \infty$ ,  $\sigma > 0$ ,  $-\infty < \xi < \infty$ .

If  $\xi = 0$ , the GEV distribution is referred to as type I or the Gumbel distribution, if  $\xi > 0$ , the GEV distribution is referred to as the type II or the Fréchet distribution, and if  $\xi < 0$ , the distribution is referred to as the type III or the Weibull distribution.



To incorporate climate trends in the modelling of extremes, the model structure of the GEV is described such that parameters are estimated as functions of time (Blain 2011) and to incorporate climate covariates in the modelling of extremes, the model structure of the GEV is described such that the parameters of the GEV are specified as functions of covariates that are themselves functions of time (Cannon 2010; Gilleland and Kartz, 2014). Under this framework, GEV models with increasing number of parameters to be estimated are added to the stationary GEV described by equation (6.6).

These parameters include:

$$\begin{cases} \mu(t) = \beta X(t) \\ \sigma(t) = \sigma_0 \\ \xi(t) = \xi \end{cases} \quad (6.7)$$

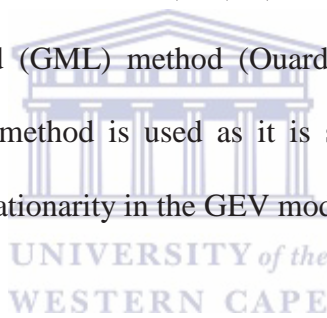
where  $X(t)$  is the covariate which is also a function of time and  $\beta$  is a regression coefficient.

In Equation (6.7), the location parameter is considered to be changing linearly with the covariate while the scale and shape parameters are constant. Equation (6.7) can also be written in such a way that the scale parameter or both scale and location parameters are changing linearly with the covariate. The shape parameter is mostly allowed to be a constant

(Cannon 2010; Gilleland and Kartz, 2014). In this study, the extReme software package written in R language by Gilleland and Katz, (2014) (R Development Core Team, 2010) was used for the GEV analysis. The choice of the package was motivated by the fact that it is an open source, and it is well oriented to climate applications. The package also allows for the incorporation of covariates into the parameters of the GEV and one can easily test for the goodness of fit between models.

### 6.3.2 Estimation of parameters of GEV distribution

The parameters of the GEV distribution may be estimated by use of several methods, and the commonly used are maximum likelihood (ML) (Gilleland and Katz, 2014) and the generalized maximum likelihood (GML) method (Ouarda and Al-Adlouni 2011). In this study, the maximum likelihood method is used as it is stable for large values (~50) and allows for the extension to non-stationarity in the GEV model.



#### *Method of maximum likelihood*

Consider  $\xi \neq 0$ , the log likelihood function of  $G_i$ s given as:

$$l(\mu, \sigma, \xi) = -m \log \sigma - \left[1 + \frac{1}{\xi}\right] \sum_{i=1}^m \log \left[1 + \xi \left(\frac{z_i - \mu}{\sigma}\right)\right] - \sum_{i=1}^m \left[1 + \xi \left(\frac{z_i - \mu}{\sigma}\right)\right]^{-1/\xi} \quad (6.8)$$

With  $1 + \xi \left(\frac{z_i - \mu}{\sigma}\right) > 0, i=1, \dots, m$

And when  $\xi=0$ , the log-likelihood function is:

$$l(\mu, \sigma, \xi) = -m \log \sigma - \sum_{i=1}^m \left(\frac{z_i - \mu}{\sigma}\right) - \sum_{i=1}^m \exp \left[-\left(\frac{z_i - \mu}{\sigma}\right)\right] \quad (6.9)$$

By maximizing the log-likelihood function of  $G$ , i.e., by letting

$$\frac{\partial l(\mu, \sigma, \xi)}{\partial \mu} = 0, \quad (6.10)$$

$$\frac{\partial l(\mu, \sigma, \xi)}{\partial \sigma} = 0, \quad (6.11)$$

$$\frac{\partial l(\mu, \sigma, \xi)}{\partial \xi} = 0 \quad (6.12)$$

for the case  $\xi \neq 0$  and

$$\frac{\partial l(\mu, \sigma, \xi)}{\partial \mu} = 0, \quad (6.13)$$

$$\frac{\partial l(\mu, \sigma, \xi)}{\partial \sigma} = 0 \quad (6.14)$$

$$\frac{\partial l(\mu, \sigma, \xi)}{\partial \xi} = 0 \quad (6.15)$$



for the case the  $\xi = 0$ , then the maximum likelihood estimator of the parameters of GEV is obtained.

### 6.3.3 Model diagnostics

The methods generally used to give an exploratory interpretation of how well a set of extreme values are fitted into GEV model are the probability-probability (PP) plots, and the quantile-quantile plots (QQ). A probability –probability (PP) plot is a graphical technique used to compare if the fitting result of the probability distribution is an acceptable model by comparing theoretical and empirical probabilities. For instance, let  $y_{(1)} \leq y_{(2)} \leq y_{(3)} \dots \dots \dots \leq y_{(n)}$  be ordered sample of independent observations from a population with distribution function  $F$ , then the estimated empirical distribution function is defined by

$$F(Y) = \frac{i}{n+1} \text{ for } y_{(1)} \leq y \leq y_{(n)} \quad (6.16)$$

Thus with an estimated distribution function  $\hat{F}$ , a p-p plot consist of plots of

$$\{(\hat{F}(y_{(i)}), (\frac{i}{n+1}), i=1, \dots, n)\}$$

A reasonable model of  $\hat{F}$  leads to p-p plot close to a diagonal (Coles 2001)

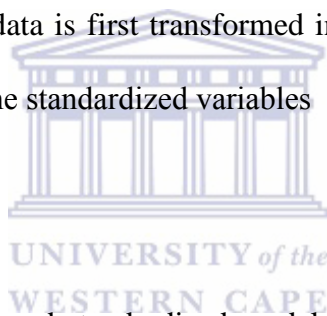
The QQ plot is also a graphical method of assessing if a fitting result of a probability distribution is a reasonable model by comparing the  $(\frac{i}{n+1})^{\text{th}}$  value derived from theoretical and empirical distributions. With an estimation distribution function  $\hat{F}$ , a q-q plot consists of the points

$$\{(\hat{F}^{-1}(\frac{i}{n+1}), y_{(i)}) \quad i=1, \dots, n\}$$

For a GEV with covariates, the data is first transformed in order to plot model diagnostics.

Consider  $z_t \sim \text{GEV}(\mu(t), \sigma(t), (t))$ , the standardized variables

$$\hat{z}_t = \frac{1}{\xi} \log\{1 + \xi(t) \left(\frac{z_t - \mu(t)}{\sigma(t)}\right)\} \quad (6.17)$$



where  $z_t$  and  $\hat{z}_t$  are the estimated and standardized models respectively each having Gumbel distribution with a probability distribution function

$$P_r\{\hat{z}_t \leq z\} = \exp\{-e^{-z}\}, z \in \mathbb{R}. \quad (6.18)$$

The probability and quantile plots can be made with Equation (6.18) as the reference distribution. if  $\hat{z}_{1:n}, \dots, \hat{z}_{n:n}$  denotes the ordered values transformed from the variable  $Z_t$ , the probability plot consist of pairs  $\{(\frac{i}{n+1}, \exp(-\exp(-\hat{z}_{i:n}))) ; i = 1, \dots, n\}$  and quantile plots consist of pairs  $\{(-\log(-\log(\frac{i}{n+1})), \hat{z}_{i:n}, i=1, \dots, n)\}$ .



### 6.3.4 Choice of model

The log-likelihood ratio test is used to determine the better model between two models of the same distribution. For instance, in this study  $M_0$  represent the stationary model and  $M_1$  a model with a covariate either in the scale or location parameters of a GEV distribution. The log-likelihood ratio test is used on the deviance statistics  $D$ , defined as:

$$D=2\{l_1(M_1)-l_0(M_0)\} \quad (6.19)$$

where  $l_1$  and  $l_0$  are the maximized log-likelihood functions of the two models  $M_1$  and  $M_0$  respectively,  $M_1$  being the more complex model.  $M_0$  asymptotically obey chi-square distribution with  $k$  degrees of freedom, i.e.  $\chi^2(k)$ , and  $k$  is the difference of the number of unknown parameters between  $M_1$  and  $M_0$ . The null hypothesis is stated that  $M_0$  is not better than  $M_1$ . If  $D$  is large and greater than  $\chi^2_{\alpha}(k)$ , ( $\alpha=0.05$ ) then  $H_0$  is rejected and model  $M_0$  is believed to perform better than the complex model  $M_1$ ; otherwise, the null hypothesis  $H_0$  is not rejected and  $M_1$  believed to perform better (Coles, 2001; Ouarda and El-Adlouni, 2011; Liu et al., 2013).

### 6.3.5 Return period and return level

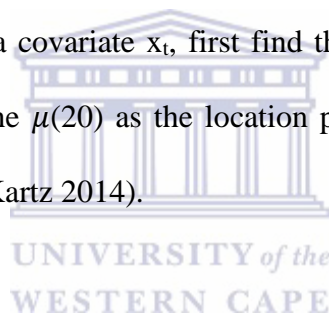
Once the appropriate model is fitted into the annual maximum rainfall time series, two statistics (the return period  $\frac{1}{p}$  and the return level  $z_p$ ) can be estimated from the GEV distribution. For instance for annual maxima, the return level  $z_p$  is an estimated high value which is expected to be exceeded in any year during the return period  $\frac{1}{p}$  with probability  $p$  where  $0 < p < 1$ . From the estimated values of the stationary GEV distribution parameters,  $\mu$ ,  $\sigma$  and  $\xi$ , the return level  $z_p$  can be estimated as:

$$z_p = \mu - \frac{\sigma}{\xi} \{1 - [-\log(1 - p)]^{-\xi}\}, \xi \neq 0$$

(6.20)

$$z_p = \mu - \sigma \log[-\log(1 - p)], \xi = 0 \quad (6.21)$$

The estimation of return levels when the parameters are fitted with covariates in any of the parameters (mainly in  $\mu$  and  $\sigma$ ), is not straightforward since the return level,  $z_p$ , will also vary with the covariate. One method of interpretation of return levels with covariates (i.e., for a non-stationary model) that was suggested by Gilleland and Kartz (2014) is to look for effective return level; defined as the level that would be got for a specific value(s) of the covariate(s) (i.e., a time varying quantile). For example, to get the 20-year return level in a model where  $\mu$  is varying with a covariate  $x_t$ , first find the  $\mu(20)$  ( $=\mu_0 + \mu(x_{t=20})$ ) and then estimate the return level using the  $\mu(20)$  as the location parameter; likewise for any of the other parameters (Gilleland and Kartz 2014).



### ***Confidence interval of return levels***

Normal method (in which normal distribution is assumed) is used to estimate the confidence intervals of the return period with considerable accuracy especially for periods of twice the data period and for GEV models whose shape parameter is close to zero (Gumbel or type I). Otherwise, the profile log-likelihood method is used more accurately than the Normal method to obtain the confidence intervals for longer period return levels and where the shape parameter is significantly positive (Fréchet or type II) or negative (Weibull or type II) (Gilleland and Kartz, 2014).

## 6.4 Results and discussion

### 6.4.1 Correlations between annual daily maximum rainfall and climate covariates

The annual maximum of daily rainfall series,  $\Omega(t)$ , of each station had no temporal trends as shown in Figure 6.1. Considering the correlations, only mean annual IOD index and its one year lag are weakly but significantly positively correlated with  $\Omega(t)$  of MU, KU (mean annual IOD) and  $NR_D$  (one year lag mean annual IOD) (Table 6.2).  $\Omega(t)$  of NKU had no significant correlation with any of these indices.

**Table 6.2: Correlations of the Annual daily maximum series with climate covariates**

$\Omega(t)$ Covariate	MU	NU	KU	NKU
IOD	<b>0.4</b>	0.1	<b>0.3</b>	-0,2
Lag IOD	-0.2	<b>0.3</b>	-0.2	0.0
SOI	-0.1	0.1	-0.1	0.0
Lag SOI	0.1	0	0.2	0.0
NINO3.4	0.2	-0.1	0.0	0.0
Lag NINO 3.4	-0.1	0.2	-0.2	0.0
Global mean Temp	0.0	0.2	-0.2	0.0
Lag GTmean	0.0	0.0	-0.2	0.0

Note: values in bold are significant at  $\alpha=0.05$ ; results for Mombasa (MU), Nairobi (NU), Kisumu (KU) and Nakuru (NKU)

Note that correlations of local temperature with  $\Omega(t)$  were not used as covariates due to short lengths of the temperature data available for this study, which affect the GEV distribution. From these results only the parameters that have significant correlations, and had the same length as the  $\Omega(t)$ , were used as covariates in the GEV analysis for each station.

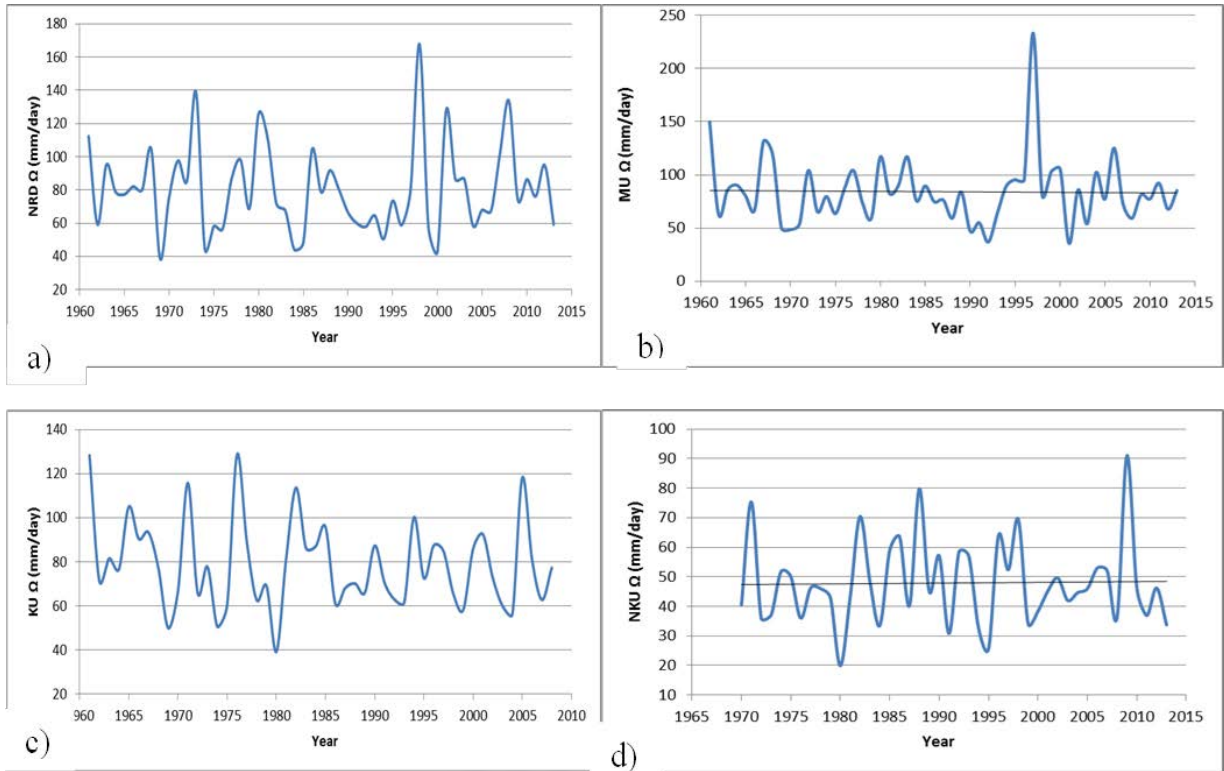
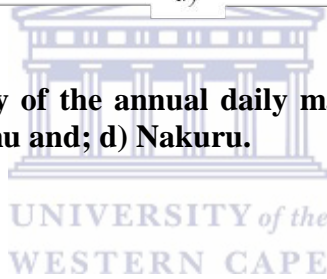


**Figure 6.1: Temporal variability of the annual daily maximum rainfall ( $\Omega(t)$ ) series a) Nairobi; b) Mombasa; c) Kisumu and; d) Nakuru.**



#### 6.4.2 GEV analysis results

Several models for each station were fitted according to Equations (6.6) (i.e., stationary) and Equation (6.7) (i.e., with covariates). Note that model with covariates was only fitted where the covariates were significantly correlated with  $\Omega(t)$ . The model parameters were estimated using the method of maximum likelihood (according to Equations ((6.8)-(6.15))). The fitted models were then tested for goodness of fit using the log likelihood ratio test according to Equation (6.16). The GEV distribution model with no trends (stationary) was first fitted for all stations. From the correlation analysis, the covariates that were significantly correlated with  $\Omega(t)$  were then used to fit the non-stationary GEV models and tested against the stationary one. The GEV analysis results for each urban area (Nairobi, Mombasa, Kisumu and Nakuru) presented below.

*Nairobi*

First the stationary model was fitted ( $M_0$ ); the three parameters were estimated, The second model was fitted with the lagged mean annual IOD indices as a covariate in the location parameter ( $M_1$ )(i.e.,  $\mu(x_t) = \mu_0 + \mu_1(x_t)$ , where  $x_t$  is the covariate representing the annual IOD indices) and a third ( $M_2$ ) one with the same covariate in the scale parameter ( $M_2$ ) (i.e.,  $\sigma(x_t) = \sigma_0 + \sigma_1(x_t)$ ). The results from the GEV analysis for models with the highest log likelihood values( $M_0$ ) and ( $M_1$ ) are shown in (Table 5.3).

**Table 6.3: Comparison of model parameters of a stationary and non-stationary GEV distribution model fitted for Nairobi**

Nairobi					
Stationary GEV model( $M_0$ )			Non-stationary model (lagIOD in scale) ( $M_1$ )		
Parameter	Estimate	Standard error	Parameter	Estimate	Standard error
Location ( $\mu$ )	68.4	3.4	location ( $\mu$ )	68.2	3.3
Scale ( $\sigma$ )	20.5	2.6	location ( $\sigma_0$ )	22.6	2.9
Shape ( $\xi$ )	-0.07	0.1	scale ( $\sigma_1$ )	8.27	3.4
Negative log likelihood 219.3			shape ( $\xi$ )	-0.09	0.1
			Negative log likelihood	218.1	

Figure 6.2 (a&b)) show the density plots of the stationary and the non-stationary model for Nairobi and Figure 6.2(c&d) are the quantile plots of the two models which show that the GEV model with no covariates has more of the quantiles almost aligned diagonally which is an indication of the suitability of the model.

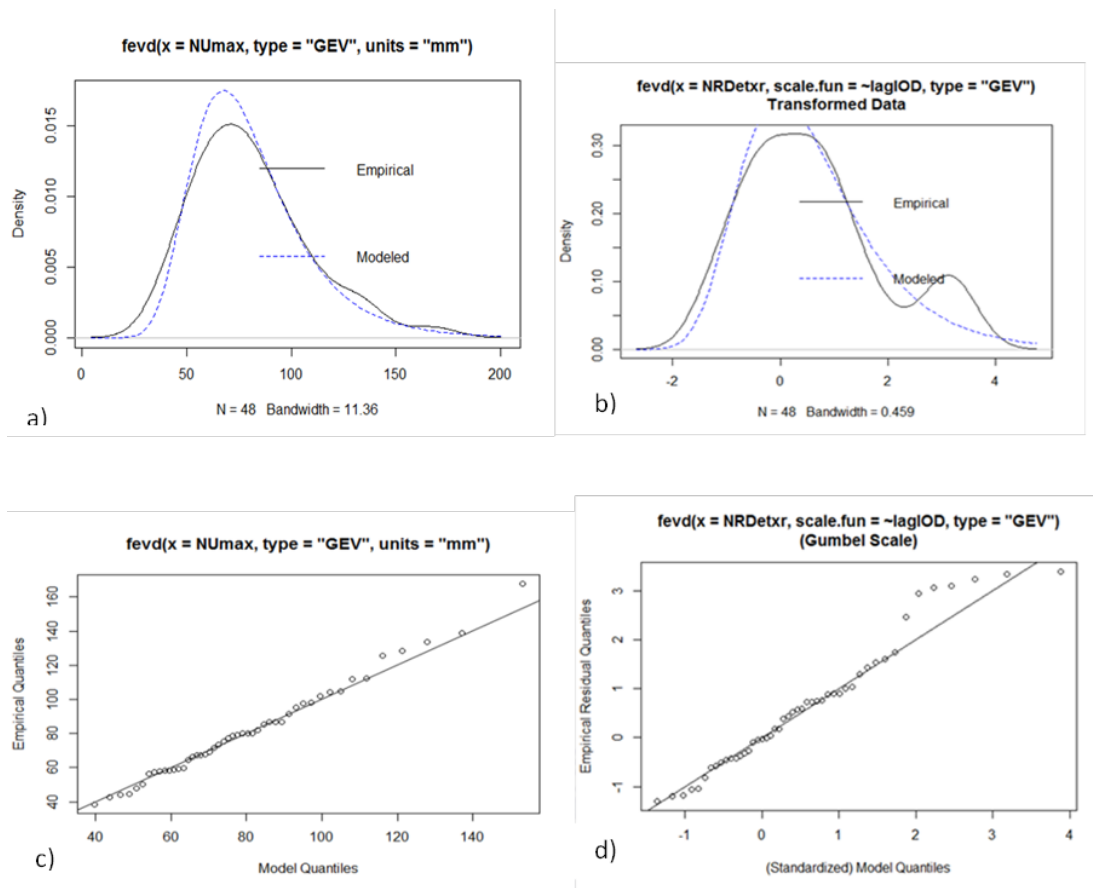


**Figure 6.2: Diagnostic plots comparing the stationary and non-stationary GEV distributions for Nairobi; a&b probability density plots; c&d) QQ plots for the same models**

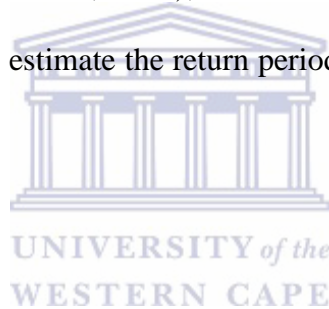
The two models ( $M_0$ ) and ( $M_1$ ) are tested using the log likelihood ratio test so as to get the better model between them. The log likelihood ratio test value ( $lr$ )=1.79,  $\chi^2_{\alpha=0.05} = 3.84$ , and p-value =0.18). Since  $lr$  is less than  $\chi^2_{\alpha=0.05}$ , and has a p-value > 0.05) then at the 5% significant level  $H_0$  is rejected. Hence the stationary model is accepted as more suitable than the non-stationary. From the small values of the shape parameter, ( $\xi$  has a range of - 0.266 < 0.07 < 0.126), and by testing  $\xi$  using the likelihood ratio test of Gumbel ( $H_0: \xi=0$  against  $H_1: \xi \neq 0$ ), the null hypothesis of a Gumbel type is not rejected (rl ratio=0.33,  $\chi^2_{\alpha=0.05} = 3.84$ , p-value=0.57) and therefore the GEV distribution is approximated to the Gumbel type. The Gumbel distribution is light tailed; meaning that although the maximum value can take on

infinitely high values, the probability of obtaining such levels becomes small exponentially. The stationary GEV equation for this station is estimated as:

$$\Omega(t) \sim \text{GEV}(\mu, \sigma) \text{ where } \mu = 68.4 (\pm 6.5); \sigma = 20.5 (\pm 5.7)$$

The values in brackets give the error bounds for the 95% level of confidence found by multiplying the standard error (Table 6.3) by  $z_{\alpha=0.05}$  (i.e., 1.96).

A simpler model that adequately describes the extreme value distribution is more preferable to a more complex one, since the more the number of parameters, the higher the uncertainty in the estimated values (Serinaldi et al., 2015); therefore for Nairobi, a stationary Gumbel distribution would be adequate to estimate the return periods and return levels of the extreme values.



### ***Mombasa***

The stationary model ( $M_0$ ) was fitted for MU station together with a second model fitted with the annual mean IOD index as a covariate in the location parameter ( $M_1$ ) (i.e.,  $\mu(x_t) = \mu_0 + \mu_1(x_t)$ , where  $x_t$  is the covariate representing annual IOD) and a third one ( $M_2$ ) with a covariate in the scale parameter (i.e.,  $\sigma(x_t) = \sigma_0 + \sigma_1(x_t)$ ). Results for two models ( $M_0$  and  $M_1$ ) with highest negative log-likelihood values are shown in (Table 6.4).

**Table 6.4: Comparison of model parameters of a stationary and non-stationary GEV distribution model for Mombasa**

Mombasa					
Stationary GEV model			Non-stationary model (IOD in location)		
Parameter	Estimate	Standard error	Parameter	Estimate	Standard error
Location ( $\mu$ )	70.2	3.7	location ( $\mu_0$ )	70.2	3.6
Scale ( $\sigma$ )	23.2	2.7	location ( $\mu_1$ )	8.48	4.6
Shape ( $\xi$ )	0.05	0.1	scale ( $\sigma$ )	22.4	2.7
Negative log likelihood		227.7	shape ( $\xi$ )	0.05	0.1
			negative log likelihood		226

Figure 6.3(a&b) show the density (P-P) plots of the stationary and the non-stationary model and (c&d) are the quantile (Q-Q) plots of the two models. From the density plot, the difference between the stationary and non-stationary models is minimal. It should be noted in the QQ plot that there is a point out of line from both the stationary and non-stationary model and the stationary model has almost all the other empirical quantiles aligned on the diagonal line (Fig 6.3(c)). The outlier quantile could be resulting from the models not able to capture properly the thickness of the tail of the distribution. The estimation procedure tries to find one single set of parameters that fit all the different parts of the distribution and the resulting compromise often penalizes the high value. The very high value recorded in this station on 19<sup>th</sup> October 1997 (233mm) could explain this case.



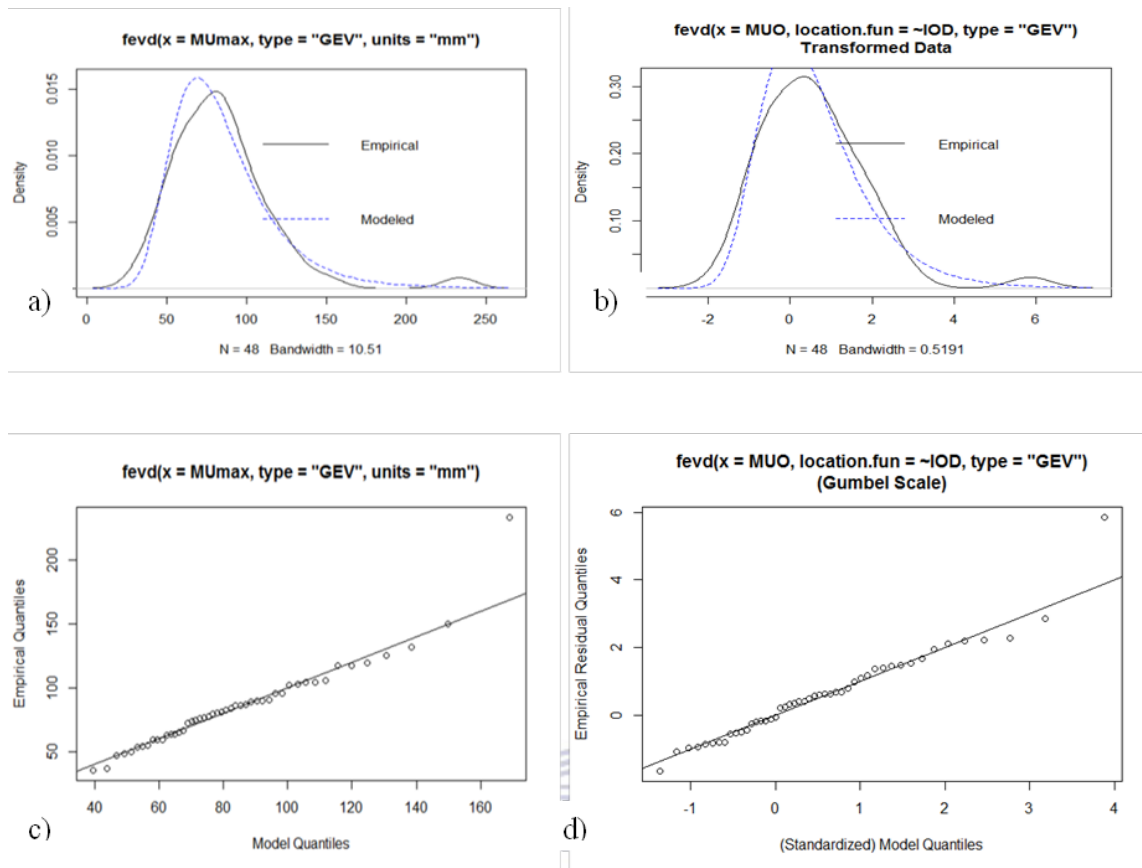


**Figure 6.3: Diagnostic plots comparing the stationary and non-stationary GEV distributions for Mombasa; a&b) Probabilityplots; c&d) QQ plots for the same models**

To determine the best model, the log likelihood ratio ( $lr$ ) test is performed between  $M_0$  (stationary model) and  $M_1$ . The results showed that  $lr$  test value = 3.17;  $\chi^2_{\alpha=0.05} = 3.84$  and;  $p$ -value = 0.07. Since  $lr$  ratio is less than  $\chi^2_{\alpha=0.05}$ , and has a higher  $p$ -value  $> 0.05$  at 5% level of significance, then  $H_0$  is rejected i.e the stationary model performs better than non-stationary one. This station model also have small value of the shape parameter,  $\xi$ , in the range of  $-0.91 < 0.05 < 1.11$ ) and from the likelihood ration test of Gumbel, GEV distribution was also approximated to the Gumbel type. The GEV equation for this station is then written as:

$$\Omega(t) \sim \text{GEV}(\mu, \sigma, \xi) \text{ where } \mu = 70.2 (\pm 7.25); \sigma(x) = 23.2 (\pm 5.3)$$

The values in brackets give the error bounds at 95% level of confidence.

***Kisumu***

The stationary model ( $M_0$ ) fitted for this station yielded the three parameters estimates as  $\mu=70.3$ ,  $\sigma=16.8$ , and  $\xi=-0.08$ . The second model ( $M_1$ ) was fitted with the annual mean IOD index as a covariate in the location parameter (i.e.,  $\mu(x_t) = \mu_0 + \mu_1(x_t)$ , where  $x_t$  is the covariate), and a third one ( $M_3$ ) with the same covariate in the scale parameter (i.e.,  $\sigma(x_t) = \sigma_0 + \sigma_1(x_t)$ ). The results from the GEV analysis for the first and second model are shown in (Table 6.5).

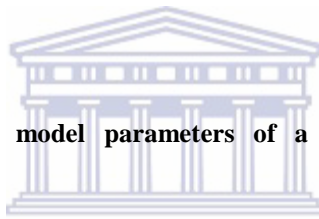


**Table 6.5: Summary comparison of model parameters of a stationary and non-stationary GEV distribution model fit for Kisumu**

Kisumu					
Stationary GEV model			Non-stationary model (IOD in location)		
Parameter	Estimate	Standard error	Parameter	Estimate	Standard error
Location ( $\mu$ )	70.3	2.7	location ( $\mu_0$ )	69.9	2.6
Scale ( $\sigma$ )	16.8	2.7	location ( $\mu_1$ )	7.7	4.6
Shape ( $\xi$ )	-0.08	0.1	scale ( $\sigma$ )	15.5	1.8
Negative log likelihood 209.2			shape ( $\xi$ )	-0.03	0.1
			negative log likelihood 226		

Figure 6.4 shows the density plots of the stationary and the non-stationary model respectively, and the quantile plots of the same models. From the probability density plot (Fig 6.4(a&b)) the non-stationary model fitted the data slightly better than the stationary model.

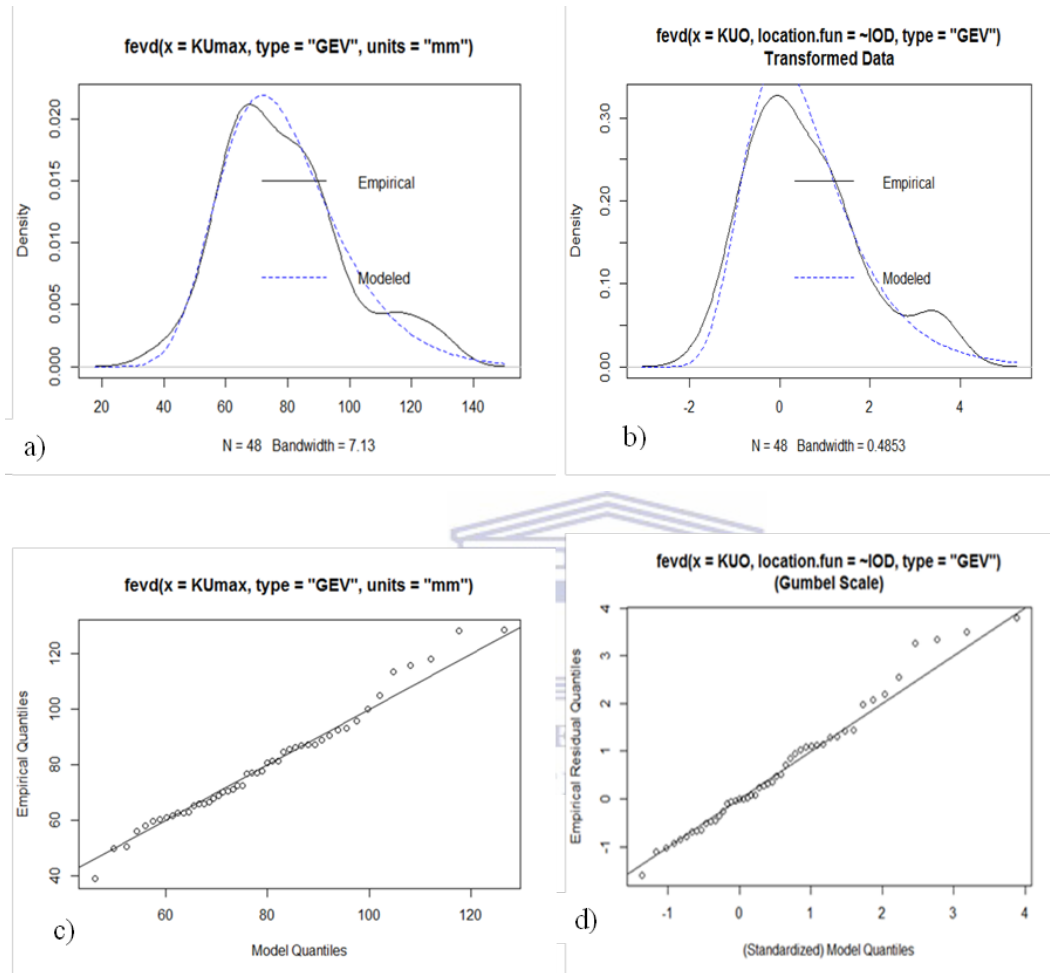


**Figure 6.4: Diagnostic plots comparing the stationary and non-stationary GEV distributions for Kisumu; a&b) Probability plots; c&d) QQ plots for the same models**

From the log likelihood ratio ( $lr$ ) test, between the  $M_0$  (stationary) and  $M_1$  (with a covariate in the location parameter),  $lr$  value = 4.5;  $\chi^2$  (at  $\alpha=0.05$ ) = 3.84; p-value = 0.03. Since  $lr$  ratio is greater than  $\chi^2_{\alpha=0.05}$ , and has a low p-value ( $<0.05$  at 5% level of significance)  $H_0$  is not rejected; therefore the non-stationary model performs better than stationary one. The shape

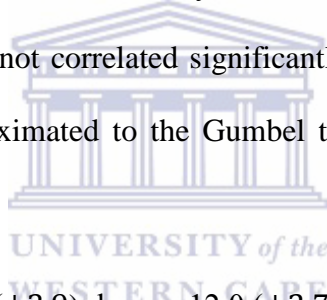
parameter,  $\xi$ , value is small of the in the range of  $-0.23 < -0.03 < 0.17$  and from the Gumbel likelihood test, GEV distribution was approximated to the Gumbel type. The GEV equation for this station is written as:

$$\Omega(t) \sim \text{GEV}(\mu(x_t), \sigma, \xi) \text{ where } \mu = 69.9(\pm 5.3) + 7.7(x_t)(\pm 6.7); \sigma = 15.5(\pm 3).$$

The values in brackets give the error bounds at 95% level of confidence.

### *Nakuru*

The estimated parameters for the stationary GEV model for Nakuru town are  $\mu=41.7$ ,  $\sigma=12.0$ , and  $\xi=0.06$ . In this particular station, only the stationary model was fitted since  $\Omega(t)$  had no temporal trends and was not correlated significantly with any one of the considered covariates. The GEV also approximated to the Gumbel type and thus distribution for this station is written as:



$$\Omega(t) \sim \text{GEV}(\mu, \sigma, \xi) \text{ where } \mu = 41.7(\pm 3.9); \log \sigma = 12.0(\pm 2.7)$$

The values in brackets give the error bounds at 95% level of confidence. The summary of the parameters is given in Table 6.6.

**Table 6.6: Parameters of a stationary GEV distribution model for Nakuru**

<b>Nakuru</b>		
<b>Parameter</b>	<b>Estimate</b>	<b>Standard error</b>
Location ( $\mu$ )	41.7	2.00
Scale ( $\sigma$ )	12.0	1.4
Shape ( $\xi$ )	0.06	0.1
Negative log likelihood 176.9		

Figure 6.5 (a) shows the density plot of the stationary and Figure 6.6 (b) shows the QQ plot. From these plots, a stationary GEV distribution adequately modeled the annual daily maximum rainfall for Nakuru.

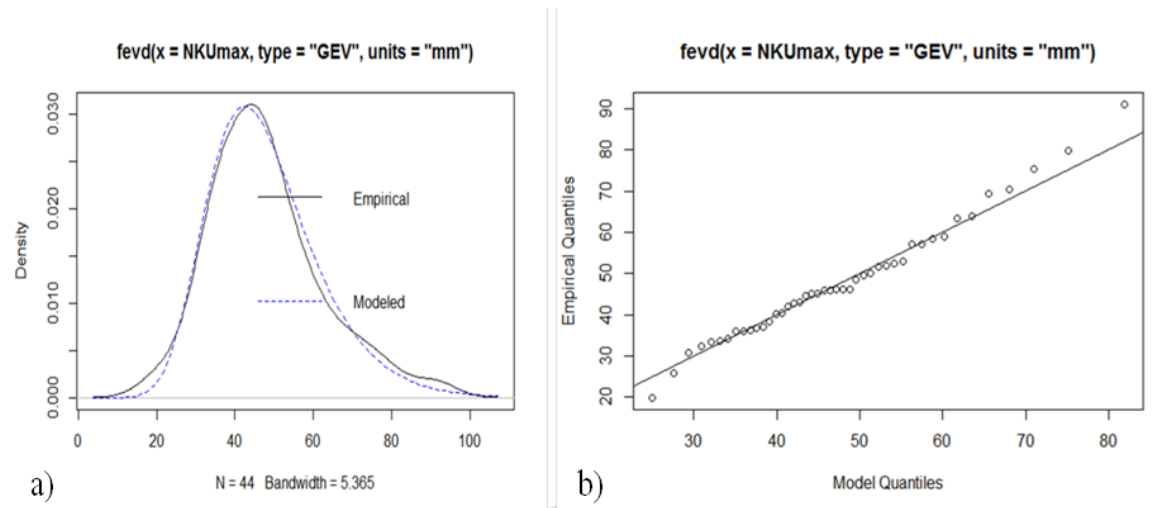
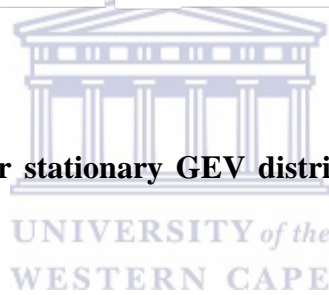


**Figure 6.5: Diagnostic plots for stationary GEV distributions for Nakuru;(a) the P-P plot; b) QQ plot**



### 6.4.3 Predicting return levels and return periods with the GEV models

Once a model for a given station was fitted, it was used to determine the return levels of extreme rainfall for given return periods using Equation (6.21). The models were also used to find the probability of occurrence of the extreme values (such as the 233 mm/day that occurred in Mombasa in 1997) by applying the same equations. Figure 6.6 shows the plots that were used to estimate the return levels for given return periods.

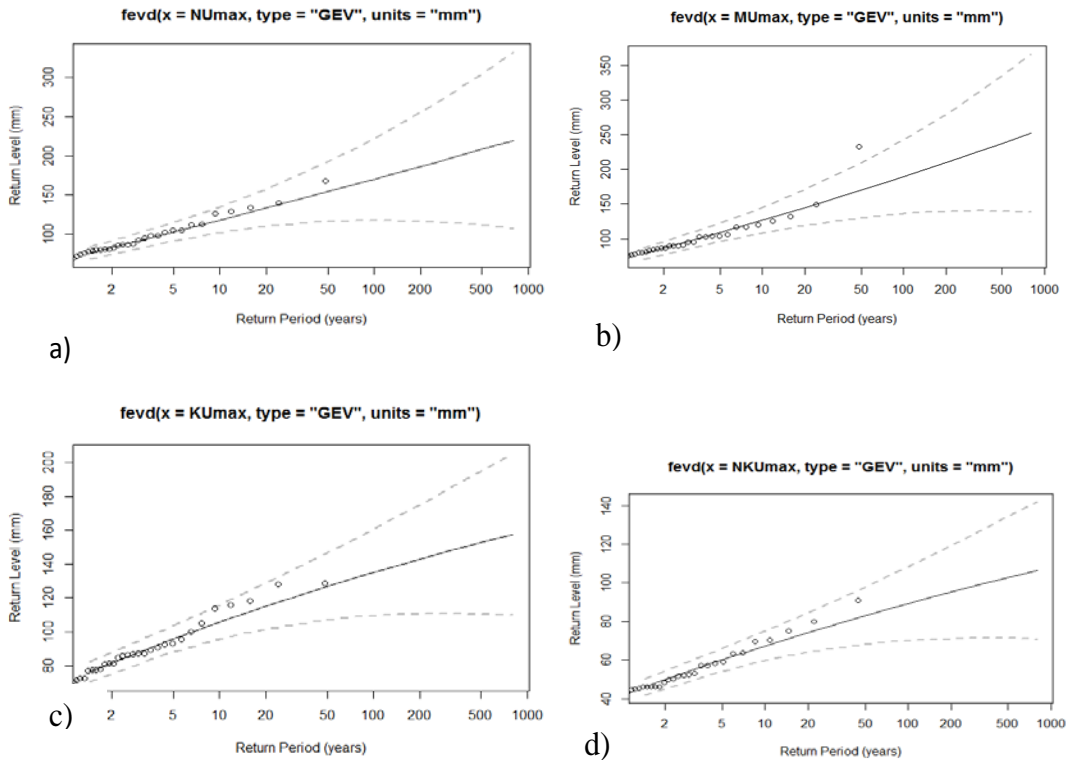


**Figure 6.6: Estimating return levels of each the four stations; a) Nairobi; b) Mombasa; c) Kisumu; d) Nakuru; in each plot the solid line estimates return levels for a given return period; the dashed lines give the upper and lower error bounds of the 95% confidence level estimated by the Normal method.**

The error region in each plot becomes broader as the return period increases. This implies that the estimation of the return levels becomes more uncertain at longer return periods. In Figure 6.6(b), the extreme value of 233mm recorded on 19<sup>th</sup> of October 1997 in Mombasa station lies outside the upper error bound meaning that the probability of occurrence of such an extreme is higher than 0.02 (i.e. the 50-year return period) and it actually lies within the error bounds of the 100-year return period (Table 6.7). The prediction line is only slightly curved in each of the four plots implying the goodness of fit of the Gumbel type of distribution ( $\xi \sim 0$ ) (Gilleland and Katz, 2011).

**Table 6.7: Return levels for some selected return periods for each of the four urban areas; the errors were estimated by the Normal method for the 95% level of confidence**

Return period (years)	Return level (mm)	lower bound (mm)	Upper bound (mm)	Return period (years)	Return level (mm)	lower bound (mm)	Upper bound (mm)
<b>Nairobi</b>				<b>Kisumu</b>			
2	75.8	68.1	83.4	2	76.5	70.7	82.2
10	116.5	100.7	132.4	10	105.0	95.2	114.9
20	132.5	109.2	155.9	20	114.8	101.6	128.1
50	153.7	115.9	191.4	50	126.7	107.1	146.2
100	169.9	117.7	221.8	100	135.0	109.6	160.5
200	186.0	126.7	255.4	200	142.9	110.7	175.1
<b>Mombasa</b>				<b>Nakuru</b>			
2	78.7	70.6	87.0	2	40.8	41.8	50.3
10	125.3	107.4	143.1	10	54.2	59.2	74.2
20	144.2	118.8	169.6	20	60.9	63.9	84.0
50	169.6	130.1	209.0	50	65.2	68.2	97.6
100	189.3	136.0	242.7	100	68.1	70.1	108.2
200	209.6	139.4	279.9	200	70.2	71.2	119.2

#### 6.4.4 Discussion

The results indicate that the GEV distribution has been able to adequately model the annual daily maxima rainfall series for each of the four stations. When the GEV was applied with covariates in the location ( $\mu$ ) and scale ( $\sigma$ ) parameters, only Kisumu's stationary model was slightly improved by an IOD covariate in the location parameter ( p-value =0.03). However, the predictions were done using the stationary model for each urban area including Kisumu. A similar study was done by Garcia-Aristizabal, et al. (2014) for Da-Es-Salaam (Tanzania) and indicated that a model with a linear trend in the location parameter only performed better than the stationary one when there was evidence of a trend. The model for each urban area

was estimated to be of the Gumbel type( $\xi \sim 0$ ). The stationary GEV distribution was found to be adequate in estimating return periods of up to 200 years but uncertainties would be less for the 100-year return periods (twice the length of data) as suggested in Gilleland et al, 2013). Most of the observed daily maximum values in each town have return periods of between 2 and 20 years, while return periods for the anomalously high values have return periods of 50-100 years.

There is a research gap in the extreme value analysis of rainfall in the EEA region. Fiddes, et al.(1974) produced a simple method of predicting the characteristics of storms for the design of hydrological structures in East Africa. However, the length of rainfall data used in that study was too short (less than 20 years) to be applicable in urban stormwater management systems. In my Thesis I have used fairly long series of maximum values of daily rainfall data (~50 years) and used the generalized extreme value analysis which does not confine the data to a particular distribution. The GEV model under non-stationary condition allowed for incorporation of climate covariates, while the rigorous method of model selection ensured that a more complex model was not chosen unnecessarily. Serinald and Kilsby, (2015) suggested that, modeling of hydro-meteorological data should start from the simplest informative approach, and that complex models produce more uncertainty when used in practical applications. Rainfall in Kenya is seasonal and highly variable, therefore the stationary GEV models should be applied while considering several factors which include that; 1) the occurrence of extreme rainfall is closely related to multi-temporal cycles that are forced by anomalies in the local and/or global climate modes of variabilities (Chapter 3). There is a possibility that any changes (either in the frequency of occurrence or intensity) in these multi-temporal modes of climate variability that affects seasonal rainfall are likely to affect the magnitude of extreme values. According to the IPCC (Stocker, 2013), the changing

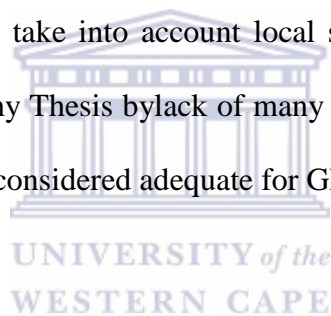


climate is likely to lead to changes in the behavior of the climate modes of variability and can result in unprecedented extreme events; In such a case, events that have been modeled to have long time return periods (i.e., have low probability of occurrence) can occur more frequently; 2) local and regional temperature were observed to influence rainfall changes in urban areas (Chapter 5) but have not been applied as climate covariates due lack of adequate length of daily temperature data for this study. Future studies should consider the influence of UHI and regional warming on the extreme value distribution of rainfall through incorporating local temperature data as covariates and comparing with the stationary models.

## 6.5 Summary

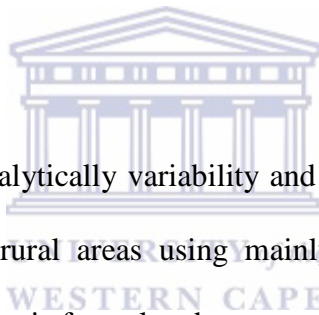
The aim of this Chapter was to establish if stationary extreme value distribution models are still applicable for estimating design storms in urban stormwater management systems in Kenya. GEV models were fitted to an annual maximum of daily rainfall series for each of the four major towns using rainfall from a station within each town that had complete and continuous daily data for close to 50 years. The stationary GEV model of the Gumbel type was found to adequately produce return levels for up to the 100 year return periods. This information is important in the development and upgrading of storm designs for effective stormwater management systems. However, in Kenya, there is almost no published work on extreme value analysis of rainfall although numerous cases of urban flooding are continuously being reported in major urban areas. Further, most cities in Kenya are in the process of creating stormwater criteria manuals in which technical information would be needed to provide the baseline knowledge for the development of the intensity- duration- frequency curves, that are used in development and upgrading of hydraulic and hydrologic structures. My Thesis, therefore, apart from providing the much needed knowledge of the

extreme value analysis of rainfall in Kenya, forms a basis upon which urban planners and engineers could get the technical information needed in developing storm water design criteria manuals. The outcome of this Chapter also forms a foundation upon which future studies of modeling of extremes in the urban areas of the EEA would be extended. Through the results of this Chapter, I have demonstrated that extreme value modeling is adequately done for each area, mainly due to the varied topography that produces spatial variability of rainfall. The parameters of the GEV models varied with the location and were highest in areas that receive high rainfall and lowest in drier areas. I, however, recommend that future work of modeling of extremes should consider the use of areal averages of the daily maximum values from a dense network of stations in each urban area instead of a representative station in order to take into account local spatial variations of rainfall. This undertaking was constrained in my Thesis by lack of many stations in one urban location that had long time series of daily data considered adequate for GEV modeling.



## 7 CHAPTERSEVEN: CONCLUSION

The aim of my Thesis was to comparatively analyse the variations of temperature and rainfall within the major urban areas of Kenya and their rural neighbourhoods in order to provide a basis upon which effective urban stormwater management can be done. To achieve this aim, five Chapters were formulated under which various climatological aspects of these two meteorological elements were analysed in order to answer the main research questions. Other atmospheric, oceanic and environmental variables needed were also sourced. The study was motivated by the need to expand the current knowledge on the variability and possible changes of these two climatic elements and their possible influence on the extreme value distribution used to prepare design storms, while considering rapid urbanization and global climate change.



The study therefore compared analytically variability and changes in temperature and rainfall in the urban and neighbouring rural areas using mainly exploratory and statistical data analysis methods in which hypothesis formulated were tested at the 5% level of significance. The thesis was organized in such a way that the first Chapter provided the background of the study, described the study area, and gave a general organization of the thesis, then: a) in Chapters 2 and 3, the long-term variations of temperature and rainfall respectively were investigated; b) in Chapter 4 existence of the urban heat islands (UHIs) using air and land surface temperature were investigated in two cities in Kenya (Nairobi and Mombasa); c) Chapter 5 addressed the effects of enhanced temperature and UHI from the previous Chapters, on rainfall at various time scales, and the implications to urban storm water management and; d) the last Chapter (6) addressed the issue of statistical modelling of the extreme rainfall series using the annual block maxima, and to establish the best statistical

models between the stationary and non-stationary that would be suitable to estimate design storms for urban stormwater management systems, in each of the four major towns.

Temperatures and rainfall from Meteorological stations within and in the neighbourhood of each town and with at least thirty (30) years of monthly (or daily) data were used for analysis. Other supporting data such as global atmospheric and oceanic indices and environmental remote sensed data such as land surface temperature (LST) were sourced from various website data banks as explained in Chapters where they were applied. Various methods of data analysis that were mainly exploratory and statistical were employed to diagnose the variations and detect changes in the temperature and rainfall, and also to examine the influence of other climatic factors on them. In particular and unique in this study was the use of the continuous wavelet transform (CWT) analysis method as a diagnostic tool to examine non-stationarity and variability of temperature and rainfall data. Different and rigorous parametric and non-parametric methods of change detection were applied to each data set in order to strengthen the statistical evidence (or lack) of change.

The main outcomes of the Thesis include that:

- a) There is warming due to urbanization as well as global warming in each of the four urban areas and their neighbourhoods, especially for the night-time temperatures. In particular, i) the rate of night-time warming is higher in urban than rural areas; more so in the last twenty years; ii) there is more evidence of day-time warming in rural areas than in urban areas, and temperature in rural areas that was fairly strongly correlated with the global warming; iii) the minimum temperature in urban areas is increasing in the lower and upper percentiles, while the maximum temperature is increasing in the upper percentiles (Chapter 2).

- b) Urban heat islands (UHIs) exist in the Kenya urban areas (Nairobi and Mombasa) both from the air and land surface temperatures. The UHI of the air temperature was found to have stronger intensities during the dry seasons (DJF and SON). Particularly; i) Nairobi is experiencing a diminishing day-time UHI intensity and increasing night-time UHI intensity relative to the stations in its outskirts to the west; the decreasing day-time UHI was attributed to effects of urban sprawl (UHI effect in sub-urban areas) and global warming which are enhancing the day-time temperature in rural more than in the urban areas. From the land surface temperature (LST) data, the day-time UHI is strongest within the CBD and the heavily built up areas particularly to the east of the CBD while at night, the UHI is mainly within the CBD; ii) the airport area of Mombasa coastal city had no significant day-time UHI intensity and a night-time cool island intensity from the surface air temperature relative to rural stations to the north-eastern side, close to the Indian Ocean. However, the intensity of the cool island had positive temporal trends partly associated with higher rate of increase of minimum temperatures within the town than over the rural areas. From LST, there were negative temperature differences between Mombasa Island town and the neighbouring land areas and positive differences between the town and the adjacent water bodies. At night-time, the surface UHI was observed within the Island and the heavily built up areas in the mainland (Chapter 4).
- c) In general rainfall totals at monthly, seasonal and annual time scales had no significant change over time with only a few exceptions where monthly and seasonal rainfall within and close to urban areas had increasing or decreasing temporal trends. The trends were attributed to the influence of changes in local and regional temperatures. High rainfall variability, especially during the OND season in which

anomalous rainfall values were observed in several years, were associated with inter-annual variability of the global atmospheric and oceanic parameters particularly when ENSO and IOD occurred simultaneously. Continuous wavelet transform (CWT) analysis revealed that local factors also enhance the global factors to produce the anomalously high seasonal rainfall (Chapter 3).

- d) There was statistical evidence that UHI and enhanced temperature within and close to urban areas have potentially influenced urban rainfall positively and negatively possibly through interactions of local thermal circulations (such as UHI) with the meso- and synoptic wind systems. The main observations in this regard were that; i) there was a general decline of rainfall during the JJA at the coast and an increase in Nairobi area downwind of the CBD that was associated with enhanced temperatures at the coast and over Nairobi; ii) the main rainfall seasons (MAM and OND) are minimally influenced by local temperature changes except in Nakuru within the Rift Valley where OND rainfall is significantly influenced by minimum temperature of regions to the east and west of the valley and; iii) rainfall in each season at the coast and Lake Victoria region is negatively associated with the maximum temperature of each region respectively while minimum temperatures of these regions are positively associated with rainfall over the central highlands and Rift Valley (Chapter 5).
- e) Stationary GEV models of annual maximum of daily rainfall series were found to apply in three of the four towns, except Kisumu whose model was only slightly improved by IOD covariate applied in the location parameter; it is worth noting that about 90% of annual daily maxima occurred within the MAM season which is least influenced by the IOD and/or ENSO. However, the highest daily totals with very low

probability of occurrence were recorded in OND season during the positive phases of ENSO and/or IOD. The stationary GEV distribution models were used to predict return levels for various return periods in each of the four urban areas. However, if the global oceanic and atmospheric modes of climate variability change either in frequency or intensity due to climate change, the probabilities of occurrence of high extreme events are also likely to change. Such changes are envisioned in climate change scenarios, and would affect the storm water management systems based on the probability of occurrence of extreme events from the GEV distribution (Chapter 6).

### **7.1 Significance of the outcomes**

Kenya is among the countries within the equatorial African region where there is limited literature on studies of variability and change of temperature (and especially urban heat islands (UHIs)), and rainfall at spatial scales relevant to stormwater management. Kenya has experienced rapid urbanization in the last five decades and the effects of urbanization (including UHI) and global temperature changes on rainfall intensity and distribution at small spatial scales have not been investigated. Rainfall in Kenya exhibits high spatial and temporal variability which poses a challenge to effective stormwater management and especially in urban areas where natural land cover have over time been replaced with impervious surfaces. Results from this study on temperature variability and change in major towns of Kenya have brought out a significant difference between the warming of the urban areas as compared to their rural surroundings; the study has shown that there is more warming in urban areas especially in the night-time (Chapter 2) due to UHI effect. Trends in rainfall characteristics were mainly found close the urban areas (Chapter 3). Such differences in rainfall that would influence the urban hydrology are usually masked in regional studies. The

factors influencing the variability of temperature and rainfall at different time scales were highlighted through the use of continuous wavelet transform (CWT) analysis. Such studies are not common in the EEA region though temperature and rainfall are highly variable and the factors influencing the variability are not well understood. The use of CWT analysis showed that although anomalous seasonal rainfall has been linked to changes in global oceanic and atmospheric systems, local factors are important during years of extreme rainfall events. In temperature time series, transient features were observed in the CWT mainly in urban stations. These high-frequency features enhance the annual temperature cycle resulting in warming. This study has therefore greatly contributed to the knowledge and has increased understanding of the variability and changes in temperature and rainfall in urban areas of Kenya and forms a strong foundation for further urban climate/hydrological studies. The extreme value distributions of extreme rainfall in Kenya have hardly been studied, although flooding in Nairobi and Mombasa have been occurring almost every year. In this study, four statistical models of extreme value distribution were developed using fairly long time series of the annual maximum of daily rainfall series for the four major towns in Kenya. This information is important to city planners, since most towns in Kenya are in the process of upgrading and developing new storm water drainage systems.

## **7.2 Implications of the findings to urban hydrology**

- a) Changes in temperature within and around urban areas, which have been shown to influence changes in rainfall at seasonal time scale, are likely to change the hydrology of the urban areas. For instance, Nairobi is likely to be wetter during the JJA season, and drier in MAM, while Mombasa is likely to be drier in JJA. However, JJA is not the main rainfall season and so such changes in wetness may not affect the design storms but is likely to change the hydrology of the affected areas. In Nakuru, OND and



annual rainfall have increasing trends that are likely to impact more on the hydrology of the town.

- b) Although rainfall of the main seasons (MAM and OND) had, in general, no significant temporal trends, multiple factors that simultaneously influence rainfall variabilities with resultant extreme events, are important in storm water management. Therefore local and or global changes that may influence changes in local and large-scale atmospheric and oceanic circulations (such as ENSO, IOD, monsoon winds, the pressure systems and UHIs) are likely to influence the occurrence of extreme events.
- c) Although the stationary GEV distribution was found to model adequately the extreme values from each urban area, the understanding of the inter-annual variability of the EEA rainfall is important for effective application of such models; therefore proper understanding and timely predictions (and projections) of the present and future behaviour of the modes of climate variability that causes anomalous rainfall is important in modelling urban storm water.

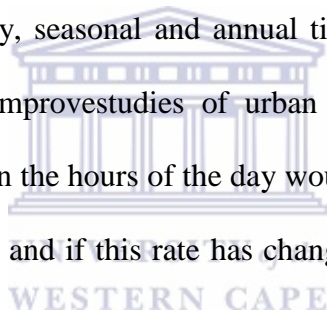
### **7.3 Recommendations**

The recommendations of my Thesis target mainly climate scientists, research institutions, urban hydrologists, urban planners and other users of urban climate information.

#### **7.3.1 Recommendations to climate scientists and research institutions**

My Thesis forms a basis under which further studies could be extended to include more urban areas within the EEA region. Rainfall and temperature are two important climate

variable that influences directly or indirectly storm water generation. The understanding of the variability and or changes of these two climatic elements and their inter-relationships, and taking into consideration the global climate change, is important for effective management of urban stormwater. Local news of damages of infrastructure and sometimes loss of human life caused by urban flooding has been associated with climate change without the benefit of a scientific enquiry. Studies should be carried out to cover wider areas so as put this notion into perspective, and so that other factors that cause urban flooding (e.g., environmental, geographical or geological) can also be explored. One of the challenges that I encountered is the limited access to climate data, especially at daily and sub-daily time-scales. Although the monthly data that meteorological services provide for research are adequate to investigate variabilities of rainfall at monthly, seasonal and annual time scales, datasets at sub-diurnal time-scales (in mm/hr) would improve studies of urban hydrology. Investigations of the distribution of daily rainfall within the hours of the day would provide information of the rate at which stormwater is generated and if this rate has changed over time, especially in urban areas with strong UHIs.



There are very few studies that have documented the existence of UHI in EEA cities. There is a need to increase such studies and further investigations of the factors influencing UHI development to be established. UHI has been shown to influence local storm intensities in other parts of the world but no such studies are available over the EEA region.

In most climate studies in EEA, local and regional air surface temperatures have not been considered as factors influencing rainfall variability. I have established (Chapter 5) local and regional statistical relationships between rainfall and temperature that should be considered in

seasonal rainfall predictions. Further studies should, however, be carried out such that wider areas and longer time series of temperature are used, and more deterministic (together with statistical) methods applied. I recommend that dynamical simulation studies be carried out to document the physical and dynamical process responsible for the observed statistical relationships. Also, further investigations possibly using dynamical simulations should be carried out to establish the influence of enhanced local and regional temperature changes on local and regional convective storm intensities at diurnal time scales. Changes in storm intensities (in mm/hr) are critical for preparation of design storms and the intensity-duration-frequency curves.

I strongly recommend the use of the wavelet analysis in studies of variability and change of climatic and hydrological variables. In Chapter 2&3 of my Thesis, I demonstrated that CWT is a strong diagnostic tool in the investigations of variabilities and changes of a meteorological time series. I found CWT to be very useful in discriminating multi-temporal cycles of a time series and give insights of how such cycles influence the meteorological variable over time. Further, spatial differences of a given variable could be observed by comparing the multi-temporal cycles among different locations. I recommend this method be used more often in climate studies and especially where spatial averages of the climatic elements into homogeneous groups would lessen the burden of too many wavelet power spectra maps; this would enable easier comparison of temporal and spatial variations of the climatic elements within and across climatic zones.

Studies on extreme value analysis of climate data in EEA are rare. In my Thesis, I have for the first time, using stationary and non-stationary generalized extreme value analysis

developed models that can be adequately applied to create design storms applicable in urban stormwater management systems in four Kenyan towns (Chapter 6). However, since each model is dependent on the rainfall climatology of a given location, this very important scientific modeling should be extended to other towns within the EEA region.

### **7.3.2 Recommendations to urban environmentalist and hydrologists**

In the Thesis, I did not investigate the hydrological response of the urban areas to rainfall or temperature variability and has not also considered other environmental factors that would influence storm water generation and urban flooding. I recommend that further research that combines the climatic with hydrological factors be undertaken for effective stormwater management.



### **7.3.3 Recommendations to urban planners**

City and municipal councils should consider the outcomes of this study (Chapter 6) to revise the design storms taking into considerations that, the occurrence of extreme values in the EEA region is very much linked to the various modes of climate variability that influence seasonal rainfall and cause the extreme rainfall events. I therefore, recommend that the revision of the design storms should be done in close consultations with climate scientist so as to incorporate safe limits from the future projections of the extreme values in climate change models.

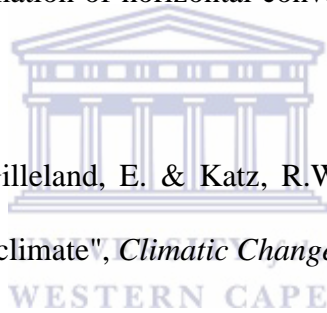
## 8 References

- Adamowski, J., Adamowski, K. & Prokoph, A. 2013, "Quantifying the spatial-temporal variability of annual streamflow and meteorological changes in eastern Ontario and southwestern Quebec using wavelet analysis and GIS", *Journal of Hydrology*, vol. 499, pp. 27-40.
- Adamowski, J., Adamowski, K. & Prokoph, A. 2013, "A Spectral Analysis Based Methodology to Detect Climatological Influences on Daily Urban Water Demand", *Mathematical Geosciences*, vol. 45, no. 1, pp. 49-68.
- Ahmed, A.Q., Ossen, D.R., Jamei, E., Manaf, N.A., Said, I. & Ahmad, M.H. 2014, "Urban surface temperature behaviour and heat island effect in a tropical planned city", *Theoretical and Applied Climatology*, , pp. 1-22.
- AlSarmi, S.H. & Washington, R. 2014, "Changes in climate extremes in the Arabian Peninsula: analysis of daily data", *International Journal of Climatology*, vol. 34, no. 5, pp. 1329-1345.
- Anghileri, D., Pianosi, F. & Soncini-Sessa, R. 2014, "Trend detection in seasonal data: from hydrology to water resources", *Journal of Hydrology*, vol. 511, pp. 171-179.
- Anyah, R.O. & Qiu, W. 2012, "Characteristic 20th and 21st century precipitation and temperature patterns and changes over the Greater Horn of Africa", *International Journal of Climatology*, vol. 32, no. 3, pp. 347-363.
- Arnfield, A.J. 2003, "Two decades of urban climate research: a review of turbulence, exchanges of energy and water, and the urban heat island", *International Journal of Climatology*, vol. 23, no. 1, pp. 1-26.

- Asnani, G. & Asnani, G. 1993, *Tropical meteorology*, GC Asnani Pune, India.
- Baik, J., Kim, Y. & Chun, H. 2001, "Dry and moist convection forced by an urban heat island", *Journal of Applied Meteorology*, vol. 40, no. 8, pp. 1462-1475.
- Barlow, J.F. 2014, "Progress in observing and modelling the urban boundary layer", *Urban Climate*, vol. 10, pp. 216-240.
- Bassett Jr, G. & Koenker, R. 1978, "Asymptotic theory of least absolute error regression", *Journal of the American Statistical Association*, vol. 73, no. 363, pp. 618-622.
- Beguiría, S., Angulo-Martínez, M., Vicente-Serrano, S.M., López-Moreno, J.I. & El-Kenawy, A. 2011, "Assessing trends in extreme precipitation events intensity and magnitude using non-stationary peaks-over-threshold analysis: a case study in northeast Spain from 1930 to 2006", *International Journal of Climatology*, vol. 31, no. 14, pp. 2102-2114.
- Biazeto, B. & Silva Dias, M.A. 2012, "Analysis of the impact of rainfall assimilation during LBA atmospheric mesoscale missions in Southwest Amazon", *Atmospheric Research*, vol. 107, pp. 126-144.
- Biggs, E.M. & Atkinson, P.M. 2011, "A characterisation of climate variability and trends in hydrological extremes in the Severn Uplands", *International Journal of Climatology*, vol. 31, no. 11, pp. 1634-1652.
- Black, E., Slingo, J. & Sperber, K.R. 2003, "An observational study of the relationship between excessively strong short rains in coastal East Africa and Indian Ocean SST", *Monthly Weather Review*, vol. 131, no. 1, pp. 74-94.

- Blain, G.C. 2011, "Incorporating climate trends in the stochastic modeling of extreme minimum air temperature series of Campinas, state of São Paulo, Brazil", *Bragantia*, vol. 70, no. 4, pp. 952-957.
- Blain, G.C. 2011, "Modeling extreme minimum air temperature series under climate change conditions", *Ciência Rural*, vol. 41, no. 11, pp. 1877-1883.
- Bornstein, R. & Lin, Q. 2000, "Urban heat islands and summertime convective thunderstorms in Atlanta: three case studies", *Atmospheric Environment*, vol. 34, no. 3, pp. 507-516.
- Braganza, K., Karoly, D.J. & Arblaster, J. 2004, "Diurnal temperature range as an index of global climate change during the twentieth century", *Geophysical Research Letters*, vol. 31, no. 13.
- Burian, S.J., Walsh, T., Kalyanapu, A.J. & Larsen, S.G. 2013, "5.06 - Climate Vulnerabilities and Adaptation of Urban Water Infrastructure Systems" in *Climate Vulnerability*, ed. R.A. Pielke, Academic Press, Oxford, pp. 87-107.
- Camberlin, P. & Philippon, N. 2002, "The East African March-May rainy season: Associated atmospheric dynamics and predictability over the 1968-97 period", *Journal of Climate*, vol. 15, no. 9, pp. 1002-1019.
- Camberlin, P., Moron, V., Okoola, R., Philippon, N. & Gitau, W. 2009, "Components of rainy seasons' variability in Equatorial East Africa: onset, cessation, rainfall frequency and intensity", *Theoretical and applied climatology*, vol. 98, no. 3-4, pp. 237-249.
- Camilloni, I. & Barros, V. 1997, "On the urban heat island effect dependence on temperature trends", *Climatic Change*, vol. 37, no. 4, pp. 665-681.

- Cannon, A.J. 2010, "A flexible nonlinear modelling framework for nonstationary generalized extreme value analysis in hydroclimatology", *Hydrological Processes*, vol. 24, no. 6, pp. 673-685.
- Changnon, S.A., Huff, F., Schickedanz, P. & Vogel, J.L. 1977, "Summary of METROMEX, Volume 1: Weather anomalies and impacts", .
- Chen, X., Zhao, H., Li, P. & Yin, Z. 2006, "Remote sensing image-based analysis of the relationship between urban heat island and land use/cover changes", *Remote Sensing of Environment*, vol. 104, no. 2, pp. 133-146.
- Chen, F. & Miao, S. 2008, "Formation of horizontal convective rolls in urban area", *Atmos*, vol. 89, pp. 298-304.
- Cheng, L., AghaKouchak, A., Gilleland, E. & Katz, R.W. 2014, "Non-stationary extreme value analysis in a changing climate", *Climatic Change*, vol. 127, no. 2, pp. 353-369.
- Cheval, S. & Dumitrescu, A. 2015, "The summer surface urban heat island of Bucharest (Romania) retrieved from MODIS images", *Theoretical and Applied Climatology*, vol. 121, no. 3-4, pp. 631-640.
- Christy, J.R., Norris, W.B. & McNider, R.T. 2009, "Surface temperature variations in East Africa and possible causes", *Journal of Climate*, vol. 22, no. 12, pp. 3342-3356.
- Clark, C.O., Webster, P.J. & Cole, J.E. 2003, "Inter-decadal variability of the relationship between the Indian Ocean zonal mode and East African coastal rainfall anomalies", *Journal of Climate*, vol. 16, no. 3, pp. 548-554.





- Coseo, P. & Larsen, L. 2014, "How factors of land use/land cover, building configuration, and adjacent heat sources and sinks explain Urban Heat Islands in Chicago", *Landscape and Urban Planning*, vol. 125, pp. 117-129.
- Coles, S., Bawa, J., Trenner, L. & Dorazio, P. 2001, "An introduction to statistical modeling of extreme values", Springer.
- Collins, J.M. 2011, "Temperature variability over Africa", *Journal of Climate*, vol. 24, no. 14, pp. 3649-3666.
- Costa, A.C. & Soares, A. 2009, "Trends in extreme precipitation indices derived from a daily rainfall database for the South of Portugal", *International Journal of Climatology*, vol. 29, no. 13, pp. 1956-1975.
- Dash, P., Göttsche, F., Olesen, F. & Fischer, H. 2002, "Land surface temperature and emissivity estimation from passive sensor data: theory and practice-current trends", *International Journal of Remote Sensing*, vol. 23, no. 13, pp. 2563-2594.
- Davies, T., Vincent, C. & Beresford, A. 1985, "July-August rainfall in West-Central Kenya", *Journal of climatology*, vol. 5, no. 1, pp. 17-33.
- Davis, R.E. 1976, "Predictability of sea surface temperature and sea level pressure anomalies over the North Pacific Ocean", *Journal of Physical Oceanography*, vol. 6, no. 3, pp. 249-266.
- Deser, C., Phillips, A.S. & Alexander, M.A. 2010, "Twentieth century tropical sea surface temperature trends revisited", *Geophysical Research Letters*, vol. 37, no. 10.

Deogun, I. Q., Rodrigues, L., & Guzman, G. (2013). Learning From the Swahili Architecture in Mombasa/Kenya. Paper presented at the Sustainable Architecture for a Renewable Future, Munich

Diaz, H.F. & Markgraf, V. 2000, *El Niño and the Southern Oscillation: multiscale variability and global and regional impacts*, Cambridge University Press.

Dixon, P.G. & Mote, T.L. 2003, "Patterns and causes of Atlanta's urban heat island-initiated precipitation", *Journal of Applied Meteorology*, vol. 42, no. 9, pp. 1273-1284.

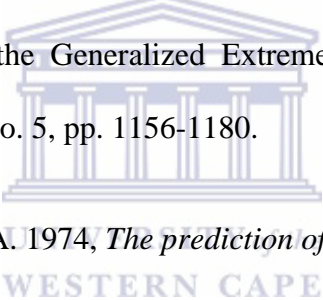
Donat, M., Peterson, T., Brunet, M., King, A., Almazroui, M., Kolli, R., Boucherf, D., Al-Mulla, A.Y., Nour, A.Y. & Aly, A.A. 2014, "Changes in extreme temperature and precipitation in the Arab region: long-term trends and variability related to ENSO and NAO", *International Journal of Climatology*, vol. 34, no. 3, pp. 581-592.

Efe, S. & Eyefia, A. 2014, "Urban Effects on the Precipitation of Benin, Nigeria", *American Journal of Climate Change*, vol. 2014.

Efstratiadis, A., Koussis, A., Koutsoyiannis, D. & Mamassis, N. 2013, "Flood design recipes vs. reality: can predictions for ungauged basins be trusted?", *Natural Hazards and Earth System Sciences Discussions*, vol. 1, no. 6, pp. 7387-7416.

Elagib, N.A. 2011, "Evolution of urban heat island in Khartoum", *International Journal of Climatology*, vol. 31, no. 9, pp. 1377-1388.

Eltahir, E.A. & Pal, J.S. 1996, "Relationship between surface conditions and subsequent rainfall in convective storms", *Journal of Geophysical Research: Atmospheres (1984–2012)*, vol. 101, no. D21, pp. 26237-26245.

- Emmanuel, R. & Johansson, E. 2006, "Influence of urban morphology and sea breeze on hot humid microclimate: the case of Colombo, Sri Lanka", *Climate research*, vol. 30, no. 3, pp. 189-200.
- Emmanuel, I., Andrieu, H., Leblois, E. & Flahaut, B. 2012, "Temporal and spatial variability of rainfall at the urban hydrological scale", *Journal of Hydrology*, vol. 430, pp. 162-172.
- Faranda, D., Lucarini, V., Turchetti, G. & Vaienti, S. 2012, "Generalized extreme value distribution parameters as dynamical indicators of stability", *International Journal of Bifurcation and Chaos*, vol. 22, no. 11.
- Faranda, D., Lucarini, V., Turchetti, G. & Vaienti, S. 2011, "Numerical convergence of the block-maxima approach to the Generalized Extreme Value distribution", *Journal of statistical physics*, vol. 145, no. 5, pp. 1156-1180.
- Fiddes, D., Forsgate, J. & Grigg, A. 1974, *The prediction of storm rainfall in East Africa*, .  

- Fisher, R.A. & Tippett, L.H.C. 1928, "Limiting forms of the frequency distribution of the largest or smallest member of a sample", *Mathematical Proceedings of the Cambridge Philosophical Society* Cambridge Univ Press, , pp. 180.
- Freitas, E.D., Rozoff, C.M., Cotton, W.R. & Dias, P.L.S. 2007, "Interactions of an urban heat island and sea-breeze circulations during winter over the metropolitan area of São Paulo, Brazil", *Boundary-Layer Meteorology*, vol. 122, no. 1, pp. 43-65.
- Fujibe, F. 2003, "Long-term surface wind changes in the Tokyo metropolitan area in the afternoon of sunny days in the warm season", *Journal of the Meteorological Society of Japan*, vol. 81, no. 1, pp. 141-149.

- Garcia-Aristizabal, A., Bucchignani, E., Palazzi, E., D'Onofrio, D., Gasparini, P. & Marzocchi, W. 2015, "Analysis of non-stationary climate-related extreme events considering climate change scenarios: an application for multi-hazard assessment in the Dar es Salaam region, Tanzania", *Natural Hazards*, vol. 75, no. 1, pp. 289-320.
- Giannini, A., Chiang, J.C., Cane, M.A., Kushnir, Y. & Seager, R. 2001, "The ENSO teleconnection to the tropical Atlantic Ocean: contributions of the remote and local SSTs to rainfall variability in the tropical Americas\*", *Journal of Climate*, vol. 14, no. 24, pp. 4530-4544.
- Giannaros, T.M. & Melas, D. 2012, "Study of the urban heat island in a coastal Mediterranean City: the case study of Thessaloniki, Greece", *Atmospheric Research*, vol. 118, pp. 103-120.
- Gilleland, E. & Katz, R.W. 2006, "Analyzing seasonal to interannual extreme weather and climate variability with the extremes toolkit", *18th Conference on Climate Variability and Change, 86th American Meteorological Society (AMS) Annual Meeting*.
- Gilleland, E., Ribatet, M. & Stephenson, A.G. 2013, "A software review for extreme value analysis", *Extremes*, vol. 16, no. 1, pp. 103-119.
- Gilleland, E. & Katz, R.W. 2014, "Extremes 2.0: an extreme value analysis package in r", *submitted to journal of statistical software*, .
- Gitau, W., Camberlin, P., Ogallo, L. & Okoola, R. 2015, "Oceanic and atmospheric linkages with short rainfall season intraseasonal statistics over Equatorial Eastern Africa and their predictive potential", *International Journal of Climatology*, vol. 35, no. 9, pp. 2382-2399.

Githui, F.W., 2008. "Assessing the impacts of environmental change on the hydrology of the Nzoia catchment, in the Lake Victoria Basin". PhD Thesis, Department of Hydrology and Hydraulic Engineering, Vrije Universiteit Brussel, Belgium.

Gocic, M. & Trajkovic, S. 2013, "Analysis of changes in meteorological variables using Mann-Kendall and Sen's slope estimator statistical tests in Serbia", *Global and Planetary Change*, vol. 100, pp. 172-182.

Grimmond, S. 2007, "Urbanization and global environmental change: local effects of urban warming", *The Geographical Journal*, vol. 173, no. 1, pp. 83-88.

Gross, G. 2014, "On the Parametrization of urban land use in mesoscale models", *Boundary-Layer Meteorology*, vol. 150, no. 2, pp. 319-326.

Habitat, U. 2008, "The state of African cities: A framework for addressing urban challenges in Africa 2008", *Nairobi, Kenya: United Nations Human Settlements Programme*, .

Han, W.S., Burian, S.J. & Shepherd, J.M. 2011, "Assessment of satellite-based rainfall estimates in urban areas in different geographic and climatic regions", *Natural Hazards*, vol. 56, no. 3, pp. 733-747.

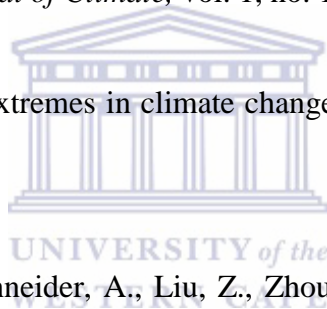
Hansen, J., Ruedy, R., Sato, M. & Lo, K. 2010, "Global surface temperature change", *Reviews of Geophysics*, vol. 48, no. 4.

Hart, M.A. & Sailor, D.J. 2009, "Quantifying the influence of land-use and surface characteristics on spatial variability in the urban heat island", *Theoretical and Applied Climatology*, vol. 95, no. 3-4, pp. 397-406.

- Hastenrath, S., Polzin, D. & Greischar, L. 2002, "Annual cycle of equatorial zonal circulations from the ECMWF reanalysis.", *气象集誌* 第2 輯, vol. 80, no. 4, pp. 755-766.
- Hastenrath, S. 2003, "TROPICAL METEOROLOGY | Tropical Climates" in *Encyclopedia of Atmospheric Sciences*, ed. J.R. Holton, Academic Press, Oxford, pp. 2338-2345.
- Hastenrath, S., Polzin, D. & Mutai, C. 2010, "Diagnosing the droughts and floods in equatorial East Africa during boreal autumn 2005-08", *Journal of Climate*, vol. 23, no. 3, pp. 813-817.
- Helsel, D.R., Mueller, D.K. & Slack, J.R. 2006, *Computer program for the Kendall family of trend tests*, US Department of the Interior, US Geological Survey Reston.
- Helsel, D.R. & Frans, L.M. 2006, "Regional Kendall test for trend", *Environmental science & technology*, vol. 40, no. 13, pp. 4066-4073.
- Hidalgo, J., Masson, V. & Gimeno, L. 2010, "Scaling the daytime urban heat island and urban-breeze circulation", *Journal of Applied Meteorology and Climatology*, vol. 49, no. 5, pp. 889-901.
- Huff, F. & Changnon Jr, S. 1972, "Climatological assessment of urban effects on precipitation at St. Louis", *Journal of Applied Meteorology*, vol. 11, no. 5, pp. 823-842.
- Huff, F. & Changnon Jr, S. 1973, "Precipitation modification by major urban areas", *Bulletin of the American Meteorological Society*, vol. 54, no. 12, pp. 1220-1232.

- Inamura, T., Izumi, T. & Matsuyama, H. 2011, "Diagnostic study of the effects of a large city on heavy rainfall as revealed by an ensemble simulation: A case study of central Tokyo, Japan", *Journal of Applied Meteorology and Climatology*, vol. 50, no. 3, pp. 713-728.
- Indeje, M. & Semazzi, F. 2000, "Relationships between QBO in the lower equatorial stratospheric zonal winds and East African seasonal rainfall", *Meteorology and Atmospheric Physics*, vol. 73, no. 3-4, pp. 227-244.
- Indeje, M., Semazzi, F.H. & Ogallo, L.J. 2000, "ENSO signals in East African rainfall seasons", *International Journal of Climatology*, vol. 20, no. 1, pp. 19-46.
- Jacobson, C.R. 2011, "Identification and quantification of the hydrological impacts of imperviousness in urban catchments: A review", *Journal of environmental management*, vol. 92, no. 6, pp. 1438-1448.
- Muthoka J,& Mundia, C. 2014, "Dynamism of land use changes on surface temperature in Kenya: a case study of Nairobi City", *International Journal of Science and Research*, vol. 3, no. 4, pp. 38-41.
- Jauregui, E. 1997, "Heat island development in Mexico City", *Atmospheric Environment*, vol. 31, no. 22, pp. 3821-3831.
- Jauregui, E. & Romales, E. 1996, "Urban effects on convective precipitation in Mexico City", *Atmospheric Environment*, vol. 30, no. 20, pp. 3383-3389.
- Jhajharia, D., Yadav, B.K., Maske, S., Chattopadhyay, S. & Kar, A.K. 2012, "Identification of trends in rainfall, rainy days and 24 h maximum rainfall over subtropical Assam in Northeast India", *Comptes Rendus Geoscience*, vol. 344, no. 1, pp. 1-13.

- Jhajharia, D. & Singh, V.P. 2011, "Trends in temperature, diurnal temperature range and sunshine duration in Northeast India", *International Journal of Climatology*, vol. 31, no. 9, pp. 1353-1367.
- Jung, I., Bae, D. & Kim, G. 2011, "Recent trends of mean and extreme precipitation in Korea", *International Journal of Climatology*, vol. 31, no. 3, pp. 359-370.
- Jury, M.R. & Funk, C. 2013, "Climatic trends over Ethiopia: regional signals and drivers", *International Journal of Climatology*, vol. 33, no. 8, pp. 1924-1935.
- Karl, T.R., Diaz, H.F. & Kukla, G. 1988, "Urbanization: Its detection and effect in the United States climate record", *Journal of Climate*, vol. 1, no. 11, pp. 1099-1123.
- Katz, R.W. 2010, "Statistics of extremes in climate change", *Climatic Change*, vol. 100, no. 1, pp. 71-76.
- Kaufmann, R.K., Seto, K.C., Schneider, A., Liu, Z., Zhou, L. & Wang, W. 2007, "Climate response to rapid urban growth: evidence of a human-induced precipitation deficit", *Journal of Climate*, vol. 20, no. 10, pp. 2299-2306.
- Keeler, J.M. & Kristovich, D.A. 2012, "Observations of urban heat island influence on lake-breeze frontal movement", *Journal of Applied Meteorology and Climatology*, vol. 51, no. 4, pp. 702-710.
- Kharin, V.V., Zwiers, F., Zhang, X. & Wehner, M. 2013, "Changes in temperature and precipitation extremes in the CMIP5 ensemble", *Climatic Change*, vol. 119, no. 2, pp. 345-357.





- Kim, Y. & Baik, J. 2002, "Maximum urban heat island intensity in Seoul", *Journal of Applied Meteorology*, vol. 41, no. 6, pp. 651-659.
- King'uyu, S., Ogallo, L. & Anyamba, E. 2000, "Recent trends of minimum and maximum surface temperatures over Eastern Africa", *Journal of Climate*, vol. 13, no. 16, pp. 2876-2886.
- Kishtawal, C.M., Niyogi, D., Tewari, M., Pielke, R.A. & Shepherd, J.M. 2010, "Urbanization signature in the observed heavy rainfall climatology over India", *International Journal of Climatology*, vol. 30, no. 13, pp. 1908-1916.
- Kizza, M., Rodhe, A., Xu, C., Ntale, H.K. & Halldin, S. 2009, "Temporal rainfall variability in the Lake Victoria Basin in East Africa during the twentieth century", *Theoretical and applied climatology*, vol. 98, no. 1-2, pp. 119-135.
- Klein Tank, A. & Können, G. 2003, "Trends in indices of daily temperature and precipitation extremes in Europe, 1946-99", *Journal of Climate*, vol. 16, no. 22, pp. 3665-3680.
- Kloog, I., Chudnovsky, A., Koutrakis, P. & Schwartz, J. 2012, "Temporal and spatial assessments of minimum air temperature using satellite surface temperature measurements in Massachusetts, USA", *Science of the total environment*, vol. 432, pp. 85-92.
- Koenker, R. & Bassett Jr, G. 1978, "Regression quantiles", *Econometrica: journal of the Econometric Society*, , pp. 33-50.
- Koenker, R. 2006, "Quantile regression", *Encyclopedia of Environmetrics*, .

- Korecha, D. & Barnston, A.G. 2007, "Predictability of June–September Rainfall in Ethiopia.", *Monthly Weather Review*, vol. 135, no. 2.
- Kruger, A. & Sekele, S. 2013, "Trends in extreme temperature indices in South Africa: 1962–2009", *International Journal of Climatology*, vol. 33, no. 3, pp. 661-676.
- Kruger, A. & Shongwe, S. 2004, "Temperature trends in South Africa: 1960–2003", *International Journal of Climatology*, vol. 24, no. 15, pp. 1929-1945.
- Kumar, P. & Foufoula-Georgiou, E. 1997, "Wavelet analysis for geophysical applications", *Reviews of Geophysics*, vol. 35, no. 4, pp. 385-412.
- Labat, D. 2005, "Recent advances in wavelet analyses: Part 1. A review of concepts", *Journal of Hydrology*, vol. 314, no. 1, pp. 275-288.
- Lamprey, B. 2010, "An analytical framework for estimating the urban effect on climate", *International Journal of Climatology*, vol. 30, no. 1, pp. 72-88.
- Lin, C., Chen, W., Chang, P. & Sheng, Y. 2011, "Impact of the urban heat island effect on precipitation over a complex geographic environment in northern Taiwan", *Journal of Applied Meteorology and Climatology*, vol. 50, no. 2, pp. 339-353.
- Liu, Y., Hao, Y., Fan, Y., Wang, T., Huo, X., Liu, Y. & Yeh, T.J. 2013, "A nonstationary extreme value distribution for analyzing the cessation of karst spring discharge", *Hydrological Processes*, .
- Liu, Y., Weaver, C.P. & Avissar, R. 1999, "Toward a parameterization of mesoscale fluxes and moist convection induced by landscape heterogeneity", *Journal of Geophysical Research: Atmospheres (1984–2012)*, vol. 104, no. D16, pp. 19515-19533.

- Li, J., Wang, X., Wang, X., Ma, W. & Zhang, H. 2009, "Remote sensing evaluation of urban heat island and its spatial pattern of the Shanghai metropolitan area, China", *Ecological Complexity*, vol. 6, no. 4, pp. 413-420.
- Liu, Y., San Liang, X. & Weisberg, R.H. 2007, "Rectification of the bias in the wavelet power spectrum", *Journal of Atmospheric and Oceanic Technology*, vol. 24, no. 12, pp. 2093-2102.
- Lyon, B. & DeWitt, D.G. 2012, "A recent and abrupt decline in the East African long rains", *Geophysical Research Letters*, vol. 39, no. 2.
- Mailhot, A. & Duchesne, S. 2009, "Design criteria of urban drainage infrastructures under climate change", *Journal of Water Resources Planning and Management*, vol. 136, no. 2, pp. 201-208.
- Makokha, G.L. & Shisanya, C.A. 2010, "Trends in mean annual minimum and maximum near surface temperature in Nairobi City, Kenya", *Advances in Meteorology*, vol. 2010.
- Marchant, R., Mumbi, C., Behera, S. & Yamagata, T. 2007, "The Indian Ocean dipole—the unsung driver of climatic variability in East Africa", *African Journal of Ecology*, vol. 45, no. 1, pp. 4-16.
- Marengo, J.A., Valverde, M.C. & Obregon, G.O. 2013, "Observed and projected changes in rainfall extremes in the Metropolitan Area of Sao Paulo", *Climate research*, vol. 57, no. 1, pp. 61-72.
- Marshall Shepherd, J., Pierce, H. & Negri, A.J. 2002, "Rainfall modification by major urban areas: Observations from space borne rain radar on the TRMM satellite.", *Journal of Applied Meteorology*, vol. 41, no. 7.

- Mazvimavi, D. 2010, "Investigating changes over time of annual rainfall in Zimbabwe", *Hydrology and Earth System Sciences*, vol. 14, no. 12, pp. 2671-2679.
- McCarthy, M.P., Best, M.J. & Betts, R.A. 2010, "Climate change in cities due to global warming and urban effects", *Geophysical Research Letters*, vol. 37, no. 9.
- McGree, S., Whan, K., Jones, D., Alexander, L., Imielska, A., Diamond, H., Ene, E., Finaulahi, S., Inape, K. & Jacklick, L. 2013, "An updated assessment of trends and variability in total and extreme rainfall in the western Pacific", *International Journal of Climatology*.
- Milly, P., Julio, B., Malin, F., Robert, M., Zbigniew, W., Dennis, P. & Ronald, J. 2007, "Stationarity is dead", *Ground Water News & Views*, vol. 4, no. 1, pp. 6-8.
- Mironga, J. 2005, "Effect of farming practices on wetlands of Kisii District, Kenya", *Applied Ecology and Environmental Research*, vol. 3, no. 2, pp. 81-91.
- Mölders, N. & Olson, M.A. 2004, "Impact of urban effects on precipitation in high latitudes", *Journal of Hydrometeorology*, vol. 5, no. 3, pp. 409-429.
- Mondal, A. & Mujumdar, P. 2015, "Modeling non-stationarity in intensity, duration and frequency of extreme rainfall over India", *Journal of Hydrology*, vol. 521, pp. 217-231.
- Morlet, J., Arens, G., Fourgeau, E. & Glard, D. 1982, "Wave propagation and sampling theory-Part I: Complex signal and scattering in multilayered media", *Geophysics*, vol. 47, no. 2, pp. 203-221.
- Mukabana, J.R. & Pielke, R.A. 1996, "Investigating the influence of synoptic-scale monsoonal winds and mesoscale circulations on diurnal weather patterns over Kenya

using a mesoscale numerical model", *Monthly Weather Review*, vol. 124, no. 2, pp. 224-244.

Mundia, C. & Aniya, M. 2006, "Dynamics of landuse/cover changes and degradation of Nairobi City, Kenya", *Land Degradation & Development*, vol. 17, no. 1, pp. 97-108.

Murphy, D.J., Hall, M.H., Hall, C.A., Heisler, G.M., Stehman, S.V. & Anselmi-Molina, C. 2011, "The relationship between land cover and the urban heat island in northeastern Puerto Rico", *International Journal of Climatology*, vol. 31, no. 8, pp. 1222-1239.

Murphy, K.W. & Ellis, A.W. 2014, "An assessment of the stationarity of climate and stream flow in watersheds of the Colorado River Basin", *Journal of Hydrology*, vol. 509, no. 0, pp. 454-473.

Mutai, C.C. & Ward, M.N. 2000, "East African rainfall and the tropical circulation/convection on intraseasonal to interannual timescales", *Journal of Climate*, vol. 13, no. 22, pp. 3915-3939.

Nakajima, J., Kuniyama, T., Omori, Y. & Frühwirth-Schnatter, S. 2012, "Generalized extreme value distribution with time-dependence using the AR and MA models in state space form", *Computational Statistics & Data Analysis*, vol. 56, no. 11, pp. 3241-3259.

Nakken, M. 1999, "Wavelet analysis of rainfall-runoff variability isolating climatic from anthropogenic patterns", *Environmental Modelling & Software*, vol. 14, no. 4, pp. 283-295.

New, M., Hewitson, B., Stephenson, D.B., Tsiga, A., Kruger, A., Manhique, A., Gomez, B., Coelho, C.A., Masisi, D.N. & Kululanga, E. 2006, "Evidence of trends in daily climate

extremes over southern and west Africa", *Journal of Geophysical Research: Atmospheres* (1984–2012), vol. 111, no. D14.

Nicholson, S. 1996, "A review of climate dynamics and climate variability in Eastern Africa", *The limnology, climatology and paleoclimatology of the East African lakes*, , pp. 25-56.

Nicholson, S.E. 2000, "The nature of rainfall variability over Africa on time scales of decades to millenia", *Global and Planetary Change*, vol. 26, no. 1–3, pp. 137-158.

Nicholson, S.E., Nash, D.J., Chase, B.M., Grab, S.W., Shanahan, T.M., Verschuren, D., Asrat, A., Lézine, A. & Umer, M. 2013, "Temperature variability over Africa during the last 2000 years", *The Holocene*, , pp. 0959683613483618.

Nicholson, S.E. 2014, "The Predictability of Rainfall over the Greater Horn of Africa. Part I: Prediction of Seasonal Rainfall", *Journal of Hydrometeorology*, vol. 15, no. 3, pp. 1011-1027.

Nicholson, S.E. 2015, "The predictability of rainfall over the Greater Horn of Africa. Part II. Prediction of monthly rainfall during the long rains.", *Journal of Hydrometeorology*, , no. 2015.

Nicholson, S.E. 2015, "Long-term variability of the East African 'short rains' and its links to large-scale factors", *International Journal of Climatology*, .

Nsubuga, F.W., Olwoch, J.M. & Rautenbach, C.d.W. 2011, "Climatic trends at Namulonge in Uganda: 1947-2009",

- Nyeko-Ogiramoi, P., Willems, P. & Ngirane-Katashaya, G. 2013, "Trend and variability in observed hydrometeorological extremes in the Lake Victoria basin", *Journal of hydrology*, vol. 489, pp. 56-73.
- Ogallo, L. 1988, "Relationships between seasonal rainfall in East Africa and the Southern Oscillation", *Journal of Climatology*, vol. 8, no. 1, pp. 31-43.
- Ohashi, Y. & Kida, H. 2002, "Effects of mountains and urban areas on daytime local-circulations in the Osaka and Kyoto regions.", *気象集誌.第2輯*, vol. 80, no. 4, pp. 539-560.
- Ohashi, Y. & Kida, H. 2002, "Local circulations developed in the vicinity of both coastal and inland urban areas: A numerical study with a mesoscale atmospheric model", *Journal of Applied Meteorology*, vol. 41, no. 1, pp. 30-45.
- Oke, T.R. 1982, "The energetic basis of the urban heat island", *Quarterly Journal of the Royal Meteorological Society*, vol. 108, no. 455, pp. 1-24.
- Oke, T. 1995, "The heat island of the urban boundary layer: characteristics, causes and effects" in *Wind climate in cities* Springer, , pp. 81-107.
- Oke, T., Johnson, G., Steyn, D. & Watson, I. 1991, "Simulation of surface urban heat islands under 'ideal' conditions at night Part 2: Diagnosis of causation", *Boundary-Layer Meteorology*, vol. 56, no. 4, pp. 339-358.
- Okoola, R.E. 1999, "A diagnostic study of the eastern Africa monsoon circulation during the Northern Hemisphere spring season", *International Journal of Climatology*, vol. 19, no. 2, pp. 143-168.

- Okoola, R.E., Camberlin, P., Ininda J. 2008, "Wet periods along the East Africa Coast and the extreme wet spell event of October 1997", *Journal of the Kenya Meteorological Society*, 2008, 2 (1), pp.67-83. <hal-00320637>
- Omondi, P.A., Awange, J.L., Forootan, E., Ogallo, L.A., Barakiza, R., Girmaw, G.B., Fesseha, I., Kululetera, V., Kilembe, C. & Mbatia, M.M. 2014, "Changes in temperature and precipitation extremes over the Greater Horn of Africa region from 1961 to 2010", *International Journal of Climatology*, vol. 34, no. 4, pp. 1262-1277.
- Omondi, P., Awange, J.L., Ogallo, L.A., Ininda, J. & Forootan, E. 2013, "The influence of low frequency sea surface temperature modes on delineated decadal rainfall zones in Eastern Africa region", *Advances in Water Resources*, vol. 54, no. 0, pp. 161-180.
- Omondi, P., Awange, J.L., Ogallo, L.A., Okoola, R.A. & Forootan, E. 2012, "Decadal rainfall variability modes in observed rainfall records over East Africa and their relations to historical sea surface temperature changes", *Journal of Hydrology*, vol. 464-465, no. 0, pp. 140-156.
- Omumbo, J.A., Lyon, B., Waweru, S.M., Connor, S.J. & Thomson, M.C. 2011, "Raised temperatures over the Kericho tea estates: revisiting the climate in the East African highlands malaria debate", *Malaria journal*, vol. 10, pp. 12-2875-10-12.
- Ongoma, V., Muthama, N. & Gitau, W. 2013, "Evaluation of urbanization influences on urban winds of Kenyan cities", *Ethiopian Journal of Environmental Studies and Management*, vol. 6, no. 3, pp. 223-231.
- Opijah, F.J., Mukabana, J.R. & Ng'ang'a, J. 2007, "Rainfall distribution over Nairobi area", *Journal Kenya Meteorological Society*, 1 (1), , pp. 3-13.



- Opijah, F.J. & Mukabana, J.R. 2004, "On the influence of urbanization on the water budget in Nairobi city: A numerical study", *GeoJournal*, vol. 61, no. 2, pp. 121-129.
- Opijah, F.J., Mukabana, J.R. & Ng'ang'a, J. 2007, "Rainfall distribution over Nairobi area", *Journal Kenya Meteorological Society*, 1 (1), , pp. 3-13.
- Opija, F.J., Ng'ang'a, J.K., Omedo, G. & Mukabana, J.R. 2008, "Contribution to the Heat Budget in Nairobi-Metro Area by the Anthropogenic Heat Component", *Journal of Kenya Meteorological Society Volume*, vol. 2, pp. 1.
- Ouarda, T. & El-Adlouni, S. 2011, "Bayesian Nonstationary Frequency Analysis of Hydrological Variables1", *JAWRA Journal of the American Water Resources Association*, vol. 47, no. 3, pp. 496-505.
- Owiti, Z., Ogallo, L.A. & Mutemi, J. 2008, "Linkages between the Indian Ocean dipole and East African seasonal rainfall anomalies", *Journal of Kenya Meteorological Society Volume*, vol. 2, pp. 1.
- Panagoulia, D., Economou, P. & Caroni, C. 2014, "Stationary and nonstationary generalized extreme value modelling of extreme precipitation over a mountainous area under climate change", *Environmetrics*, vol. 25, no. 1, pp. 29-43.
- Parkinson, J. & Mark, O. 2005, *Urban stormwater management in developing countries*, IWA publishing.
- Peng, S., Piao, S., Ciais, P., Friedlingstein, P., Oettle, C., Bréon, F., Nan, H., Zhou, L. & Myneni, R.B. 2011, "Surface urban heat island across 419 global big cities", *Environmental science & technology*, vol. 46, no. 2, pp. 696-703.

- Pielke, R.A. 2001, "Influence of the spatial distribution of vegetation and soils on the prediction of cumulus convective rainfall", *Reviews of Geophysics*, vol. 39, no. 2, pp. 151-177.
- Prokoph, A. & Barthelmes, F. 1996, "Detection of nonstationarities in geological time series: wavelet transform of chaotic and cyclic sequences", *Computers & Geosciences*, vol. 22, no. 10, pp. 1097-1108.
- Prokoph, A. & Patterson, R.T. 2004, "Application of wavelet and regression analysis in assessing temporal and geographic climate variability: Eastern Ontario, Canada as a case study", *Atmosphere-Ocean*, vol. 42, no. 3, pp. 201-212.
- Rizwan, A.M., Dennis, L.Y. & Chunho, L. 2008, "A review on the generation, determination and mitigation of Urban Heat Island", *Journal of Environmental Sciences*, vol. 20, no. 1, pp. 120-128.
- Robaa, S. 2003, "Urban-suburban/rural differences over Greater Cairo, Egypt", *Atmósfera*, vol. 16, no. 3, pp. 157-172.
- Rosenzweig, C., Solecki, W.D., Blake, R., Bowman, M., Faris, C., Gornitz, V., Horton, R., Jacob, K., LeBlanc, A. & Leichenko, R. 2011, "Developing coastal adaptation to climate change in the New York City infrastructure-shed: process, approach, tools, and strategies", *Climatic Change*, vol. 106, no. 1, pp. 93-127.
- Roxy, M. 2014, "Sensitivity of precipitation to sea surface temperature over the tropical summer monsoon region—and its quantification", *Climate Dynamics*, vol. 43, no. 5-6, pp. 1159-1169.



- Roxy, M.K., Ritika, K., Terray, P. & Masson, S. 2014, "The Curious Case of Indian Ocean Warming\*", *Journal of Climate*, vol. 27, no. 22, pp. 8501-8509.
- Sang, Y., Wang, Z. & Liu, C. 2013, "Discrete wavelet-based trend identification in hydrologic time series", *Hydrological Processes*, vol. 27, no. 14, pp. 2021-2031.
- Savić, S., Milošević, D., Lazić, L., Marković, V., Arsenović, D. & Pavić, D. 2013, "Classifying Urban Meteorological Stations Sites by “Local Climate Zones”: Preliminary Results for the City of Novi Sad (Serbia)", *Geographica Pannonica*, vol. 17, no. 3, pp. 60-68.
- Sen, A.K. & Ogrin, D. 2015, "Analysis of monthly, winter, and annual temperatures in Zagreb, Croatia, from 1864 to 2010: the 7.7-year cycle and the North Atlantic Oscillation", *Theoretical and Applied Climatology*, , pp. 1-7.
- Schreck, C.J. & Semazzi, F.H. 2004, "Variability of the recent climate of eastern Africa", *International Journal of Climatology*, vol. 24, no. 6, pp. 681-701.
- Schwarz, N., Lautenbach, S. & Seppelt, R. 2011, "Exploring indicators for quantifying surface urban heat islands of European cities with MODIS land surface temperatures", *Remote Sensing of Environment*, vol. 115, no. 12, pp. 3175-3186.
- Serinaldi, F. & Kilsby, C.G. 2015, "Stationarity is undead: uncertainty dominates the distribution of extremes", *Advances in Water Resources*, vol. 77, pp. 17-36.
- Shepherd, J.M., Pierce, H. & Negri, A.J. 2002, "Rainfall modification by major urban areas: Observations from spaceborne rain radar on the TRMM satellite", *Journal of Applied Meteorology*, vol. 41, no. 7, pp. 689-701.

- Shepherd, J.M. & Burian, S.J. 2003, "Detection of urban-induced rainfall anomalies in a major coastal city.", *Earth Interactions*, vol. 7, no. 1.
- Shepherd, J.M. 2005, "A review of current investigations of urban-induced rainfall and recommendations for the future.", *Earth Interactions*, vol. 9, no. 1.
- Shepherd, J.M. 2006, "Evidence of urban-induced precipitation variability in arid climate regimes", *Journal of Arid Environments*, vol. 67, no. 4, pp. 607-628.
- Shepherd, J.M., Carter, M., Manyin, M., Messen, D. & Burian, S. 2010, "The impact of urbanization on current and future coastal precipitation: a case study for Houston", *Environment and planning B: Planning and Design*, vol. 37, no. 2, pp. 284-304.
- Shepherd, J., Stallins, J., Jin, M. & Mote, T. 2010, "Urbanization: Impacts on clouds, precipitation, and lightning", *Urban ecosystem ecology*, , no. urbanecosysteme, pp. 1-27.
- Shongwe, M., Van Oldenborgh, G., Van Den Hurk, B., De Boer, B., Coelho, C. & Van Aalst, M. 2009, "Projected changes in mean and extreme precipitation in Africa under global warming. Part I: Southern Africa", *Journal of Climate*, vol. 22, no. 13, pp. 3819-3837.
- Shongwe, M.E., van Oldenborgh, G.J., van den Hurk, B. & van Aalst, M. 2011, "Projected changes in mean and extreme precipitation in Africa under global warming. Part II: East Africa", *Journal of Climate*, vol. 24, no. 14, pp. 3718-3733.
- Skansi, María de los Milagros, Brunet, M., Sigró, J., Aguilar, E., Arevalo Groening, J.A., Bentancur, O.J., Castellón Geier, Y.R., Correa Amaya, R.L., Jácome, H. & Malheiros Ramos, A. 2013, "Warming and wetting signals emerging from analysis of changes in climate extreme indices over South America", *Global and Planetary Change*, vol. 100, pp. 295-307.

- Sonali, P. & Kumar, D.N. 2013, "Review of trend detection methods and their application to detect temperature changes in India", *Journal of Hydrology*, vol. 476, pp. 212-227.
- Song, Y., Achberger, C. & Linderholm, H.W. 2011, "Rain-season trends in precipitation and their effect in different climate regions of China during 1961–2008", *Environmental Research Letters*, vol. 6, no. 3, pp. 034025.
- Stephenson, T.S., Vincent, L.A., Allen, T., Van Meerbeek, C.J., McLean, N., Peterson, T.C., Taylor, M.A., Aaron-Morrison, A.P., Auguste, T. & Bernard, D. 2014, "Changes in extreme temperature and precipitation in the Caribbean region, 1961–2010", *International Journal of Climatology*, .
- Stocker, D.Q. 2013, "Climate change 2013: The physical science basis", *Working Group I Contribution to the Fifth Assessment Report of the Intergovernmental Panel on Climate Change, Summary for Policymakers, IPCC*, .
- Stewart, I.D. & Oke, T.R. 2012, "Local climate zones for urban temperature studies", *Bulletin of the American Meteorological Society*, vol. 93, no. 12, pp. 1879-1900.
- Stewart, I.D., Oke, T. & Krayenhoff, E.S. 2014, "Evaluation of the 'local climate zone' scheme using temperature observations and model simulations", *International Journal of Climatology*, vol. 34, no. 4, pp. 1062-1080.
- Sugahara, S., Da Rocha, R.P. & Silveira, R. 2009, "Non-stationary frequency analysis of extreme daily rainfall in Sao Paulo, Brazil", *International Journal of Climatology*, vol. 29, no. 9, pp. 1339-1349.
- Suriya, S. & Mudgal, B.V. 2012, "Impact of urbanization on flooding: The Thirusoolam sub watershed – A case study", *Journal of Hydrology*, vol. 412–413, no. 0, pp. 210-219.

- Tabari, H., Abghari, H. & Hosseinzadeh Talaee, P. 2012, "Temporal trends and spatial characteristics of drought and rainfall in arid and semiarid regions of Iran", *Hydrological Processes*, vol. 26, no. 22, pp. 3351-3361.
- Tabari, H. & Talaee, P.H. 2011, "Temporal variability of precipitation over Iran: 1966–2005", *Journal of Hydrology*, vol. 396, no. 3, pp. 313-320.
- Tayanc, M. & Toros, H. 1997, "Urbanization effects on regional climate change in the case of four large cities of Turkey", *Climatic Change*, vol. 35, no. 4, pp. 501-524.
- Tomas, R.A. & Webster, P.J. 2003, "TROPICAL METEOROLOGY | Overview and Theory" in *Encyclopedia of Atmospheric Sciences*, ed. J.R. Holton, Academic Press, Oxford, pp. 2306-2313.
- Tomás, R., Li, Z., Lopez-Sanchez, J., Liu, P. & Singleton, A. 2015, "Using wavelet tools to analyse seasonal variations from InSAR time-series data: a case study of the Huangtupo landslide", *Landslides*, , pp. 1-14.
- Torrence, C. & Compo, G.P. 1998, "A practical guide to wavelet analysis", *Bulletin of the American Meteorological Society*, vol. 79, no. 1, pp. 61-78.
- Travis, D.J., Meentemeyer, V. & Suckling, P.W. 1987, "Influence of meteorological conditions on urban/rural temperature and humidity differences for a small city", *Southeastern Geographer*, vol. 27, no. 2, pp. 90-100.
- Turki, I., Laignel, B., Laftouhi, N., Nouaceur, Z. & Zamrane, Z. 2016, "Investigating possible links between the North Atlantic Oscillation and rainfall variability in Marrakech (Morocco)", *Arabian Journal of Geosciences*, vol. 9, no. 3, pp. 1-14.

- Unger, J., Sümeghy, Z. & Zoboki, J. 2001, "Temperature cross-section features in an urban area", *Atmospheric Research*, vol. 58, no. 2, pp. 117-127.
- Veleda, D., Montagne, R. & Araujo, M. 2012, "Cross-wavelet bias corrected by normalizing scales", *Journal of Atmospheric and Oceanic Technology*, vol. 29, no. 9, pp. 1401-1408.
- Vasiliades, L., Galiatsatou, P. & Loukas, A. 2015, "Nonstationary frequency analysis of annual maximum rainfall using climate covariates", *Water Resources Management*, vol. 29, no. 2, pp. 339-358.
- Vardoulakis, E., Karamanis, D., Fotiadi, A. & Mihalakakou, G. 2013, "The urban heat island effect in a small Mediterranean city of high summer temperatures and cooling energy demands", *Solar Energy*, vol. 94, pp. 128-144.
- Waliser, D.E. 2003, "TROPICAL METEOROLOGY | Inter Tropical Convergence Zones" in *Encyclopedia of Atmospheric Sciences*, ed. J.R. Holton, Academic Press, Oxford, pp. 2325-2334.
- Wan, Z. & Dozier, J. 1996, "A generalized split-window algorithm for retrieving land-surface temperature from space", *Geoscience and Remote Sensing, IEEE Transactions on*, vol. 34, no. 4, pp. 892-905.
- Wang, J., Wang, K. & Wang, P. 2007, "Urban heat (or cool) island over Beijing from MODIS land surface temperature", *JOURNAL OF REMOTE SENSING-BEIJING-*, vol. 11, no. 3, pp. 330.
- Wang, F., Yang, S., Higgins, W., Li, Q. & Zuo, Z. 2014, "Long-term changes in total and extreme precipitation over China and the United States and their links to oceanic-atmospheric features", *International Journal of Climatology*, vol. 34, no. 2, pp. 286-302.

Wang, H., Chen, Y., Xun, S., Lai, D., Fan, Y. & Li, Z. 2013, "Changes in daily climate extremes in the arid area of northwestern China", *Theoretical and applied climatology*, vol. 112, no. 1-2, pp. 15-28.

Wang, C., Lin, W., Peng, T. & Tsai, H. 2008, "Temperature and hydrological variations of the urban environment in the Taipei metropolitan area, Taiwan", *Science of The Total Environment*, vol. 404, no. 2-3, pp. 393-400.

Weaver, C.P. & Avissar, R. 2001, "Atmospheric disturbances caused by human modification of the landscape", *Bulletin of the American Meteorological Society*, vol. 82, no. 2, pp. 269-281.

Whan, K., Alexander, L., Imielska, A., McGree, S., Jones, D., Ene, E., Finaulahi, S., Inape, K., Jacklick, L. & Kumar, R. 2013, "Trends and variability of temperature extremes in the tropical Western Pacific", *International Journal of Climatology*, .

Williams, A.P., Funk, C., Michaelsen, J., Rauscher, S.A., Robertson, I., Wils, T.H., Koprowski, M., Eshetu, Z. & Loader, N.J. 2012, "Recent summer precipitation trends in the Greater Horn of Africa and the emerging role of Indian Ocean sea surface temperature", *Climate Dynamics*, vol. 39, no. 9-10, pp. 2307-2328.

Williams, A.P. & Funk, C. 2011, "A westward extension of the warm pool leads to a westward extension of the Walker circulation, drying eastern Africa", *Climate Dynamics*, vol. 37, no. 11-12, pp. 2417-2435.

WMO, 2008: Guide to meteorological instruments and methods of observation.

7th ed. WMO-8. [Available online at [www.wmo.int/pages/prog/gcos](http://www.wmo.int/pages/prog/gcos)

/documents/gruanmanuals/CIMO/CIMO\_Guide- 7th\_Edition-2008.pdf.]



WMO, 2011: Guide to climatological practices. WMO-100. [Available online at [www.wmo.int/pages/prog/wcp/ccl/documents/WMO\\_100\\_en.pdf](http://www.wmo.int/pages/prog/wcp/ccl/documents/WMO_100_en.pdf).]

Yagüe, C., Zurita, E. & Martinez, A. 1991, "Statistical analysis of the Madrid urban heat island", *Atmospheric Environment. Part B. Urban Atmosphere*, vol. 25, no. 3, pp. 327-332.

Yang, J., Liu, H., Fei, S., Zhang, N., Jiang, W., Jianguo, M.O.C. & Jianguo, M.B. 2013, "The impact of urbanization on the urban heat island in Suzhou under the influence of Taihu lake-land breeze", *Journal of the Meteorological Sciences*, vol. 5, pp. 001.

Yamagata, T., Behera, S.K., Luo, J., Masson, S., Jury, M.R. & Rao, S.A. 2004, "Coupled ocean-atmosphere variability in the tropical Indian Ocean", *Earth's Climate*, pp. 189-211.

Yamagata, T., Behera, S.K., Rao, S.A., Guan, Z., Ashok, K. & Saji, H.N. 2003, "Comments on "Dipoles, temperature gradients, and tropical climate anomalies"", *Bulletin of the American Meteorological Society*, vol. 84, no. 10, pp. 1418-1422.

Zhang, N., Wang, X. & Peng, Z. 2014, "Large-eddy simulation of mesoscale circulations forced by inhomogeneous urban heat island", *Boundary-Layer Meteorology*, vol. 151, no. 1, pp. 179-194.

Zhang, X., Alexander, L., Hegerl, G.C., Jones, P., Tank, A.K., Peterson, T.C., Trewin, B. & Zwiers, F.W. 2011, "Indices for monitoring changes in extremes based on daily temperature and precipitation data", *Wiley Interdisciplinary Reviews: Climate Change*, vol. 2, no. 6, pp. 851-870.

Zhao, W. & Khalil, M. 1993, "The relationship between precipitation and temperature over the contiguous United States", *Journal of Climate*, vol. 6, no. 6, pp. 1232-1236.

Zhong, S. & Yang, X. 2015, "Ensemble simulations of the urban effect on a summer rainfall event in the Great Beijing Metropolitan Area", *Atmospheric Research*, vol. 153, pp. 318-334.



## 9 Appendices

**Appendix 5.1: Stations used for computing inter-station correlations of rainfall; rainfall homogeneous zones from Indeje, et al., (2000) is shown in column 3; the stations and their acronyms were as used in Chapters 2, 3 & 4.**

Station name	Station acronym	Region	Latitude °S or °N °S =(-)	Long. (°E)	Altitude (m)	Length of rainfall data
Wilson	NU	Central highlands and Rift Valley	-1.32	36.82	1679	1961-2013
Dagoretti	NR <sub>D</sub>		-1.30	36.70	1798	1961-2013
Thika	NR <sub>T</sub>		-0.98	37.07	1549	1961-2013
Nyeri	NYR		0.43	36.97	1815	1970-2008
Narok	NRK		-1.13	35.83	1890	1961-2008
Nakuru	NKU		0.27	36.12	1901	1970-2013
Mombasa	MU	The coastal regions	-4.03	39.60	55	1961-2013
Mtwapa	MR <sub>Mt</sub>		-3.93	39.73	20	1961-2013
Msabaha	MR <sub>Ms</sub>		-3.27	40.05	91	1961-2013
Makindu	MKD		-2.28	37.83	1000	1961-2008
Voi	VOI		-3.70	38.57	560	1961-2008
Malindi	MLD		-3.23	40.10	20	1961-2008
Lamu	LAM		-2.27	40.90	30	1961-2008
Kisumu	KU	Lake victoria region	-0.100	34.70	1146	1961-2013
Kakamega	KKM		0.28	34.75	1580	1961-2008
Kisii	KR		-0.68	34.73	1493	1963-2013

Appendix 5.2: Seasonal rainfall Inter-station correlations a) MAM; b) JJA and c); OND; all the values highlighted in red ( $r \geq \pm 0.27$ ) are significant at  $\alpha = 0.05$ ; the black rectangles show inter-correlations of NU and MU with neighbouring rural stations; the station names are as shown in Table 5.1

a)	MAM	NU	NR <sub>D</sub>	NR <sub>T</sub>	NYR	NRK	NKU	KU	KR	KKM	MKD	VOI	MU	MR <sub>Mt</sub>	MR <sub>Ms</sub>	MLD
NR <sub>D</sub>		0,63														
NR <sub>T</sub>		0,71	0,51													
NYR		0,44	0,33	0,49												
NRK		0,58	0,43	0,59	0,24											
NKU		0,57	0,35	0,44	0,27	0,50										
KU		0,29	0,12	0,35	0,25	0,46	0,18									
KR		0,12	0,18	0,24	0,09	0,13	0,16	0,32								
KKM		0,24	0,15	0,20	0,36	0,42	0,22	0,49	0,14							
MKD		0,48	0,65	0,61	0,33	0,44	0,38	0,19	0,26	0,17						
VOI		0,16	0,30	0,34	0,39	0,29	0,02	0,03	0,08	0,10	0,61					
MU		0,08	-0,01	0,06	0,28	0,11	-0,17	0,04	-0,25	0,15	0,22	0,34				
MR <sub>Mt</sub>		0,04	-0,03	0,07	0,17	-0,02	-0,11	0,05	-0,20	0,06	0,13	0,10	0,85			
MR <sub>Ms</sub>		0,10	0,08	0,18	0,37	0,09	0,02	0,08	-0,05	0,07	0,24	0,37	0,76	0,70		
MLD		0,02	0,07	0,01	0,18	-0,03	-0,05	-0,07	-0,19	-0,02	0,11	0,17	0,66	0,66	0,75	
LAM		0,17	0,16	0,17	0,45	0,06	0,01	-0,04	0,03	0,18	0,13	0,21	0,58	0,61	0,77	0,62

b)	JJA	NU	NR <sub>D</sub>	NR <sub>T</sub>	NYR	NRK	NKU	KU	KR	KKM	MKD	VOI	MU	MR <sub>Mt</sub>	MR <sub>Ms</sub>	MLD
NR <sub>D</sub>		0,46														
NR <sub>T</sub>		0,25	0,02													
NYR		0,32	0,28	0,54												
NRK		0,42	0,03	0,36	0,35											
NKU		0,17	0,23	0,01	0,30	0,21										
KU		0,28	0,22	0,07	-0,08	0,01	0,31									
KR		0,06	0,06	0,26	0,05	0,24	0,06	0,21								
KKM		0,15	0,10	-0,07	0,08	0,01	0,27	0,24	0,28							
MKD		0,07	-0,06	0,34	0,28	0,07	0,00	-0,19	0,18	-0,13						
VOI		-0,17	0,02	0,02	0,19	-0,19	-0,06	-0,11	-0,11	-0,08	0,37					
MU		-0,20	-0,22	0,00	-0,08	-0,33	-0,11	-0,09	0,02	0,08	0,09	0,68				
MR <sub>Mt</sub>		0,01	-0,19	-0,09	-0,09	-0,10	-0,21	-0,01	-0,08	0,00	-0,04	0,51	0,67			
MR <sub>Ms</sub>		-0,17	-0,24	0,20	0,00	0,04	-0,19	0,07	0,08	-0,18	0,07	0,27	0,51	0,53		
MLD		-0,03	-0,09	0,25	0,07	0,28	-0,01	0,01	0,10	-0,15	0,12	0,33	0,42	0,24	0,60	
LAM		-0,14	0,13	0,02	-0,25	-0,03	0,02	-0,06	0,03	-0,17	-0,04	-0,06	0,15	0,25	0,40	0,31

c)	OND	NU	NR <sub>D</sub>	NR <sub>T</sub>	NYR	NRK	NKU	KU	KR	KKM	MKD	VOI	MU	MR <sub>Mt</sub>	MR <sub>Ms</sub>	MLD
NR <sub>D</sub>		0,76														
NR <sub>T</sub>		0,76	0,63													
NYR		0,59	0,49	0,77												
NRK		0,88	0,82	0,68	0,68											
NKU		0,74	0,56	0,65	0,67	0,81										
KU		0,72	0,65	0,70	0,73	0,76	0,71									
KR		0,43	0,35	0,39	0,27	0,46	0,39	0,61								
KKM		0,76	0,64	0,60	0,44	0,76	0,70	0,69	0,33							
MKD		0,72	0,59	0,66	0,56	0,68	0,44	0,65	0,34	0,49						
VOI		0,62	0,49	0,50	0,50	0,64	0,55	0,52	0,21	0,45	0,72					
MU		0,46	0,47	0,66	0,78	0,57	0,65	0,63	0,24	0,43	0,52	0,60				
MR <sub>Mt</sub>		0,53	0,46	0,62	0,77	0,56	0,64	0,68	0,24	0,51	0,50	0,63	0,88			
MR <sub>Ms</sub>		0,61	0,59	0,72	0,81	0,63	0,76	0,76	0,31	0,52	0,58	0,57	0,87	0,86		
MLD		0,35	0,32	0,64	0,62	0,46	0,61	0,59	0,27	0,33	0,33	0,37	0,75	0,61	0,76	
LAM		0,44	0,45	0,66	0,79	0,51	0,68	0,62	0,27	0,38	0,46	0,51	0,89	0,79	0,86	0,75